STUDIES OF SLOPE STABILITY PROBLEMS BY LEM, SRM AND DEM

SUN YINGJIE

Ph.D
The Hong Kong
Polytechnic University

2013

THE HONGKONG POLYTECHNIC UNIVERSITY

DEPARTMENT OF CIVIL AND ENVIRONMENTAL ENGINEERING

STUDIES OF SLOPE STABILITY PROBLEMS BY LEM, SRM AND DEM

SUN Yingjie

A Thesis Submitted in Partial Fulfilment of the Requirements
for the Degree of Doctor of Philosophy

May 2012

CERTIFICATE OF ORIGINALITY

I hereby declare that this thesis is my own work and that, to the best of my knowledge and belief, it reproduces no material previously published or written, nor material that has been accepted for the award of any other degree of diploma, except where due acknowledgement has been made in the text.

Signature:

Name: SUN Yingjie

Abstract of thesis entitled

STUDIES OF SLOPE STABILITY PROBLEMS BY LIMIT EQUILIBRIUM METHOD, STRENGTH REDUCTION METHOD AND DISTINCT ELEMENT METHOD

for the degree of Doctor of Philosophy
at The Hong Kong Polytechnic University in May 2012

Slope stability problem is a major problem in geotechnical engineering with influence on structure and human life, and slope stability problem has drawn the attentions of many researchers and engineers for the past several decades. This study is aimed to investigate slope stability problem with a better understanding of the failure mechanism and some fundamental principles in slope stability analysis by several methods so that the complete stability and failure processes are investigated. From the present study, some outstanding fundamental questions in slope stability problem have been settled, and the works are beneficial to both academic and practical aspects.

This study first begins with the typical upper bound limit equilibrium analysis where different modern heuristic optimization algorithms are modified and improved to locate the critical slip surface efficiently and precisely. This problem has been studied by many researchers in the past, but there is a major difficulty in this problem in that the objective function is non-smooth and non-convex and the solution might be trapped into local minimum easily. Towards this complicated problems, two modified optimization algorithms: improved harmony search method MHS and coupled algorithm of HS/PSO are developed. These two algorithms are demonstrated to be more efficient than the

original methods, and are particularly suitable for highly complicated problems where there are several strong local minima in the solution domain. The knowledge and works gained in this part of work are useful for practical engineering and also become part of the tools for the later sections.

Secondly, the extremum principle and the concept of variable factor of safety based on Pan's postulate and equivalent variational principle are developed in this study. Using the new concept which can be viewed as an equivalent lower bound method, the long outstanding question on the interslice force function is finally settled using the mathematical tool developed in the first part of the present study. Slope stability problem can now become a statically determinate problem, and the interslice force function is actually taken as a variable instead of a prescribed function. This function is now determined by an equivalent lower bound principle which is missing in all the previous limit equilibrium formulation, which is major breakthrough in the basic formulation of the limit equilibrium method. Besides the new extremum LEM formulation, the author has also employed SRM to study the interslice force function. In general, it is found that the interslice force function is close to a bell shape and is also in agreement with the results from LEM, and such results clearly demonstrates that this function cannot be arbitrarily specified as what has been done for more than 40 years. The location of the thrust line also agrees well with the Janbu's Rigorous method which is at 1/3 of slice height from the base for normal cases. As a further extension of the works, the extremum formulations are further extended to the concept of variable factor of safety formulation which can satisfy all the global and local equilibrium. Using this new concept, the stress re-distribution and residual strength concept can be cast into the LEM framework under a rigorous lower bound formulation. Progressive failure can now be cast into the framework of limit equilibrium method which is not possible in the past.

The limitation of both LEM and SRM is the requirement on continuity which is not possible after the initiation of failure. The failure and post-failure mechanism are investigated by the use of Distinct Element Method (DEM) due to the demand in the consideration of large scale post-failure deformation. The use of DEM to investigate the slip surface is seldom considered in the past but has been achieved in the present study. The effect of water seepage on slope stability using a DEM approach is also an outstanding work which is worth to be investigated. In this study, it is found that the geometry of slope changes continuously, and tensile failure at the crest and shear failure in the middle of the slope are found. The failure mode for soil nailed slope and slope with by water flow are also studied by the DEM with interesting results obtained.

For three-dimensional problems, there are several interesting problems to be considered. Three-dimensional effect of curvature with different nailing modes is considered by SRM, and the intercolumn force function is investigated (which is an outstanding item up to present). It is found that the intercolumn force function within the principal section containing the sliding direction is dominating over other sections. Concave geometry also gives higher global stability which is important for many highway slopes. For nailing pattern, the radial nailing mode gives lower factor of safety for convex slope but higher factor of safety for concave slope as compared with the parallel nailing mode. These results are both useful to the engineers as well as to the basic understanding of three-dimensional slope stability problem.

Based on the above research involving different methods, many fundamental principles and outstanding problems in slope stability analysis have been settled in the present research. For example, the search for critical failure surface can now be carried out with very high level of confidence even for very complicated problem. Many engineers arbitrarily assign interslice force function (f(x)) equal to 1.0 (or sine function) without any thought, as all textbooks and research papers give the view that this function is "fundamentally indeterminate" and is not critical for normal condition. The author has however pointed out the mistake of this common belief accepted by engineers/researchers for more than 40 years, and has also demonstrated that there are also cases where f(x) is important and has proposed a systematic way to determine this function for arbitrary problem based on the equivalent lower bound principle. This work is then extended to three-dimensional condition where no one has ever proposed any interslice force function, and this three-dimensional function can now be treated as determinate function. The knowledge about the initiation and post failure movement of slope by DEM has also provided clearer picture about the movement and internal stress distribution within a slope at different stages which is useful to assess the post-failure behaviour and the precautions that are required.

LIST OF PUBLICATIONS DURING THE COURSE OF STUDY

Y. M. Cheng, Liang Li, Lansivaara T, S. C. Chi, **Y.J. Sun** (2008). An Improved harmony search minimization algorithm using different slip surface generation methods for slope stability analysis. Engineering optimization. vol.40(2): 95-115.

Y.J. Sun, S.C. Lam, C.W. Law and Y.M. Cheng (2009). Elasto-plastic analysis of raft footing on continuum. Proceedings of international conference on Computational Design in Engineering 2009: 78.

Cheng Y.M., Zhao Z.H. and **Sun Y.J.** (2010), Evaluation of interslice force function and discussion on convergence in slope stability analysis by the lower bound method, Journal of Geotechnical and Geoenvironmental Engineering, 136(8):1103-1113. (Grade A)

Cheng Y.M., Li L, **Sun Y.J.**, Au S.K.(2010). A coupled particle swarm and harmony search optimization algorithm for difficult geotechnical problems. Structural and Multidisciplinary Optimization. Volume 45, Number 4, 489-501.

Y.M. Cheng, **Y.J. Sun** (2010). Investigation on interslice forces function/thrust line in slope stability problem by strength reduction and lower bound methods. Proceedings of 2nd International Postgraduate Conference on Infrastructure and Environment, Vol.2: 323-329.

Y.M. Cheng, D.Z. Li, L Li, **Y.J. Sun**, R. Baker, Y Yang(2011). Limit equilibrium method based on an approximate lower bound method with a variable factor of safety that can consider residual strength. Computers and Geotechnics, Vol 38: 623-637.

Y.J. Sun and Y.M. Cheng, Interslice force function in two and three-dimensional problems, Computers and Geotechnics (under review)

ACKNOWLEDGEMENTS

I would like to express my sincere gratitude to my supervisor, Dr Y.M. Cheng, for all the inspiration, guidance and support throughout the study. His invaluable supports and experienced guidance made this work possible. The privilege of working with Dr Y.M. Cheng has appreciably influenced my professional development as well as perspectives on life.

Financial support for this research work from The Hong Kong Polytechnic University is greatly acknowledged. Administrative and technical supports from the staff of the Department of Civil and Structural Engineering are also deeply appreciated.

Professor J. A. Wang of University of Science and Technology, Beijing is truly appreciated due to the continued caring and concerning about my study and life during the past decade. I would also like to express my great thanks to Dr. Wei W.B., Dr. Li L., Mr. Zhao Z.H., Mr. Li D.Z., Miss Li N. and Mr. Yang Y. for fruitful and unforgettable suggestions and discussions they have made for my work.

Finally, special thanks shall go to my dearest parents, teachers, and friends whose endless understanding, encouragement, and love have enabled me to go through all the difficulties and reach a new level in my life.

TABLE OF CONTENTS

LIST OF TABLES

LIST OF FIGURES

CHAPTER 1 Introduction

1.1 Background and motivation

Slope stability problem is always a main concern in geotechnical engineering. Natural or cut slopes have greatly influenced human's properties and life, and for area like Hong Kong, slope failures can be fatal. There are many research works on the assessment of the stability of slopes under different geometry, soil properties and groundwater conditions in the past. Each stability analysis method differs from the others in some of the basic assumptions, but most of the stability analysis methods will give similar factors of safety for normal cases which are sufficient for normal engineering uses. Besides the factor of safety, the failure mechanism and post-failure mechanism are also important in some cases, and different methods of analysis are more suitable and efficient for specific aspects. In literature, limit equilibrium method, strength reduction method, limit analysis and distinct element method have been used for this problem, and the applications and limitations of these methods have been investigated and discussed by various researchers over the past 40 years.

Even though LEM has been studied in details by various researchers in the past 40 years, there are still different variations of LEM and numerical techniques being put forward each year. In Hong Kong, possibly more than 98% of the analyses are still based on the LEM, as LEM possesses the advantages of simple in operation, fast in computation, easy to understand and the support from many engineers' experience. Limit equilibrium method (LEM) using the method of slices is the classical slope stability analysis which requires assumptions on the interslices force distribution before the problem can be solved. LEM can broadly be classified into ‘simplified’ and ‘rigorous’ approaches. In the simplified approach, either force or moment equilibrium is satisfied, but not both equilibrium conditions at the same time. Though this approach is a highly simplified method of analysis, it is still flavored by many engineers at present, as the concept behind the stability formulation is simple and straightforward. For the rigorous approach, both force and moment equilibrium have to be satisfied simultaneously, and assumptions on the interslices force distribution must be specified before the problem can be solved. Morgenstern and Price (1965) have proposed a relation between the interslice shear and normal force as a general formulation, and this interslice force function has drawn considerable attention by many researchers in the past. There is however no theoretical background to specify this function for an arbitrary problem, though Morgenstern (1992) has discussed that this function is not critical for normal cases if both force and moment equilibrium are satisfied. In some cases, the interslice force function can be critical which has been discussed by Abramson et al. (2002) and Cheng et al. (2010). A more in-depth investigation on the interslice force function and the basic problems in LEM is hence necessary and this will be carried out in this study.

Strength Reduction Method (SRM), which is considered as an effective alternative to LEM, is becoming popular in recent decades. The concept of SRM is to modify the material properties and apply body forces due to the self weight and applied loadings to render the slope to the ultimate limit state. Such approach is also well accepted by engineers and researchers, and SRM is now available in some commercial geotechnical programs. Though SRM requires lengthy modeling and computational time compared with LEM, the factor of safety of a slope can be obtained with few assumptions (the main assumption is the flow rule), and the critical failure surface is automatically generated in SRM without any search. Cheng et al. (2007) have tested many commercial SRM programs and have pointed out that every commercial program may come across some technical problems. The reasons behind these problems are related to the difficulties in defining the ultimate limit state for a complicated system and the solution of the nonlinear system (and the corresponding redistribution of unbalanced force) where the Hessian of the system matrix approaches zero near to the ultimate limit state.

At present, there are only limited applications of the Distinct Element Method (DEM) for slope stability problem, and DEM is more suitable for qualitative instead of quantitative assessment of the stability of slope. The movement and growth after slope failure has launched is also important in many cases. Continuum based LEM or SRM are not capable to capture the post-failure mechanism, and this case should be analyzed by DEM. There is virtually no application of DEM to consider the important action of soil nail and the effect of seepage at present, and there are many outstanding works to be considered in this respect. This problem will be assessed by the use of two-dimensional particle flow program PFC in the present study.

Although slope stability analysis has been well considered by many researchers in the past, there are still several major outstanding items which are worth considering. Since the interslice force function proposed by Morgenstern and Price (1965) cannot be determined within the classical context, an arbitrary value of 1.0 is commonly used by the engineers (commonly known as the Spencer's method). The validity of this assumption has been questioned by many engineers in Hong Kong (and other countries). This is an important outstanding issue which will be considered in this study by LEM and SRM.

The general interslice force function which is an interesting and pioneer work is established and studied in the present work.

For the classical stability analysis methods, a single factor of safety is assumed and failure is defined with respect to a failure mechanism (apply to both LEM and SRM). This condition applies to the complete failure condition but should be not realistic for normal cases where the slope is still stable. In real case, progressive failure is however commonly found, and this is particularly important when slope failure is induced by rainfall. Some efforts have been taken to study the failure mechanism with the concept of variable factor of safety (Chugh, 1986; Sarma and Tan, 2006), but these methods require assumptions which are actually questionable. To assess the progressive failure mode, a variable factor of safety LEM method is proposed in this study. This method can be considered as an equivalent lower bound method, and an improved optimization algorithm is proposed for the solution of this problem in this study. This new formulation is based on an equivalent variational principle and is much stronger in the foundation as compared with all the existing variable factor of safety formulations.

Unlike idealized numerical modeling, most of the slope is three-dimensional in nature. Based on the investigation of 2D internal force function, 3D internal force distribution is also studied in form of intercolumn force function and thrust line. Besides, the effect of the curvature of slope will also be considered. The beneficial action of soil nail under the effect of curvature as another outstanding problem will also be studied in the present work.

1.2 Objectives

This study will consider various aspects (which are not well considered in the past) about slope stability problems in greater depth which include:

1. The interslice force function for two-dimensional slope will be evaluated and studied in details by LEM and SRM
2. A variable factor of safety approach by the use of modern optimization algorithms will be proposed for LEM, and the concept of progressive failure can be considered by the LEM which is not possible for all the previous formulations.
3. To investigate the progressive failure of slope and the post-failure conditions in more details, DEM based particle flow analysis for slope with soil nail and water seepage effect will be considered.
4. Three-dimensional analysis on the stability of slope to assess the effect of curvature and soil nail on the stability of slopes. Three-dimensional intercolumn force function which is an outstanding item at present will be determined in the present study.

1.3 Organization of thesis

In **Chapter 2**, the advantages and limitations of different theories and methods for slope stability analysis will be discussed, and this chapter will concentrate on the classical limit equilibrium methods and strength reduction methods.

Chapter 3 aims to establish the computational algorithm required for upper bound analysis of complicated geotechnical problems using the LEM. Two new global optimization algorithms have been proposed with illustration, and these methods will be used for the variable factor of safety limit equilibrium method required in Chapter 4.

Chapter 4 is devoted to the progressive failure of slope under simple and also complex conditions by DEM. This analysis gives clearer insight about the development of failure, microcosmic failure mechanism and the post-failure mechanism for slope.

Chapter 5 will focus on the investigation of the interslice force function by both the limit equilibrium method and strength reduction method. Besides that, the variable factor of safety concept using new optimization algorithms will be proposed for the study of progressive failure using the LEM.

Chapter 6 is about three dimensional slope failure which will be particularly useful for many highway slopes where curvature play an important effect on the stability of slopes. Three-dimensional intercolumn force function which is an outstanding item at present will be determined in the present study.

Chapter 7 will be the overall discussion and conclusion of the whole study with recommendations.

CHAPTER 2 Literature Review

2.1 Analysis methods of slope stability problems

Slope stability problems have attracted considerable attention from many researchers and engineers, from the past till present. Even though this problem has been studied in great details in the past, there are still many new methods coming up for slope stability analysis at present. In general, slope stability analysis methods can be classified as: limit equilibrium method, finite element / finite difference (strength reduction) method, limit analysis method, variational principle method and distinct element method. Limit equilibrium method (LEM) has the advantages of efficiency and the ease to determine the factor of safety, so it is still favoured by most of the engineers in routine analysis and design. LEM however requires assumptions on the distributions of the internal forces and location of the critical failure surface which can be critical and difficult for some complicated cases. Strength reduction methods (SRM) which is a stress field analysis usually does not suffer from convergence problem, and the limitations of LEM do not apply to SRM in general. SRM however requires more time in setting up the problem and solution of the problem, and SRM needs the assumption on flow rule which is not easily defined. In particular, it is very difficult to define nonuniform flow rule in a solution domain, and a single dilation angle (usually nonassociative) is assigned for an arbitrary problem. LEM and SRM methods are continuum based method which is not suitable if the post-failure mechanism has to be assessed, and distinct element method (DEM) which is discontinuity based method will be more suitable for this case. In literature, there are applications of limit analysis method and variational approach in slope stability analysis, but these two methods are difficult to be used for real complicated problems and will not be discussed in details in the present work.

2.1.1 Limit equilibrium method

The limit equilibrium method (LEM) is well known to be a statically indeterminate problem, and method of slices based on the LEM is commonly used by engineers for assessing the factor of safety of slopes. To determine the factor of safety, assumptions on the distributions of internal forces (or thrust line) are required.

Two of most famous LEM methods in the early development based on classical method of circular slip surface are Bishop's Method and Janbu's Method. Bishop (1955) assumed the interslice force is horizontal and determined the factor of safety by employing overall moment equilibrium. Janbu's method (1975) also prescribed only horizontal interslice force (thrust line) but overall force equilibrium was considered.

Morgenstern and Price (1965) adopted an assumption that the relation between the interslice normal and shear force could be specified to make the stability problem statically determinate and by the assumption, both force and moment equilibrium can be satisfied. In this method, the relation between interslice normal and shear force can be described as

$$X = \lambda f(x)E \text{ or } \frac{X}{E} = \lambda f(x)$$

in which X is the vertical component of the interslice force along the interslice surface; E is the normal component; $\lambda f(x)$ is the inclination of interslice force and λ can be determined by the condition that both force and moment equilibrium are satisfied when a given f(x) is prescribed by the engineers.

Later, Spencer (1967) indicated that the interslice forces could be assumed to be parallel to obtain the factor of safety. $f(x)$ is hence actually specified to be 1, and $\lambda f(x)$ is constant in the Spencer's method. Spencer's method is essentially a specific case of Morgenstern-Price's Method. Some researchers have also made different efforts on the investigation of interslice force function. Chen and Morgenstern (1983) have proposed that the interslice force relations for the first and last slices should be based on the Mohr-circle consideration. Fan, Fredlund and Wilson (1986) have proposed a function similar to the error function which is derived from an elastic finite element stress analysis. The validity of this function should actually be questioned as the stress state for slope stability analysis should be the ultimate limit state instead of the elastic stress state. Liang, Zhao and Vitton (1997) adopted the hypothesis of least resistance which stated that among all the forces satisfying the geometrical boundary conditions of a system, the smallest interslice force derived from local moment equilibrium of a slice will be the required force. This method will eliminate the requirement for f(x) at the expense that the hypothesis is not necessarily the true phenomenon. The moment equilibrium of the last slice is also not considered in this formulation, and this formulation is very similar to the original Janbu's rigorous method (1973) and can be modified from the Janbu's rigorous method (1973) by varying the thrust line until the smallest interslice force is obtained. Convergence is also a problem in the real application of this method so that this method appears to be never used in practice.

For "rigorous" methods, "failure to converge" is well known among many engineers, in particular, for complicated problems with heavy external loads or soil reinforcement.

Cheng et al. (2008b) have carried out a detailed study on the convergence problem in stability analysis and have concluded that there are two reasons for failure to converge with the rigorous methods. Firstly, the iteration method that is commonly used to determine the factor of safety may fail to converge because the interslice shear force is assumed to be zero in the first step of the iterative analysis. Cheng (2003) has developed the double QR method, which can evaluate the factor of safety and internal forces directly from a Hessenberg matrix. Based on this method, failure to converge in stability calculations due to the first reason can be eliminated. There are however some cases for which the double QR method determines that a physically acceptable answer does not exist for a given f(x), which means that no meaningful factor of safety will be available unless f(x) can be varied. Actually, some engineers have questioned the meaning of "no factor of safety available" for a given failure surface, as such a concept does not appear in structural engineering. So far, there is little previous study on this type of failure to converge, and no rigorous method can guarantee convergence for the general case. Since the critical failure surface may not necessarily converge according to the existing "rigorous" methods of analysis (Cheng et al. 2008b), there is always a chance that the critical failure surface may be missed during optimization analysis. It is also interesting to note that it has never been proved that a slip surface that fails to converge in stability analysis is not a critical slip surface, but all commercial programs will simply neglect those slip surfaces which fail to converge. On the other hand, Cheng et al. (2010) have proved that the critical slip surface may fail to converge using the classical rigorous method. Although this problem may not be critical in general, a failure surface with no factor of safety is still physically surprising. A system without factor of safety is not real and is just a human deficiency in making the wrong assumption, and this situation never appears in structural engineering or other similar disciplines. Factor of safety always exist for a problem, but it is possible that we are not able to determine it simply because of the use of wrong assumption, and this is supported by the study by Cheng et al. (2008b) that many smooth slip surfaces can fail to converge using the popular Spencer's analysis.

For the LEM, one of the basic assumptions common to all of the traditional methods is a single factor of safety for the entire solution domain. Without this assumption, the slope stability problem will be statically indeterminate unless additional assumptions are used. The actual failure of a slope is however usually a progressive phenomenon. Chugh (1986) presented a procedure for determining a varying factor of safety along the failure surface within the framework of the LEM. Chugh (1986) predefined a characteristic shape for the variation of the local factor of safety along a failure surface, and this idea actually follows the idea of the inter-slice shear force function in the Morgenstern-Price's method (1965). The suitability of this varying factor of safety distribution function is however questionable, and there is no simple way to define this function for a general problem, as the local factor of safety should be mainly controlled by the local soil properties, topography and shape of failure surface. Sarma and Tan (2006) have recently proposed a new formulation with varying factor of safety based on the critical acceleration concept. No factor of safety distribution function is required in this formulation, and the varying factor of safety can be approximately viewed as an indication of the progressive failure mechanism of the slope. The problem to this method is that the energy balance equation based on the limit analysis is used across the interface between adjacent blocks which is an assumption without proof. Lam et al. (1987) proposed a limit equilibrium method for the study of the progressive failure in slope under long-term condition. His main idea involved the recognition of the local failure and the operation of the post-peak strength. This concept is one of the progressive failure phenomena which applies when the deformation is very large and there is a major reduction in the strength of soil, but this approach is not easy to implement and cannot be applied to the general progressive failure phenomenon. The formulations by Sarma and Tan (2006) or Chugh (1986) are not satisfactory but are easy to implement with an estimation of the progressive failure except that they cannot accept the post-peak strength in the analysis.

2.1.2 Strength reduction method

The strength reduction method (SRM) is first used in 2D slope stability analysis by Zienkiewicz et al. (1975). The concept of SRM analysis is to reduce the strength parameters (cohesion strength c' and frictional strength tan ϕ ' for example) by the factor of safety (larger than 1.0 in concept) in an implicit form while the body forces due to weight of soil and other external loads are applied until the system cannot maintain a stable condition. Such instable condition is usually indicated by (1) fail to converge in static equilibrium; (2) thorough plastic zone from toe to crest of slope; (3) large strain or strain increment and displacement. This procedure can determine the safety factor within a single framework for both two and three dimensional slopes, and it is implemented in some commercial geotechnical programs for engineering uses. The advantages of the SRM are: (1) the critical failure surface is found automatically from the application of gravity loads and/or the reduction of shear strength; (2) it requires no assumption on the interslice shear force distribution; and (3) it is applicable to many complex conditions and can give information such as stresses, movements, and pore water pressures. On the other hand, SRM suffers from long solution time required to develop the computer model and to perform the analysis, and SRM relies on the assumption of flow rule which is actually unknown in general.

In strength reduction analysis, the convergence criterion is the most critical factor for the assessment of the factor of safety. Different criteria for the ultimate state have been used in practice according to the choice of the program: (1) maximum number of iteration is reached; (2) formation of a continuous failure mechanism; (3) sudden change in the displacement for some selected points. For simple problems, there are no major differences between these criteria, while greater differences may be obtained by different convergence criteria for some special cases.

Recently, SRM appears to be a popular alternative to the LEM, but Cheng et al. (2007, 2008) and Wei et al. (2008) have carried out extensive SRM studies and have found that there are also many practical limitations to the SRM. Cheng et al. (2007, 2008) and Wei et al. (2008) concluded that both LEM and SRM are useful to slope stability analysis, and each method cannot totally replace the other method in practical use.

2.1.3 Distinct element method

Distinct element analysis (DEM) discretizes the domain into discrete elements. The elements can be blocks (DDA by Shi, 1988) or particles (Cundall and Strack 1979). Program PFC models the movement and interaction of particles by the distinct element method, as described by Cundall and Strack (1979). The major application of distinct element method is to assess the behaviour of granular materials. The continuous deformations take account of 1) sliding and rotation of particles as rigid bodies and 2) elasticity of individual particles. Although the particles can be assumed as rigid elements, the behavior of the contacts is characterized using soft contact approach in which finite normal stiffness is taken to represent the stiffness which exists at the contact surface. The soft contact approach allows small overlapping area of particles which can be easily observed. Stress on particle is then measured from this overlapping through the particle interface.

While FEM and FDM are applied for investigation of the interslice force function and thrust line in Chapter 5, DEM will be adopted for the analysis of the slope failure mechanism in Chapter 4.

2.1.4 Limit analysis method

The limit analysis method includes the upper bound approach and the lower bound approach, and the general analysis process is the construction of a statically admissible stress field for the lower bound analysis or a kinematically admissible velocity field for an upper bound analysis. The lower bound approach has been used in 2D slope stability analysis by Chen (1975), Bottero et al. (1980), Zhang (1999), Kim et al. (2002), and Loukidis et al. (2003), while the application of this approach in 3D slope stability analysis has been conducted by Lyamin (1999), Lyamin and Sloan (2002a). Stress fields employed in the lower bound solutions are usually assumed without an apparent relation to the actual stress fields, and it is usually not easy to obtain the lower bound solutions for a practical slope problem. Therefore, the lower bound approach is seldom adopted as compared with the upper bound approach in slope stability analysis. Cheng et al. (2010) however proposed an equivalent lower bound approach by generalized interslice force function according to Pan extremum principles (1980).

The upper bound approach was first used by Drucker and Prager (1952) to determine the critical height of a slope. Subsequently, Chen and Giger (1971), Chen (1975), Karal (1977a, 1977b) and Izbicki (1981) also applied and extended the upper bound approaches in 2D slope analysis. Donald and Chen (1997) presented an upper bound method on the basis of a multi-wedge failure mechanism, and the sliding body was divided into a small number of discrete blocks. Some researchers have tried to use the finite element method to obtain the upper bound solution for structures and geotechnical problems (Anderheggen and Knopfel, 1972; Bottero et al., 1980; Sloan, 1988, 1989; Sloan and Kleeman, 1995; Kim et al., 2002; Loukidis et al., 2003). Chen (2004) and Chen et al. (2003b, 2004, 2005a) used rigid finite element method to establish a new upper bound formulation which renders the limit analysis of slope stability suitable to be conducted for different complex conditions.

2.1.5 Variational calculus

Baker and Garber (1978), Baker (1980) and Revilla and Castillo (1977) applied the calculus of variation to determine the factor of safety of a 2D slope. This approach was subsequently employed by Jong (1980) for vertical cut analysis in cohesive frictionless soil. Baker (2003) later has incorporated some additional physical restrictions into the basic limiting equilibrium framework so as to guarantee that the problem has a well-defined minimum solution. Although the variational principle requires very few assumptions with no convergence problem during the solution, it is difficult to be adopted when the geometry or the ground/loading condition are complicated. Cheng et al. (2010) have developed the numerical algorithm based on the Pan's extremum principle, and the formulation which relies on the use of modern heuristic optimization method can be viewed as an equivalent form of the variational method in a discretized form but is applicable for complicated real problem.

2.2 Optimization algorithms applied for slope stability problems

Many geotechnical problems are governed by an optimization / extremum process. For example, the location of the critical failure surface is a typical minimization process while the lower bound principle is a typical optimization process. There are many mathematical techniques available for optimization analysis. While classical simplex or gradient methods can work for relatively simple problems, they can easily be trapped by a local minimum which may occur for a complicated problem. Currently, many researchers are turning to the modern global optimization methods which are not limited by the presence of a local minimum during the optimization process.

Most of the modern global optimization algorithms are based on certain characteristics and behavior of biological, molecular, swarm of insects, and neurobiological systems. The *genetic algorithms* are based on the principles of natural genetics and natural selection; the s*imulated annealing method* is based on the simulation of thermal annealing of critically heated solids; the *particle swarm optimization* is based on the behavior of a colony of living things, such as a swarm of insects or a flock of birds; the *harmony search* algorithm is conceptually based on the musical process of searching for a perfect state of harmony; the *tabu search* is the search strategy that uses memory and search history as its integrated component; the *ant colony optimization* is based on the cooperative behavior of real ant colonies, which are able to find the shortest path from their nest to a food source.

Heuristic optimization algorithms are more suitable for complicated geotechnical problems where the global minimum is required but is difficult to be determined by the classical methods. More detailed discussion about the modern optimization methods will be discussed in Chapter 3.

2.3 Three-dimensional slope stability analysis and internal force function

For simplicity, most of the slope stability problems are usually analyzed as two-dimensional (2D) problem while slope failure is always three-dimensional (3D) in nature. Many researchers have considered on 3D slope study and various 3D slope stability methods are proposed basically by the extensions of the corresponding 2D analysis.

Cavounidis (1987) has demonstrated that the factor of safety of a 3D slope should normally be greater than that for a corresponding 2D slope. The common 3D methods include those by Baligh and Azzouz (1975), Hovland (1977), Chen and Chameau (1982), Azzouz and Baligh (1983), Hungr (1987), Gens et al. (1988), Zhang (1988), Ugai (1988), Huang and Tsai (2000), Huang et al. (2002), Chang (2002), Chen et al. (2003a). The assumption which is adopted in most of these methods is that the failure mass is symmetrical about a known sliding direction, so asymmetric slope failure cannot be modeled directly by the classical 3D methods. Jiang and Yamagami (1999) proposed the axis rotation concept and the minimum factor of safety to determine the sliding direction, but this approach is time consuming in the geometry calculation. Huang and Tsai (2000) proposed a 3D asymmetrical slope stability analysis method where the sliding direction can be obtained with the direct determination of the factor of safety, but it is unreasonable that the sliding direction will be different for different soil columns. Lam and Fredlund (1993) in their development of a general LEM method have found that dominating intercolumn force functions are applied for normal and vertical shear forces on the xy- and yz- plane (xz- and yz- plane in this study) respectively. Cheng and Yip (2007) have developed a new asymmetric 3D analysis model under which there is only one sliding direction for the whole sliding mass, and this simplification has overcome the convergence problem under transverse load in the formulation by Huang and Tsai (2000) and Huang et al. (2002).

Giger and Krizek (1975, 1976) applied the upper bound approach in 3D slope stability analysis, where the stability of a vertical cut with a variable corner angle was analyzed. Michalowski (1989) proposed an upper bound formulation for 3D analysis of locally loaded slopes. Farzaneh and Askari (2003) later improved and extended this method to non-homogeneous 3D slopes. Chen et al. (2001a, 2001b) proposed another 3D upper bound approach which is extended from the corresponding 2D approaches by Donald and Chen (1997). In most of the 3D limit analysis methods, the column techniques which are usually used in 3D LEM are employed to construct the kinematically admissible velocity field. The finite element method has also been also used by some researchers (Lyamin and Sloan 2002b, Chen et al. 2005b) to obtain 3D upper bound solution.

The variational method has been employed in 3D slope stability analysis by Leshchinsky et al. (1985), Ugai (1985), Leshchinsky and Baker (1986), Baker and Leshchinsky (1987), and Leshchinsky and Huang (1992). By such approaches, the minimum factor of safety and the associated failure surface can be obtained at the same time and the assumptions on the internal force distribution are not required. However, these methods are limited to homogeneous and symmetrical problems, so further study is required on the application in practical problems with complicated geometric and loading conditions.

CHAPTER 3 Optimization Algorithms and Applications in Geotechnical Engineering

3.1 Introduction

Optimization can be defined as the process of finding the conditions that give the maximum or minimum value of a function (Rao, 2009). In general, the optimum solution can be the maximum or minimum within a given solution domain, and can be classified as the global or local minimum.

In the location of critical slip surface in slope stability analysis, the current trend is the adoption of the modern heuristic optimization algorithm instead of the gradient type optimization algorithms because:

1. the objective function of the factor of safety f can be a non-continuous function and is usually non-smooth and non-convex so that gradient type optimization methods where continuity is required may not work (Cheng et al. 2008a). Most of gradient type methods rely on a creditable initial trial, otherwise, the results would be trapped into a local minima which normally exist in geotechnical engineering problems. Figure 3.1 shows the typical domain with multiple local minima. If the initial trial starts near point C, the optimization procedure will easily find this local minimum but thereafter be trapped at C. The global minimum point E will then not be obtained.
2. Some researchers set a series of sub-range for the whole search domain and multiple initials are established to avoid the influence of local minimum. Such effort is time-consuming and cannot overcome the problems of discontinuity. When the number of

control variables is great, this method is still not satisfactory.

3. Gradient type algorithms find the minimum by the condition of $\nabla f=0$. If the global minimum lies at the edge of search domain like point B in Figure 3.1 where gradient $\nabla f\neq 0$, the gradient type algorithm will fail.

In recent years, some optimization methods that are conceptually different from the traditional mathematical programming techniques have been developed. These methods are labeled as modern or nontraditional methods of optimization. Most of these methods are emerging as popular methods for the solution of complex engineering problems, and these methods aims at the global optimum solution without the derivatives and the need for a continuous function or a good initial trial. The increasing number of published papers and applications in this area shows the growing attention from the geotechnical engineers and researchers for the efficiency and robustness of the modern optimization methods. This trend can also be seen from the optimization algorithms used in the commercial slope stability programs where the traditional optimization methods are now replaced with the use of modern heuristic optimization algorithms.

3.2 Popular global optimization algorithms and comparison

Most of the modern global optimization algorithms are based on certain characteristics and behavior of biological, molecular, swarm of insects, and neurobiological systems such as the Genetic Algorithm (GA), Simulated Annealing method (SA), Particle Swarm Optimization method (PSO), Harmony Search method (HS), Tabu Search (TS) and Ant Colony Optimization method (ACO). These methods are useful for both upper and lower bound analysis and will be briefly discussed in this section.

3.2.1 Genetic algorithm

Although genetic algorithm (GA) was first presented systematically by Holland (1975), the basic ideas of analysis and design based on the concepts of biological evolution can be found in the work by Rechenberg (1965). Philosophically, GA is based on Darwin's theory of survival of the fittest. The basic elements of natural genetics - reproduction, crossover, and mutation - are used in the genetic search procedure.

In GA, the design variables are represented as strings of binary numbers, 0 and 1. For example, if a design variable x_i is denoted by a string of length four (or a four-bit string) as 0 1 0 1, its integer (decimal equivalent) value will be (1) 2^0 + (0) 2^1 + (1) 2^2 + (0) 2^3 =1+0+4+0=5. If each design variable x_i , i = 1, 2, . . . , n is coded in a string of length q, a design vector is represented using a string of total length nq. In general, if a binary number is given by $b_{q-1} \cdots b_2 b_1 b_0$, where b_k = 0 or 1, k = 0, 1, 2, . . . , q-1, then its equivalent decimal number y (integer) is given by

$$y = \sum_{k=0}^{q-1} 2^k b_k \tag{3.1}$$

This indicates that a continuous design variable x can only be represented by a set of discrete values if binary representation is used. If a variable x (whose bounds are given by $x^{(l)}$ and $x^{(u)}$) is represented by a string of q binary numbers, as shown in Eq. (3.1), its decimal value can be computed as

$$x = x^{(l)} + \frac{x^{(u)} - x^{(l)}}{2^q - 1} \sum_{k=0}^{q-1} 2^k b_k \tag{3.2}$$

Thus, if a continuous variable is to be represented with high accuracy, we need to use a large value of q in its binary representation. In fact, the number of binary digits needed (q) to represent a continuous variable in steps (accuracy) of Δx can be computed from the relation

$$2^{q} \geq \frac{x^{(u)} - x^{(l)}}{\Delta x} + 1 \tag{3.3}$$

For example, if a continuous variable x with bounds 1 and 5 is to be represented with an accuracy of 0.01, we need to use a binary representation with q digits where

$$2^{q} \geq \frac{5-1}{0.01} + 1 = 401 \quad \text{or} \quad q = 9 \tag{3.4}$$

Eq. (3.4) shows why GA is naturally suited for solving discrete optimization problems.

The computational procedure involved in maximizing the fitness function $G(x_1, x_2, x_3, \ldots, x_n)$ in the GA can be described by the following steps:

1. Choose a suitable string length $l = nq$ to represent the n design variables of the design vector **X**. Assume suitable values for the following parameters: population size m, crossover probability p_c, mutation probability p_m, permissible value of standard deviation of fitness values of the population $(s_f)_{\max}$ to use as a convergence criterion, and maximum number of generations ($i_{\max}$) to be used as the second convergence criterion.
2. Generate a random population of size m, each consisting of a string of length $l = nq$. Evaluate the fitness values G_i , $i = 1, 2, \ldots, m$, of the m strings.
3. Carry out the reproduction process.
4. Carry out the crossover operation using the crossover probability p_c.
5. Carry out the mutation operation using the mutation probability p_m to find the new generation of m strings.
6. Evaluate the fitness values G_i, $i = 1, 2, \ldots, m$ of the m strings of the new population. Find the standard deviation of the m fitness values.
7. Test for the convergence of the algorithm or process. If $s_f \leq (s_f)_{\max}$, the convergence criterion is satisfied and hence the process may be stopped. Otherwise, go to step 8.

8. Test for the generation number. If $i \geq i_{max}$, the computations have been performed for the maximum permissible number of generations and hence the process may be stopped. Otherwise, set the generation number as $i = i + 1$ and go to step 3.

GA differs from the traditional methods of optimization in the following respects (Rao 2009):

1. A population of points (trial design vectors) is used to start the procedure instead of a single design point. If the number of design variables is n, usually the size of the population is taken as $2n$ to $4n$. Since several points are used as candidate solutions, GA is less likely to get trapped at a local optimum.
2. GA uses only the values of the objective function while the derivatives are not used.
3. In GA, the design variables are represented as strings of binary variables that correspond to the chromosomes in natural genetics. Thus, the search method is naturally applicable for solving discrete and integer programming problems. For continuous design variables, the string length can be varied to achieve any desired resolution.
4. The objective function value corresponding to a design vector plays the role of fitness in natural genetics.
5. In every new generation, a new set of strings is produced by using randomized parents selection and crossover from the old generation (old set of strings). Although randomized, GA efficiently explores the new combinations with the available knowledge to find a new generation with better fitness or objective function value.

3.2.2 Simulated annealing

Simulated Annealing (SA) pioneered by Kirkpatrick, Gelatt and Vecchi in 1983 mimics the annealing process in material processing when a metal cools and freezes into a crystalline state with minimum energy and larger crystal size so as to reduce the defects in metallic structures. The annealing process involves the careful control of temperature and cooling rate (often called annealing schedule). It has been proved that SA will converge to its global optimality if enough randomness is used in combination with very slow cooling (Yang 2008).

Metaphorically speaking, this is equivalent to dropping some bouncing balls over a landscape, as the balls bounce and loose energy, they will settle down to some local minima. If the balls are allowed to bounce enough times and loose energy slowly enough, some of the balls will eventually fall into the global lowest locations, and hence the global minimum will be reached. The basic idea of SA algorithm is to use random search which not only accepts changes that improve the objective function, but also keeps some changes that are not ideal. In a minimization problem, for example, any better moves or changes that decrease the cost (or the value) of the objective function f will be accepted. However, some changes that increase f will also be accepted with a probability p. This probability p, also called the transition probability, is determined by

$$p = e^{-\delta E / kT} \tag{3.5}$$

where k is the Boltzmann's constant, and T is the temperature for controlling the annealing process. δE is the change of the energy level. This transition probability is based on the Boltzmann distribution in physics. The simplest way to link δE with the change of the objective function δf is to use

$$\delta E = \gamma \delta f \tag{3.6}$$

where γ is a real constant. For simplicity without losing generality, we can use $k = 1$ and $\gamma = 1$. Thus, the probability p simply becomes

$$p(\delta f, T) = e^{-\frac{\delta f}{T}} \tag{3.7}$$

Whether or not we accept a change, we usually use a random number r as a threshold. Thus, if $p > r$ or

$$p = e^{-\frac{\delta f}{T}} > r \tag{3.8}$$

this solution is accepted.

Here, the choice of the right temperature is crucial. The special case $T \to 0$ corresponds to the gradient based method because only better solutions are accepted, and the system is essentially ascending or descending along a hill. For a given change δf, if T is too high ($T \to \infty$), then $p \to 1$, which means almost all changes will be accepted; the system is at a high energy state on the topological landscape, and the minima are not easily reached. On the other hand, if T is too low ($T \to 0$), the system may be trapped in a local minimum (not necessarily the global minimum), and there is not enough energy for the system to jump out of the local minimum to explore other potential global minima.

Another important issue in SA is how to control the annealing or cooling process in order to ensure the system cools down gradually from a higher temperature to ultimately freeze to a global minimum state. There are many ways of controlling the cooling rate or the decrease of the temperature. Two commonly used annealing schedules are: linear and geometric cooling.

For a linear cooling process, we have $T = T_0 - \beta t$ or $T \to T - \delta T$, where T_0 is the initial temperature, and t is the pseudo time for iterations. β is the cooling rate and should be chosen in such way that $T \to 0$ when $t \to t_f$ (maximum number of iterations). This usually renders $\beta = T_0/t_f$. The geometric cooling essentially decreases the temperature by a cooling factor $0 < \alpha < 1$ so that T is replaced by αT or

$$T(t) = T_0 \alpha^t,\ t = 1, 2, ..., t_f \tag{3.9}$$

Since $0 < \alpha < 1$, $T \rightarrow 0$ when $t \rightarrow \infty$ in Eq.(3.9), thus there is no need to specify the maximum number of iterations t_f. The cooling process should be slow enough to allow the system to remain stable. In practice, α = 0.7~0.9 is commonly used. In the case of a given temperature, multiple evaluations of the objective function are required. If too few evaluations are considered, the system will be at a risk of being unstable and subsequently fails to converge to the global optimum. On the other hand, if there are too many evaluations, it is time-consuming and the system will usually converge too slowly as the number of iterations to achieve stability might be exponential to the problem size. Therefore, there is a balance of the number of evaluations and solution quality. Either many evaluations at a few temperature levels or few evaluations at many temperature levels can be adopted.

Some of the features of SA method are as follows (Yang, 2008):

1. The quality of the final solution is not affected by the initial trials, except that the computational effort may increase with worse starting designs.
2. Because of the discrete nature of the function and constraint evaluations, the convergence or transition characteristics are not affected by the continuity or differentiability of the functions.
3. The convergence is also not influenced by the convexity status of the feasible space.
4. The design variables are not required to be positive.
5. The method can be used to solve mixed-integer, discrete, or continuous problems.

3.2.3 Particle swarm optimization

Particle swarm optimization (PSO) was developed by Kennedy and Eberhart in 1995, based on the swarm behaviour such as fish and bird schooling in nature. Though PSO has many similarities with GA, it is much simpler because it does not use mutation/crossover operators or pheromone (Yang 2008). Instead, it uses the real-number randomness and the global communication among the swarm particles. In this sense, it is also easier to implement as there is no encoding or decoding of the parameters into binary strings as those in GA. This algorithm searches a space of an objective function by adjusting the trajectories of individual agents, called particles, as the piecewise path formed by positional vectors in a quasi-stochastic manner. The particle movement has two major components: a stochastic component and a deterministic component. The particle is attracted toward the position of the current global best while at the same time it has a tendency to move randomly. When a particle finds a location that is better than any previously found locations, it updates it as the new current best for particle *i*. The aim is to find the global best among all the current best until the objective no longer improves or beyond a certain number of iterations.

Consider an unconstrained maximization problem:

$$\text{Maximize } f(\mathbf{X})$$
$$\text{with } \mathbf{X}^{(l)} \leq \mathbf{X} \leq \mathbf{X}^{(u)} \tag{3.10}$$

where $\mathbf{X}^{(l)}$ and $\mathbf{X}^{(u)}$ denote the lower and upper bounds on $\mathbf{X}$, respectively. The PSO procedure can be implemented through the following steps:

1. Assume the size of the swarm (number of particles) is N. If a swarm size is too small, it is likely that it will take longer time to find a solution, or in some cases, we may not be able to find a solution at all. Usually a size of 20 to 30 particles is assumed for the swarm

as a compromise.

2. Generate the initial population of $\mathbf{X}$ in the range $\mathbf{X}^{(l)}$ and $\mathbf{X}^{(u)}$ randomly as $\mathbf{X}_1, \mathbf{X}_2, \ldots, \mathbf{X}_N$. Hereafter, for convenience, the particle (position of) j and its velocity in iteration i are denoted as $\mathbf{X}_j^{(i)}$ and $\mathbf{V}_j^{(i)}$, respectively. Thus the particles generated initially are denoted $\mathbf{X}_1(0)$, $\mathbf{X}_2(0)$, . . . ,$\mathbf{X}_N(0)$. The vectors $\mathbf{X}_j$ (0) (j = 1, 2, . . . ,N) are called particles or vectors of coordinates of particles (similar to chromosomes in GA). Evaluate the objective function values corresponding to the particles as $f[\mathbf{X}_1(0)]$, $f[\mathbf{X}_2(0)]$,…, $f[\mathbf{X}_N(0)]$.

3. Find the velocities of particles. All particles will be moving to the optimal point with a velocity. Initially, all particle velocities are assumed to be zero. Set the iteration number as $i = 1$.

4. In the ith iteration, find the following two important parameters used by a typical particle j:

(a) The historical best value of $\mathbf{X}_j(i)$ (coordinates of jth particle in the current iteration i), $\mathbf{P}_i$, with the highest value of the objective function, $f[\mathbf{X}_j(i)]$, encountered by particle j in all the previous iterations. The historical best value of $\mathbf{X}_j(i)$ (coordinates of all particles up to that iteration), $\mathbf{P}_g$, with the highest value of the objective function $f[\mathbf{X}_j(i)]$, encountered in all the previous iterations by any of the N particles.

(b) Find the velocity of particle j in the ith iteration as follows:

$$\mathbf{V}_j(i) = \mathbf{V}_j(i-1) + c_1 r_1[\mathbf{P}_i - \mathbf{X}_j(i-1)] + c_2 r_2[\mathbf{P}_g - \mathbf{X}_j(i-1)];$$

$$j = 1, 2, \ldots, N \tag{3.11}$$

where c_1 and c_2 are the cognitive (individual) and social (group) learning rates, respectively, and r_1 and r_2 are uniformly distributed random numbers in the range [0,1]. The parameters c_1 and c_2 denote the relative importance of the memory (position) of the particle itself to the memory (position) of the swarm. The values of

c_1 and c_2 are usually assumed to be 2 so that c_1r_1 and c_2r_2 ensure that the particles would overfly the target about half the time.

(c) Find the position or coordinate of the jth particle in ith iteration as

$$\mathbf{X}_j(i) = \mathbf{X}_j(i-1) + \mathbf{V}_j(i);\ j = 1, 2, \ldots, N \tag{3.12}$$

where a time step of unity is assumed in the velocity term in Eq.(3.12). Evaluate the objective function values corresponding to the particles as $f[\mathbf{X}_1(i)]$, $F[\mathbf{X}_2(i)], \ldots$, $F[\mathbf{X}_N(i)]$.

5. Check the convergence of the current solution. If the positions of all particles converge to the same set of values, the method is assumed to have converged. If the convergence criterion is not satisfied, step 4 is repeated by updating the iteration number as $i= i+1$, and by computing the new values of $\mathbf{P}_i$ and $\mathbf{P}_g$. The iterative process is continued until all particles converge to the same optimum solution.

It is found that usually the particle velocities build up too fast and the maximum of the objective function is skipped (Rao 2009). Hence an inertia term, θ, is added to reduce the velocity. Usually, the value of θ is assumed to vary linearly from 0.9 to 0.4 as the iterative process progresses. The velocity of the jth particle, with the inertia term, is assumed as

$$\mathbf{V}_j(i) = \theta\mathbf{V}_j(i-1) + c_1r_1[\mathbf{P}_i - \mathbf{X}_j(i-1)] + c_2r_2[\mathbf{P}_g - \mathbf{X}_j(i-1)];$$

$$j=1, 2, \ldots, N \tag{3.13}$$

The inertia weight coefficient θ was originally introduced by Shi and Eberhart in 1999 to dampen the velocities over time (or iterations), enabling the swarm to converge more accurately and efficiently compared to the original PSO algorithm with Eq.(3.11). Eq.(3.13) denotes an adapting velocity formulation, which improves its fine tuning ability in solution search. Eq.(3.13) shows that a larger value of θ promotes global exploration and a smaller value promotes a local search. To achieve a balance between global and local exploration to speed up convergence to the true optimum, an inertia weight whose value decreases linearly with the iteration number has been used:

$$\theta(i) = \theta_{max} - \left(\frac{\theta_{max} - \theta_{min}}{i_{max}} \right) \cdot i \tag{3.14}$$

where θ_{max} and θ_{min} are the initial and final values of the inertia weight, respectively, and i_{max} is the maximum number of iterations used in PSO.

3.2.4 Harmony search

Geem et al. (2001) and Lee and Geem (2005) developed a harmony search (HS) meta-heuristic algorithm which is conceptually based on the musical process of searching for a perfect state of harmony. Harmony in music is analogous to the optimization solution vector, and the musician's improvisations are analogous to local and global search schemes in optimization techniques. The HS algorithm does not require initial values for the decision variables. Furthermore, instead of a gradient search, the HS algorithm uses a stochastic random search which is based on the harmony memory consideration rate *HR* and the pitch adjustment rate *PR* so that the gradient of the objective function is not necessary during the analysis. The HS algorithm is a population-based search method. A harmony memory *HM* of size *M* is used to generate a new harmony which is probably better than the optimum in the current harmony memory. The harmony memory consists of *M* harmonies (slip surfaces) which are usually generated randomly. Consider $HM = \{hm_1 \quad hm_2 \quad ,..., \quad hm_M\}$

$$hm_i = (v_{i1}, v_{i2}, ..., v_{im}) \tag{3.15}$$

where each element of hm_i corresponds to that in vector $\mathbf{V}$ representing certain harmony. Consider the following optimization problem, where M=4, m=2. Suppose that HR=0.9,

PR=0.1.

$$\begin{cases} \min & f(x_1, x_2) = (x_1 - 1)^2 + x_2^{\ 2} \\ s.t. & 0 \le x_1 \le 2 \quad 1 \le x_2 \le 3 \end{cases} \tag{3.16}$$

The structure of *HM* is comprised of four randomly generated harmonies as shown in Table 3.1. The new harmony can be obtained using the harmony search algorithm as follows. A random number in the range [0, 1] is generated, for example 0.6 (<*HR*). One of the values from {1.0, 1.5, 0.5, 1.8} is chosen as the value of x_1 in the new harmony. If the value of x_1 is set to 1.0, another random number 0.95 (>*HR*) and a random value in the range [1, 3] are obtained. Suppose that a number 1.2 is obtained from the range [1,3]; then a coarse new harmony $hm'_n = (1.0, 1.2)$ is generated. Fine tuning of the new harmony is obtained by adjusting the coarse new harmony according to the parameter *PR*. Suppose that two random values in the range [0,1] are generated, say 0.7 and 0.05. Since the former value of 0.7 is greater than *PR*, the value of x_1 in hm_n will remain unchanged. The latter value of 0.05 is less than *PR* and therefore the value of 1.2 should be adjusted; say 1.10 is assigned to the new value of x_2 until the fine new harmony hm_n = (1.0*,* 1.10) is obtained. The objective function of the new harmony is then calculated as 1.21. The objective function value of 1.21 is better than that of the worst harmony hm_4; therefore hm_4 is excluded from the current *HM* and hm_n is included in the *HM.* This completes one iteration loop. The algorithm continues until the termination criterion is satisfied.

The iterative steps of the HS algorithm in the optimization are as follows.

Step 1. Initialize the algorithm parameters *HR*, *PR*, and *M*, and randomly generate *M* harmonies (slip surfaces).

Step 2. Generate a new harmony and evaluate it.

Step 3. Update the *HM*, i.e. if the new harmony is better than the worst harmony in the

HM in terms of factor of safety, the worst harmony is replaced with the new harmony.

Step 4. Repeat steps 2 and 3 until the termination criterion is achieved.

Take the *i*th value of the coarse harmony $h_n^{'}$, $v_{ni}^{'}$, for instance, with its lower bound and upper bounds named herein as $v_{i\min}, v_{i\max}$. A random number r_0 in the range [0,1] is generated. If $r_0 > 0.5$, $v_{ni}^{'}$ is adjusted to v_{ni} using the Eq.(3.17), otherwise, Eq.(3.18) is used to calculate the new value of v_{ni}.

$$v_{ni} = v_{ni}^{'} + \left(v_{i\max} - v_{ni}^{'}\right) \times rand \quad r_0 > 0.5 \tag{3.17}$$

$$v_{ni} = v_{ni}^{'} - \left(v_{ni}^{'} - v_{i\min}\right) \times rand \quad r_0 \leq 0.5 \tag{3.18}$$

where *rand* denotes a random number in the range [0,1], is used to calculate the new value of v_{ni}.

The number of objective function evaluations during the search for the optimum, denoted by *NOF*, can represent the computation time required by the optimization algorithm. The termination criterion is not reported by Geem et al. (2001), and many researchers just specify a fixed number of trials and take the minimum value from the trials as the global minimum. The original formulation is not good in that there is no guideline for the selection of a suitable number of trials and many researchers find this by a trial and error process. It is found that if a very large number of trials are specified, the optimum solution may be found at a relatively early stage and many unnecessary computations will be carried out (Cheng et al. 2008b), and Cheng has proposed the termination criterion for the harmony search algorithm (Cheng et al. 2007).

3.2.5 Tabu search

Tabu search (TS) developed by Fred Glover in 1970s is a search strategy that uses memory and search history as its integrated component. Memory could introduce many degrees of freedom, especially for the adaptive memory use, which makes it almost impossible to use the rigorous theorems-and-proof approach to establish the convergence and efficiency of such algorithms. Therefore, even though TS works well for certain problems, it is difficult to analyze mathematically why it works well. Consequently, Tabu search remains a heuristic approach. TS is an intensive local search algorithm and the use of memory avoids the potential cycling of local solutions so as to increase the search efficiency. The recent tried or visited solutions are recorded and put into a Tabu list and new solutions should avoid those in the Tabu list. The Tabu list is an important concept in Tabu search, and it records the search moves as the recent history, and any new search move should avoid this list of previous moves. This will inevitably save time as previous moves are not repeated. Over a large number of iterations, this Tabu list could save tremendous amount of computing time and thus increase the search efficiency significantly (Yang 2008).

3.2.6 Ant colony optimization

Ant colony optimization (ACO) is based on the cooperative behavior of real ant colonies which find the shortest path from their nest to a food source. The method was developed by Dorigo et al. in the early 1990s. The ACO process can be explained by representing the optimization problem as a multilayered graph, where the number of layers is equal to the number of design variables and the number of nodes in a particular layer is equal to the number of discrete values permitted for the corresponding design variable. Thus each node is associated with a permissible discrete value of a design variable. More particularly, let the colony consist of *N* ants. The ants start at the home node, travel through the various layers from the first layer to the last or final layer, and end at the destination node in each cycle or iteration. Each ant can select only one node in each layer in accordance with the state transition rule. The nodes selected along the path visited by an ant represent a candidate solution. Once the path is completed, the ant deposits some pheromone on the path based on the local updating rule. When all the ants complete their paths, the pheromones on the globally best path are updated using the global updating rule. In the beginning of the optimization process (i.e., in iteration 1), all the edges or rays are initialized with an equal amount of pheromone. So, in iteration 1, all the ants start from the home node and end at the destination node by randomly selecting a node in each layer. The optimization process is terminated if either the prescribed maximum number of iterations is reached or no better solution is found in a prescribed number of successive cycles or iterations. The values of the design variables denoted by the nodes on the path with the largest amount of pheromone are considered as the components of the optimum solution vector. In general, at the optimum solution, all ants travel along the same best (converged) path (Rao 2009).

3.2.7 Comparisons and discussions on different heuristic algorithms

Many practical optimization design problems are characterized by mixed continuous–discrete variables, and discontinuous and nonconvex design spaces. If standard nonlinear programming techniques are used for this type of problem, they will be inefficient, computationally expensive, and, in most cases, find a relative (local) optimum that is closest to the starting point (Rao 2009). In views of these limitations, the current trend is the adoption of the modern global optimization methods in this type of problem.

The uses of optimization methods in slope stability analysis have been discussed by Cheng (2007). For clarity, the procedures for the optimization algorithms are given in Figures 3.2-3.7. Cheng et al. (2007a) examined the performance of these major heuristic algorithms in geotechnical engineering. It is found that every global optimization method can be tuned to work well if suitable optimization parameters or initial trial are adopted. Since the suitable optimization parameters or the initial trial are difficult to be established for a general problem, the performance of a good optimization method should be relatively insensitive to these factors. The general comments on these heuristic optimization methods are:

(1) For normal and simple problems, practically every method can work well. The HS and the GA are the most efficient method when the number of control variable is less than 20. The TS and the ACO are sometimes extremely efficient in the optimization process, but the efficiency of these two methods fluctuates significantly between different problems and these two methods not recommended to be used.

(2) For normal and simple problems where the number of control variables exceeds 20, the HS and the PSO are the recommended solution as they are more efficient in the solution, and the solution time will not vary significantly between different problems.

(3) For more complicated problems or when the number of control variables is great, the effectiveness and efficiency of the PSO is nearly the best in all of the studied examples.

(4) Thin soft band create great difficulty in the global optimization analysis, and the PSO will be the best method in this case. However, using the domain transformation strategy by Cheng (2007), all the global optimization methods can work well for this case.

(5) For complicated problems, where an appreciable amount of trial failure surfaces will fail to converge, the simulated annealing method and the PSO are the recommended

solutions. In views of the differences in the performance between different global optimization algorithms, a more satisfactory solution is the combined used of two different algorithms. For example, the PSO or the HS can be adopted for normal problems, while the SA can be adopted when the 'failure to convergence' counter is high. Further improvement can be achieved by using the optimized results from a particular optimization method as a good initial trial, and a second optimization method adopts the initial trial from the first optimization algorithm for the second stage of optimization with a reduced solution domain for each control variable.

Heuristic algorithms are approximate and not accurate algorithms. These algorithms usually find a solution close to the best one, and they usually find it fast and easily. Cheng et al. (2008a) have commented that no particular optimization method is superior under all cases, but some methods (ACO and TS) may be less effective for problem where the objective functions are highly discontinuous. Cheng et al. (2007a) adopt a uniform set of parameters for every optimization method for all the problems. In normal most cases, it is found that these global optimization algorithms are relatively insensitive to the use of the optimization parameters.

3.3 Modified harmony search algorithm for optimization problem (MHS)

3.3.1 Modified harmony search algorithm

There are many hydropower projects in China where the ground conditions are complicated with contrasting soil properties between each soil layer. The scale of the problem is also large so that the numbers of control variables become high. The problem is further complicated by the presence of several layers of weak zones which are usually irregular in the geometry. To overcome these difficulties, two global optimization methods are developed in this study.

Cheng et al. (2008b) have found that the original harmony search (OHS) algorithm works well for simple optimization problem with less than 25 control variables. For more complicated problems with a large number of control variables, the OHS algorithm requires a large number of trials before a good solution can be achieved. A new type of harmony search algorithm called the modified harmony search (MHS) algorithm has been developed in the present study to ensure the efficiency in the analysis.

The MHS method differs from the original method in two aspects. The first difference is the probability of each harmony. The better the objective function value of one harmony, the more probable will it be chosen for the generation of a new harmony. A parameter δ ($0 < \delta \leq 1$) is introduced. All the harmonies in *HM* are sorted by ascending order (for minimization problems, and by descending order for the maximization problem), and a probability is assigned to each of them. For instance, $pr(i)$ indicates the probability to choose the *i*th harmony

$$pr(i) = \delta \times (1-\delta)^{i-1} \qquad i=1,2,\ldots,M \tag{3.19}$$

From Eq.(3.19), it can be seen that the larger the value of δ, the more probable that it is the first harmony to be chosen. A new array $ST(i), i = 0,1,2,..,M$ should be used to implement the above procedure of choosing the harmony.

$$ST(i) = \sum_{j=1}^{i} pr(j) \tag{3.20}$$

where $ST(i)$ represents the accumulating probability for the *i*th harmony. $ST(0)$ equals to 0.0 in the implementation. A random number r_c is chosen from the range [0, $ST(M)$], and the *k*th harmony in *HM* is chosen if the following criterion is satisfied:

$$ST(k-1) < r_c \leq ST(k), k = 1,2,..., M \tag{3.21}$$

The second modification in the MHS method is that other than one new harmony being generated in the OHS, a certain number of new harmonies (Nhm) are generated during each iteration step. The utilization of *HM* is intuitively more exhaustive when generating several new harmonies than when generating one new harmony during one iteration. In order to retain the structure of *HM*, the M harmonies with lower objective functions (for the minimization optimization problem) from $M + Nhm$ harmonies are included in the structure of *HM* again and Nhm harmonies with higher objective functions are rejected.

As described above, the *HM* as shown in Table 3.1 are reordered in ascending order. The new structure is demonstrated in Table 3.2. Suppose $\delta = 0.5, Nhm = 2$, the arrays pr and ST obtained are given in column 5 and 6, respectively, in Table 3.2. As discussed above, a random number in the range [0, 1] is generated, e.g., 0.6($< HR$). One of the values from {1.0, 1.5, 0.5, 1.8} should be chosen as the value of x_1 in the new harmony. Given the value of r_c, for example 0.7, by using criterion Eq.(3.21) 0.5 is chosen to be the value of x_1. Another random number of 0.95($> HR$) is then chosen, and a random value in the range [1, 3], e.g., 1.2, is obtained, thus a coarse new harmony $hm'_n = (0.5,1.2)$ is generated. The fine tuned new harmony is obtained by adjusting the coarse new harmony according to the parameter PR. Suppose two random values in the range [0, 1], say 0.7, 0.05, are generated randomly. Because the former is greater than PR, so the value of x_1 in hm'_n remains unchanged. The latter is lower than PR, so the value of 1.2 should then be adjusted. For example, 1.10, is the new value of x_2, and the fine tuned new harmony $hm_n = (0.5,1.10)$ is obtained. Similarly, the second new harmony $hm''_n = (0.9,1.5)$ is also obtained. The objective functions of the two new harmonies are calculated as 1.46 and 2.26, respectively. So the four harmonies with lower objective functions as $hm_1, hm_2, hm_n^{'}, hm_n^{''}$ are introduced into HM as illustrated in Table 3.3, and one iteration loop is then finished. The algorithm continues until the termination criterion is satisfied.

Besides the three parameters *HR*, *PR*, and *M* as used in the OHS algorithm, there are another two parameters δ, Nhm which can influence the performance of the proposed algorithm. Usually, the larger the value of Nhm is, the more iterations are investigated to achieve the termination criterion. Also, the larger the value of δ is, the fewer harmonies in HM are employed to generate the new harmonies. There is no simple way to determine the values of δ and Nhm. Three different values 0.1, 0.5 and 0.8 for δ are found by trial and error in the MHS. Each δ can be considered to be controlling a specific domain within [0,1]. For example, δ=0.1 can be considered as a controlling domain [0,0.3] where 0.3 is the average of 0.1 and 0.5. Similarly, δ=0.1 controls domain [0.3,0.65] while δ=0.8 controls domain [0.65,1.0]. The present algorithm is not sensitive to the exact choice of δ provided that the weighting of each δ is approximately the same. Firstly, N_{m1} iterations are performed yielding the best harmony hm_{g1} with the objective function value of f_{g1}, then N_{m2} iterations are continued and hm_{g2} and f_{g2} are obtained. If Eq.(3.22) is satisfied, $M-1$ harmonies are randomly generated with the extra hm_{g2} comprising the initial HM for next value of δ ; otherwise, hm_{g1} and f_{g1} are replaced with hm_{g2} and f_{g2} respectively. N_{m2} iterations are performed until Eq.(3.22) is satisfied. After Eq.(3.22) is satisfied, another value of δ is examined until all three values are tested.

$$\left| f_{g1} - f_{g2} \right| \le eps \qquad (3.22)$$

where eps is the termination tolerance of the algorithm and is specified as 0.0001 in the present study. After the three values of δ are applied, the search domain for the optimization problem is reduced as follows:

$$\begin{aligned} v'_{i\min} &= v_{gi} - (v_{i\max} - v_{i\min}) \times \eta \\ v'_{i\max} &= v_{gi} + (v_{i\max} - v_{i\min}) \times \eta \end{aligned} \tag{3.23}$$

where v_{gi} represents the ith element of the best harmony so far (hm_g), and η is the reduced percentage. In this study, η is set to 0.1. $v'_{i\min}$ and $v'_{i\max}$ are the reduced minimum and maximum bounds to the value of the ith control variable, respectively. Besides hm_g, $M-1$ harmonies are randomly generated within the reduced search domains, both of which comprise the new initial *HM* for iteration. Figure 3.8 shows the flowchart of the MHS algorithm.

3.3.2 Case studies for modified harmony search algorithm

Most of the existing global optimization methods can work well for relatively simple problems. When the problem has complicated geometry with major differences in soil parameters between different soils, there might be no solution to the objective functions at discrete regions or points, the efficiency and the capability to escape from local minima for the solution algorithm will become important.

To compare the performance of different algorithms, five procedures of slip surface generation (Cheng et. al, 2008b) are adopted as shown in Figure 3.9. In general, kinematically acceptable slip surface is concave upward and for failure soil mass to be divided into n slices, the slip surface is represented by n+1 vertices [V_1,V_2,…,V_{n+1}] with coordinates $(x_1, y_1), (x_2, y_2), \ldots, (x_{n+1}, y_{n+1})$. The first vertex (x_1, y_1) is usually at the toe of simple slope and the last vertex (x_{n+1}, y_{n+1}) can be defined easily by engineering experience based on slope geometry or sufficiently wide domains can be specified by the engineers. In the first method of slip surface generation, P1, x-ordinates are decided by evenly dividing the slices on the horizontal direction and y-ordinates can be determined by slope geometry, properties and especially, rectifying the convex segments into concave segments as shown in Figure 3.9(a); In the second procedure, P2 shown in Figure 3.9(b), equal horizontal extent of each slice is also adopted, y_2 is determined by the geometry and bedrock line, y_{i+1} (i=2,…,n-1) is randomly generated between point G (intersection of line x=x_{i+1} and line between V_i and V_{n+1}) and bedrock line or point H (intersection of line x=x_{i+1} and line between V_{i-1} and V_i), and therefore the convex segments can be avoided automatically in the generation of slip surface; The third procedure, P3 shown in Figure 3.9(c), is conceptually similar with P2 except that it uses angle between the slices as control variable instead of y-ordinates; In the fourth procedure P4 as shown in Figure 3.9(d), both x-ordinates and angle between the slices are control variables and the trial slip surface is generated in the similar procedure as P2 and P3; The fifth procedure P5 shown in Figure 3.9(e) is based on the generation method by Greco (1996) and Malkawi et al. (2001): the x-ordinates and angles of first and last vertices are control variables, as well as n random numbers in the range (-0.5, 0.5) representing the horizontal distance ratio which are adopted to determine the vertices at the middle portion of the slip surface (for example, the ratio of the horizontal distance between V_2 and mid-point of line V_1V_6 to the horizontal distance between V_2 and V_6 is a control variable used to determine V_2). The number of control variables in different generation procedures are listed in Table 3.4. From the procedures to generate the slip surface and corresponding number of control variables, it is anticipated that P1 requesting rectification of convex segments would employ more computation time, i.e. the *NOF* of P1 would be larger than the other procedures before the optimization algorithm can obtain the satisfactory factor of safety.

Several published examples are considered in this section to illustrate the effectiveness of the proposed algorithm MHS based on different slip surface generation methods. The first example is a simple homogeneous slope. The geotechnical parameters are: friction angle $\phi = 10.0^\circ$, cohesion $c = 9.8$ kPa, unit weight $\gamma = 17.64$ kN/m^3. Different researchers have examined this example using different optimization methods. Yamagami and Ueta (1988) used nonlinear programming methods to search for the critical slip surfaces and adopted Morgenstern and Price's method assuming $f(x) = 1.0$ to calculate the factor of safety. Greco (1996) analyzed this example using pattern search and a Monte Carlo type method. Malkawi et al. (2001) used the Monte Carlo technique to solve this problem. In this study, the number of slices is specified as 20, 25, and 30. The MHS and Morgenstern and Price method are used to analyze this example. The minimum factors of safety corresponding to different number of slices and the associated critical slip surfaces are shown in Table 3.5 and Figure 3.10, respectively. It must be noted that the result by P1 is slightly less satisfactory than the other results because the *NOF* required by P1 is up to 210308 which is much more than all the other procedures. Except for the results by P1, all the results are almost the same both in the factors of safety and the critical slip surfaces which are illustrated in Table 3.5 and Figure 3.10, respectively. In view of the differences in the precision used for the geometry and factor of safety calculation, it can be concluded that all the minimum factors of safety from different researchers are practically the same, except for the result 1.238 by Malkawai et al. (2001) (when the result by P1 is excluded). When the critical solution reached by Malkawai et al. (2001) is analyzed, a factor of safety of 1.37 is, however, obtained by the present method instead of the value 1.238 by Malkawai et al. (2001). It appears that the result by Malkawai et al. (2001) is affected by the multi-solution problem as discussed by Cheng (2003).

The second example is taken from the study by Bolton et al. (2003). It is a case where a weak layer is sandwiched between two strong layers. The geotechnical properties for layers 1 to 3 respectively are friction angle 20°, 10° and 20°; cohesion 28.73kPa, 0.0kPa, and 28.73kPa; and the unit weight is taken as 18.84kN/m^3 for all three layers. Different researchers used different methods to perform this example. Bolton et al. (2003) used Spencer's method to calculate the factor of safety, and the leap-frog algorithm was employed to search for the critical slip surface. The number of slices is assumed to be 20, 25, and 30 as in example 1. The minimum factors of safety under different numbers of slices and the associated critical slip surfaces are shown in Table 3.6 and Figure 3.11 respectively. The critical slip surfaces obtained by Bolton et al. (2003) are also illustrated in Figure 3.11 for comparison. As shown in Table 3.6, P1 is always inefficient for different number of slices in different cases because it requires large number of *NOF* to obtain a relatively high factor of safety. When the number of slices is equal to 30, the factor of safety by P4 is the best solution. However, the *NOF* required by P4 is the largest among all the five procedures. The result obtained by Bolton et al. (2003) is greater than those obtained by P2 to P4. The result 1.3086 is obtained by P5 which is slightly bigger than that by Bolton et al. (2003), but the number of iterations required is only 3362, which is smaller than all the other procedures.

The third example is a case considered by Goh (1999) and the geotechnical parameters are listed in Table 3.7. The cross section of the example is sketched in Figure 3.12. Goh (1999) used a genetic algorithm for this example and obtained a minimum factor of safety equal to 1.387. Bolton et al. (2003) adopted the leap-frog optimization algorithm and

Spencer's method to analyze this example and a minimum factor of safety equal to 1.359 is obtained. It can be seen from Figure 3.13 and Table 3.8 that the results obtained by different researchers are practically the same except those by P1. The critical slip surface obtained by P5 is slightly upwards concave as compared with the solutions from other procedures or researchers. Once again, the results obtained by P1 are poor even for a large number of iterations while the performance of P5 appears to be very efficient.

Example 4 is taken from the study by Arai and Tagyo (1985) where a layer of low resistance soil is interposed between two layers of soil with higher strengths. Geometrical features of the slope and values of shear-strength parameters of various layers are reported in Figure 3.14 and Table 3.9, respectively. Arai and Tagyo (1985) used Janbu's simplified method in combination with the conjugate gradient method and obtained a minimum factor of safety of 0.405. The same example was also examined by Sridevi and Deep (1991) using the random search technique and a value of 0.401 is obtained. Greco (1996) used the Monte-Carlo method to solve the same problem and obtained a factor of safety of 0.388. Malkawi et al. (2001) also adopted the Monte Carlo technique with a factor of safety equal to 0.401 but the critical slip surface was very close to that by Greco (1996). Results by different researchers are shown in Table 3.10. The critical slip surfaces are summarized in Figure 3.15. The factors of safety obtained by P1 vary from 0.42 to 1.17 and are totally unacceptable. The critical slip surfaces using 30 slices and P1 to P5 are shown in Figure 3.15 and they are much different from those found by Arai and Tagyo (1985), Sridevi and Deep (1991), Greco (1996), and Malkawi et al. (2001) in the exit part of the slip surface (right hand side in Figure 3.15). The factors of safety found using P1 to P5 and the simplified Janbu's method as given in Table 3.10 fall in between those obtained by Arai and Tagyo (1985) and by Greco (1996). Also, the critical slip surfaces obtained by P1 to P4 are close to that obtained by Malkawi et al. (2001). The critical slip surfaces obtained by Arai and Tagyo (1985) and Sridevi and Deep (1991) pass through the stronger layer, whereas the critical slip surfaces found in this study, by Greco (1996), and by Malkawi et al. (2001) are all located in the weak layer. It is interesting to note that if the critical failure surface found by Greco (1996) is used for analysis, a factor of safety of 0.401 instead of 0.388 as reported by Greco (1996) is obtained. It appears that the result by Greco (1996) is questionable.

Example 5 is considered by Zolfaghari et al. (2005) where a slope in layered soil is analyzed using the GA and the Morgenstern and Price method. Figure 3.16 shows the geometrical features of the analyzed slope, while Table 3.11 gives the geotechnical properties in layers 1 to 4. The number of slices used in this study is assumed to be 20, 25, and 30 and the results obtained are given in Table 3.12 and Figure 3.17. P1 appears to be always ineffective and the factors of safety range from 2.80 to 2.90. The results in Table 3.12 are all smaller than that obtained by Zolfaghari et al. (2005) except for P1 and P2. A very surprising result is that the result 1.11 by P5 which is the best among all the different procedures has the smallest *NOF*. The results obtained by P2 and P4 are almost the same and the result obtained by P3 is slightly larger than that by Zolfaghari et al. (2005). Although the number of slices used by Zolfaghari et al. (2005) is not clearly stated, it can be seen from Figure 3.17 that greater portions of the critical slip surfaces found by P2, P3, P4 and P5 lie within the weakest layer as compared with that obtained by Zolfaghari et al. (2005) which are clearly more reasonable results.

3.3.3 Differences between the original harmony search and modified harmony search methods

The MHS is developed because of the poor performance of the original method when the number of control variables exceeds 25. In order to compare the efficiency between the OHS and MHS, P2 is used to generate the trial slip surfaces, assuming the number of slices to be 20, 25 and 30 or equivalently the number of control variables are 21, 26 and 31, respectively. The OHS algorithm is tested in the above five examples using *NOF* equal to 30000, 40000 and 50000 respectively. The comparison of the results obtained by the OHS and MHS is given in Table 3.13.

From Figure 3.18 and Table 3.13, it can be concluded that the MHS attains the optimal solution with no loss of accuracy and with much less effort. In addition to that, considering the OHS requires a large number of trials for complicated problems with a large number of control variables (larger than 25) , the MHS is superior to the OHS algorithm in most cases. Since the MHS is more stable than OHS for most cases, harmony search algorithm that is referred at the rest of this chapter actually refers to the MHS instead of OHS.

3.4 A coupled particle swarm optimization and harmony search algorithm

3.4.1 Mixed optimization algorithm of particle swarm optimization and harmony search

Another modified algorithm denoted as HS/PSO is developed in present study for cases where there are several strong local minima in the present. In the original PSO, the locations of the particles are updated by modifying the corresponding velocity vectors, and it is found that incorrect value of θ may lead to the trap into the local minimum which will be demonstrated in a later section. Generally speaking, a moderate value of 0.5 for θ is used for all the problems, otherwise, a larger value of θ can be applied at the initial analysis to search the solution space, which is then reduced linearly to a small value to find better results near the existing best position (Cheng et al. 2010b). On the other hand, the HS method is efficient and effective global optimization method when the number of control variables is less than 25 for many geotechnical problems as mentioned before. Modified harmony search (MHS) method as proposed in this study can overcome the limitation of the OHS method. From the study by Cheng et al. (2007a), the PSO is found to be a more stable method in the optimization analysis while the HS is a fast solution algorithm in some cases. So the combination of two optimization method can possibly result in a better performance under difficult cases.

The procedure to generate a new harmony in HS can be introduced into the PSO to determine the locations of the particles beyond the boundary, thus the mixed optimization algorithm can make good use of the advantages in both the PSO and the HS. The detailed procedures for the presented mixed algorithm are as follows, and flow chart is shown in Figure 3.19:

Step 1: Randomly generate N particles comprising a group of particles, and initialize the values of parameters. Set the counter of iteration $j = 0$.

Step 2: If $j = 0$, evaluate all the particles in the group, else the particles with the modified positions are evaluated. Update $\mathbf{P}_i$ and $\mathbf{P}_g$.

Step 3: Randomly choose N_z particles to 'move' by Eqs.(3.12) and (3.13)

Step 4: Determine whether there are particles outside the allowable bounds. If yes, replace the old values with the new ones obtained by the MHS procedure.

Step 5: The counter of iteration j is increased by 1, and the termination criterion is checked. If the termination criterion is satisfied, the algorithm will terminate, else, go to step 2 and continue.

Only N_z particles other than all the particles are allowed to 'move' during each iteration in the mixed optimization. By this means, the computation result and the computation time can be maintained at a balance. In this study, N_z is set to 5. Several different values of N_z have been tried and it is found that the value of N_z has no major effect on the results. The other parameters are chosen to be the same as the PSO by Cheng et al. (2008d). The maximum and minimum extremum principles to be discussed in chapter 4 is implemented by using the mixed optimization algorithm as given above, and it is found that this approach is highly effective and efficient so that the factor of safety can be determined within a reasonable time suitable for routine design works.

3.4.2 Case studies for coupled particle swarm optimization and harmony search algorithm

To demonstrate the effectiveness of the present coupled optimization method HS/PSO, we will consider example 5 again as shown in Figure 3.20. Again, the soil parameters are shown in Table 3.11. The soil parameters for soil layer 3 are particularly low so that the majority of the slip surface will lie within this layer of soil. The minimum factors of safety using Spencer method for this problem are 1.50, 1.11, 1.361 and 1.09 by the GA (Zolfaghari et al.(2005)), the artificial fish swarm algorithm (AFSA) (Cheng et al. (2008c), the ACO (Kahatadeniya et al. (2009)) and the present algorithm. Since the soft band soil is a strong local minimum and the thickness of this layer is relatively small, the

GA and the ACO fail to provide a good solution for this problem. On the other hand, the AFSA and the present HS/PSO optimization analysis provide solutions which are nearly the same. In fact, it is difficult to differentiate precisely the critical slip surfaces from these two methods.

The second geotechnical example is taken from example 2, and it is less difficult than the first case in term of optimization. For this problem, there is a “strong” minimum while the geometry is relatively simple, so the global minimum will attract the optimization solution paths for the HS and PSO which will be very efficient in the analysis. For the HS/PSO method, it is less affected by the attraction of any local minimum, so it is actually less efficient than the original HS or PSO methods for the present example. This feature is however important when a difficult problem is encountered, as the HS/PSO method will be less affected by the presence of several “strong” minimum so that it will be actually more efficient and effective for difficult problems.

Another example is shown in Figure 3.21. It is one of the sections for a major hydropower project founded at a location with complicated ground conditions in China. There are several different layers of soft materials which are shown in shaded in Figure 3.21 while the material parameters are shown in Table 3.14. Detailed studies of this project using various methods and computer programs have been carried out by Cheng et al. (2008b), and satisfactory results have been obtained for most of the difficult sections. There are however some special sections where the results are very sensitive to the initial solution and a wide range of minimized results are obtained which are shown in Table 3.15. It is not easy to determine the critical failure surface automatically by the classical optimization methods, as there are several layers of soft materials which are strong local minima affecting the direction of search for the global minimum as shown in Figure 3.22. For the present analysis, the left exit end of the failure surface is searched within the domain of x=260m to 330m while the right exit end is searched within the domain of x=520m to 575m. The failure surface based on the MHS is close to the original PSO methods and they are not shown for clarity in Figure 3.23. It is noticed that the failure surfaces from all the optimization methods are virtually the same at the right hand side as this is governed by the soil profiles and the geometry of this project. The major differences between the failure surfaces from different methods of optimization as shown in Figure 3.23 are: (1) the starting point of the critical failure surface from HS/PSO is x=278.0 while it ranges from 320.25 to 320.38 for all the other methods; (2) the exit angle of the failure surface for HS/PSO method is smaller than all the other methods; (3) all the optimization methods except for the HS/PSO is more attracted by soil 13 in the analysis so that the critical failure surfaces are deeper than that by the HS/PSO. In Table 3.15, it is clear that most of the global optimization methods are not satisfactory except for the AFSA which gives a factor of safety less than 2.0 (but still not good enough while HS, PSO are actually poor in performance) but requires 394527 trials in the analysis. Actually, when the number of control variable is large, it is found that HS can be very inefficient and sometimes non-effective. It can be viewed that all the optimization methods are attracted by the presence of the “strong” local minima during the search, except for the coupled HS/PSO analysis which is less affected by the “attraction” of the local minima. Based on the proposed coupling method, the minimum factor of safety is obtained as 1.65 with 130156 evaluations, and the result is the best among all the five different global optimization as shown in Table 3.15. It is true that the present coupled optimization method is less efficient for simple problem which is demonstrated in examples 5 and 2, but the method is also more stable for problems where there are several “strong” local minima. For the present large scale construction work, a good result is much more important than the time of computation, and the proposed coupled method has provided a good result without excessive computations.

3.5 Conclusions and Discussions

In slope stability analysis, the minimum factor of safety for all possible failure surfaces has to be determined, and this is a typical global optimization upper bound problem. For slope stability problems, practically all the modern optimization methods can work well if the geometry and ground conditions are relatively simple. For complicated problems, the factor of safety is very sensitive to the precise location of the critical solution and differences between different global optimization methods are found to be large. Since the ground topography, the boundary between individual soil layers and soil parameters distribution can be highly irregular in some cases, the objective function will be non-convex in general. Furthermore, there are cases (about 10-15% of all the total trials) where there will be no solution available for the trial vectors, hence the objective function is also not continuous over the whole solution domain (Cheng et al. 2010b).

An improved harmony search method MHS is developed in the present study. It is found that the MHS is highly efficient with no loss of accuracy. In fact, it performs better than the original harmony method in most cases. When the number of control variables is large, it is always found to be better than the original method but requires much less trials.

The coupling of the PSO and HS as presented is a new approach in global optimization. It has been demonstrated that HS/PSO algorithm is efficient and effective for complicated geotechnical problems. Most of the examples in this study are difficult problems in global optimization analysis, as the factors of safety are very sensitive to the precise locations of the critical failure surfaces. In addition, when Morgenstern-Price method is used for the analysis, ‘failure to converge’ is also relatively common and a large value is assigned to those cases that fail to converge (equivalent to a discontinuous objective function), and this will create further difficulties in the search direction. The proposed coupled optimization method has clearly demonstrated the advantages under these difficult cases.

Table 3.1 The structure of HM

Control variables / HM	x_1	x_2	Objective function
hm_1	1.0	1.5	2.25
hm_2	1.5	2.0	4.25
hm_3	0.5	1.5	2.50
hm_4	1.8	2.5	6.89

Table 3.2 The reordered structure of HM

Control variables / HM	x_1	x_2	Objective function	$pr(\ )$	$ST(\ )$
hm_1	1.0	1.5	2.25	0.5	0.5
hm_2	0.5	1.5	2.50	0.25	0.75
hm_3	1.5	2.0	4.25	0.125	0.875
hm_4	1.8	2.5	6.89	0.0625	0.9375

Table 3.3 The structure of HM obtained after the first iteration in the modified harmony search algorithm

Control variables / HM	x_1	x_2	Objective function	$pr(\ )$	$ST(\ )$
hm_1	0.5	1.10	1.46	0.5	0.5
hm_2	1.0	1.5	2.25	0.25	0.75
hm_3	0.9	1.5	2.26	0.125	0.875
hm_4	0.5	1.5	2.50	0.0625	0.9375

Table 3.4 Summary of the number of control variables for different procedures

Procedure	P1	P2	P3	P4	P5
Number of control variables	n+1	n+1	n+1	2n	2n

Table 3.5 Summary of results for example 1 using Morgenstern-Price's method in determining the factor of safety

Different procedures		Minimum factors of safety	NOFs
P1	Number of slices=20	1.3380	97598
	Number of slices=25	1.3512	175147
	Number of slices=30	1.3656	210308
P2	Number of slices=20	1.3379	10568
	Number of slices=25	1.3246	15208
	Number of slices=30	1.3365	15848
P3	Number of slices=20	1.3242	6862
	Number of slices=25	1.3248	10581
	Number of slices=30	1.3230	13882
P4	Number of slices=20	1.3235	16880
	Number of slices=25	1.3228	19126
	Number of slices=30	1.3224	23006

P5	Number of slices=20	1.3264	4072
	Number of slices=25	1.3295	4125
	Number of slices=30	1.3257	3973
Yamagami And Ueta (1988)	BFGS	1.338	unknown
	DFP	1.338	unknown
	Powell	1.338	unknown
	Simplex	1.339-1.348	unknown
Greco(1996)	Pattern search	1.327-1.33	unknown
	Monte Carlo	1.327-1.333	unknown
Malkawi et al. (2001)	Monte Carlo	1.238	unknown

Table 3.6 Results from different procedures for example 2

Different procedures		Minimum factors of safety	NOFs
P1	Number of slices=20	1.9904	43868
	Number of slices=25	2.0257	78314
	Number of slices=30	2.4619	35330
P2	Number of slices=20	1.2568	19368
	Number of slices=25	1.2408	16208
	Number of slices=30	1.2953	26648
P3	Number of slices=20	1.3028	10019
	Number of slices=25	1.2473	11524
	Number of slices=30	1.2755	18456
P4	Number of slices=20	1.2368	29512
	Number of slices=25	1.2564	25072
	Number of slices=30	1.2570	51168
P5	Number of slices=20	1.2825	3201
	Number of slices=25	1.3103	5284
	Number of slices=30	1.3086	3362
Bolton et al. (2003)	Leap-frog (Spencer)	1.305	unknown

Table 3.7 Geotechnical parameters for example 3

layers	γ (kN/m^3)	c (kPa)	ϕ (degree)
1	19.5	0.0	38.0
2	19.5	5.3	23.0
3	19.5	7.2	20.0

Table 3.8 Factors of safety obtained by different researchers for example 3 (Spencer's method)

Different procedures		Minimum factors of safety	NOFs
P1	Number of slices=20	1.4142	47113
	Number of slices=25	1.4211	92060
	Number of slices=30	1.4220	161445

P2	Number of slices=20	1.3599	10926
	Number of slices=25	1.3659	10656
	Number of slices=30	1.3622	21186
P3	Number of slices=20	1.3619	11428
	Number of slices=25	1.3603	13258
	Number of slices=30	1.3600	14988
P4	Number of slices=20	1.3591	24763
	Number of slices=25	1.3568	31039
	Number of slices=30	1.3578	34779
P5	Number of slices=20	1.3599	2289
	Number of slices=25	1.3598	3519
	Number of slices=30	1.3683	3579
Bolton et al. (2003)	Leap-frog(Spencer)	1.359	unknown
Goh (1999)	GA(Spencer)	1.387	unknown

Table 3.9 Geotechnical parameters for example 4

layers	γ (kN/m^3)	c (kPa)	ϕ (degree)
1	18.82	29.4	12.0
2	18.82	9.8	5.0
3	18.82	294.0	40.0

Table 3.10 The factors of safety for example 4

Different procedures		Minimum factors of safety	NOFs
P1	Number of slices=20	0.4272	72657
	Number of slices=25	0.6696	117943
	Number of slices=30	1.1731	232967
P2	Number of slices=20	0.3962	13768
	Number of slices=25	0.4006	13208
	Number of slices=30	0.3958	20648
P3	Number of slices=20	0.4008	6871
	Number of slices=25	0.3959	12593
	Number of slices=30	0.3956	13908
P4	Number of slices=20	0.3959	16929
	Number of slices=25	0.3959	21120
	Number of slices=30	0.3959	25448
P5	Number of slices=20	0.4014	2458
	Number of slices=25	0.4138	3862
	Number of slices=30	0.3990	2148
Arai and Tagyo (1985)	Conjugate gradient	0.405	unknown
Sridevi and Deep (1991)	RST-2	0.401	unknown
Greco (1996)	Monte Carlo	0.388	unknown
Malkawi et al. (2001)	Monte Carlo	0.401	unknown

Table 3.11 Geotechnical parameters for example 5

Layers	γ (kN/m^3)	c (kPa)	ϕ (degree)
1	19.0	15.0	20.0
2	19.0	17.0	21.0
3	19.0	5.00	10.0
4	19.0	35.0	28.0

Table 3.12 Summary of results for example 5

Different procedures		Minimum factors of safety	NOFs
P1	Number of slices=20	2.8342	64900
	Number of slices=25	2.8408	124659
	Number of slices=30	2.9055	86332
P2	Number of slices=20	1.2400	16968
	Number of slices=25	1.2674	20208
	Number of slices=30	1.1959	21848
P3	Number of slices=20	1.2302	9969
	Number of slices=25	1.1394	13515
	Number of slices=30	1.2509	25703
P4	Number of slices=20	1.1692	24756
	Number of slices=25	1.2154	50869
	Number of slices=30	1.2032	56059
P5	Number of slices=20	1.1181	3881
	Number of slices=25	1.1117	5904
	Number of slices=30	1.1299	2371
Zolfaghari et al. (2005)	Genetic algorithm	1.24	unknown

Table 3.13 Comparison between OHS and MHS

Different cases and methods			results	NOFs
	OHS	Number of slices=20	1.3387	30000
Example 1		Number of slices=25	1.3236	40000
		Number of slices=30	1.3442	50000
	MHS	Number of slices=20	1.3379	10568
		Number of slices=25	1.3246	15208
		Number of slices=30	1.3365	15848
Example 2	OHS	Number of slices=20	1.3175	30000
		Number of slices=25	1.2370	40000
		Number of slices=30	1.2858	50000
	MHS	Number of slices=20	1.2568	19368
		Number of slices=25	1.2408	16208
		Number of slices=30	1.2953	26648
Example 3	OHS	Number of slices=20	1.3830	30000
		Number of slices=25	1.3719	40000
		Number of slices=30	1.3837	50000
	MHS	Number of slices=20	1.3599	10926
		Number of slices=25	1.3659	10656
		Number of slices=30	1.3622	21186
Example 4	OHS	Number of slices=20	0.3979	30000
		Number of slices=25	0.3967	40000

		Number of slices=30	0.3970	50000
	MHS	Number of slices=20	0.3962	13768
		Number of slices=25	0.4006	13208
		Number of slices=30	0.3958	20648
Example 5	OHS	Number of slices=20	1.2205	30000
		Number of slices=25	1.2827	40000
		Number of slices=30	1.2130	50000
	MHS	Number of slices=20	1.2400	16968
		Number of slices=25	1.2674	20208
		Number of slices=30	1.1959	21848

Table 3.14 Geotechnical parameters for example 6

layers	γ(kN/m^3)	c' (kPa)	ϕ'(degree)
1	16.00	2000.	56.31
2	24.00	2000.	56.31
3	24.00	2000.	56.31
4	26.00	1000.	50.20
5	26.00	1400.	54.50
6	26.00	1000.	44.70
7	26.00	100.0	19.30
8	26.00	100.0	19.30
9	26.00	1000.	44.70
10	26.00	1400.	54.50
11	26.00	100.0	19.30
12	26.00	100.0	19.30
13	26.00	100.0	19.30
14	23.00	130.0	22.30
15	26.00	1400.	54.50
16	26.00	100.0	19.30
17	26.00	1400.	54.50

Table 3.15 Minimum factors of safety for example 6 based on Spencer method (41 control variables)

Method of global optimization	PSO	MPSO	AFSA	MHM	HM/PSO
Min. factor of safety	2.18	2.15	1.83	1.98	1.65
No. of trials	121124	59288	394527	132098	130156
Min. factor of safety at evaluation number	99824	35460	219284	98426	112342

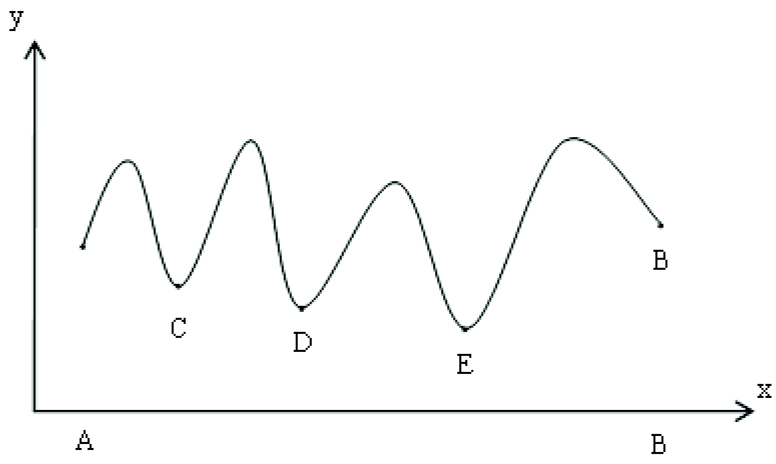

Figure 3.1 Typical search domain with multiple local minimum

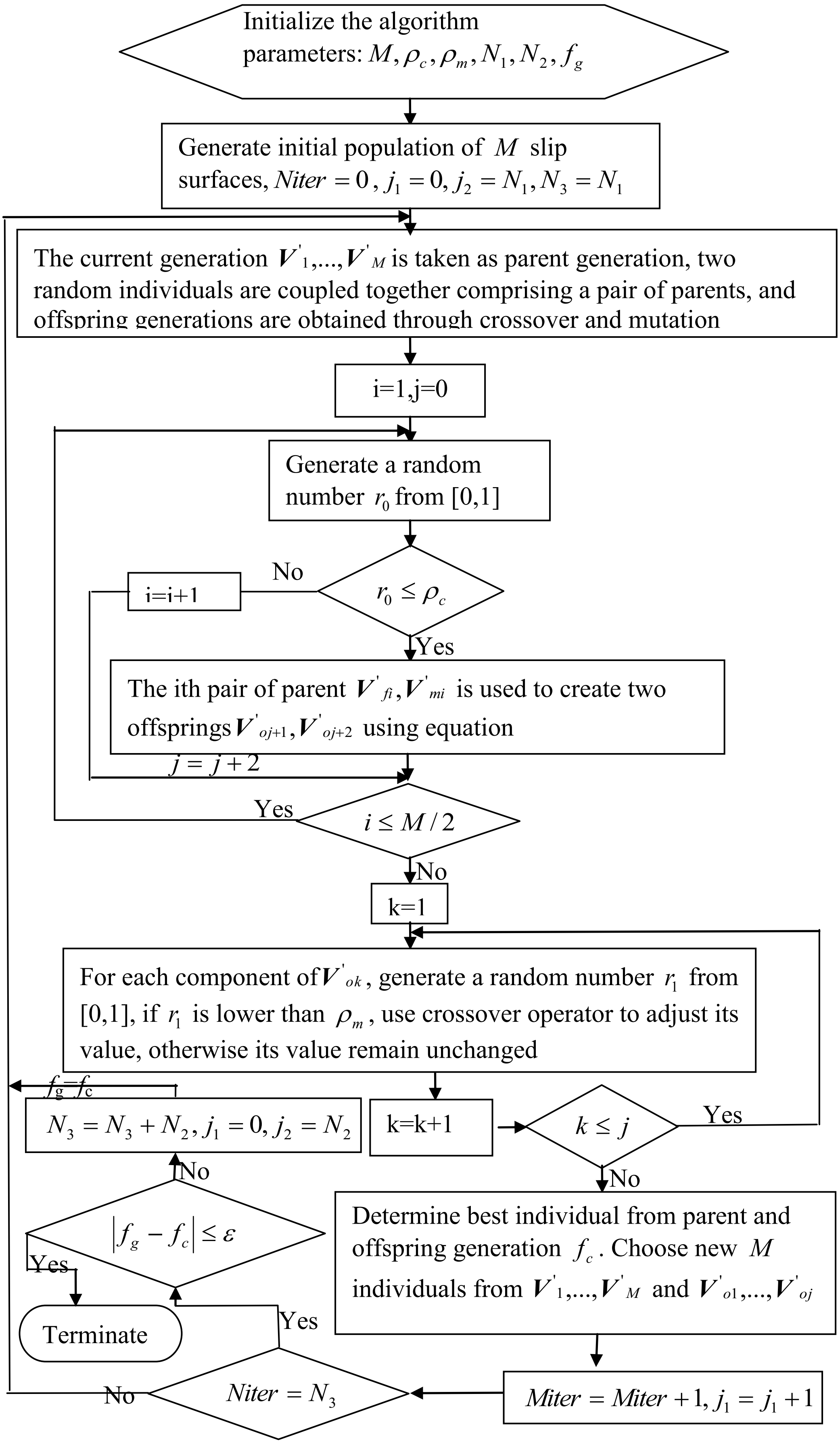

Figure 3.2 Flowchart for the genetic algorithm (GA)

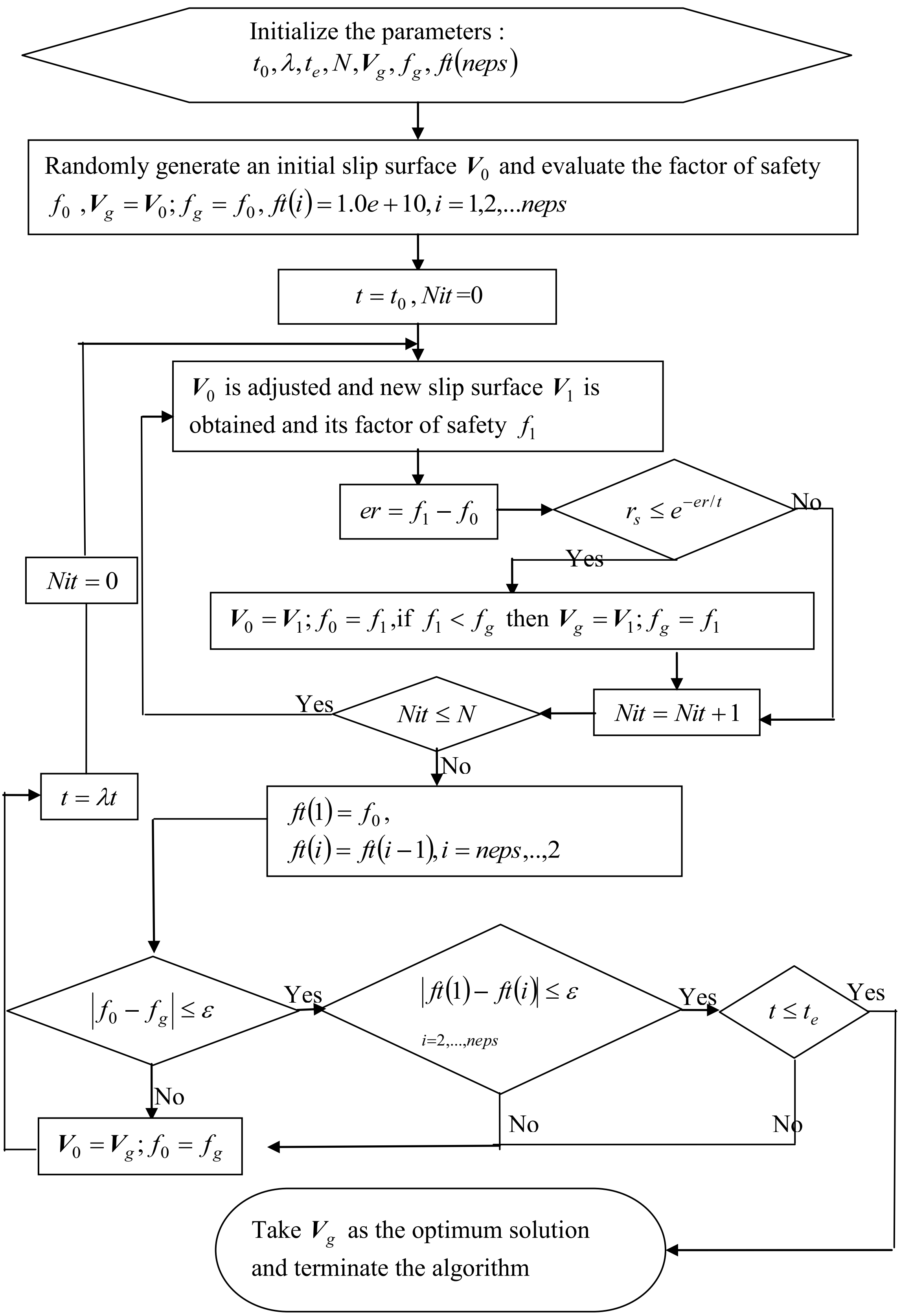

Figure 3.3 Flowchart for the simulated annealing algorithm (SA)

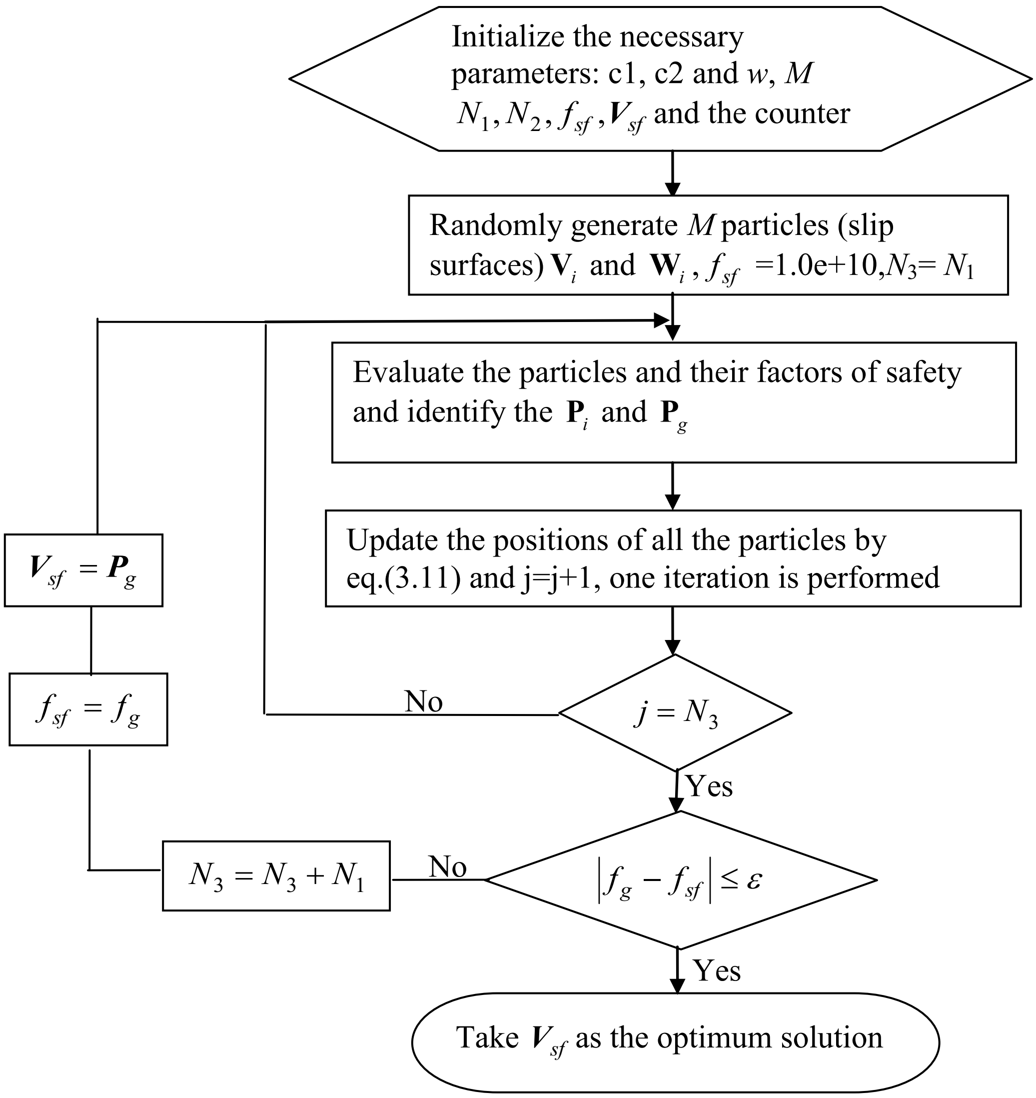

Figure 3.4 Flowchart for the particle swarm optimization method (PSO)

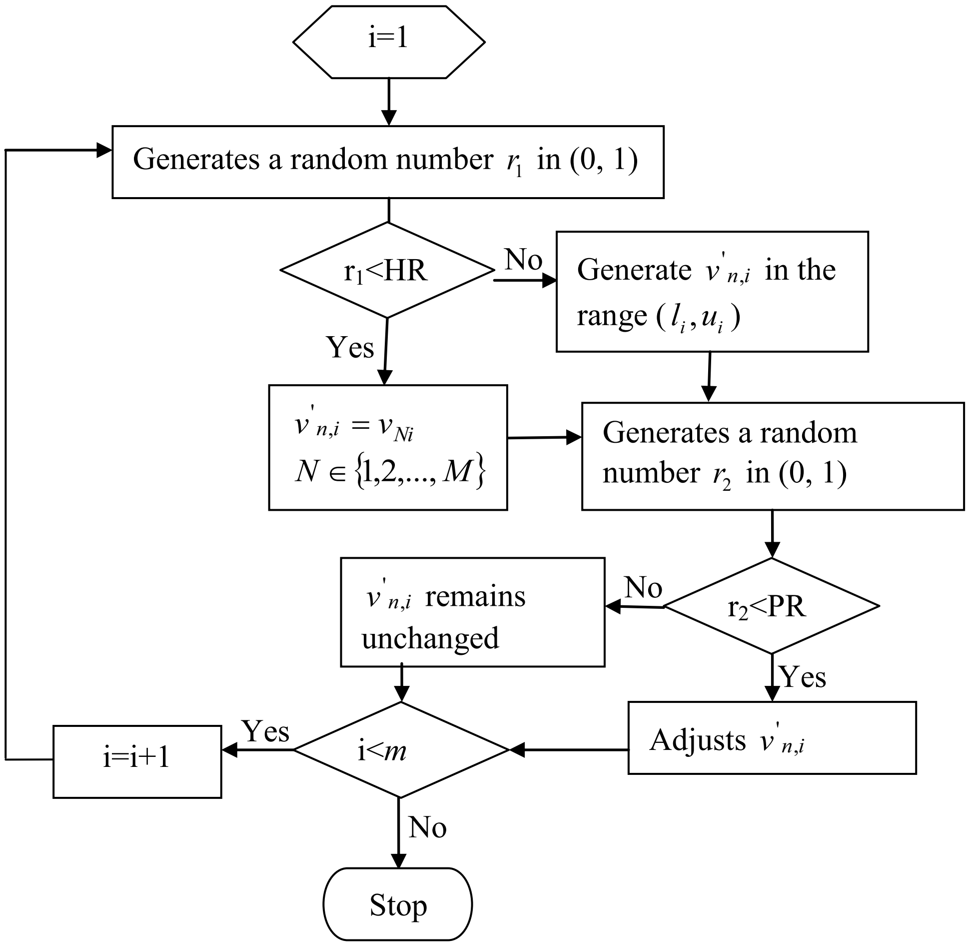

Figure 3.5 Flowchart for generating a new harmony (HS)

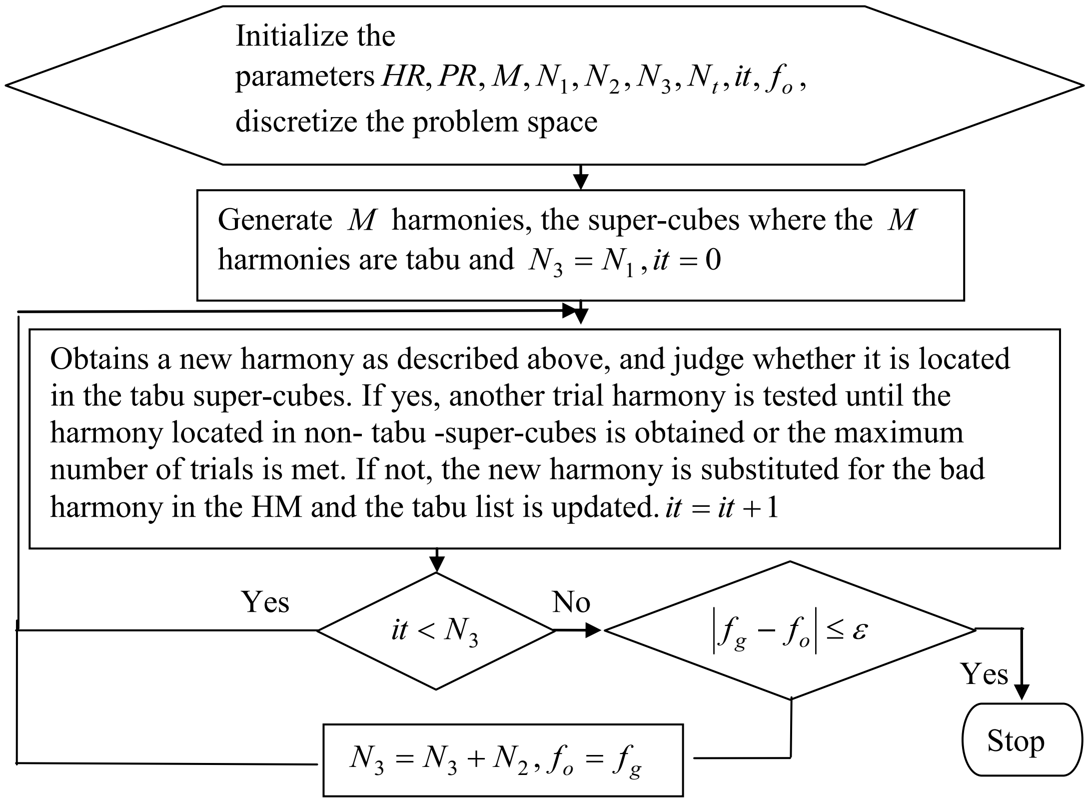

Figure 3.6 Flowchart for the Tabu search (TS)

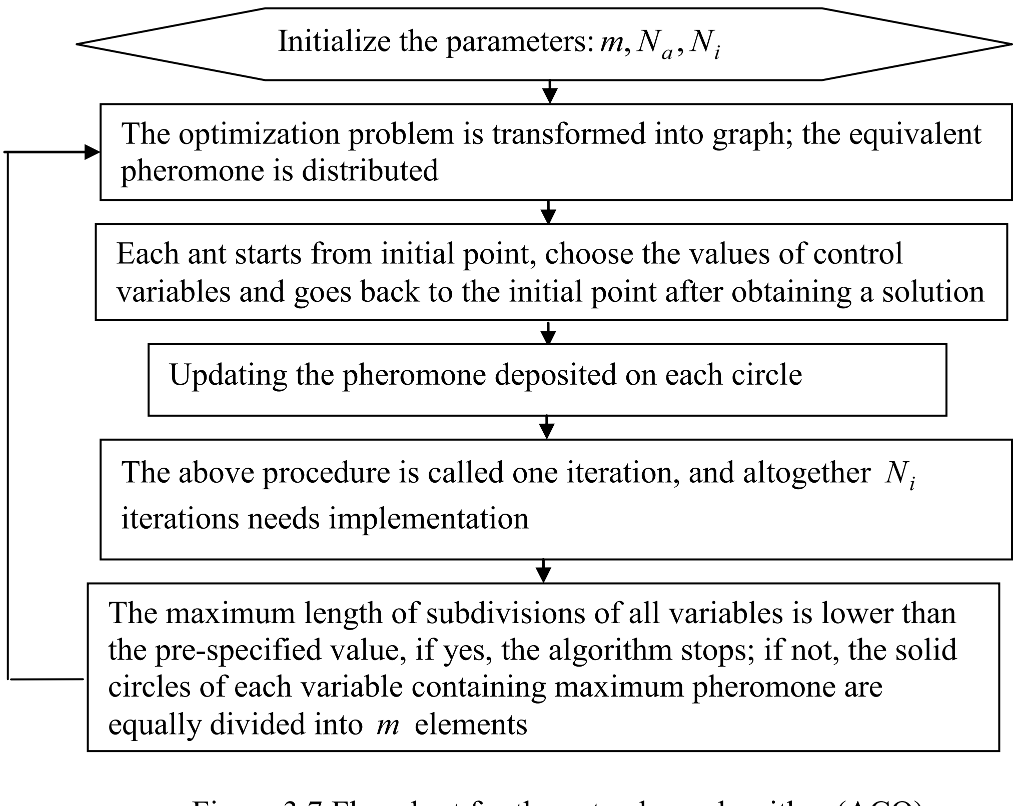

Figure 3.7 Flowchart for the ant colony algorithm (ACO)

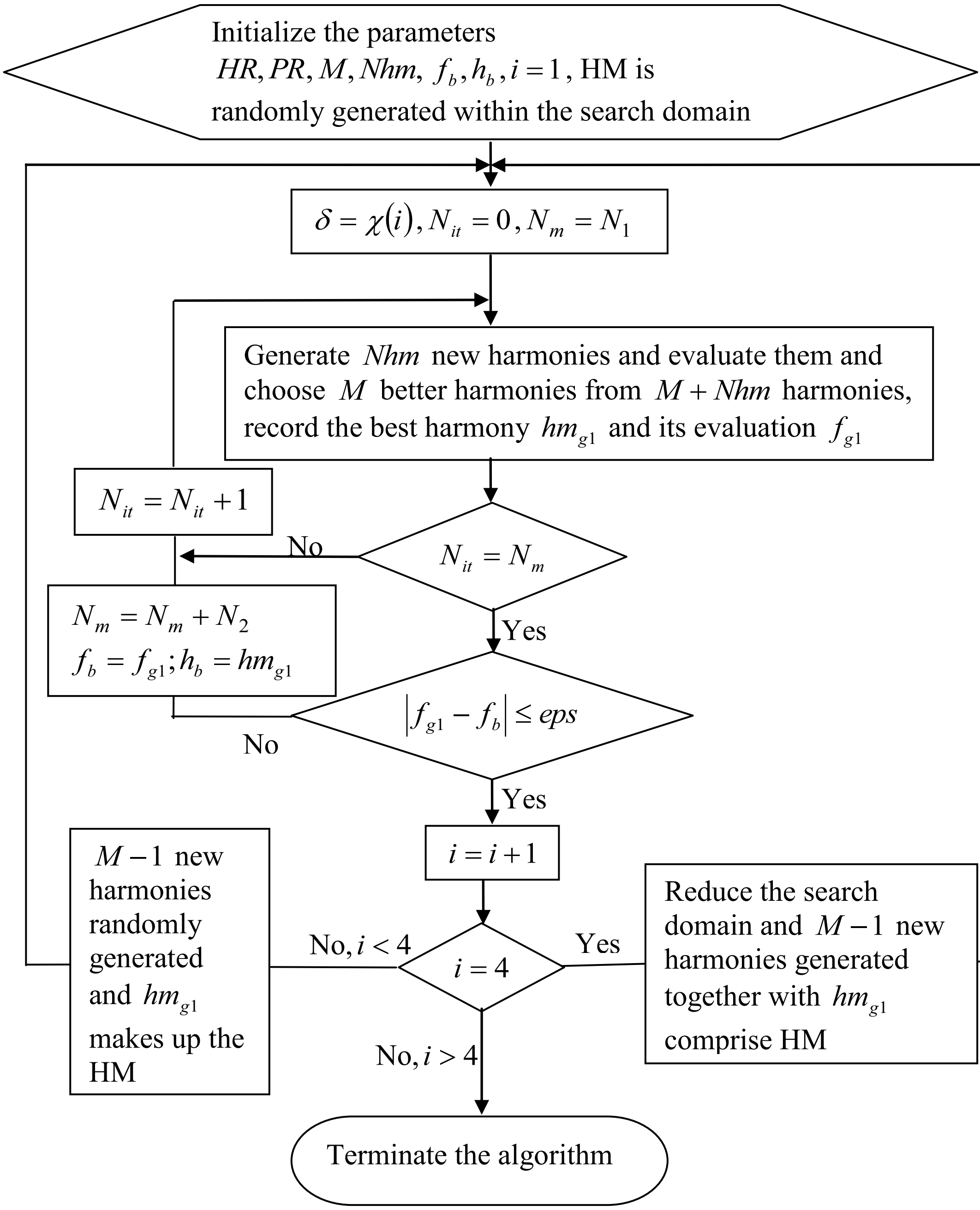

Figure 3.8 Flowchart for the modified harmony search algorithm (MHS)

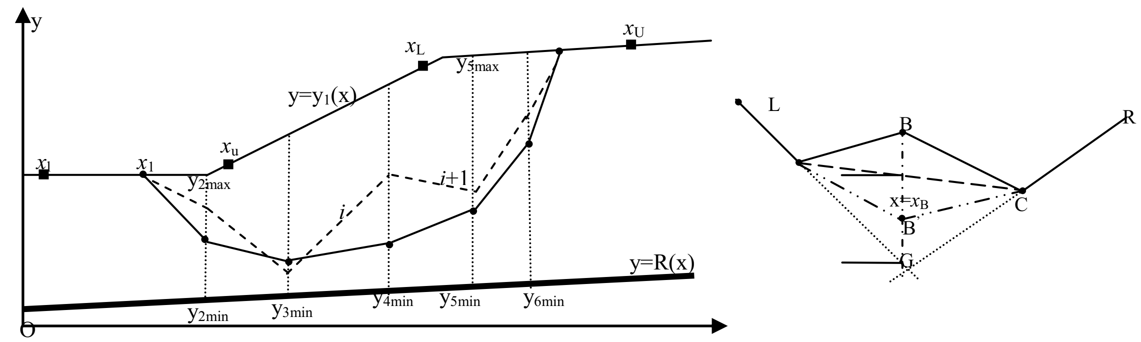

(a) Generation method P1 and rectifying procedure for convex segments in P1

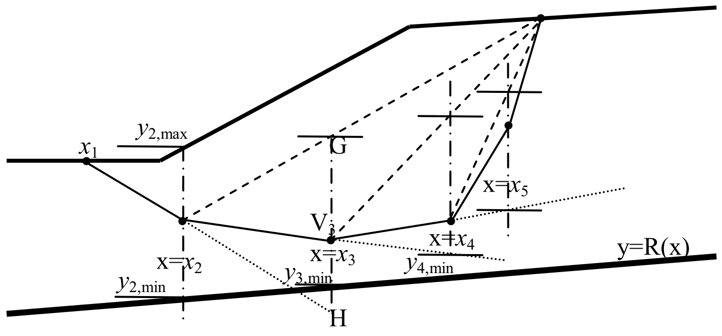

(b) Generation method P2

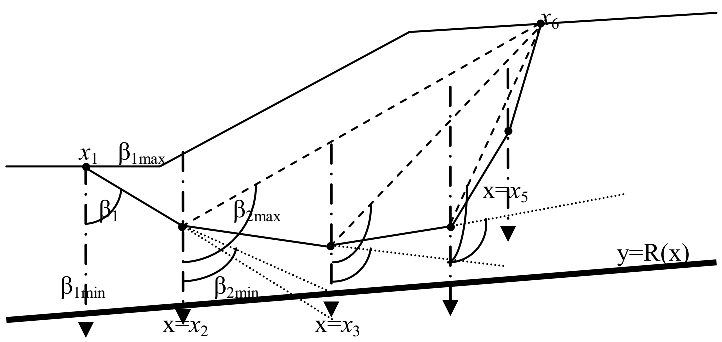

(c) Generation methods P3 & P4

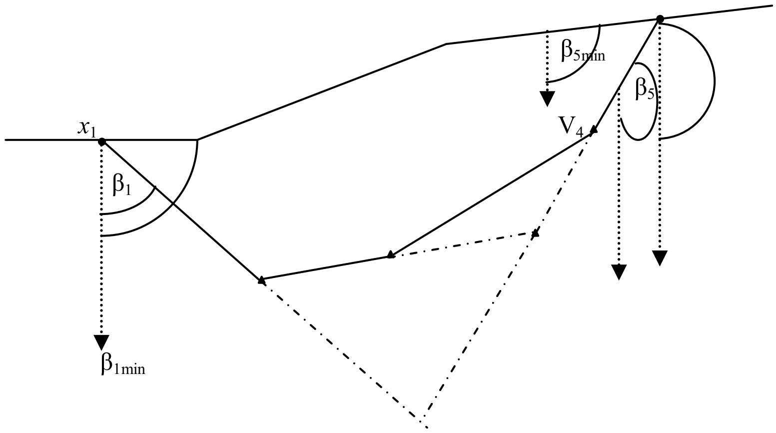

(d) Generation method P5

Figure 3.9 Different generation methods of critical slip surfaces

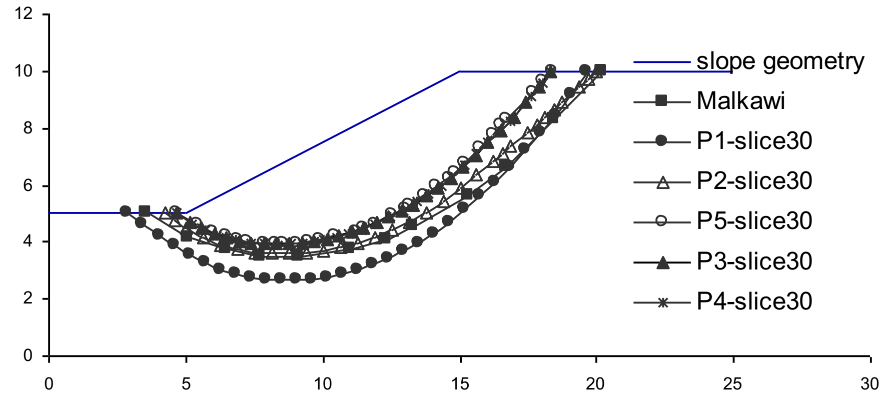

Figure 3.10 Critical slip surfaces obtained by different procedures for example 1

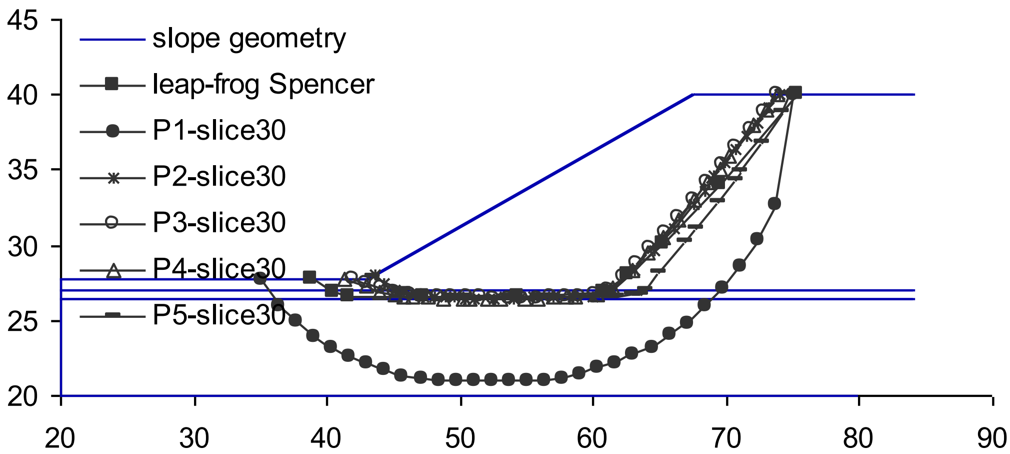

Figure 3.11 Comparison of different critical slip surfaces for example 2

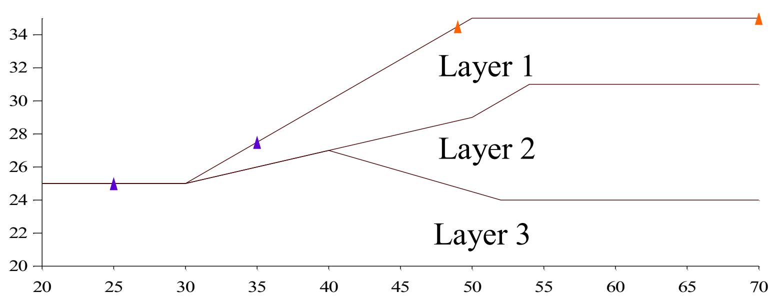

Figure 3.12 The cross-section of example 3

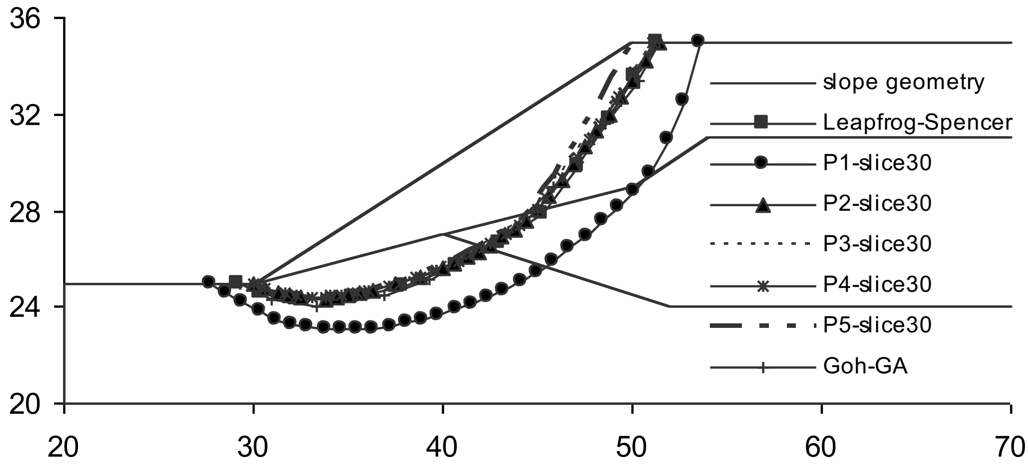

Figure 3.13 Comparison of different critical slip surfaces for example 3

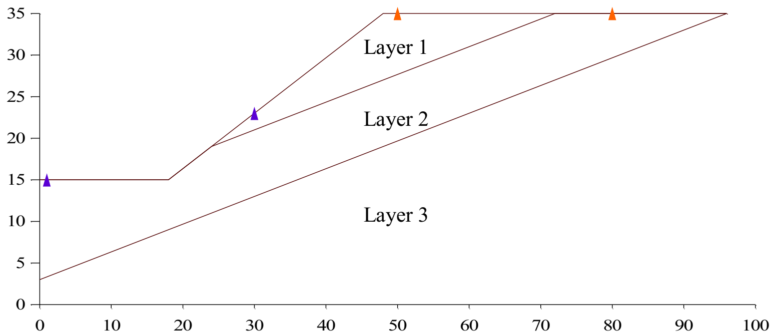

Figure 3.14 Cross-section for example 4

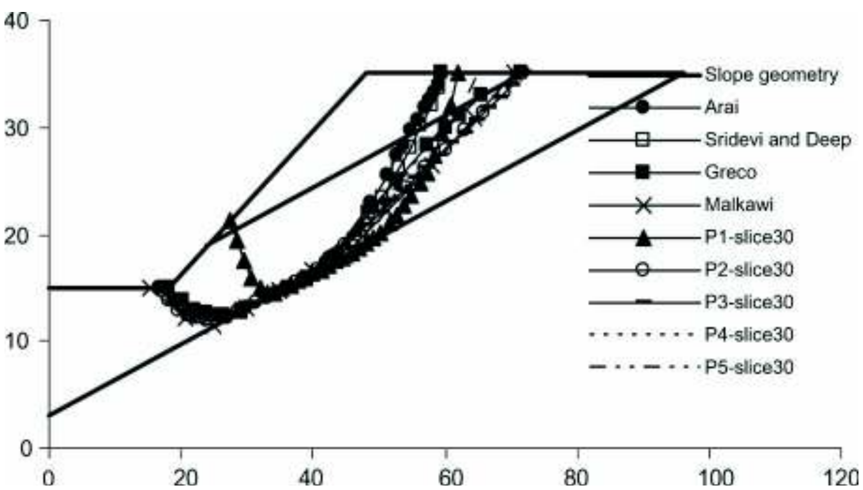

Figure 3.15 Critical slip surfaces obtained by different researchers for example 4

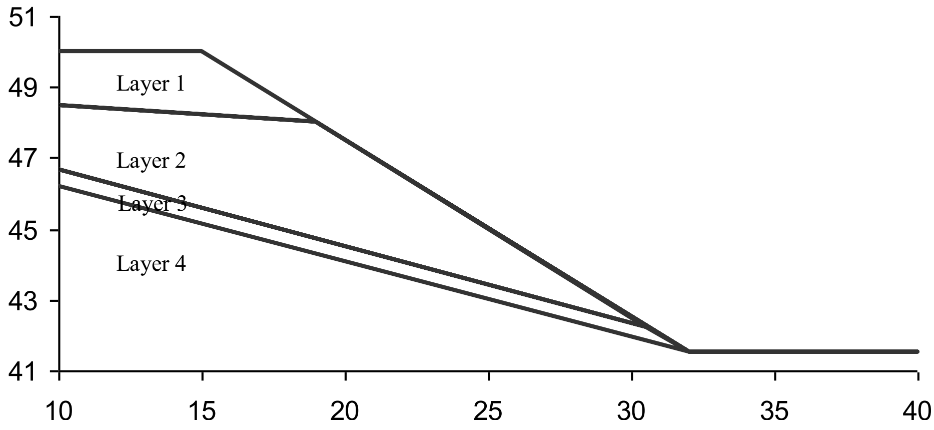

Figure 3.16 The geometry for example 5

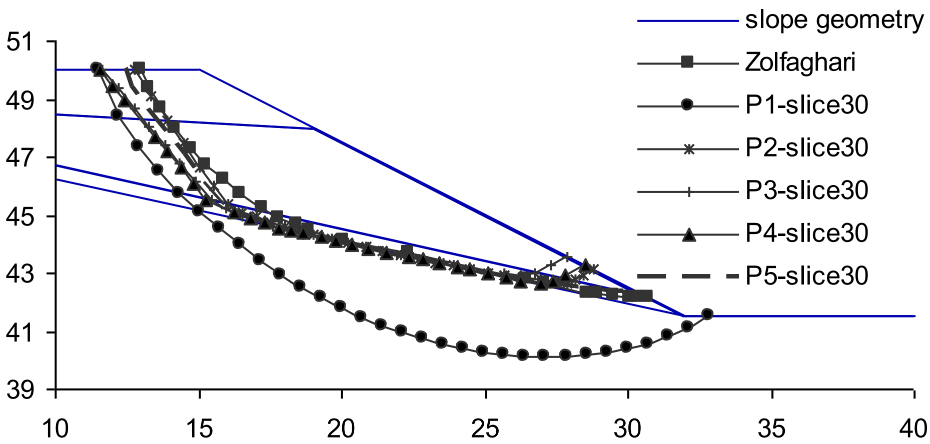

Figure 3.17 Summary of critical slip surfaces for example 5

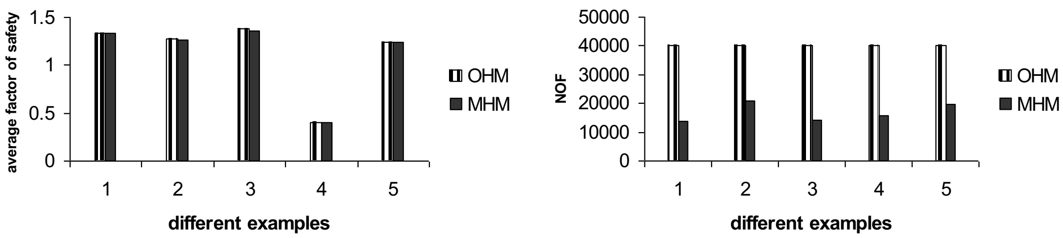

Figure 3.18 The comparison of the average factor of safety and NOF between OHS and MHS

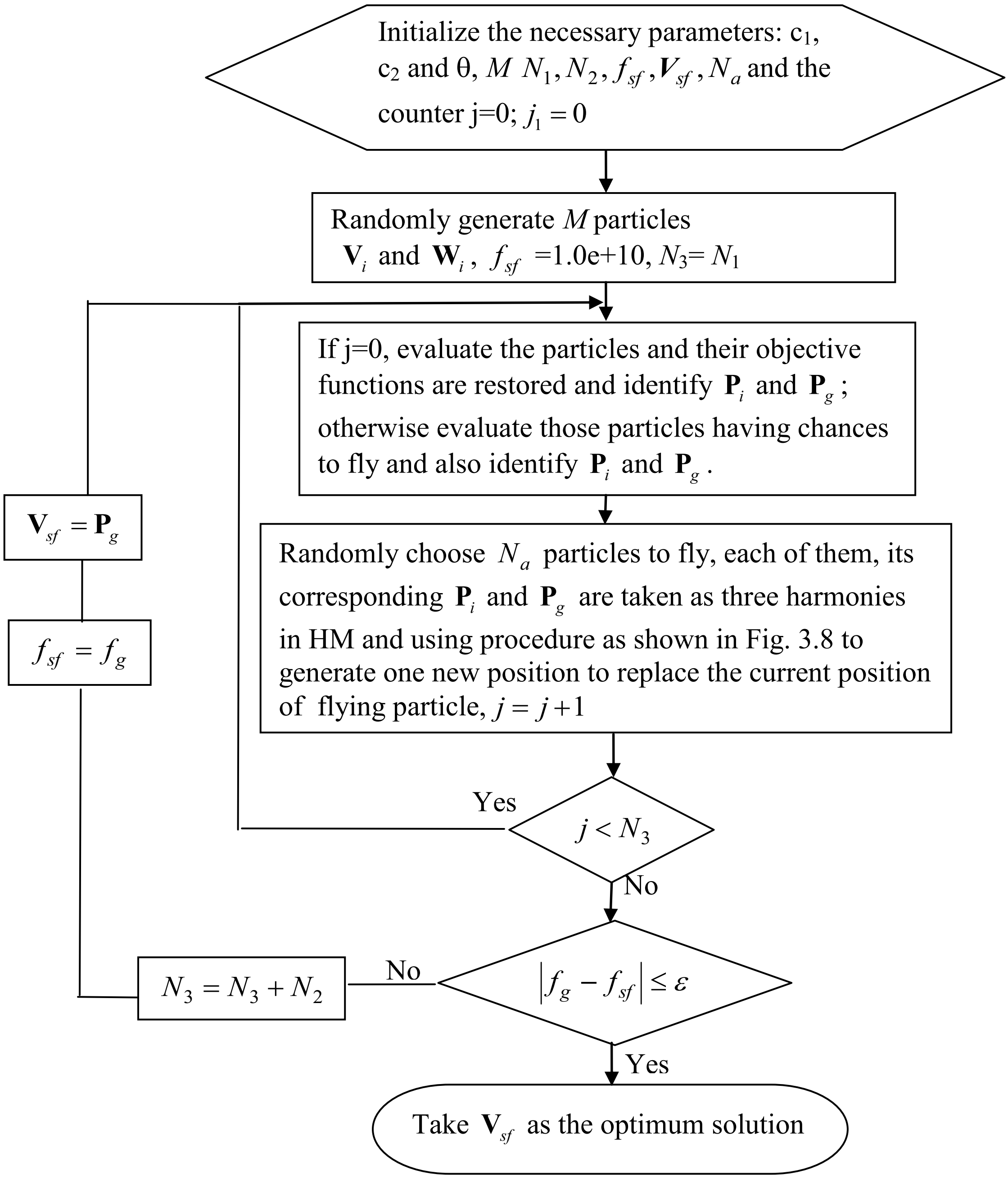

Figure 3.19 The flowchart of the coupled optimization method HS/PSO

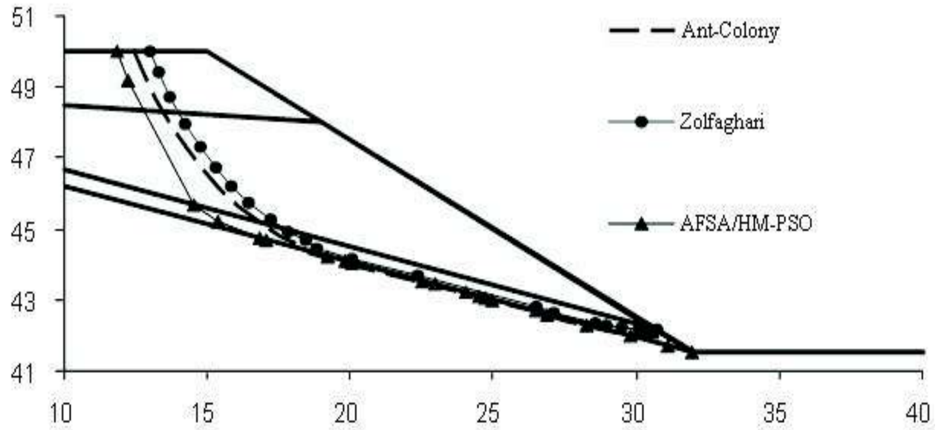

Figure 3.20 Critical slip surface of example 5 using different kinds of optimization methods

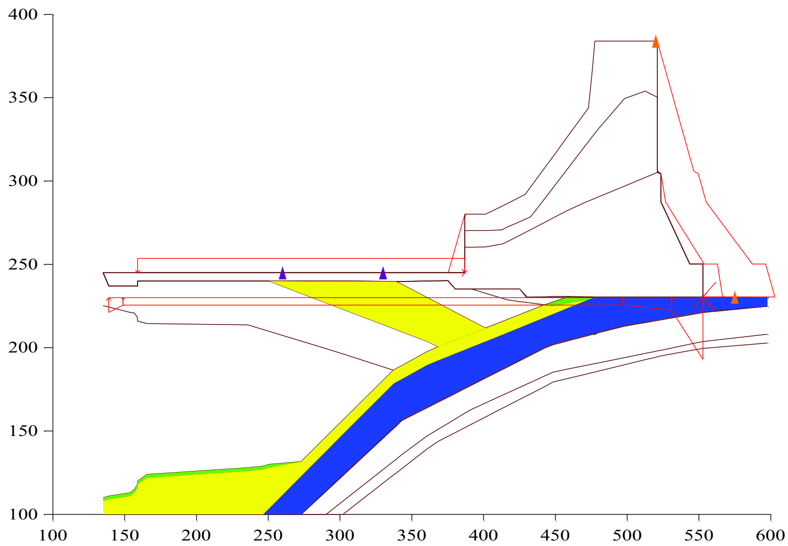

Figure 3.21 Soft soil in shaded area for a dam project

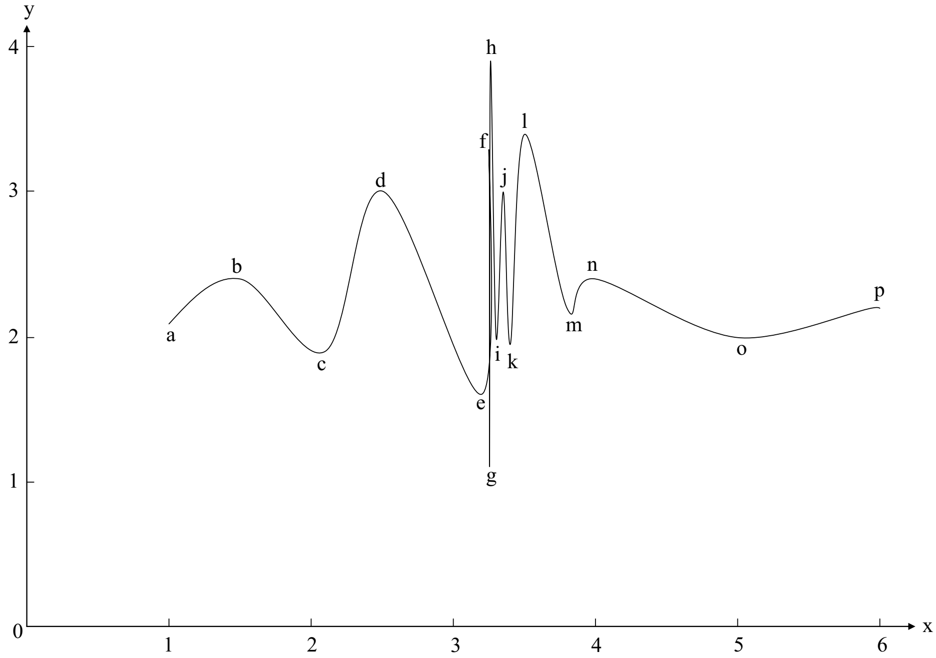

Figure 3.22 A simple one-dimensional function with the presence of several "strong" maxima and minima for illustration of optimization

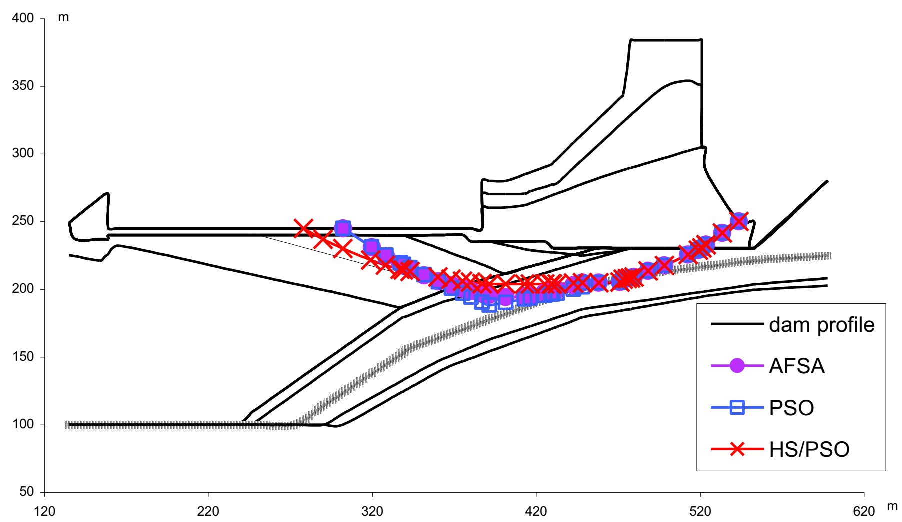

Figure 3.23 Critical failure surfaces by different global optimization methods based on the Spencer's method (critical failure surface by MHS and MPSO are not shown for clarity)

CHAPTER 4 Study on the Failure Mechanism under Several Conditions by Distinct Element Method

4.1 Introduction

In practical applications, limit equilibrium method based on the method of slices or method of columns and strength reduction method based on the finite element method or finite difference method are used for slope stability analysis. These two major analysis methods take the advantage that the insitu stress field which is usually not known with good accuracy is not required in the analysis. The uncertainties associated with the stress-strain relation can also be avoided by a simple concept of factor of safety. In general, this approach is sufficient for engineering analysis and design. If the condition of the slope after failure has initiated is required to be assessed, these two methods will not be applicable. Even if the insitu stress field and the stress-strain relation can be defined, the post-failure collapse is difficult to be assessed using the conventional continuum based numerical method, as sliding, rotation and collapse of the slope involve very large displacement or even separation without the requirement of continuity.

The most commonly used numerical methods for continuous systems are the FDM, the FEM and the boundary element method (BEM). The basic assumption adopted in these numerical methods is that the materials concerned are continuous throughout the physical processes. This assumption of continuity requires that at all points in a problem domain, the material cannot be torn open or broken into pieces. All material points originally in the neighborhood of a certain point in the problem domain remain in the same neighborhood throughout the whole physical process. Some special algorithms have been developed to deal with material fractures in continuum mechanics based methods, such as the special joint elements by Goodman (1976) and the displacement discontinuity technique in BEM by Crouch and Starfield (1983). However, these methods can only be applied with limitations (Jing and Stephansson, 1993):

(1) large-scale slip and opening of fracture elements are prevented in order to maintain the macroscopic material continuity;

(2) the amount of fracture elements must be kept to relatively small so that the global stiffness matrix can be maintained well-posed, without causing severe numerical instabilities; and

(3) complete detachment and rotation of elements or groups of elements as a consequence of deformation are either not allowed or treated with special algorithms.

Before the slope starts to collapse, the factor of safety serves as an important index in both the LEM and SRM to assess the stability of the slope. The movement and growth after failure has launched which is also important in many cases cannot be simulated on the continuum model, and this should be analyzed by the distinct element method (DEM).

The distinct element method is an explicit method based on the finite difference principles which is originated in the early 1970s by a landmark work on the progressive movements of rock masses as 2D rigid block assemblages (Cundall, 1971a,b). Later, the works by Cundall are developed to the early versions of the UDEC and 3DEC codes (Cundall, 1980; Cundall and Hart, 1985). The method has also been developed for simulating the mechanical behavior of granular materials (Cundall and Strack, 1979a,b,c, 1982), with a typical early code BALL (Cundall, 1978) which later evolved into the codes of the PFC group for 2D and 3D problems of particle systems (Itasca, 1995). Through continuous developments and extensive applications over the last three decades, there has accumulated a great body of knowledge and a rich field of literature about the distinct element method. The main trend in the development and application of the method in rock engineering is represented by the history and results of the code groups UDEC/3DEC.

In this chapter, Particle Flow Code (PFC2D) is used for the detailed investigation of the failure mechanism of slopes under several conditions. PFC models the movement and interaction of circular particles by the distinct element method, as described by Cundall and Strack (1979). The packing of granular material can be defined from statistical distributions of grain size and porosity, and the constitutive model acting at a particular contact consists of a stiffness model, a slip model, and a bonding model: the stiffness model establishes an elastic relation between the contact force and relative displacement; the slip model allows a relation between shear and normal contact forces such that two contacting balls may slip relative to one another; the bonding model serves to limit the total normal and shear forces that the contact can carry by enforcing bond-strength limits. Two types of bonds can be represented either individually or simultaneously – contact-bond and parallel-bond; these bonds are referred to the contact and parallel bonds respectively (Itasca, 1995a,b). Although the individual particles are solid, these particles are only partially connected at the contact points which will change at different time step. Under low normal stresses, the strength of the tangential bonds of most granular materials will be weak and the material may flow like a fluid under very small shear stresses. Therefore, the behaviour of granular material in motion can be studied as a fluid-mechanical phenomenon of particle flow where individual particles may be treated as 'molecules' of the flowing granular material. In many particle models for geological materials in practice, the number of particles contained in a typical domain of interest will be very large, similar to the large numbers of molecules.

PFC runs according to a time-difference scheme in which calculation includes the repeated application of the law of motion to each particle, a force-displacement law to each contact, and a contact updating scheme. In each cycle, the set of contacts is updated from the known particles and known wall positions. Force-displacement law is firstly applied on each contact, and new contact force is then calculated according to the relative motion and constitutive relation. Law of motion is then applied to each particle to update the velocity, the direction of travel based on the resultant force, and the moment and contact acting on the particles. Although every particle is assumed as rigid material, the behavior of the contacts is characterized using soft contact approach in which finite normal stiffness is taken to represent the stiffness which exists at the contact. The soft contact approach allows small overlap between the particles which can be easily observed. Stress on particles is then determined from this overlapping through the particle interface.

One of the primary objectives of the particle model is the establishment of the relations between microscopic and macroscopic variables/parameters of the particle systems, mainly through micromechanical constitutive relations at the contacts. It seems that the constitutive models of PFC are possible to be linked to those commonly used in continuum based methods: the stiffness linked to modulus of elasticity, friction coefficient to tan ϕ ' (It should be pointed out that the friction coefficient in PFC is aimed to check whether the ratio of shear contact force to normal contact force is large enough to render the particles slip. So it is a strength parameter and cannot be correlated directly to the ratio of shear stress to normal stress) and bond strength to c'. But we should recognize that the adopted microscopic parameters, including circular or spherical particles and their sizes and the contact relation between each two particles are established based on macroscopic parameters of whole mass from simulation experiment. Difference between both natures of parameters is inevitable. Therefore the parameters, particle sizes and distribution and model assembling should be carefully tested in trials before calculation in order to better reflect real behavior of soil.

On the other hand, compared with a continuum, particles have an additional degree of freedom of rotation which enables them to transmit couple stresses, besides forces through their translational degrees of freedom. At certain moment, the positions and velocities of the particles can be obtained by translational and rotational movement equations and any special physical phenomenon can be traced back from every single particle interactions. Therefore, it is possible for PFC to analyze large deformation problems and flow process which will occur after slope failure has initiated. The main limitation of DEM is that there is great difficulty in relating the microscopic and macroscopic variables/parameters, hence DEM is mainly tailored towards qualitative instead of quantitative analysis.

4.2 Large displacement simulation of slope failure by PFC

4.2.1 Failure pattern of simple slope

To assess the failure mechanism of slope, particularly the situation after the initiation of failure, PFC is used for the study of several slopes in this section. For simplicity, simple slope with slope angle 45° and 60° are firstly considered. The height of slope is set as 3m, and the base of both models is 14m long and 7m high. Friction is set to 0.4 and the density of particle is set to 1000kg/m^3. Mohr-Coulomb criterion is adopted through the entire failure process. The typical numerical model for a soil nailed slope is shown in Figure 4.1, and the use of measure circles to recover the average stresses are also illustrated in this figure. It should be pointed out the local stresses from PFC can fluctuate rapidly and may be not realistic in the value because of the highly localized effect, and the use of averaged stress can give a much better picture about the stresses.

Based on Figures 4.2-4.4 which show the progressive failure of a simple slope (without and with cohesive strength) under gravity, the progress failure of the slope, the post-failure mechanism and a typical failure surfaces are clearly shown in Figure 4.3. From parametric study (not shown here), it is found that the collapse is more sensitive to the cohesive strength than the slope angle or friction angle, and the cohesive strength can be considered as a controlling variable when friction is fixed. This result is actually well known among the engineers that cohesive strength is more important in the design in general. Actually, if c is large enough, the slope is stable which is shown in Figure 4.4. The failure mechanisms as shown in these figures are generally similar to that as predicted from LEM or SRM. It is noticed that failure seems to start from the crest of slope while in practical cases, failure seems to initiate from the toe in Hong Kong (usually in rainy times). The displacements at different phases are therefore investigated in this study.

For the simple slope where gravity is the sole factor in the failure, the toe of the slope is the exit end of slip surface in classical slope stability theory. However, during the initial failure as shown in Figures 4.5-4.8, the horizontal and vertical displacements are only slightly changed at the toe, while more than 0.5m movement in both the horizontal and vertical directions can be found at the crest. The results indicate that failure occurs firstly at the crest of the slope which this is a typical local failure while failure at toe is the initiation of global failure. The rotation and sliding along the assumed slip surface in classical concept seem not to dominate the initial failure mechanism. This is a clear illustration of the progressive failure of slope which can be modeled by PFC but not in FDM and FEM. In PFC, the failure of cohesionless slope initiates when the grains at the top firstly roll downwards with the resulted grains flow to the base of the slope. This flow causes the accumulation of grains near to the toe and finally sliding out. When the resistance at the toe is fully mobilized, the extent of the collapse is enlarged which is a global failure. In reality, completely cohesionless soil is not commonly found in practice, and the actual slope failure is usually induced by ground water flow under raining. Actually, failures initiated at the crest of slopes are also found in Hong Kong. In general, the prediction by the PFC computations is acceptable, and DEM has the ability to assess the progressive failure which is not possible for the continuum based methods.

The typical displacement of the simple slope with c=0 and α=60° is given in Figure 4.3. The advantage of PFC over continuum based methods is also evident, as the displacement vectors clearly demonstrate the locations of the mobilized particles at different phases with different slope geometries due to the progressive failure. At the initial stage, basically only the particles around the slope face are mobilized. The grains at the crest slide down under the gravity and hence large-scale deformation of the slope start to initiate. The contact forces among particles are re-distributed and further failure develops gradually. When the slope angle approaches the natural angle of repose, the slope has achieved a stable displacement. Such failure development demonstrates that the tension failure occurs firstly at the top of the slope, and hence accumulation of soil particles at the toe at the later stages. Of course, the concept of one “safety of factor” on a “critical slip surface” normally accomplished in LEM and SRM cannot predict such “progressive” failure procedure with the presence of continuously modified large displacement movement. Nevertheless, rough “critical slip surface” can be determined at the later stage of failure based on the displacement vectors at the later stage of failure in Figure 4.3g which is the global failure.

4.2.2 Influence of soil-nail on the slope failure

Soil nail is a common reinforcement used for slope stabilization. The essential concept of soil nailing is reinforcing the slope with closely spaced inclusions to increase the stability. When soil movement is induced by excavation for cut slopes or by natural environment changes for existing slopes, resistant tension force is generated in the soil nail and is transferred to the soil by the friction mobilized at the soil-nail interface. Three models of soil-nailed slope with slope angle of 60° are conducted in this section: (1) c=0; (2) c=2kPa and (3) c=5kPa. A set of two soil nails of density 2000kg/m^3, stiffness 10MN/m, friction=0.4, contact-bond strength 10MN is introduced in the slope to study the effects of the soil nail on slope stability and failure mechanism. Since there is no soil nail in the original PFC program, in this study, the soil nails are simulated by installing and clumping grains along the excavated hole in the original model. If the grains are clumped rigidly, then the action is practically equivalent to that of a soil nail.

The use of soil nail head in continuum model has been demonstrated to be important by Cheng et al. (2007) by SRM, and the effect of soil nail head is also studied in this section. From Figures 4.9-4.11, it is obvious that the stability of the slope is increased by the use of soil nails, especially for the region close to the soil nails, though falling and accumulation of soil particles still exist at the crest and around the toe respectively. Due to the resistance provided by the soil nails, massive failure indicating the shear failure located inside the slope is not formed, which is a good illustration about the stabilizing effect of soil nail. Furthermore, basically only local failure by tension at the top of slope and shear at the interface between soil nail and soil mass can be found. From Figure 4.9 where there is no nail head in the problem, it can be noticed that the region located near to the slope face between the soil nails seems not to be reinforced which is not surprising, and this is also the worry of many local engineers towards the use of soil nails in loose fill slope where the cohesive strength of soil is practically zero near to the slope surface. The stability of this local region has to be provided by the soil nail head and facing (if any), and this is a common understanding among the engineers in Hong Kong that a large soil nail head or even facing is required for a good slope stabilization work, even these elements do not appear in their computer model analysis. Without the soil nail head, the confining action from the soil nail cannot be transferred to the slope surface. For soil nailed slopes, failure initiates when the soil falls down by gravity at the upper part of the slope, and also the area between and beneath the soil nails to form tension failure. Similar to the situation without soil nail, the resulted accumulation of soil particles can later be found at the bottom of the slope. Therefore, in the view of geometry change, the progressive failure of soil-nailed slope is basically the same as that of slope without nail, except that the region of shear failure is smaller and the movement is smaller than an unreinforced slope. For soil-nailed without nail head or facing, local failure is however dominant and must be controlled.

Soil nail head is generally used in construction and is an effective component to the local stability of the slope. If nail head is used in the analysis (by bonding the adjacent grains to the exit end of nail on the slope face together), confining action is provided by the nail head to increase the local stability (Figures 4.12-4.14). For the slope failure, failure occurs only at the toe and crest without surface failure. The effect of cohesive strength can also be summarized from the displacement graph. Higher cohesion of soil will give higher stability with less failure which is obvious. More importantly, in Figure 4.14, there is no obvious tension crack at the upper part of the slope and the rundown to the bottom is also less noticeable if c is high enough.

Figures 4.15-4.18 illustrate the local failure at the toe and the crest in more details. By logging the displacement history of ball 2673 at crest, it can be found that the particles around the top of the slope move downwards along the face and are limited by the soil nail after a short displacement has occurred and the corresponding loading is taken by the soil nails. For the bottom of the slope, the particles show the trend of moving out with upheaval. This failure is later controlled by the mobilized resistance of the soil nail. To sum up, soil nailing reinforces the global stability of the slope by resisting the formation of extended shear failure as well as limiting the local failure at the crest and toe.

4.3 Stress state analysis by PFC

Though it is difficult for PFC to give an over-all stress field similar to that in FLAC, measure circle (for instance as shown in Figure 4.1) can be specified to compute the average stress within the circle at specified calculation step. For the stress state of the simple sandy slope, the stress is released and re-distributed during the collapse, so the majority of the changes take place at the initial stage of the failure as shown in Figure 4.19. The same phenomenon exists for clay slope (tested but not shown) and soil-nailed slope (as shown in Figure 4.20).

For cohesionless slope as shown in Figure 4.19, gradually increasing stress field can be found at the toe and decreasing stress field can be found at the crest. This result is reasonable as the stress descends at the crest under the unloading action. Due to limited amount of confining soil mass within this zone, the vertical stress dominates over the horizontal stress in the whole process. Both the vertical and horizontal stress drop to zero in the later stage when the soil collapses at the crest. At the toe, the state of stress is more complicated because of the continuous accumulation of sliding soil mass from the upper part of the slope. The comparison of the stress on the slip surface in Figure 4.19 shows that normal stress on the failure surface is nearly equal to the vertical normal stress and is much greater than the shear stress on the failure surface, which indicates that the vertical stress still dominates near the slope face at the toe. Tension failure at the crest is not obvious from the stress analysis, and this may be due to the stress from the measure circle being the averaged value instead of the local value.

Soil nail is an efficient measure to reinforce the slope, as it mobilizes the shear strength on the contact surface to resist further failure. As shown in Figure 4.20, once there is slight displacement of soil, the tensile strength of the soil nails can be activated to take over the loading which will effectively reduce the instability of the stress field. The effect is particularly obvious for the soil mass below the nails. The particles slide out at the toe only while the upper part of the slope which is well supported by the nails has almost no failure. So the normal and shear stress are very stable as compared with the situation without the nails. The soil mass above the nails is also well stabilized against collapse. There is only slight collapse but no obvious loss at the crest (referring to Figure 4.12), and the stress maintains stable which is different from the slope without nails (referring to Figure 4.19). Overall speaking, the soil nails effectively help the slope to maintain a stable stress field.

The shear stress along the soil nails is also checked by several measure circles (Figure 4.21). The action of the soil nails after the initiation of failure is clearly shown in Figure 4.22. The value of the shear stress on the nails firstly increases after nails are installed and slight movement has occurred. The tensile strength of the soil nail is then mobilized to resist further shear failure and maintain the reinforced soil mass at a stable stress. It is reasonable that the lower soil nail has larger stress than the upper one as it bears more loading, while attention should be paid to the shear stress versus different positions of nails where there are large differences in the results. The shear stress at the bottom of the nail is much higher than that in the middle and the direction of the shear stress is even reversed. This indicates that the neutral point is approximately at the middle of the nails for the present problem, and the shear stress on the nails should be zero at the neutral point which is a well known result and is supported by various laboratory and field tests. The results also demonstrate that the portions of nails outside the failure zone actually take up the stabilization action.

If the shear stress along the soil nails is investigated from the initial condition to the reinforced state with the installed soil nails, the results can be found in Figure 4.23. The nail head moves with the surrounding soil so that the shear stress around the nail head is very small. At a distance away from the soil nail head, shear stress on the soil nails increases significantly, which indicates that this portion of soil nail is mobilized to resist further sliding and turns gradually to approximately zero at middle where the neutral point situates. At the bottom of both soil nails, the shear stress becomes positive and the lower soil nail sn2 obtains greatly larger stress than upper nail sn1. Such finding once again convinces the reinforcement mechanism by soil nails.

4.4 Failure mode of slope influenced by water flow

Most of the slope failures in Hong Kong occur within May to September. Within this period, heavy rain which may last for many hours are not uncommon. Besides the saturation of the soil, the seepage of water can also create a major effect to the stability of slope which is however not considered in routine analysis and design in Hong Kong. The influence of underground water and water flow is always an important concern in slope stability problems. Infiltration from the watershed or runoff on the ground surface can even cause a thrust to the impacted area and accelerate the failure. After the initiation of the failure, water acts a lubricant and the soil will experience very large movement and finally debris flow will occur. PFC has the particular advantage over continuum based method in that very large scale soil movement or even debris flow can be modeled by distinct element analysis. The models selected in this section take the properties of c=0.65kPa and density of soil particles equal to 1000kg/m^3. In PFC the applied loading can be simulated by velocity field on wall, velocity on particles or external forces. The external forces are simulated by the following procedure: fix all boundary particles and remove the walls; execute one cycle to make the unbalanced force resulting from the wall deletion equal on each boundary particle; apply a force opposite to the unbalanced force to each boundary particle. That is to say, such external forces can only be applied to boundary particles by use of a wall. Such limitation of PFC incurs that the effect of saturation and seepage is not possible to be done by directly applying negative body forces, and applying external forces by velocity field, as an approximate method, is used in the present study. The submerged effect of water is modeled layer by layer while the seepage effect due to water flow is simulated by an inclined velocity field of 5 gradually changing velocities (from 0.01/s to 0.001/s) oriented from the upper far-end of the underground water table. The polygonal line as shown in Figure 4.24 is the approximate imposed water table, and a smooth water table is not easily defined using the approximate numerical modeling method as discussed above.

The progressive failure mechanism due to underground water flow in Figure 4.25 shows that slope failure is accelerated by the water as compared with a simple slope. Unlike the failure (both sliding at the crest and the accumulation at the toe) in simple slope which are influenced only by gravity, the pore water pressure induces a continuous sliding failure on the slope face. The failure zone develops towards the inside of the slope and results in obvious loss of soil grains as shown in Figure 4.25(c) and (d). In the later stage of failure, the driving force tends to be gentle with changed geometry and reduced slope angle and the development of failure becomes slower.

If both the effect of underground water (reduce the effective density only) and water flow (including the seepage force) are taken into consideration, the failure becomes more complicated. The forward movement and upheaval at the toe are quite considerable as shown in Figure 4.26. The seepage force reduces the stability above the water table accompanying with an obvious settlements at the top of the slope. If the velocity (equivalently seepage force) is reduced by half which indicates weaker water seepage force, the entire soil mass is pushed outwards, as shown in Figure 4.27. For the groundwater, the combined effects of buoyance force and water seepage induce deeper failure with large extent above the water table, and obvious zone of shear failure can be found.

For the effective stress on the failure surface, smooth and relative stable normal and shear stresses at the crest and decreasing normal and shear stresses at the toe can be found as shown in Figure 4.28. The seepage force from the water flow induces buoyance force to the soil and reduces the effective stress, so the stress decreases as the time steps increase. Such phenomenon demonstrates that the water does not simply reduce the strength by reducing the effective stress, but the seepage force can greatly magnify the instability of the whole slope.

4.5 Conclusions and Discussions

This chapter is mainly focused on the failure mechanism of slope under the action of self weight, soil nail and water flow. It is found that for a slope with cohesionless soil, failure firstly occurs at the crest of the slope, and the failure gradually extends to the base of the slope and finally the slope angle will be equal to the friction angle of soil. The failure is generally caused by soil sliding where a precise slip surface cannot be found, and this is a typical surface slope failure. Considering the overall particles flow will reveal that the downward movement of the particles at the crest induces tensile failure, and tension crack may also be found at the crest of slope. The deposition of the particles at the toe causes the failure in the forms of sliding out and upheaval; and the area in the middle of the slope actually turns into a shear failure zone due to the continuous sliding of soil. When the cohesive strength is relatively high, the overall instability can be reduced and the displacement is limited. The cohesive strength is hence an important factor in slope stability which is actually a well-known fact. In Hong Kong, the soil cohesive strength is usually controlled to a threshold limit even the soil tests may indicate a very high cohesive value. This practice is adopted because of the doubt on the long term cohesive strength of soil and the factor of safety is rather sensitive to the cohesive strength of soil. From this study, it seems that this practice is reasonable for Hong Kong where there are many slope failures each year.

Soil nails can effectively reinforce the slope stability, especially when nail head is used in the numerical analysis, and the overall stability is greatly enhanced. Soil nail provides the resistance to soil movement by mobilizing the shear strength along the nail and massive movement of soil is restrained and limited. The stress field is also more stable under the action of soil nails. Failure for soil nailed slope is hence generally comprised of the tensile failure at the crest and the shear failure at the base.

The effect of water flow in slope stability problem by PFC is more complicated in nature. The basic failure mechanism is similar to that of a simple slope: failure begins from the crest of slope due to gravity and extends to the middle of slope and then the toe. The sliding mass and accumulated particles can also be found for the case with water flow. On the other hand, water flow results in a thrust pushing the soil mass above the water table outwards with an obvious decrease in the stability of the slope and extended failure zone.

To sum up, by the use of the distinct element method, it is found that slope failure occurs firstly at the crest because of insufficient resistance to driving forces like gravity or combined influence of gravity and water. The soil particles slide continuously and enlarge the extent of failure to the lower part of the slope and eventually sliding out at the toe. Sliding out can further decrease the support to the upper soil mass and promote the whole failure, especially in the cases where water takes effect. The stability of the toe is hence also an important factor in maintaining the overall stability of a slope. The progressive failure of a slope is clearly investigated by the use of DEM which is not possible for LEM or SRM. On the other hand, it is very difficult to obtain a nice stress distribution by DEM, as the local results can fluctuate significantly in DEM. The use of average results will give a better picture about the stress distribution within the failed soil mass, but there will be a lack of accurate local results from the use DEM. Another major limitation of DEM is that the results are only qualitative instead of quantitative. Furthermore, the time required by DEM for computation is excessively long, and each example in the present chapter can takes several days to more than a week for the analysis. For design purpose, the use of LEM and SRM appears to be unavoidable at present.

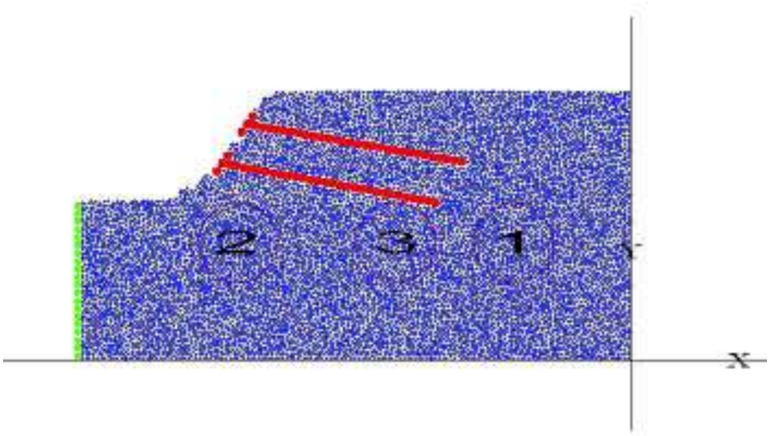

Figure 4.1 Basic numerical model of soil-nailed slope in PFC (α=60°, with nail head)

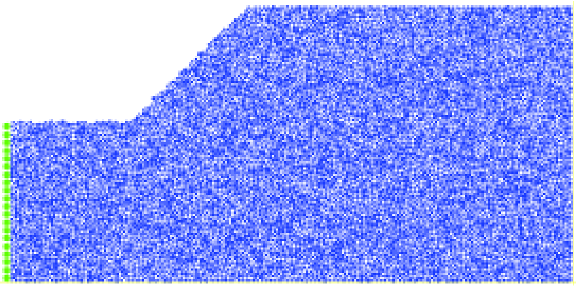

(a)Initial state of slope

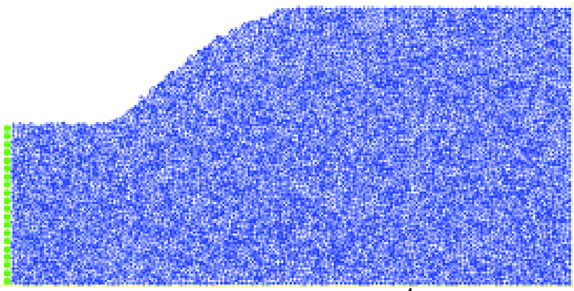

(b) 5x10^4 step

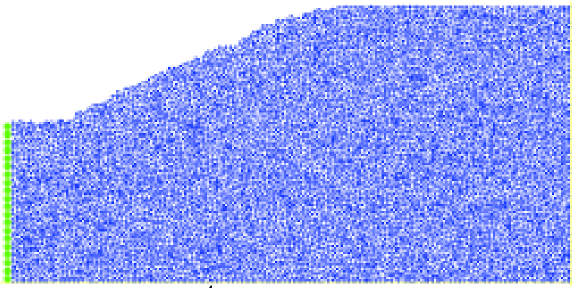

(c) 30x10^4 step

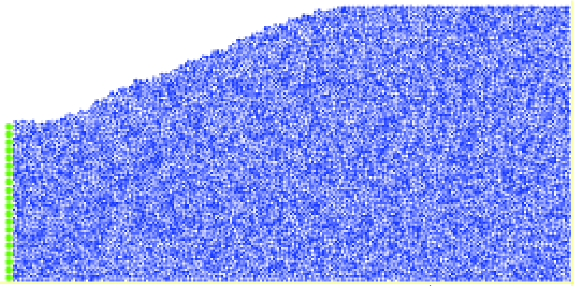

(d) 120x10^4 step

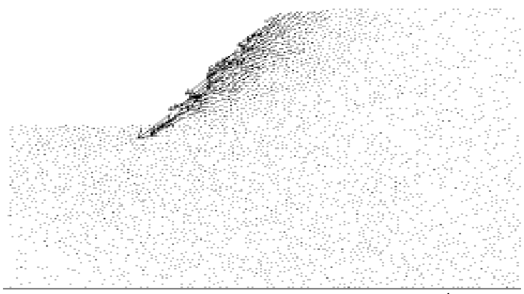

(e) displacement vector at120x10^4 step

Figure 4.2 Failure development of simple slope with c=0 and α=45°

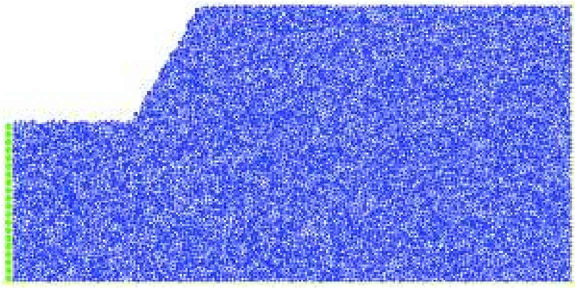

(a) Initial state of slope

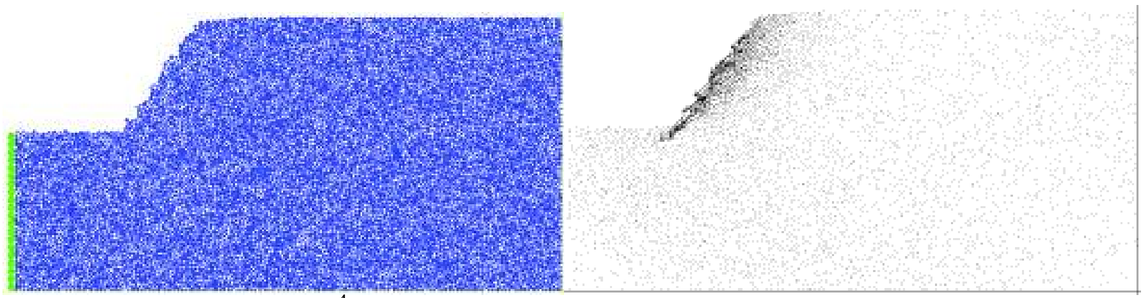

(b) $1x10^4$ step and corresponding displacement vector

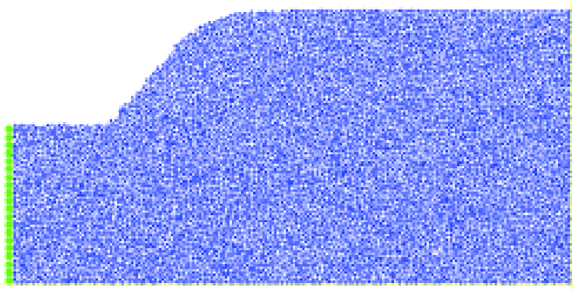

(c) $3x10^4$ step

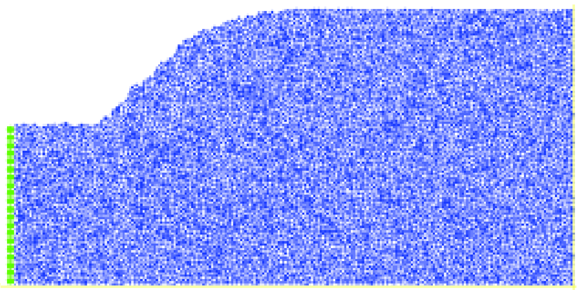

(d) $5x10^4$ step

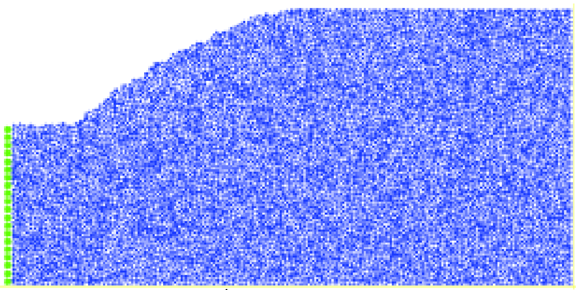

(e) $10x10^4$ step

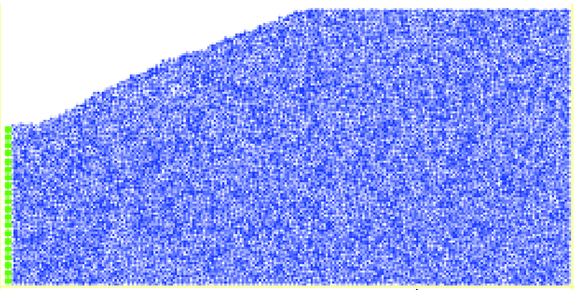

(f) $30x10^4$ step

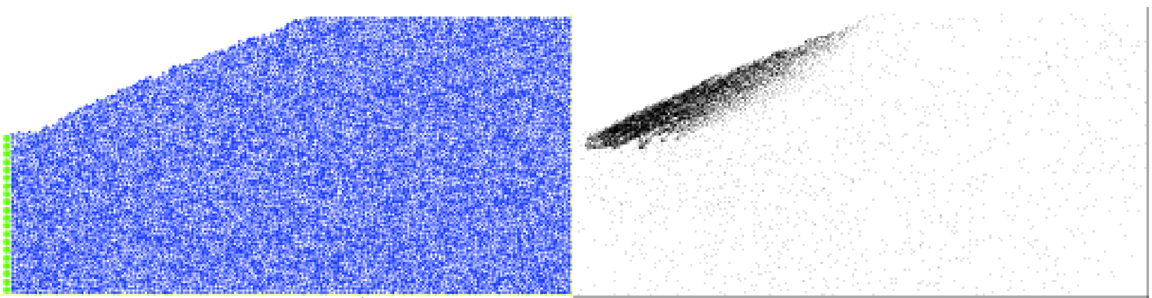

(g) $200x10^4$ step and corresponding displacement vector

Figure 4.3 Failure development of simple slope with c=0 and α=60°

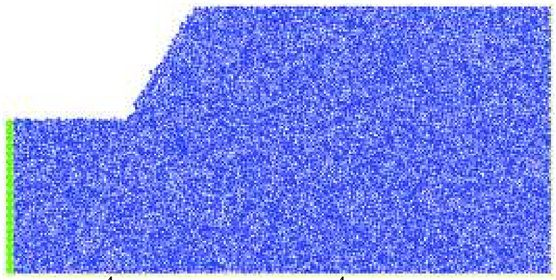

$1x10^4$ step ~ $200x10^4$ step Stable

Figure 4.4 Failure development of simple slope with c=5kPa and α=60°

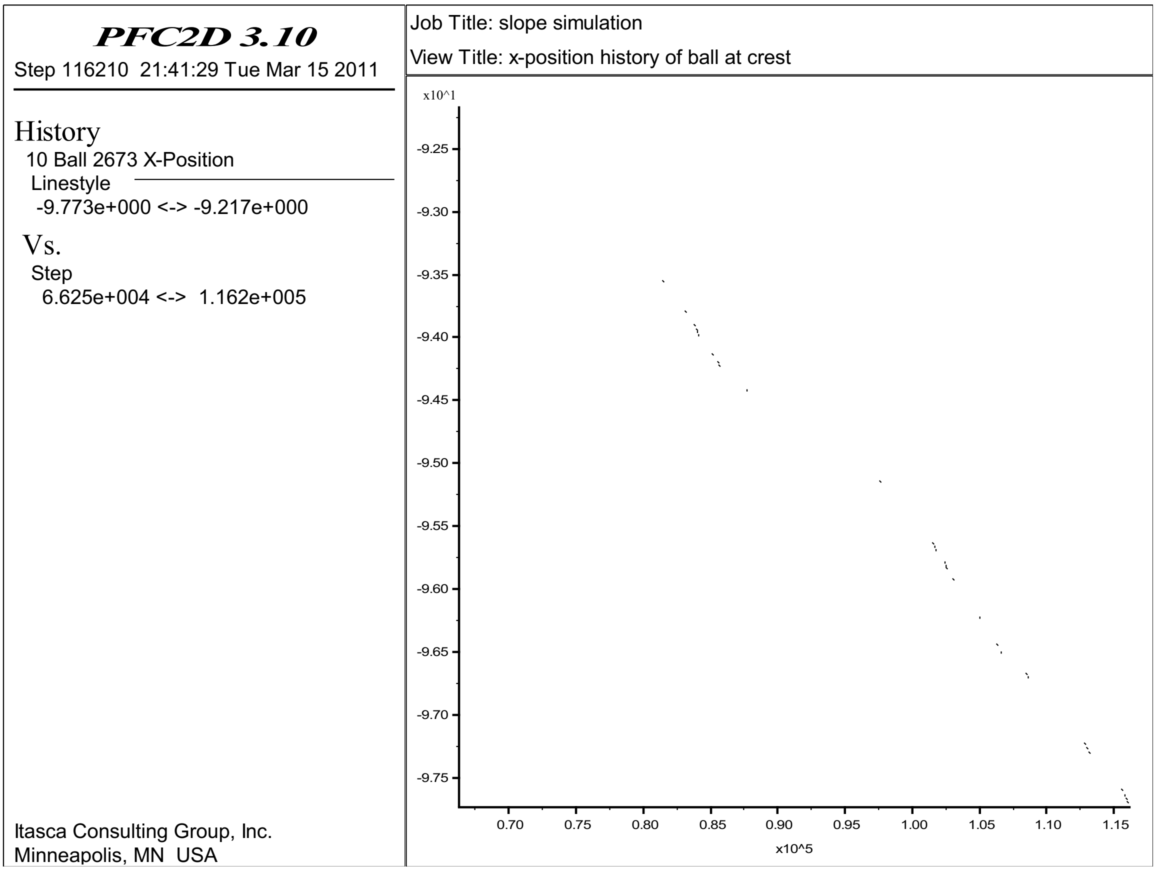

Figure 4.5 X-position history of ball 2673 at crest (c=0, α=60°)

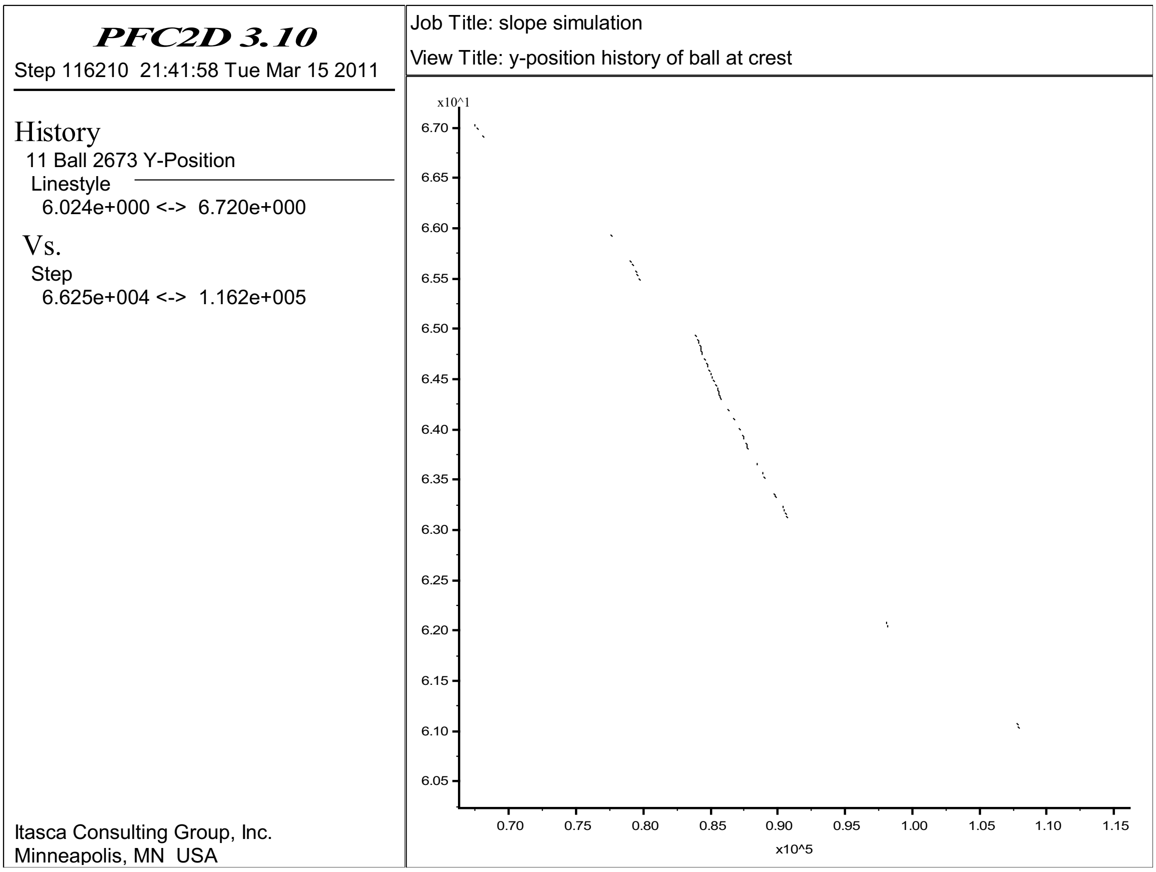

Figure 4.6 Y-position history of ball 2673 at crest (c=0, α=60°)

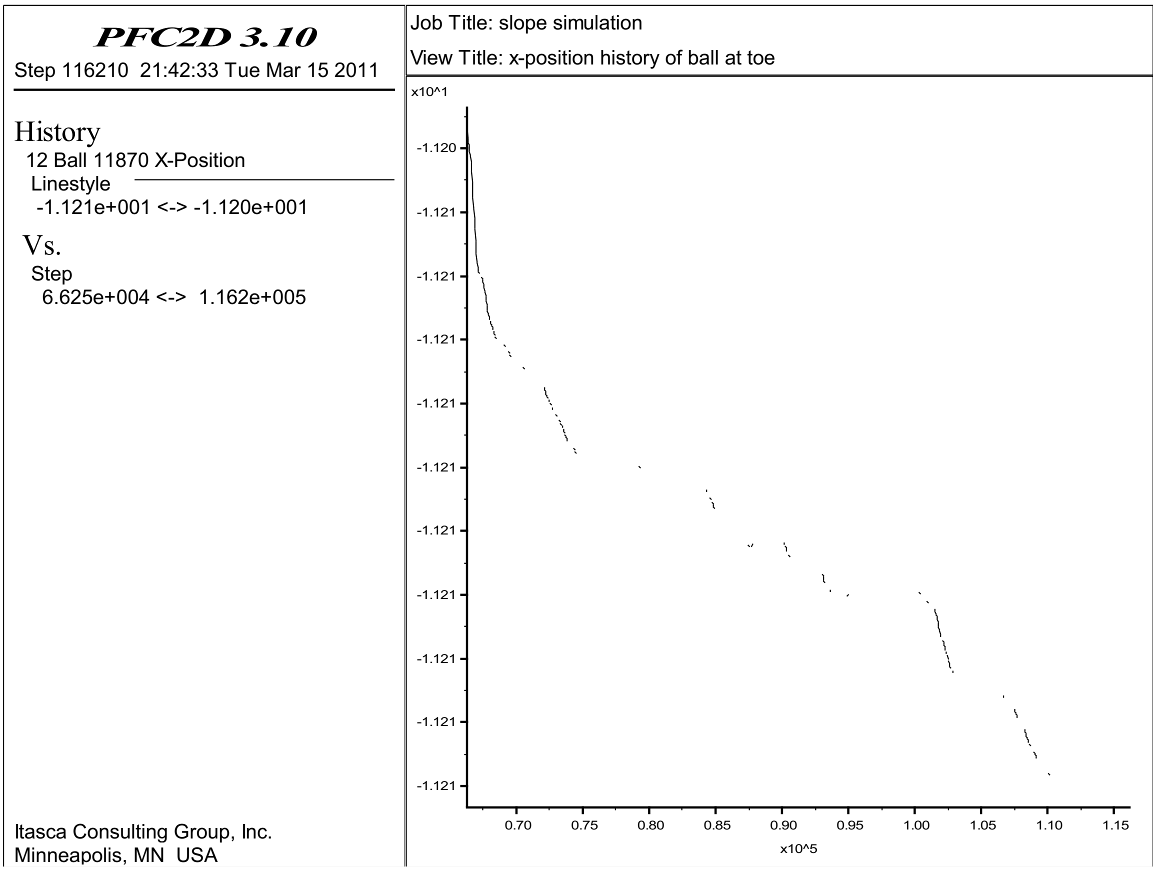

Figure 4.7 X-position history of ball 11870 at toe (c=0, α=60°)

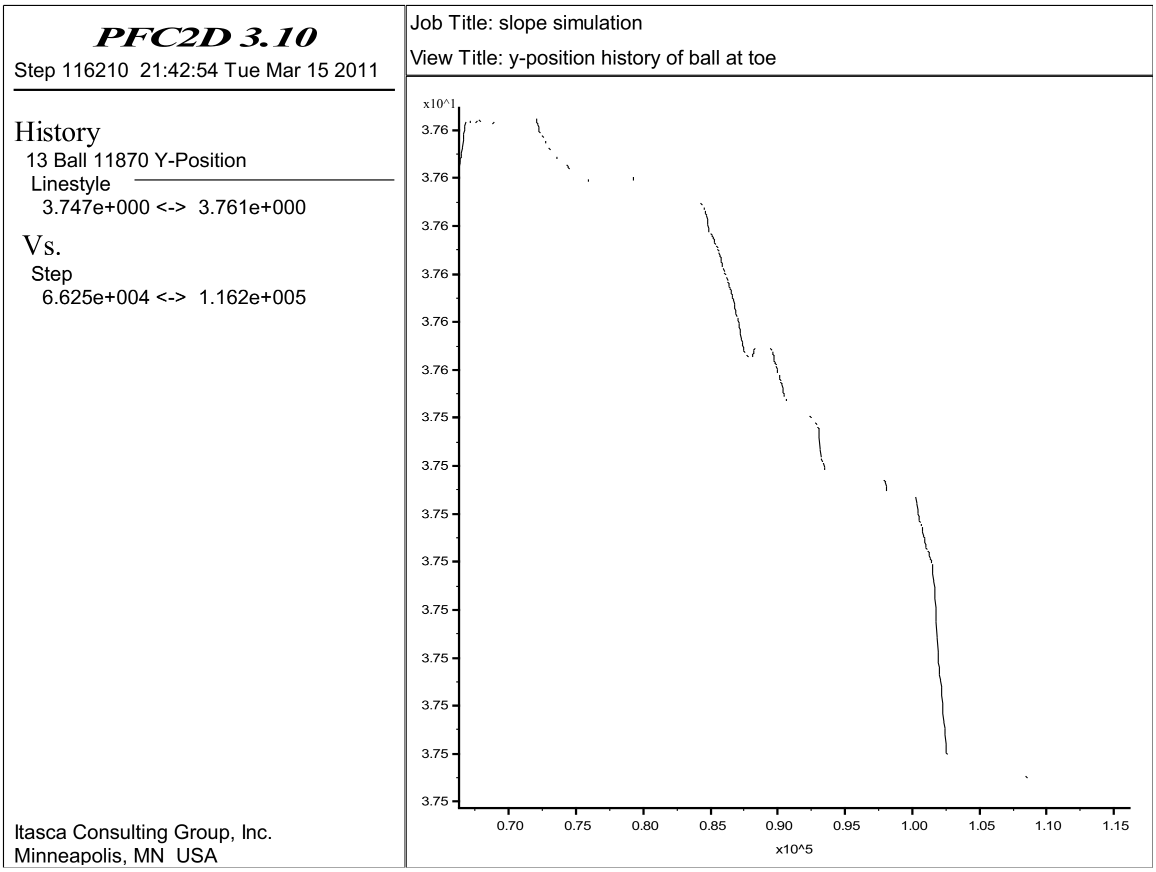

Figure 4.8 Y-position history of ball 11870 at toe (c=0, α=60°)

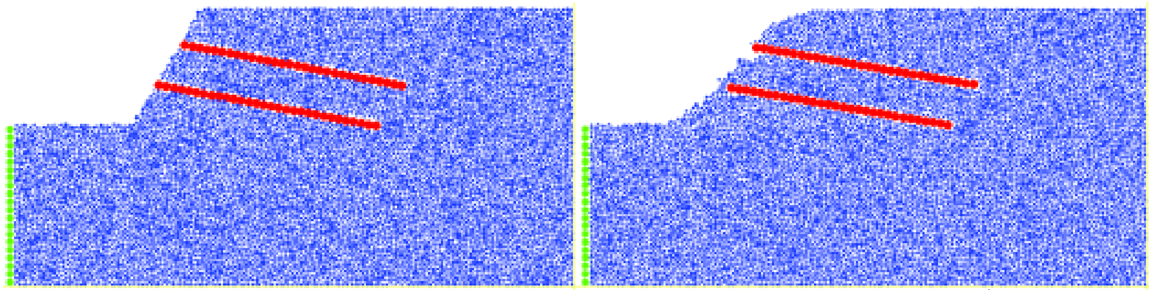

(a)Initial state of slope (b) 5×10^4 step

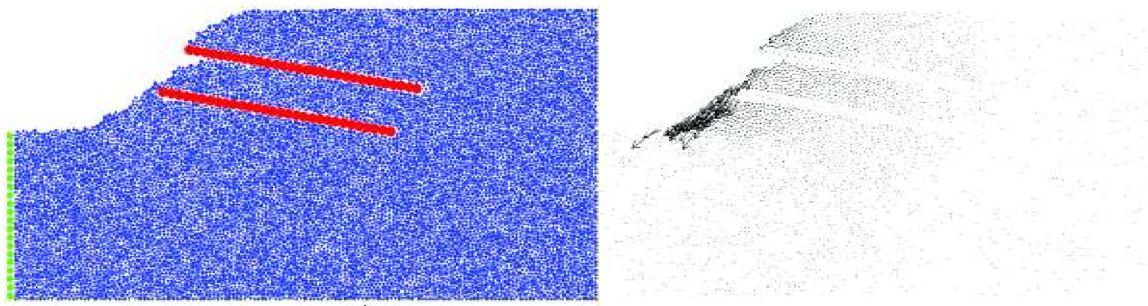

(c) 200×10^4 step and corresponding displacement vector

Figure 4.9 Failure development of nailed slope with c=0 and no nail head

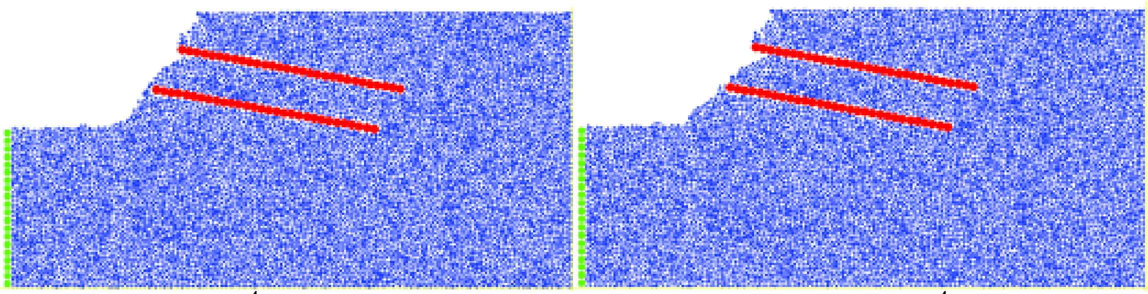

(a) $3x10^4$ step (b) $10x10^4$ step

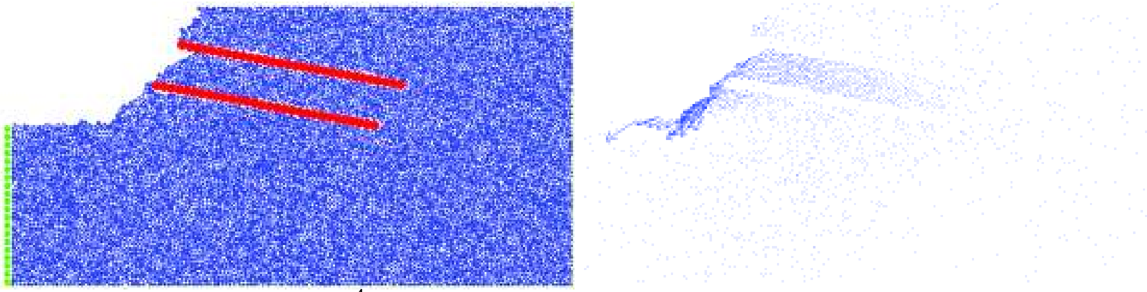

(c) $200x10^4$ step and corresponding displacement vector

Figure 4.10 Failure development of simple slope with c=2kPa and no nail head

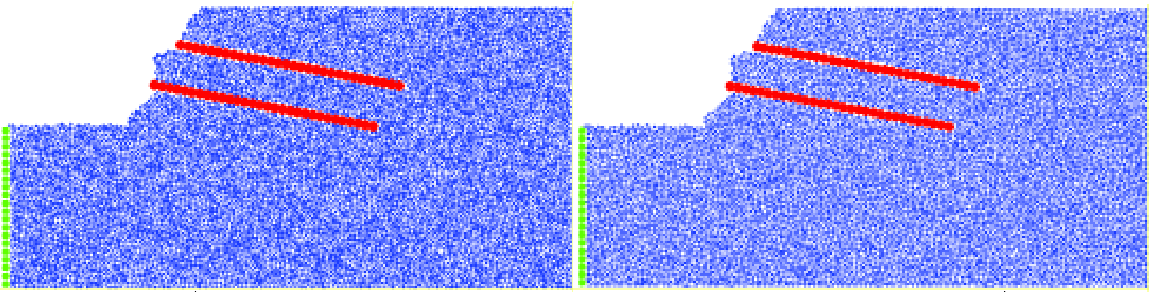

(a) $3x10^4$ step (b) $200x10^4$ step

Figure 4.11 Failure development of simple slope with c=5kPa and no nail head

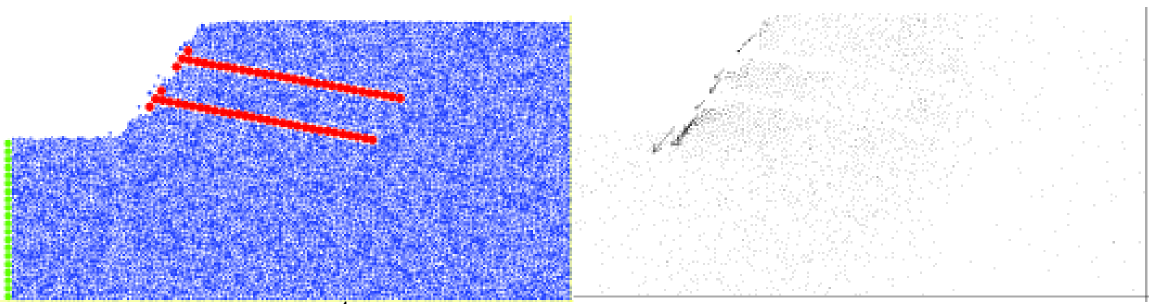

(a) $1x10^4$ step and corresponding displacement vector

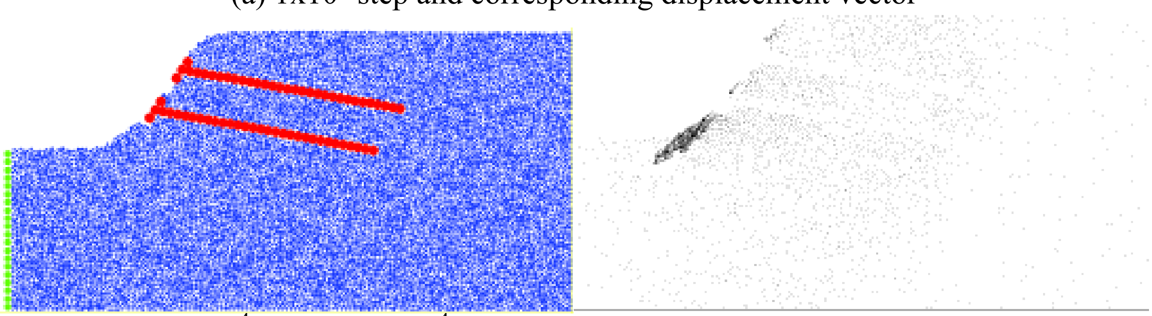

(b) $5x10^4$ step ~ $200x10^4$ step and corresponding displacement vector

Figure 4.12 Failure development of simple slope with c=0 and nail head

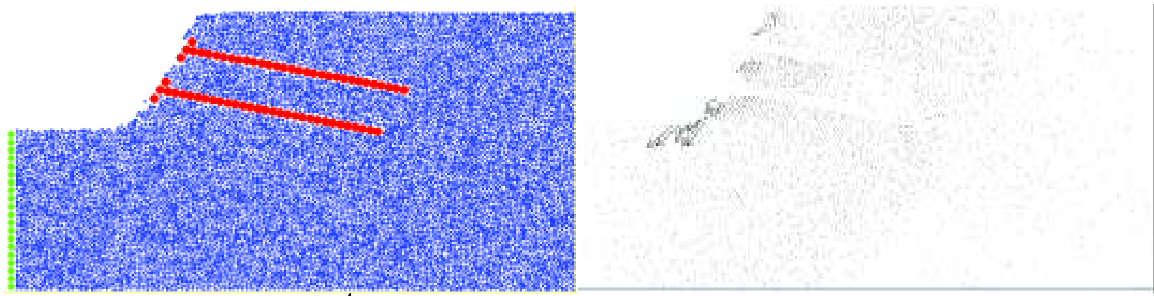

(a) 1×10^4 step and corresponding displacement vector

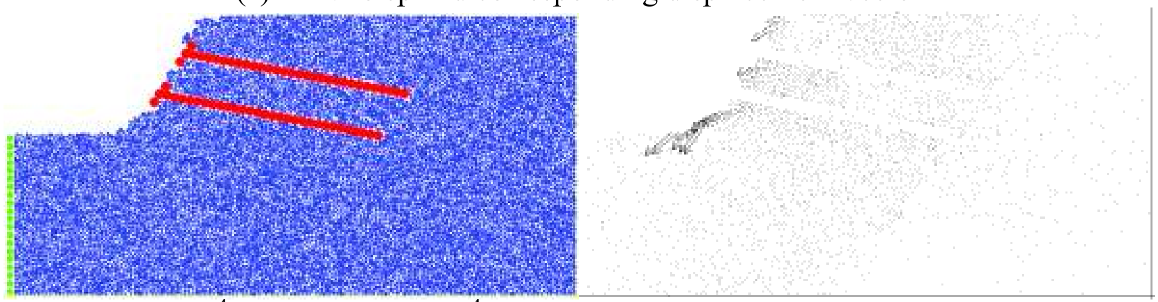

(b) 3×10^4 step and ~ 200×10^4 step and corresponding displacement vector

Figure 4.13 Failure development of simple slope with c=2kPa and nail head

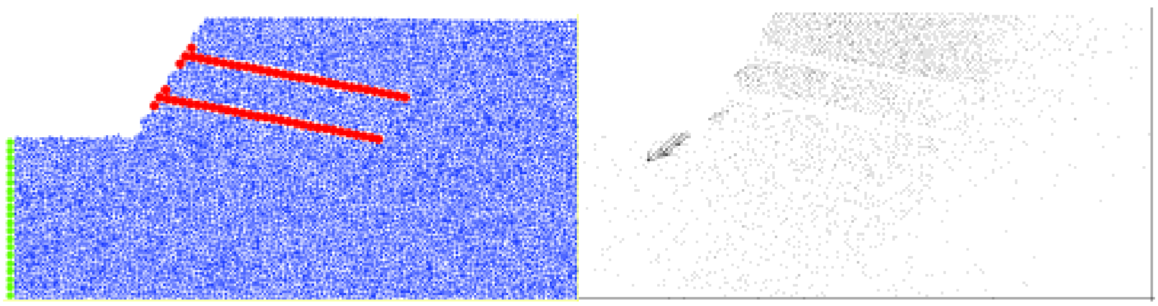

Figure 4.14 Failure development of simple slope with c=5kPa and nail head (very stable)

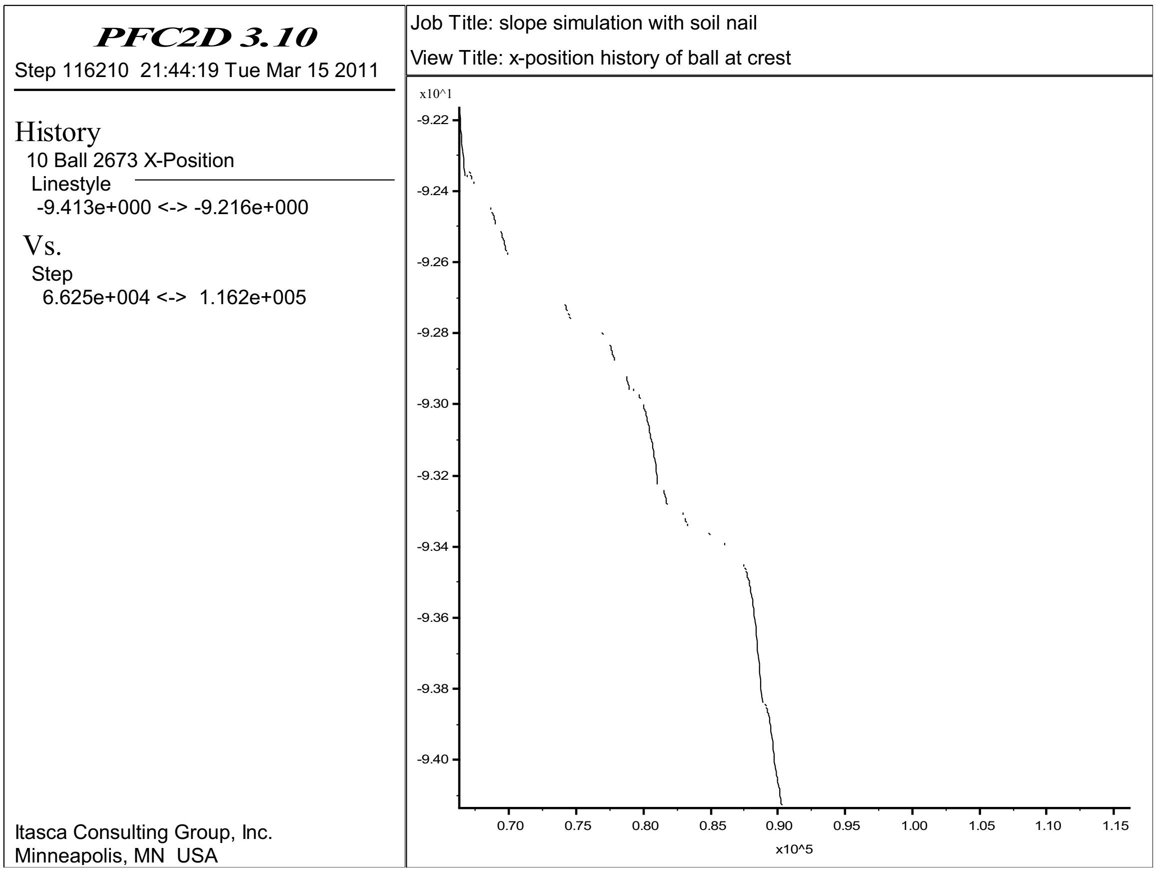

Figure 4.15 X-position history of ball 2673 at crest (c=0, soil nailed with head)

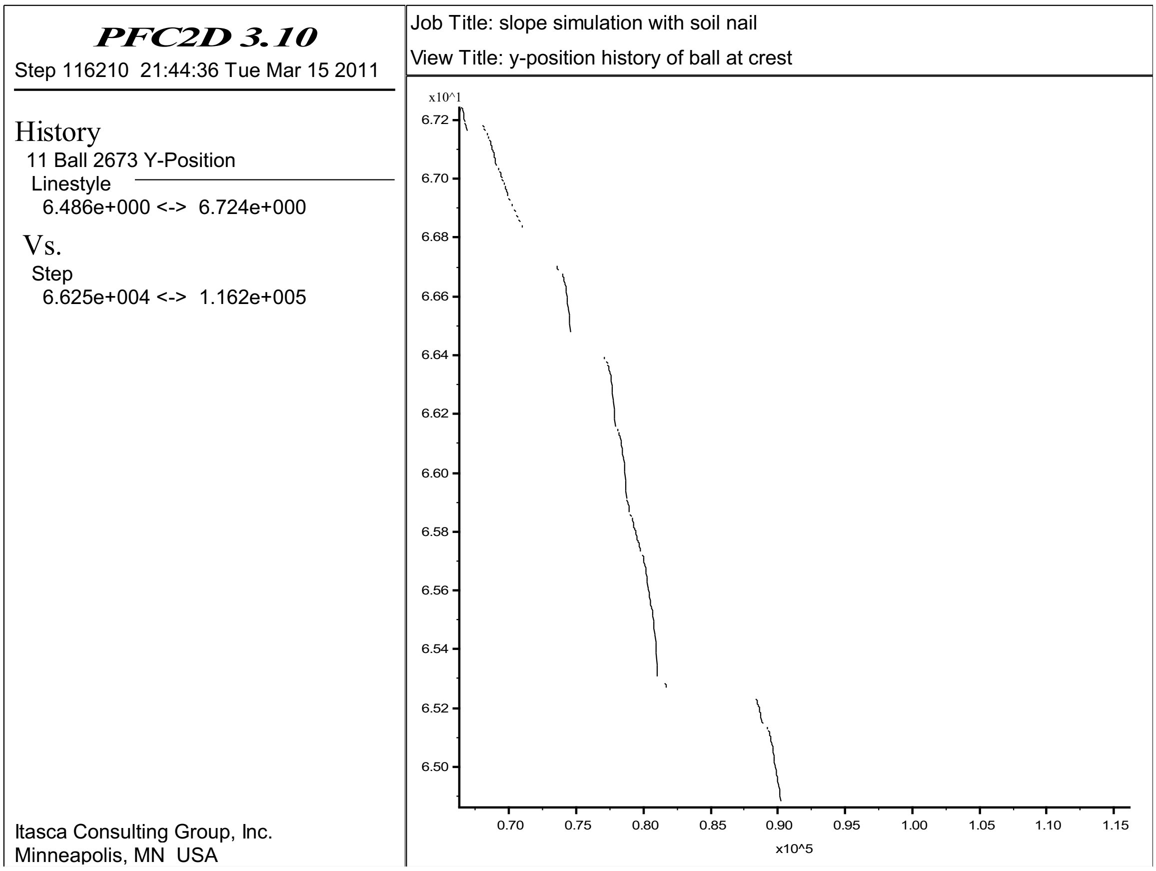

Figure 4.16 Y-position history of ball 2673 at crest (c=0, soil nailed with head)

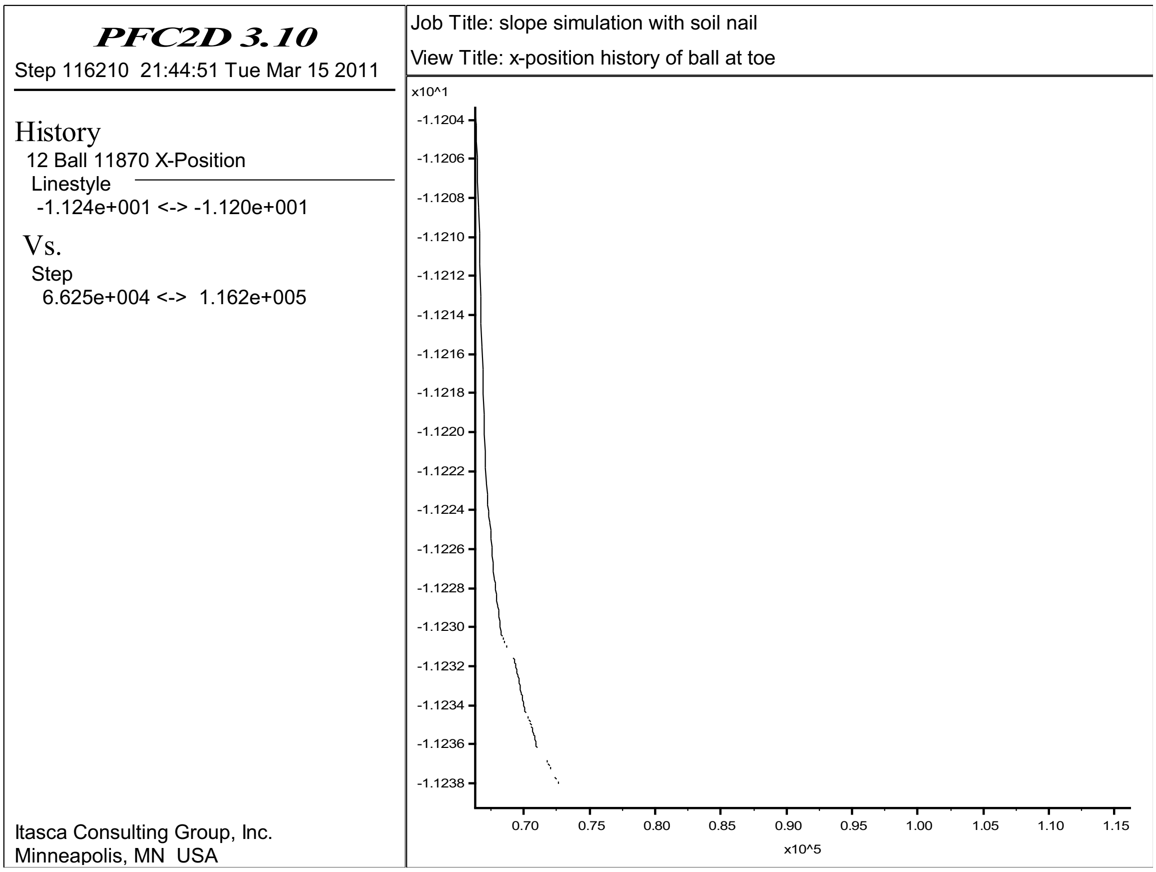

Figure 4.17 X-position history of ball 11870 at toe (c=0, soil nailed with head)

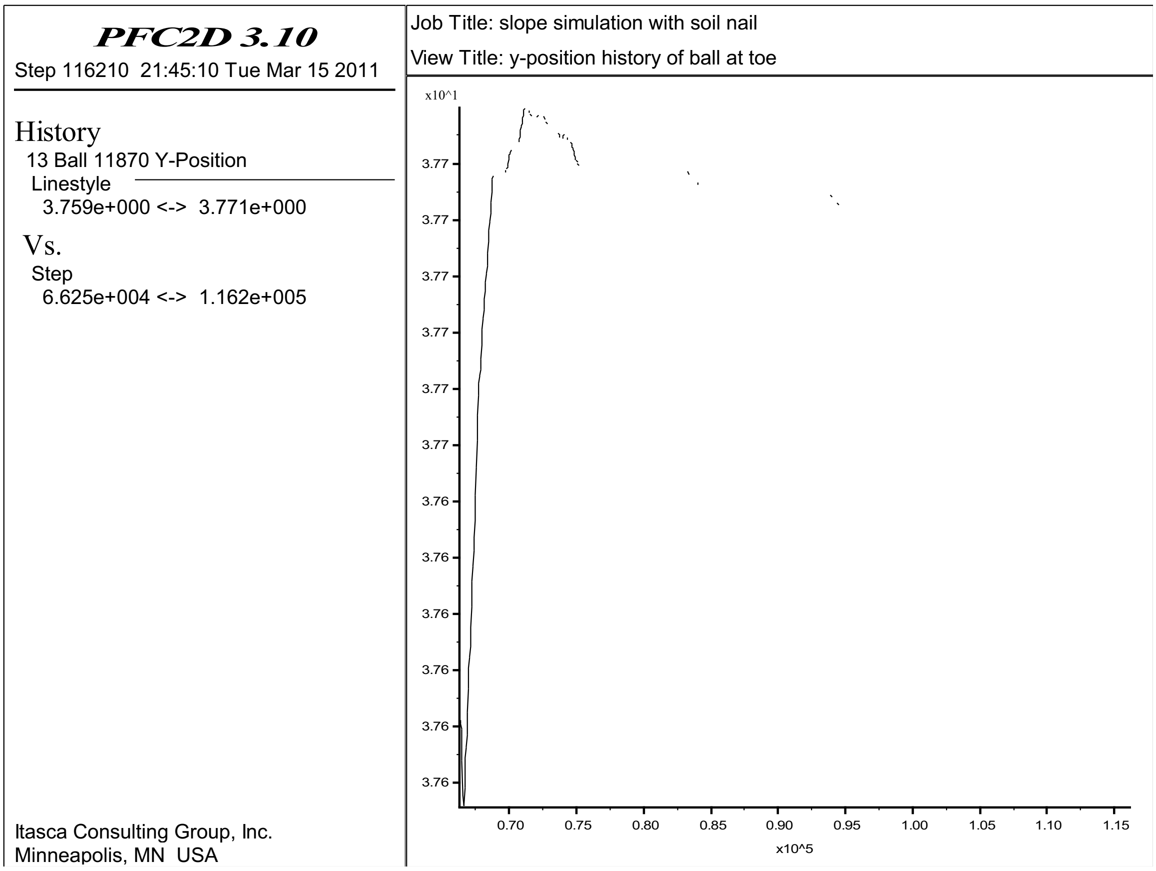

Figure 4.18 Y-position history of ball 11870 at toe (c=0, soil nailed with head)

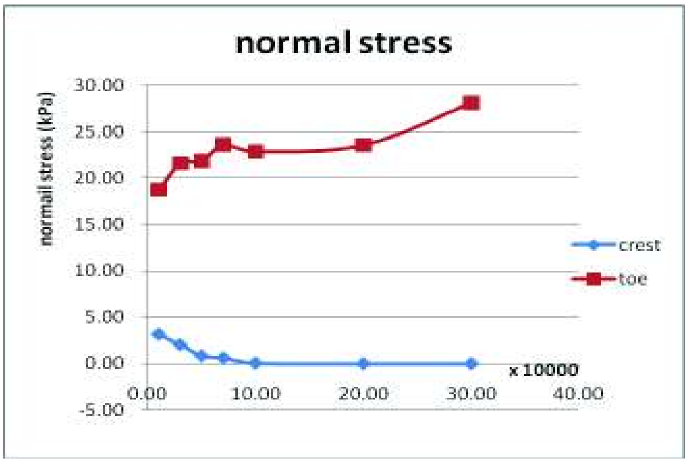

(a) normal stress on failure surface vs. time steps

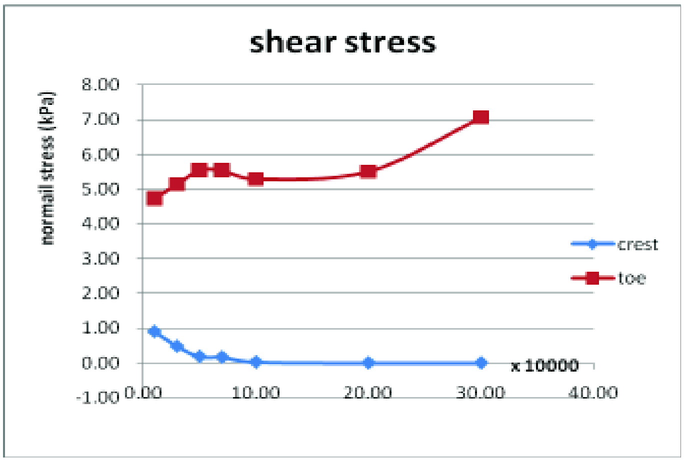

(b) shear stress on failure surface vs. time steps

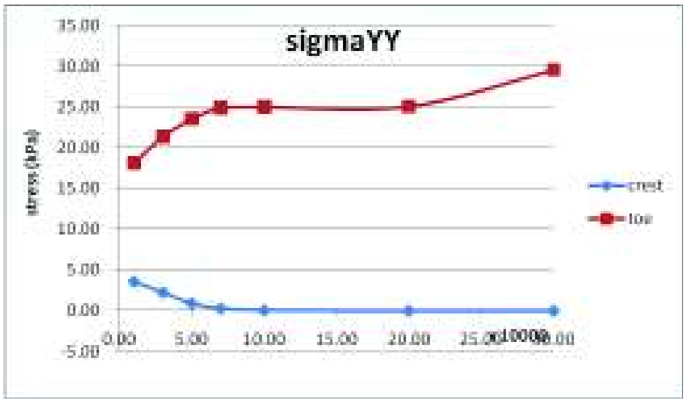

(c) vertical normal stress vs. time steps

Figure 4.19 The stress state of simple sandy slope (c=0)

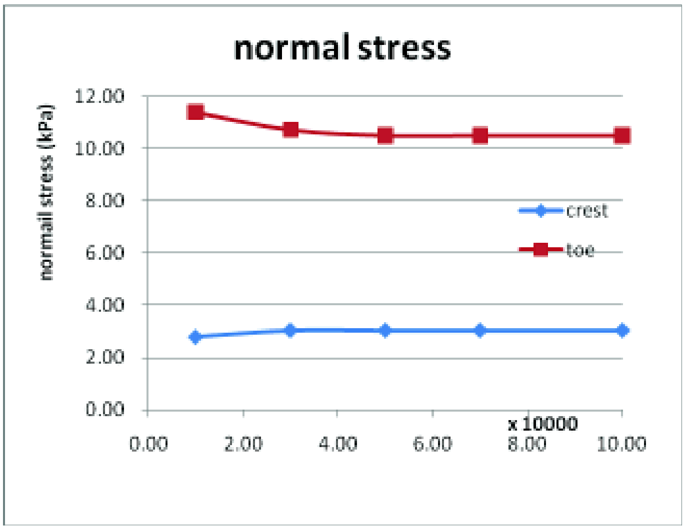

(a) normal stress on failure surface vs. time steps

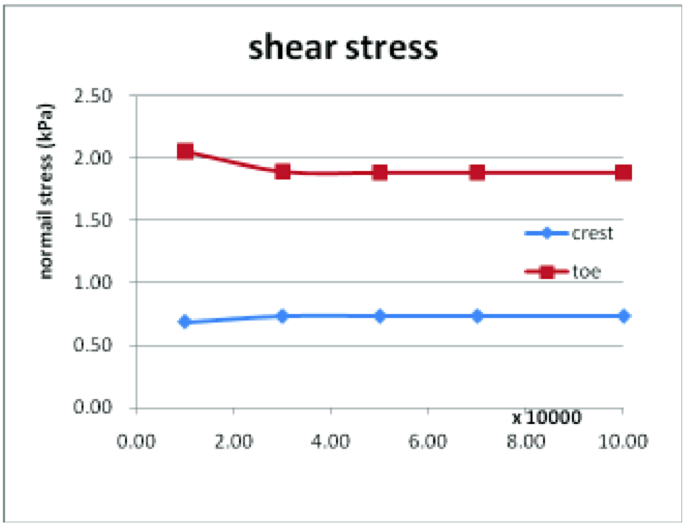

(b) shear stress on failure surface vs. time steps

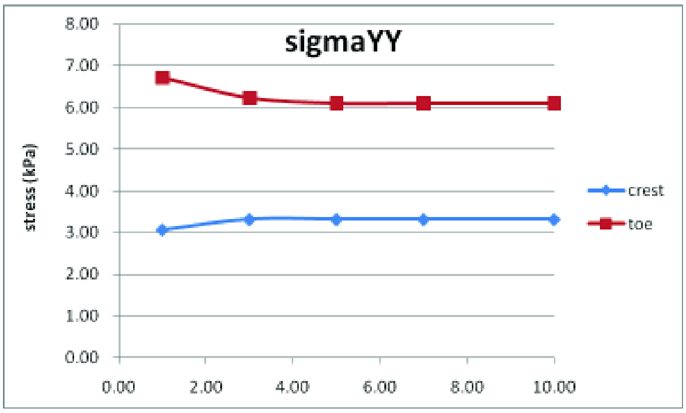

(c) vertical normal stress vs. time steps

Figure 4.20 Stress state of soil-nailed sandy slope (c=0)

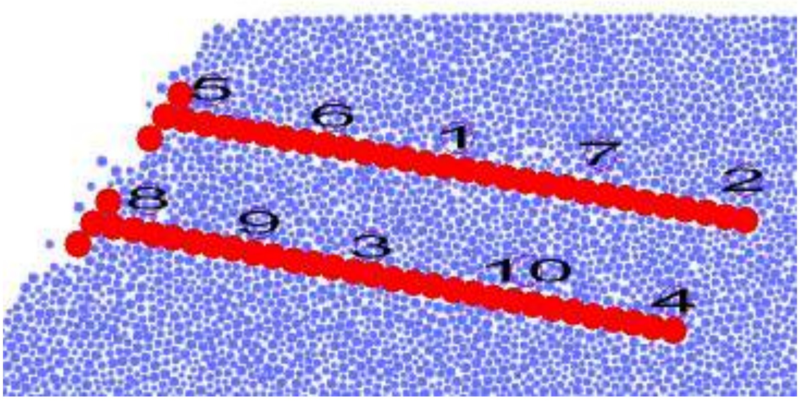

Figure 4.21 Measure circles next to the soil nails

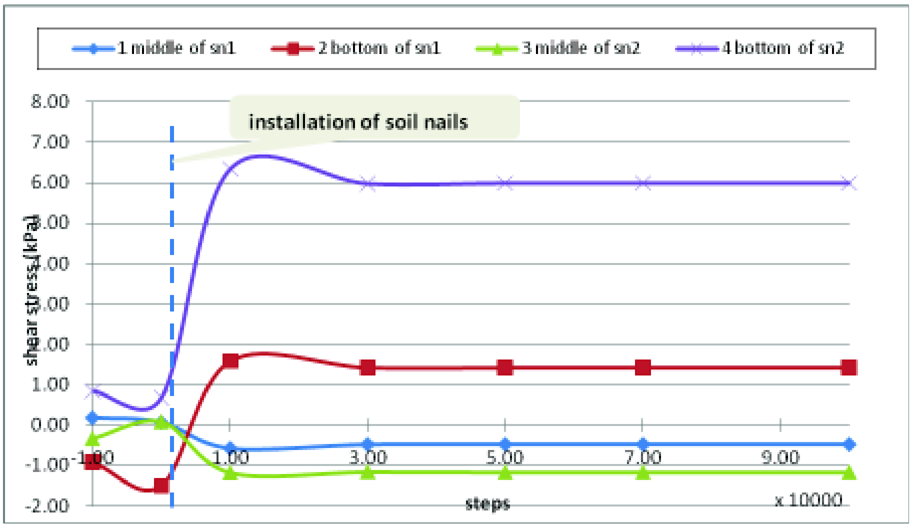

Figure 4.22 Stress analysis of soil nail during failure (c=0)

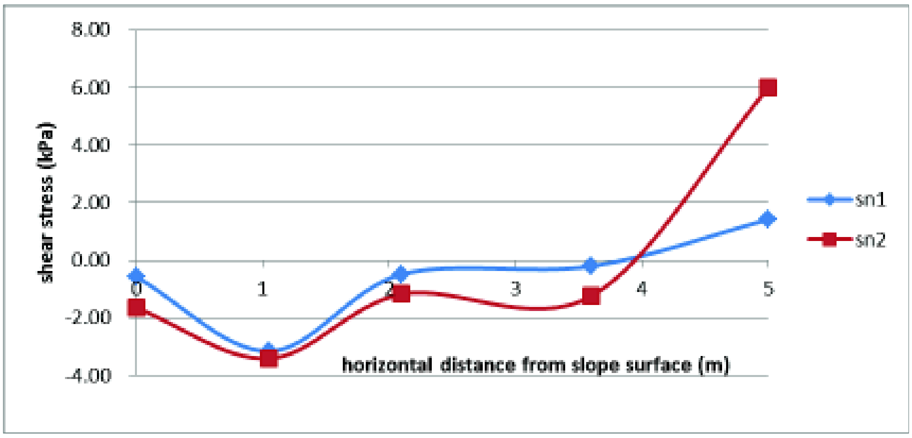

Figure 4.23 Stress analysis along soil nails (c=0)

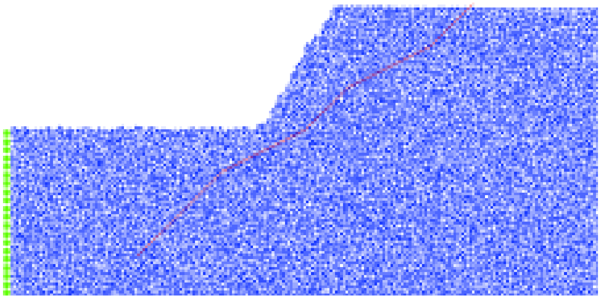

Figure 4.24 Initial state of modeling considering pore water pressure and water flow

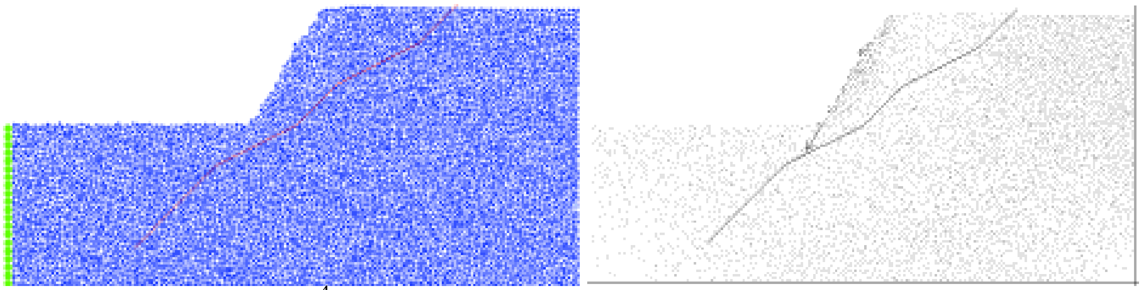

(a) 1×10^4 step Displacement graph

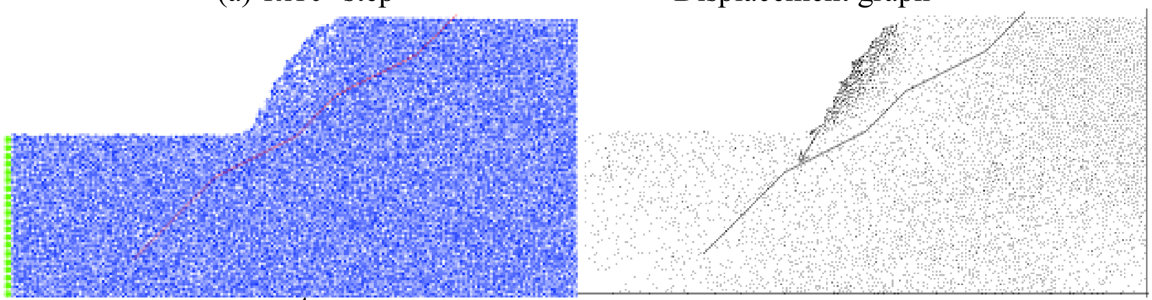

(b) 3×10^4 step Displacement graph

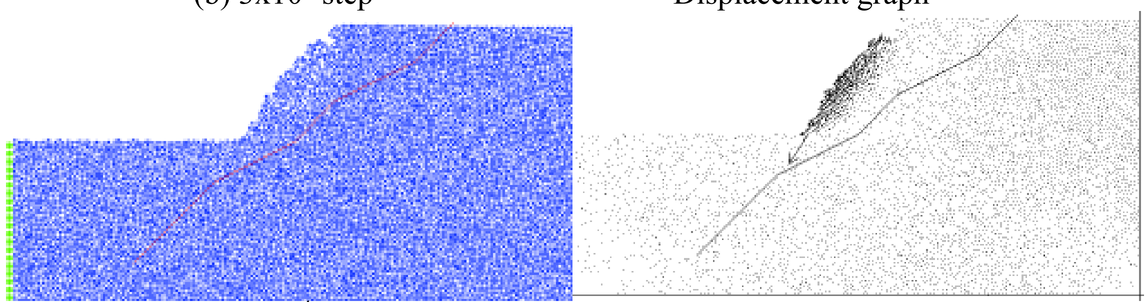

(c) 5×10^4 step Displacement graph

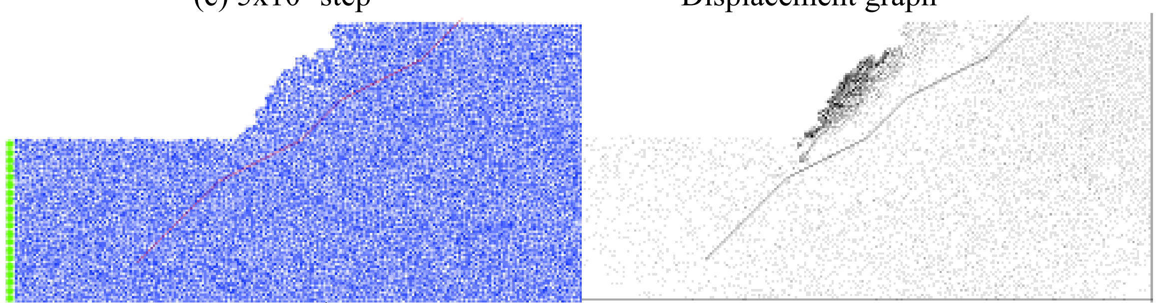

(d) 10×10^4 step Displacement graph

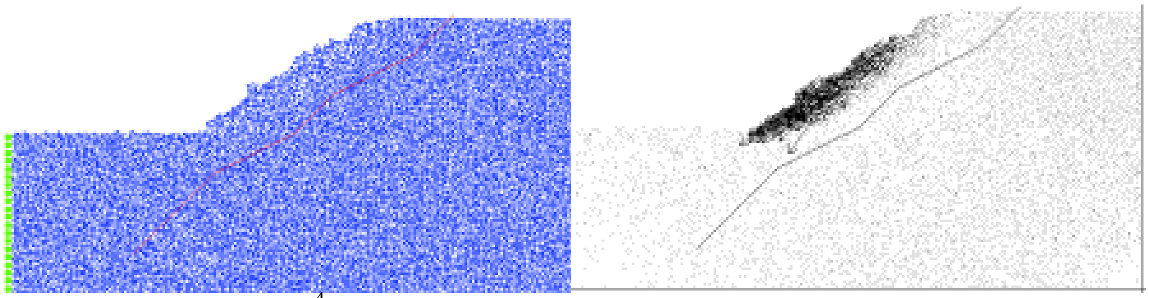

(e) 30x10^4 step Displacement graph

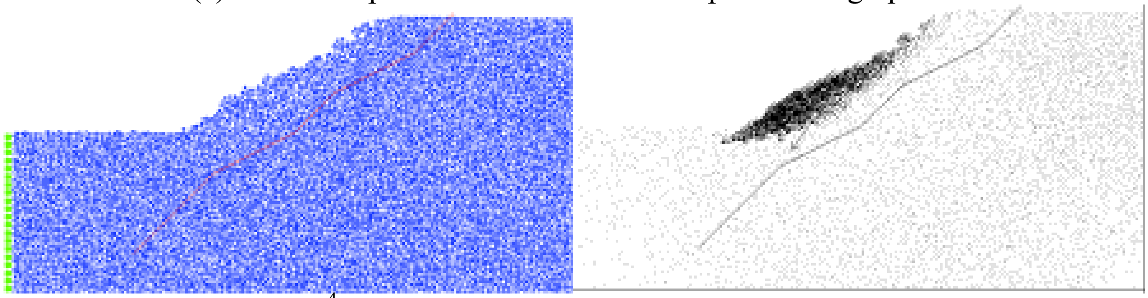

(f) 100x10^4 step Displacement graph

Figure 4.25 Failure development of slope with underground water

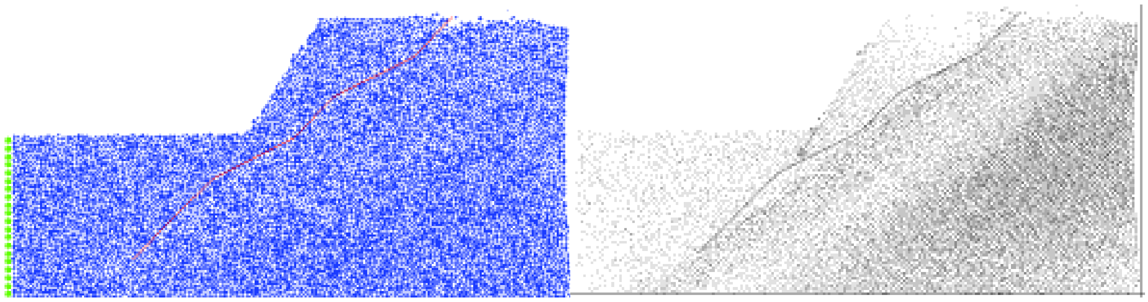

(a) initial state after adding velocity of 5 inclined layers Displacement graph

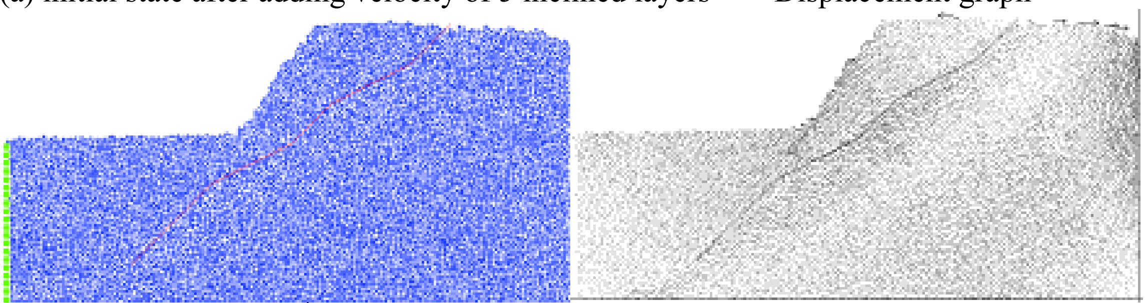

(b) 1x10^4 step Displacement graph

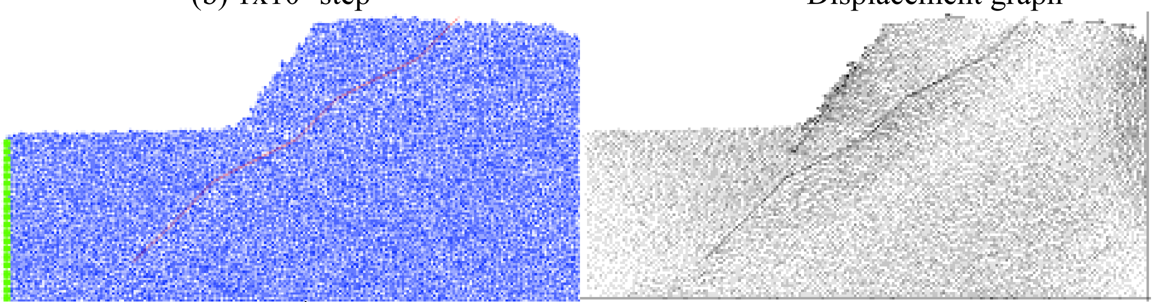

(c) 3x10^4 step Displacement graph

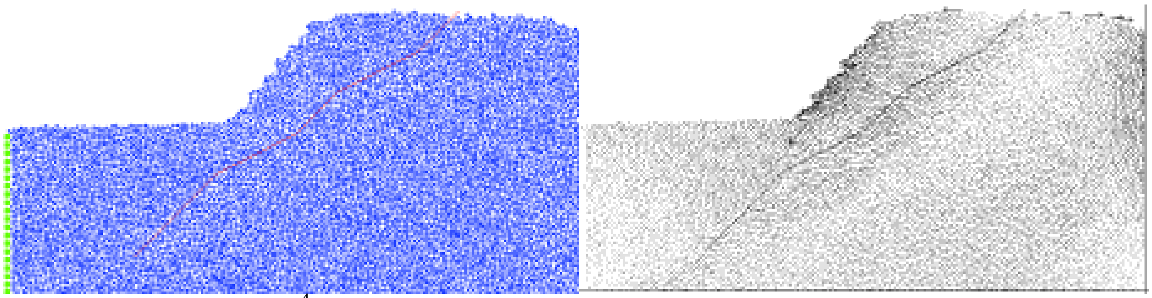

(d) $5x10^4$ step Displacement graph

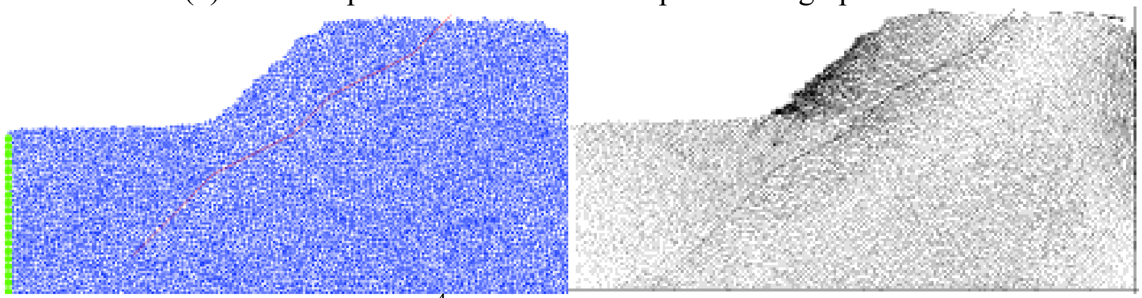

(e) $10x10^4$ step Displacement graph

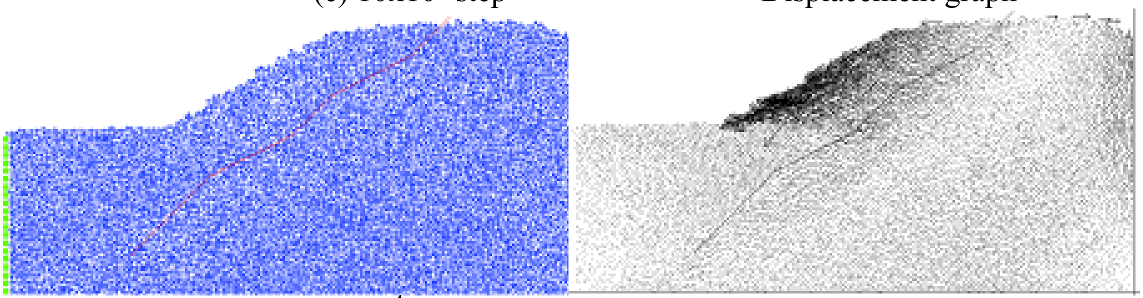

(f) $30x10^4$ step Displacement graph

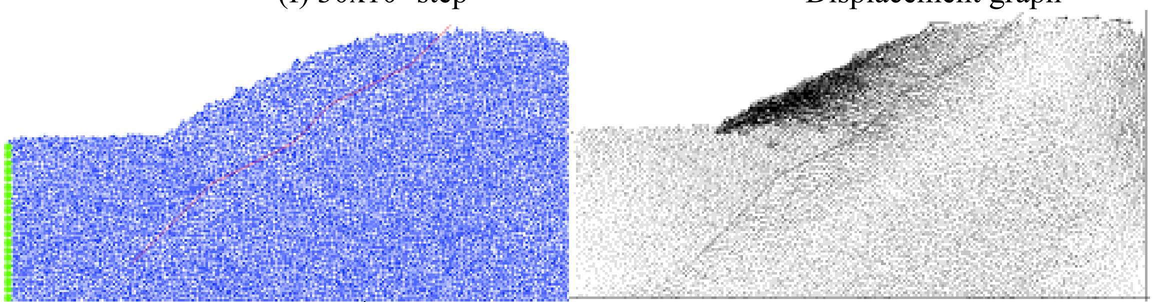

(g) $100x10^4$ step Displacement graph

Figure 4.26 Failure development of slope with underground and water flow

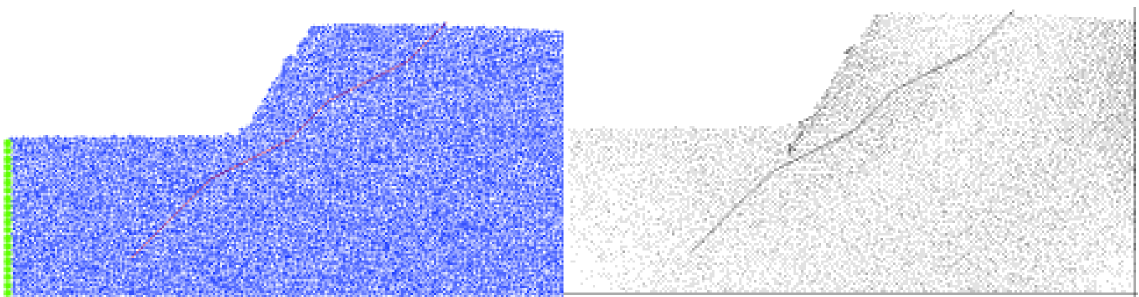

(a) $1x10^4$ step Displacement graph

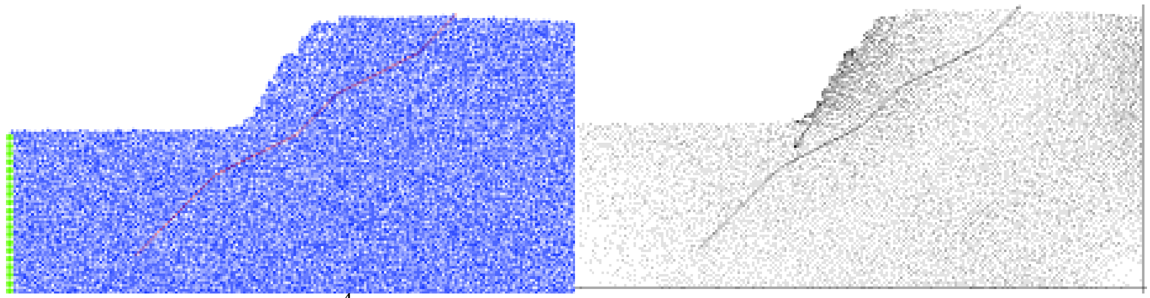

(b) $3x10^4$ step Displacement graph

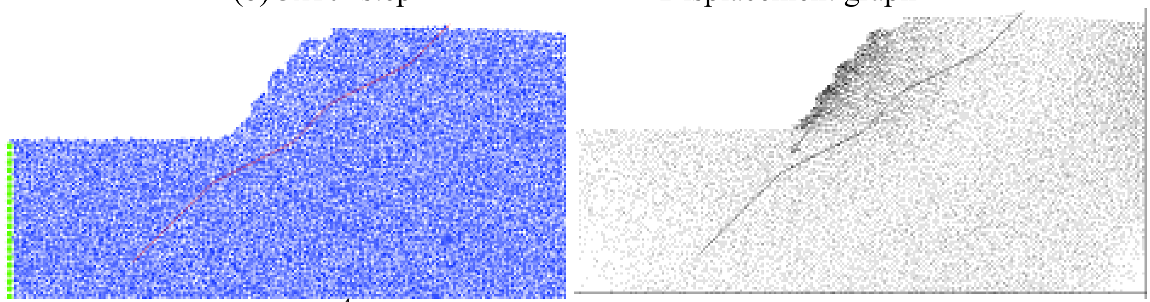

(c) $5x10^4$ step Displacement graph

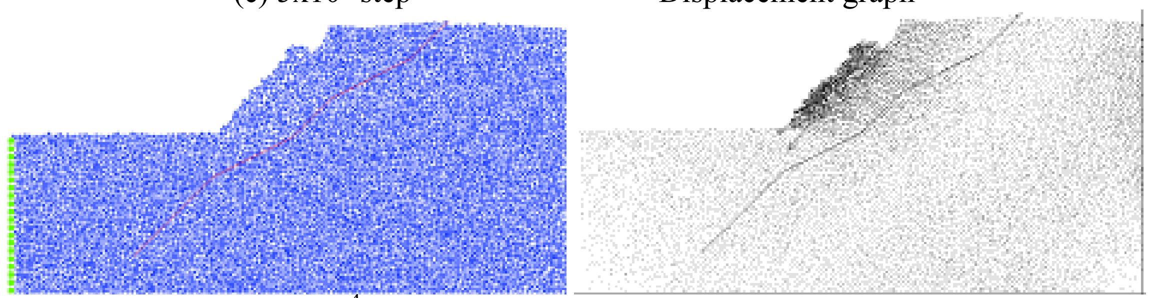

(d) $10x10^4$ step Displacement graph

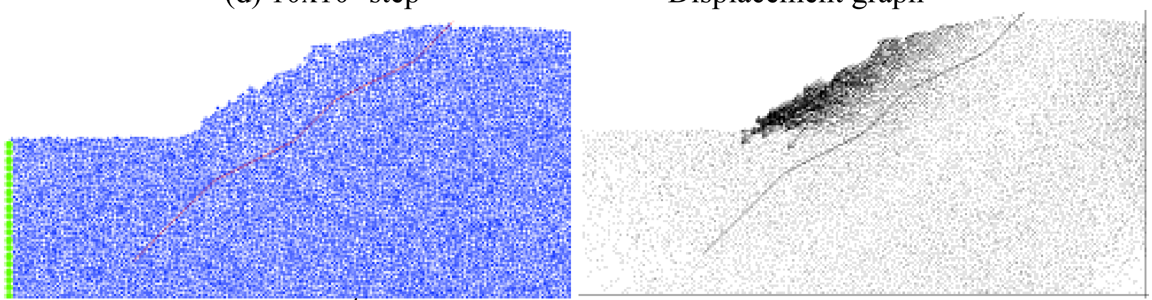

(e) $30x10^4$ step Displacement graph

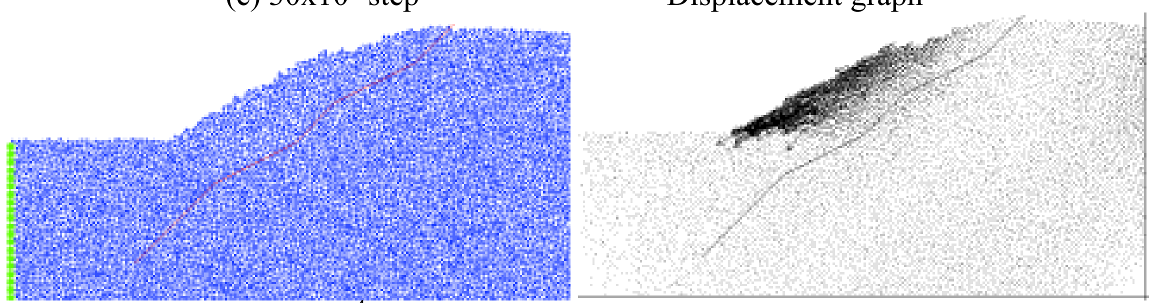

(f) $100x10^4$ step Displacement graph

Figure 4.27 Failure development of slope with underground and water flow (Half velocity)

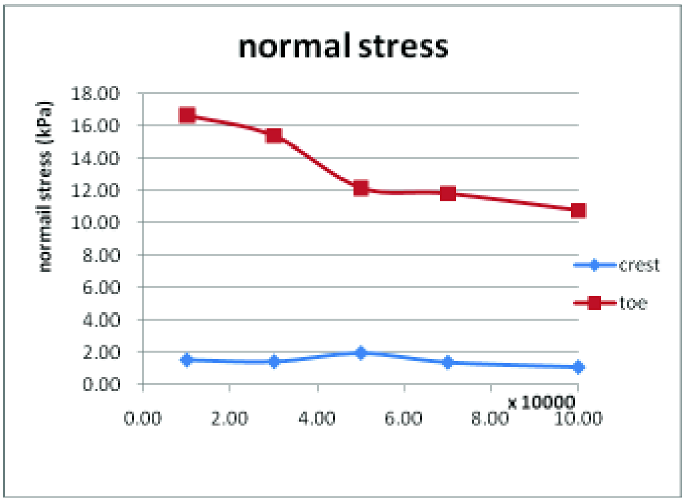

(a) normal stress on failure surface

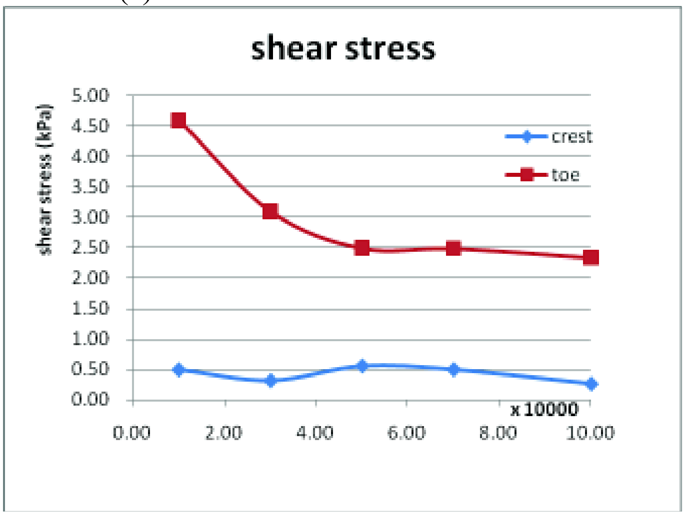

(b) shear stress on failure surface

Figure 4.28 The stress state of slope influenced by water flow (vel=0.01/s)

CHAPTER 5 Study on some Slope Stability Methods, the Problems and New Solutions

5.1 Introduction

Slope stability analysis using the limit equilibrium method is well known to be a statically indeterminate problem. All the slope stability methods must require assumptions on the internal forces or base forces before the problem can be solved. Broadly speaking, there are two major groups of "rigorous" methods in the limit equilibrium analysis: (1) internal variables in form of interslice forces relation or the thrust line locations; (2) boundary stresses in form of base normal forces.

For the first group of methods, the Morgenstern-Price's method (1965) and the Janbu's rigorous method (1973) are the most important formulations. In the Morgenstern-Price's method (1965) which is a method popular to many engineers, the inclination of the total internal force is usually expressed as $\lambda f(x)$, where λ is the mobilization factor while $f(x)$ is a function between 0 to 1 and x (within 0 to 1.0) is the ratio of the distance of any section from the left end of the failure surface to the total horizontal length of the failure surface. Since only the global moment equilibrium is used in the Morgenstern-Price's formulation (1965), the back-calculated thrust line may lie outside the soil mass which is not possible, and this situation is equivalent to the violation of local moment equilibrium. In the Janbu's method (1973), the distance between the thrust line and the base of slip surface is assumed to be known while the local moment equilibrium is used in the formulation. By taking moments about the centre of the base of each slice, the local and overall moment equilibrium is implicitly satisfied, and the interslice shear forces can be calculated. As the problem is actually over-specified by 1 unknown, the moment equilibrium of the last slice is not checked or enforced in the Janbu's rigorous method (1973), hence true moment equilibrium is still not maintained in this method. Besides these two methods, there are many other variants of slope stability methods which are usually based on these two important slope stability formulations. As long as a statically admissible stress field is defined over a domain, the solution will be a lower bound of the ultimate limit state. In this respect, LEM is an approximate but not an exact lower bound solution (Chen 1975), as force (lumped the stresses over a finite length) instead of stress at each region is considered in the classical LEM.

In the second group of method, the variational principle by Baker and Garber (1978) using the base normal stress distribution along the potential slip surfaces is the representative method. The minimum factor of safety with respect to the base normal force as well as the location of the failure surface is then determined by the variational principle. It should be noted that in the Baker and Garber formulation (1978), the failure mass bounded by the potential slip surface and the ground surface is not divided into slices, and complete equilibrium can be achieved using this group of method which is not possible with the first group of method. The second group of method is however difficult to be adopted when the geometry or the ground/loading conditions are complicated.

In the SRM, the major assumption is the use of flow rule. Since there is practically no restraint to the soil at the surface of the slope, Griffiths and Lane (1999) suggested that non-associated flow rule can be a good approximation in the analysis. For soil under the ground surface, the use of the flow rule is an open question, and engineers either adopt non-associated flow rule (more common approach) or associated flow rule in the whole analysis. In this respect, SRM is not actually better than the LEM. SRM also suffers from the difficulties in defining the ultimate condition and the slip surface in complicated problems which are discussed by Cheng et al. (2007) and Wei and Cheng (2010).

Some of the important questions about the fundamental problems of the LEM as raised by the engineers include:

1. The meaning of failure to converge during stability analysis – this is particularly serious for slopes with external loads and soil reinforcement, as the external loads and soil reinforcement may create local stress concentration so that the problem is difficult to be defined by a simple interslice force function.
2. Choice of $f(x)$ for some special problems where $f(x)$ is important in the analysis.
3. For cases where $f(x)$ is important, there will be a wide range of results based on different classical stability formulations, and the acceptability of the result is difficult.

These questions are important to both researchers and engineers for certain difficult problems, but there are very few previous studies devoted to these three questions.

In 1965, Morgenstern and Price (MP method) proposed that the relation between the interslice normal and shear force could be specified to make the stability problem statically determinate which is shown in Figure 5.1. Currently, most of the engineers adopt an interslice force relation in the form of

$$X = \lambda f(x) E \tag{5.1}$$

where X and E are the interslice shear force and interslice normal force respectively.

Spencer (1967) later proposed that all the interslice forces could be assumed to be parallel to obtain the factor of safety, and $f(x)$ will then be equal to be 1 and hence $\lambda f(x)$ is a constant to be determined. Lam and Fredlund (1993) introduced interslice force function to specify the relationships between intercolumn normal and horizontal shear forces, intercolumn normal and vertical shear forces for three-dimensional problems, but the three-dimensional intercolumn function $f(x,y)$ was actually set to 1 in order to determine λ and the safety factor. Cheng and Yip (2007) have found that $f(x,y)$ is not sensitive to the factor of safety based on some limited studies for simple slopes.

The major assumption in LEM is $f(x)$ which is important but is not adequately considered in the past. In this chapter, $f(x)$ is taken as the control variable, and the upper and lower limits of the factor of safety will be determined by global optimization analysis which is actually mathematically equivalent to the use of variational principle. Based on this approach, $f(x)$ will be determined and investigated. Furthermore, $f(x)$ will also be determined by the strength reduction method, and the results from LEM and SRM will be compared.

5.2 Investigation of interslice forces by limit equilibrium method

5.2.1 Determination of bounds of safety factor and f(x)

For a failure surface with n slices, there are n-1 interfaces and hence n-1 $f(x_i)$. $f(x)$ will lie within the range of 0 to 1.0, while the mobilization factor λ and the objective function factor of safety based on MP method will be determined for each set of $f(x_i)$. The maximum and minimum factors of safety of a prescribed failure surface satisfying force and moment equilibrium will then be given by the various possible $f(x_i)$ satisfying Eq.(5.2).

Maximize (or minimize) factor of safety subject to $0 \leq f(x_i) \leq 1.0$ for all i (5.2)

In carrying out the optimization analysis as given by Eq.(5.2), the constraints from the Mohr-Coulomb relation along the vertical interfaces between slices as given by Eq.(5.3) should be considered.

$$X \leq E \tan(\phi') + c'L \tag{5.3}$$

where L is the vertical length of the interface between slices. The constraint given by Eq.(5.3) should also satisfy the requirement that the line of thrust of the internal forces lies within the soil mass, and Eq.(5.3) can have a major impact on the factor of safety in some cases, which will be illustrated by numerical examples in the following section. Since other than the $f(x)$, the MP method is totally governed by force and moment equilibrium, the maximum and minimum factors of safety found from varying $f(x)$ will provide the upper and lower bounds to the factor of safety of the slope that are useful for some difficult problems.

Pan (1980) has stated that the slope stability problem is actually a dual optimization problem which is not well known outside China. On one hand, the soil mass should redistribute the internal forces to resist the failure, which will result in a maximum factor of safety for any given slip surface, and this is called the maximum extremum principle. On the other hand, the slip surface with the minimum factor of safety is the most possible failure surface, which is called the minimum extremum principle. The maximum and minimum extremum principles are actually equivalent to the lower and upper bound methods, which are well known. Mathematically, the solution from the use of variational principles is an extremum of a function, and this is also equal to the global maximum/minimum of the function, which can also be determined from an optimization process. The "present proposal" can be viewed as a form of the discretized variational principle (Cheng et al. 2011).

Since the objective function is highly discontinuous, the factor of safety is obtained by the double QR method by Cheng (2003). The simulated annealing method which is more stable but less efficient is used to determine the extrema with any given slip surface according to Eq.(5.2). To evaluate the global minimum factor of safety of a slope, another global optimization analysis should be carried out for the factor of safety, which is an outer loop of the global optimization analysis. To ensure that "false" failure-to-converge due to iteration analysis (Cheng et al. (2008b)) is not encountered so as to reduce the discontinuity of the objective function, the factor of safety is determined by the more time-consuming but robust double QR method. Since the factor of safety is available for practically all of the failure surfaces, the more efficient modified harmony search method as developed previously can be used for locating the critical failure surface. The complete process is computationally intensive, but the use of modern global optimization processes can make this process a reality on a personal computer within an acceptable computation time. Most of the problems can be completed within 1 hour which is considered to be acceptable for engineering use.

The maximum extremum principle is not new in engineering, and the ultimate limit state of a reinforced concrete beam is actually the maximum extremum state where the compressive zone of the concrete beam will propagate until a failure mechanism is formed. The ultimate limit state design of a reinforced concrete beam under the application of a moment is equivalent to the maximum extremum principle. For any prescribed failure surface, the maximum "strength" of the system will be mobilized when a continuous yield zone is formed which is similar to a concrete beam. Pan's extremum principle (1980) can provide a practical guideline for slope stability analysis, and it is equivalent to the calculus of variation method used by Baker and Garber (1978), Baker (1980) and Revilla and Castillo (1977). This dual extremum principle is proved by Chen (1998) based on lower and upper bound analyses, and it is further elaborated upon with applications to rock slope problems by Chen et al. (2001). The maximum extremum is actually the lower bound solution, and the present approach is actually a lower bound approach as well as a variational principle approach.

5.2.2 Numerical studies of *f(x)* and comparisons with classical methods of analysis

Cheng et al. (2010) have applied the simulated annealing method complying with Eqs. (5.2) and (5.3) to evaluate the two extrema of the factor of safety. To determine the maximum and minimum extrema by the simulated annealing method, a tolerance of 0.0001 is used to control the optimization search and the factor of safety determination. This tolerance will terminate the search in a particular solution path during the optimization process (see also Cheng et al. 2007a for details of the heuristic optimization methods). Since 15 slices are adopted in the computation, there are in total 14 $f(x_i)$ unknowns in the analysis, and the number of trials required to evaluate the two extrema ranges from 25000 to 32000, which is controlled by the tolerance during the optimization search. Based on this study, it was found that about 30-80% of the trials can converge when $f(x)$ is varied, and those trials that fail to converge are controlled by either Eq.(5.3), or no physically acceptable answer can be found from the double QR method. The number of trials which fail to comply with Eq.(5.3) is about 3-5 times that where no physically acceptable answer can be found by the double QR method, so the compliance with Eq.(5.3) (together with the requirement on the line of thrust), which has been neglected in the MP method, is actually important if an arbitrary $f(x)$ is defined.

Consider a very simple 45° 6 m high slope with a circular failure surface (example 1) as shown in Figure 5.2. The unit weight of the soil is 19 kN/m^3, while c' and ϕ' vary as shown in Tables 5.1a and 5.1b. The differences between the two extrema are less than 2% of the results given by Spencer's method (1967), which clearly indicates that the factor of safety is not sensitive to $f(x)$ and that Spencer's method (1967) gives a good result for this example (see Table 5.1a). It is also interesting to find that while the factor of safety is not sensitive to Eq.(5.3), λ is quite sensitive to the Mohr-Coulomb relation along the interfaces as the mobilization of interslice shear force to achieve maximum and minimum resistance will involve higher λ value. It is also observed that the values of λ from the two extrema are generally greater than that from Spencer's analysis (1967), and these observations also apply to all the other examples in this study.

For the slope as shown in Figure 5.3 (example 2) with the soil parameters given in Table 5.2, the various factors of safety are given in Tables 5.3a and 4.3b. With only the lower nail present, the differences between the two extrema as compared with Spencer's result (1967) are about 5.9% and 4.4% when Eq.(5.3) is used or not used, respectively (see Table 5.1b). The corresponding results/differences when the two soil nails are present are 10.5% and 4.1%. It can be observed that when the soil nail or external load is present, the choice of $f(x)$ has a noticeable impact on the results, and the compliance with Eq.(5.3) is also a critical issue which should be considered in the determination of extrema.

For example 3 in Figure 5.4, if a deep-seated failure surface is considered with a uniform pressure 30 kPa on top of the slope, the two extrema are 1.236 and 1.091 if Eq.(5.3) is not applied, and the two extrema are 1.221 and 1.184 if Eq.(5.3) is considered. The corresponding factor of safety from Spencer's method (1967) is 1.200. Once again, Eq.(5.3) appears to be important in the factor of safety determination.

For examples 1 and 3, Spencer's method (1967) is adequate for practical purposes. On the other hand, for example 4 as shown in Figure 5.5 where there are many external loads and several weak zones, the two extrema are given by 3.24 and 3.98, indicating that the choice of $f(x)$ is actually important. For more complicated problems similar to examples 2 and 4 where $f(x)$ is important, the present approach can avoid the dilemma of choosing a suitable $f(x)$ and can provide a solution with acceptable internal forces to the engineers.

It is clearly demonstrated that based on the lower bound principle/extremum principle, the interslice force function which is considered to be an indeterminate relation for the last 40 year can now be determined. This is also an outstanding and important breakthrough to be added to the classical LEM formulation, and every problem will be statically determinate when the concept of lower bound principle is fully utilized.

5.3 Investigation of interslice forces by strength reduction method

5.3.1 Calculation of the interslice force function by strength reduction method

Recently, the strength reduction method (SRM) appears to be a popular alternative to the LEM, and Eq.(5.1) is not required in the analysis. Cheng et al. (2007, 2008) and Wei et al. (2009) have carried out extensive SRM studies and have found that there are many practical limitations to the SRM. Cheng et al. (2007, 2008) and Wei et al. (2008)

concluded that both LEM and SRM are useful to slope stability analysis, and each method cannot replace the other method in practical use. Based on the stresses at the ultimate limit state from SRM, $f(x)$ can also be determined from the SRM. The procedures to determine $f(x)$ from SRM are:

1. Conduct the SRM to determine the stress and factor of safety.
2. Determine the location of the failure surface and the failure soil mass is divided into slices.
3. Determine the normal and shear stresses on the vertical interfaces between slices and carry out the integration to evaluate the interslice normal and shear forces. The ratio between the interslice shear force and normal force is denoted as $\lambda f(x_i)$. The largest $\lambda f(x_i)$ is taken as the reference and $f(x)$ will be set to 1.0 at this location and λ will be denoted as λ_{max}.
4. $f(x_i)$ will be determined as $\lambda f(x_i)/\lambda_{max}$.

When the factor of safety (FOS) is taken into consideration for defining the $f(x)$, c' and $\tan\phi$' are reduced and the author proposes another interslice force function $f_2(x)$ which should be expressed as

$$F_2(x) = \frac{X}{E(\tan\phi)_r + C_r} = \frac{X}{\frac{E\tan\phi'}{FOS} + \frac{C}{FOS}} = FOS \cdot \frac{X}{E\tan\phi' + C} = FOS \cdot f_2(x)$$

or $$f_2(x) = \frac{F_2(x)}{FOS} \tag{5.4}$$

It will be shown later that the uses of the two $f(x)$ can give useful insight about the internal forces distribution of a slope under the ultimate limit state.

For the SRM analysis, program Phase2 based on the finite element analysis and FLAC3D based on the finite difference method (FDM) are adopted. Non-associated flow rule is used for the analysis (dilation angle is set to 0), and maximum shear strain criterion is used for the definition of the critical slip surface. Cheng et al. (2007) have established that the uses of associated or non-associated flow rule are not critical in most cases, and associated flow rule has also been used for some cases in this study to confirm that this assumption is not critical to the present study in general. The numerical modeling is shown in Figure 5.6. The cohesive strength c' varies from 2kPa, 10kPa, 20kPa to 30kPa, whereas the friction angle ϕ' varies from 10°, 20°, 30° to 40°. The effect of the slope geometry will be discussed later while the unit weight, Young's modulus and Poisson's ratio are taken as 18.84kN/m^3, 18MPa and 0.25 respectively in this study. As established by Cheng et al. (2007), the effects of Young's modulus and Poisson's ratio are generally negligible for most cases and will not be considered.

In general, the critical failure surfaces from the SRM and LEM are close in most cases which are shown in Figure 5.7, and these results are similar to the results by Cheng et al. (2007). It can be noted that:

1. Factor of safety from LEM and FDM agrees well with few exceptions, while results from FDM are usually higher than those from FEM.
2. When c' is small, differences in factor of safety are greatest for higher ϕ', and when c' is relatively large, differences in factor of safety are greatest for lower ϕ'.

The investigation on $f(x)$ for constant c'=2kPa and varying ϕ' from 10° to 40° is shown in Figure 5.8, which is followed by Figure 5.9 for the interslice force function with constant ϕ'=10° and varying c' from 2kPa to 30kPa. It should also be noted that interslice tension normal forces have developed in the later portion of the soil mass which is actually not possible. To deal with this, two approaches are commonly adopted. Tension crack can be introduced and the portion of soil mass beyond the tension crack is neglected in the calculation (or a tensile cut off stress can be introduced if necessary). The location of the tension crack will be varied until no tension is found in the failure soil mass. Alternatively, most of the engineers or researchers will simply allow tension which is a simpler procedure, and this is the approach adopted in the present study. The results for $f(x)$ or thrust line are hence illustrated up to the compression zone only and the general trend of $f(x)$ is not greatly affected by this tension cut-off.

As shown in Figures 5.8 and 5.9, the general shape of $f_1(x)$ for a 1:1 slope is an asymmetrical bell which can be divided into three segments. For the left exit end of the sliding soil mass where is near to the toe of slope, $f(x)$ ascends rapidly to the peak value at around x=0.2. Such result is similar to the result based on the lower bound method by Cheng et al. (2010). Beyond the peak, $f(x)$ maintains a relatively high value until x is close to 0.6. Beyond x=0.6, $f(x)$ drops rapidly until tension develops between slices. In general, the results from SRM and LEM agree well. Based on the results in Figures 5.8 and 5.9, it is clear that $f(x)$ is close to 1.0 at region close to the toe of slope. Such results imply that the shear strength of soil is virtually fully mobilized near to the toe of the slope, which is in agreement with the understanding that the most of the slope failures initiate from the toe of slope.

If the percentage of shear resistance mobilized along the interface between slices is considered, $f_2(x)$ should be used instead of $f_1(x)$ in the formulation. The results of analysis using $f_2(x)$ are shown in Figures 5.10 and 5.11 for illustration. Initially, *F2(x)* was calculated without consideration of factor of safety along the interface and the results are shown in Figures 5.10a and c and 5.11a. After the application of the factor of safety by Eq.(5.4), $f_2(x)$ will give a much more reasonable distribution of the internal forces.

The variations of the interslice force function for simple slopes with different geometries have also been investigated. Slopes of c=30kPa and ϕ=40° with the same height and slope angle of 30°, 45° and 60° have been considered. For the $f_1(x)$ as shown in Figure 5.12, steeper slope possesses lower horizontal extent of bell-shaped function. For the $f_2(x)$ as shown in Figure 5.13, similar relationship between the slope angle and the function region can be found. Because of the narrower region and similar gradient, larger slope angle seems to be related to acuter bell-shaped function. Similar to the previous case, even though great differences in the gradient and peak value exist among different geometries when the factor of safety is not considered, similar forms of bell shape with or without obvious flatness for the interslice function can be obtained if the factor of safety is involved in $f_2(x)$.

The λ obtained by different methods are tabulated in Table 5.4. The data shows that generally larger λ is obtained with larger ϕ', which means that more shear resistance is mobilized while less percentage of resistance is mobilized as c gets larger. When the angle of slope is large, λ increases which indicates that more shear force is mobilized.

To sum up, the two definitions of $f(x)$ agree well with each other if the factors of safety are taken into calculation on the interslice surface. $f_1(x)$ is generally used in the original MP method but it ignores the shear strength effect so it might induce fluctuations in the results. The method presented in this study has however considered this problem indirectly by enforcing the Mohr-Coulomb relation along the vertical interface. $f_2(x)$

which is proposed in the present study considers factor of safety directly along interslice surface. The interslice force function can be divided into two major forms: with or without obvious platform. SRM and LEM can both obtain similar forms of interslice force function corresponding to similar critical slip surface and factor of safety. Interslice force function is mainly related to the geometry of the slope, influenced by the cohesive strength and friction angle, and less affected by Poisson's ratio, dilation angle and tensile strength which are not important or required in LEM. Considering such characteristic and the efficiency of LEM, specified reasonable interslice force function within LEM framework could give results more rapidly than SRM and more accurately than classical LEM with arbitrarily specified interslice force relationship. The use of the extremum principle can also effectively avoid convergence problem which is not possible with the classical limit equilibrium methods.

As mentioned by Cheng et al. (2010), for practical purposes, a simple formula as given by Eq.(5.5) will be sufficiently good for practical purposes. This will greatly simplify the definition of interslice force function with only 3 parameters a, b and c. Maximum location of $f(x)$ by Eq.(5.5) will be located at x=0 which is slightly different from the present study. Such small differences are generally acceptable for practical purposes, and the addition of 1 more parameter to Eq.(5.5) will improve the curve fitting at the expense of 1 more parameter as shown in Figure 5.14. Eq.(5.5) is adequate for simple problems, while the numerical procedure as suggested in present study can be adopted for more general and complicated problems.

$$f(x) = \cot^{-1} (ax+b)/c \qquad (5.5)$$

5.3.2 Back-calculation of thrust line

Besides $f(x)$, the thrust line in the Janbu's Rigorous Method (1973) can also be used to determine the factor of safety. Janbu (1973) assumed the thrust line is located at 1/3 interface height as measured from the base on each slice and formulated the general equations of equilibrium by resolving vertically and parallel to the base of each slice. By taking moments about the centre of the base for each slice, overall moment equilibrium is implicitly satisfied, and the interslice shear forces can be calculated.

The procedure to determine the acting position of the thrust line on the interslice surface (as shown in Figure 5.1) is actually a back-calculation procedure. To calculate the interslice force, the total moment of the normal stresses with respect to the bottom of the slice is determined, and the centroid of the interslice normal force (thrust line) can then be evaluated. The interslice surface is subdivided into small segments which allow acceptable accuracy for the assumption that for each segment, the resultant force of the thrusting stress acted at the middle of the segment, therefore, the location of thrust line can be determined if the stresses are known.

The position of the thrust line with various cohesion, friction angle and slope angle are shown in Figures 5.15-5.17. For comparison, the critical slip surface and thrust line with 1/3 height from slice base according to the assumption in the Janbu's Rigorous Method (1973) are also included. Basically, the thrust line calculated by SRM is almost the same as the thrust line assumed in the Janbu's Rigorous Method (1973), except that there are minor difference when c' is small. The results agree well with the assumption of 1/3 slice height which indicates that after stress re-distribution at ultimate limit state, the resultant interslice forces satisfy the general consideration that the lateral pressure acts at 1/3 height from the slice base. From Figure 5.15, the effect of the friction angle seems to be not critical to the position of the thrust line. The thrust line however deviates from the 1/3 slice height apparently around the crest of the slope, and larger cohesive strength tends to cause the thrust line to move up. This is reasonable as the stress condition is composite in multiple slices and re-distribution cannot thoroughly render the interslice forces to classical soil pressure. The influence of the slope angle on the thrust line is also investigated and is shown in Figure 5.17. The thrust line deviates slightly from the generally assumed 1/3 height condition.

Based on the above observation, re-distribution of stress drives the thrust line partially coincident with general soil pressure acting on the 1/3 from the base on each slice. It should be noticed that two probabilities may exist here: the difference between the thrust line from SRM and the assumed 1/3 height is relatively small; the difference is actually large but seems negligible. The latter situation can be caused by relatively small length of slice around the toe of slope. To further investigate the thrust line location from the slice base, more results are given in Figure 5.18.

From the four typical slopes of (i) c’=2kPa, ϕ’=10°; (ii) c’=2kPa, ϕ’=40°; (iii) c’=30kPa, ϕ’=10°; (iv) c’=30kPa, ϕ’=40° in Figure 5.18, the thrust lines for the first few slices around the toe of slope are located at the half of the slice height, then drop rapidly to 0.40 slice height and is located at about 0.3 slice height (which is close to assumption of 1/3) for more than 50% of the horizontal extent of the sliding soil mass. It is also illustrated that around the crest of the slope and forwards, the thrust line fluctuates which depends on different type of slope. If c’ is relatively large, the thrust line fluctuates more at the top of the slope, while for larger ϕ’, the thrust line seems to be flatter. Therefore, the slope of type (ii) possesses most well-proportioned thrust line. More importantly, as shown clearly in Figure 5.18, the starting position of the thrust line around the toe of slope is not sensitive to different types of slopes, while the existence of tension crack is more important which causes the thrust line to deviate from the assumption by Janbu at the top of the slope.

5.4 Variable factor of safety method

5.4.1 Variable factor of safety formulation

For the LEM, one of the basic assumptions common to all of the traditional soil and rock slope stability methods is a single factor of safety for the entire solution domain. Without this assumption, the slope stability problem will be statically indeterminate unless additional assumptions are used. The actual failure of a slope is however usually a progressive phenomenon. If the shear strengths between adjacent blocks are fully mobilized, the unbalanced forces will distribute to the adjacent blocks until a failure mechanism is formed. This process is called the progressive failure of slope. This phenomenon is well known, but is difficult to be considered by the classical LEM. For a system with a factor of safety close to 1.0, the choices of the shear strength parameters become critical. The adoption of the maximum shear strength or the residual strength and the extent in the adoption of different design parameters for the analysis is difficult to be decided, but the results of analysis will be greatly affected by the choice of the parameters. In this section, a discretized numerical formulation for LEM will be provided based on the extremum principle by Cheng et al. (2010), which can be viewed as an equivalent form of the variational principle. Through such numerical procedures, a limit equilibrium formulation which can satisfy all the equilibrium conditions can be achieved.

A variable factor of safety LEM formulation using mixed optimization method combining the particle swarm optimization (PSO) with the harmony search (HS) (developed in chapter 3) is proposed in this chapter. It will be demonstrated that the overall factor of safety from this approach is close to the classical methods of analysis for normal problems, but the present approach can accept the post-peak strength in the analysis which provides an estimate to the progressive failure mechanism. With minor modification, the present formulation can also reduce to a special form of the classical Janbu's rigorous method (1973).

In the classical LEM, most of the formulations consider only the global moment (local moment equilibrium is not enforced) except for the Janbu's rigorous method which however cannot satisfy the moment equilibrium for the last slice. Cheng et al. (2010) enforce the local moment by rejecting the $f(x)$ associated with an unacceptable thrust line. In this chapter, the proposed formulation considers the local moment equilibrium explicitly with re-distribution of forces and the allowance of post-peak strength in the analysis. The values and the locations of the inter-slices forces are viewed as the control variables, and the group of inter-slices forces satisfying static equilibrium will be optimized to determine the maximum factor of safety. Consider the slope as shown in Figure 5.1, the soil mass between the potential slip surface and the ground surface is divided into n slices numbering from 1 to n. K_0 represents the boundary thrust force and its value is usually equal to 0. Points A and B are the entrance and exit points of the sliding surface respectively with their x-coordinates denoted as x_A and x_B. The forces acting on a typical slice i are also illustrated in Figure 5.1. The boundary between i-1 slice and i slice intersects with the slip surface and the ground surface at point C and E respectively. Similarly, points D and F are also defined. K_{i-1} is the thrust force between i-

1 and i slice and h_{i-1} is the vertical distance from the thrust point of K_{i-1} to point C, while K_i represents the thrust force between i slice and i+1 slice, and h_i is the vertical distance from the thrust point of K_i to point D. β_{i-1} is the angle between K_{i-1} and the horizontal direction. W_i is the weight of slice i. v_i is the horizontal distance from the thrust line of W_i to the center point of slice base (used for moment arm). P_i and U_i are the effective normal force and the pore water pressure acting on the slice base respectively. T_i is the mobilized shear force required to maintain the static equilibrium condition. Q_i is the external forces induced by earthquake. d_i is the distance from the thrust line of Q_i to O (also used for the moment arm). b_i is the slice width. α_i is the inclination of slice base, namely, the angle from horizontal to the slice base in clockwise direction. g_i is the distance from the thrust line of P_i to point O along the slice base. Usually, the centroid of P_i is assumed to be at point O, that is, $g_i = 0$ under the classical formulation. In this study, g_i can changes during the optimization process which is a more flexible arrangement. In addition, the distance from point C to the thrust line of P_i is named as λ_i. The local factor of safety for slice i is defined as the ratio of the available shear strength along a slice base to the driving shear stress along the slice as:

$$F_s^i = \frac{P_i \tan\phi_i + c_i}{T_i} \tag{5.6}$$

where F_s^i is the local factor of safety for slice i, ϕ_i is the effective friction angle of slice base, c_i equals $c_i'l_i$ and l_i is the base length of slice i. The total/global factor of safety can be defined as the ratio of the available shear strength along the slip surface to the driving shear stress along the whole slip surface, and it is given by Eq.(5.7) as:

$$F_s = \frac{\sum_{i=1}^{n}(P_i \tan\phi_i + c_i)}{\sum_{i=1}^{n} T_i} \tag{5.7}$$

If we define a force vector $H_i = (K_{i-1}, K_i, W_i, Q_i, U_i.P_i, T_i)$, the maximum extremum can be stated as Eq.(5.8):

$$\begin{cases} \max F_s(H_1, H_2, ..., H_n; h_1, ..., h_n; g_1, ..., g_n; \beta_1, ..., \beta_n) \\ s.t. \quad \sum_{i=1}^{n} H_i\big|_x = 0 \quad \sum_{i=1}^{n} H_i\big|_y = 0 \\ \qquad \sum_{i=1}^{n} H_i \times M_o = 0 \end{cases} \tag{5.8}$$

where H_i represents the total forces imposed on slice *i*, $\big|_x$ means the projection of force vectors in *x*-direction, $\big|_y$ means the projection of force vectors in *y*-direction. $H_i \times M_o$ is the moment of vector H_i about point O. That means, the force vectors H_i (*i*=1,2,…,*n*) and the variables of h_i, g_i, β_i (*i*=1,2,…,*n*) must satisfy the static equilibrium condition. There exist infinite groups of force vectors H_i and variables of h_i, g_i, β_i which can satisfy the static equilibrium condition, and they will lead to different factors of safety according to Eq.(5.7). The factor of safety for a given slip surface will be the maximum value based on the lower bound principle (see Cheng et al. 2010) which can be determined from an optimization process.

The next step is to determine the control variables for the maximum extremum principle. If $h_{i-1}, K_{i-1}, \beta_{i-1}$ are known, there will be six remaining variables $h_i, \beta_{i-1}, P_i, T_i, K_i, g_i$ to be determined based on the static equilibrium. Since there are only three static equilibrium equations available for slice *i,* in order to make the problem determinate, three variables should be taken as the control variables in the optimization process. In this study, we assume that $g_i = 0$ in the initial trial and take h_i, β_i as the control variables. The boundary conditions give $h_0 = h_n = 0$ and $\beta_0 = \beta_n = 0$, so there are totally 2n-2 variables ($h_1,...,h_{n-1};\beta_1,...,\beta_{n-1}$) to be optimized. Based on the boundary conditions, the recursive procedures will determine the local factor of safety and the related normal forces, shear forces on the slice base and the thrust forces for all the slices. The global factor of safety is then determined by Eq.(5.7). P_i is limited to positive value in the optimization analysis which is also a constraint in the analysis.

Furthermore, during the implementation of the maximum extremum principle, there is the possibility that F_s^i<1.0. Two approaches are adopted in this study. The first approach allows the occurrence of F_s^i <1.0, and the other approach will assign F_s^i =1.0 by transferring the unbalanced thrust forces to its adjacent slice in the sliding direction. The former approach is called the approach of instantaneous loading condition (Ailc), and the latter is called the approach of gradual loading condition (Aglc). The details of the Aglc are as follows (take slice *i* for example):

Step 1: The force equilibrium equations in the *x*- and *y*-directions give:

$$\begin{cases} Q_i + K_{i-1}\cos\beta_{i-1} - K_i\cos\beta_i + P_i\sin\alpha_i - T_i\cos\alpha_i = 0 & \mathrm{x-direction} \\ -W_i - K_{i-1}\sin\beta_{i-1} + K_i\sin\beta_i + P_i\cos\alpha_i + T_i\sin\alpha_i = 0 & \mathrm{y-direction} \end{cases} \tag{5.9}$$

$$K_i = \frac{W_i v_i + Q_i d_i - K_{i-1}\sin\beta_{i-1}\dfrac{b_i}{2} + K_{i-1}\cos\beta_{i-1}(h_{i-1} + \dfrac{b_i}{2}\tan\alpha_i)}{\sin\beta_i\dfrac{b_i}{2} + \cos\beta_i(h_i - \dfrac{b_i}{2}\tan\alpha_i)} \tag{5.10}$$

Assuming $g_i = 0$ initially, the moment equilibrium about point O leads to Eq.(5.10). In the following, we denote the nominator in Eq.(5.9) as M^i for sake of clearer interpretation. P_i, T_i can be obtained as Eq.(5.11) by using the force Eq.(5.9) in *x*-and *y*-

directions and Eq.(5.10).

$$\begin{cases} P_i = -Ca_1 \sin\alpha_i - Ca_2 \cos\alpha_i \\ T_i = -Ca_2 \sin\alpha_i + Ca_1 \cos\alpha_i \end{cases} \tag{5.11}$$

where Ca_1 equals to $Q_i + K_{i-1}\cos\beta_{i-1} - K_i \cos\beta_i$, and Ca_2 equals to $-W_i - K_{i-1}\sin\beta_{i-1} + K_i \sin\beta$.

Step 2: Calculate the global factor of safety F_s^i by Eq.(5.6). If F_s^i<1.0, local failure will occur, and T_i is adjusted to $P_i \tan\phi_i + c_i$ (or the residual strength if it is defined) with F_s^i=1.0. The unbalanced thrust force will be distributed to K_i and P_i. P_i and K_i will be adjusted according to Eq.(5.12):

$$\begin{cases} P_i = \dfrac{-Cb_1 \sin\beta_i - Cb_2 \cos\beta_i}{Cd_1 \sin\beta_i + Cd_2 \cos\beta_i} \\ K_i = \dfrac{-Cb_2 Cd_1 + Cb_1 Cd_2}{Cd_1 \sin\beta_i + Cd_2 \cos\beta_i} \end{cases} \tag{5.12}$$

where Cb_1 equals $Q_i + K_{i-1}\cos\beta_{i-1} - c_i \cos\alpha_i$, Cb_2 equals $-W_i - K_{i-1}\sin\beta_{i-1} + c_i \sin\alpha_i$, Cd_1 equals $\sin\alpha_i - \tan\phi_i \cos\alpha_i$, and Cd_2 equals $\cos\alpha_i + \tan\phi_i \sin\alpha_i$. Residual strength can hence be considered easily by step 2 in the present formulation. The moment equilibrium about an arbitrary moment point O will then be checked again. The variable h_i is calculated by Eq.(5.13) as follows:

$$h_{i-1} = \frac{M^i F_i + Q_i d_i + F_{i-1}\sin\beta_{i-1}\dfrac{b_i}{2}}{F_{i-1}\cos\beta_{i-1}} - \frac{b_i}{2}\tan\alpha_i \tag{5.13}$$

Pan (1980) has pointed out that the acceptable h_i should be in the range between $0.25|\mathrm{DF}|$ and $0.5|\mathrm{DF}|$, which is basically similar to the suggestion by Janbu in his "rigorous" method (1973). $|\mathrm{DF}|$ represents the vertical distance from point D to point F which can be adjusted if necessary. If the constraint $0.25|\mathrm{DF}| \le h_i \le 0.5|\mathrm{DF}|$ (or any other similar range defined by the engineer) is not satisfied, the boundary value will be set to h_i. That is to say, if $h_i < 0.25|\mathrm{DF}|$ then $h_i = 0.25|\mathrm{DF}|$. The unbalanced moment induced by the violation of this constraint drives the force P_i to move along the slice base within a certain range. The maximum length for which P_i can move is set to $\frac{b_i}{\cos\alpha_i}\psi$, where $0 < \psi \le 0.5$. If g_i is lower than $\frac{b_i}{\cos\alpha_i}\psi$, the computation for slice *i* will finish. ψ is set to 0.1 in the present study, otherwise, the centroids of the base normal forces will be close to the edges of the slice and are not acceptable. The effect of this value on the factor of safety can be considered by using Eq.(5.14):

$$g_i = \frac{M^i - K_i\left(\sin\beta_i \frac{b_i}{2} + \cos\beta_i\left(h_i - \frac{b_i}{2}\tan\alpha_i\right)\right)}{P_i} \tag{5.14}$$

The above-mentioned steps are applicable to all the slices except for the last one. For the last slice, h_n, F_n are equal to 0 from the boundary condition, so F_n can be pre-determined as 0.0 instead of using Eq.(5.10). By Eq.(5.9), P_i and T_i are determined and the local factor of safety F_s^n is obtained. The moment equilibrium condition is maintained by varying P_i within the acceptable range between 0 (at middle of slice) and $\frac{b_n}{\cos\alpha_n}\psi$ (close to the edge of slice).

For Ailc, only step 1 is required as $F_s^i < 1.0$ is allowed. The optimization problem related to the maximum extremum principle (or lower bound method, Cheng et al. (2010)) for a given slip surface $\mathbf{Z}'$ is stated as follows:

$$\begin{cases} \max \quad g\left(h_{1,} \ldots, h_{n-1}; \beta_1, \ldots, \beta_{n-1}, \beta_-, \beta_+\right) \\ 0.25\left|\mathrm{DF}\right| \le h_i \le 0.50\left|\mathrm{DF}\right| \\ P_i > 0; \beta_- \le \beta_i \le \beta_+ \end{cases} \tag{5.15}$$

where β_-, β_+ are the minimum allowed angle and the maximum allowed angle respectively. In the present study, the lower and upper limits of β_- and β_+ are -45° to 0° and 0° to 70° respectively (it should be noted that β less than zero is allowed by many commercial software). There are totally 2n variables to be optimized for the maximum extremum, and the global factor of safety will be obtained from this optimization procedure based on the mixed optimization algorithm which will be discussed below.

In the Aglc formulation, progressive failure can be considered approximately in two ways. If the global factor of safety exceeds 1.0, the system can redistribute the stresses for local yielding by Eqs.(5.12) and (5.13). That means, part of the failure surface can yield locally (with a local factor of safety 1.0) while the whole soil mass is still maintained in a stable state by the remaining portion of the failure surface where the local factors of safety exceed 1.0. If a residual strength is specified, the Aglc formulation can allow the use of the residual strength according to step 2 above during the stress-redistribution, which will further extend the local yield zone in the analysis.

The present formulation is similar to that by Cheng et al. (2010) while a varying local factor of safety is defined with the explicit consideration of the local moment equilibrium of every slice which is not possible with other classical formulation. In the formulation by Cheng et al. (2010), the violation of local moment equilibrium (actually thrust line) is enforced indirectly by rejecting the trial $f(x)$ which give a thrust line outside the soil mass (as Morgenstern-Price's method does not consider local moment). The local moment equilibrium is however automatically enforced for every slice in the present formulation which is not possible with the other existing methods. On the other hand, this method requires the concept of local and global factor of safety which is different from the previous lower bound method by Cheng et al. (2010). The incorporation of the residual strength is simple and direct in the present formulation, and progressive failure mechanism can be approximately estimated from the stress-redistribution in the present formulation.

The present formulation requires the optimization analysis for any prescribed failure surface. The difficulties of the present optimization analysis are:

1. Large number of control variables for the N-P type optimization problem.
2. No solution may be obtained for some combinations of internal forces or thrust line locations, as the factor of safety function is a highly discontinuous function for the present formulation.
3. Presence of multiple local minima for the objective function, and the objective function is not necessarily a convex function.

To overcome the highly discontinuous nature of the objective function in the present formulation, a powerful, stable and fast global optimization method is required for the analysis. To maintain effectiveness and efficiency, a combination of the PSO and the HS algorithms for the present problem is proposed in chapter 3. The combination of the two algorithms is usually more stable towards difficult problems, but will be less efficient for simple problems. This optimization method is used for the present difficult optimization problem.

5.4.2 Comparisons among different methods

We can find that the present maximum extremum method of analysis gives results similar to the classical methods of analysis for many prescribed failure surfaces. Example 5 as shown in Figure 5.19 is a simple slope considered by Greco (1996) and Yamagami and Ueta (1988). The geotechnical parameters for example 5 are: $\phi'=10°$, $c'=9.8$kPa, unit weight $\gamma = 17.64$ kN/m^3. Yamagami and Ueta (1988) used nonlinear programming methods and the Spencer's method to search for the critical factor of safety. The optimization search algorithms included the DFP, BFGS, Powell, and simplex methods. Greco (1996) analyzed this example using the pattern search and the Monte Carlo method. Cheng et al. (2007a) have also obtained a minimum factor of safety 1.325 using the Spencer's analysis by the PSO method. The results by Ailc, Aglc and MP (extremum principle) as shown in Table 5.5 are slightly higher than those by Greco (1996) and Yamagami and Ueta (1988) and Cheng (2008a). The number of slices n is assumed to be 11 and 15 respectively for Ailc and Aglc while 15 slices are used in the MP approach in the present study. The critical failure surfaces by MP are not shown in the present chapter for clarity, as the failure surface usually lie between those from Ailc and Aglc.

These results are normal as the present formulation is practically equal to the extremum of the lower bound solution, while the use of the Spencer's method is actually a lower bound solution. These results are also similar to the lower bound results by Cheng et al. (2010). The critical slip surfaces and the thrust lines by Aglc and Ailc are generally quite similar. The line of thrust for the MP approach is not shown in Figure 5.19, as the local moment equilibrium is not enforced in the MP approach and there are locations where the line of thrust located outside the soil mass which is not correct (the MP method cannot automatically ensure the thrust line to lie within the soil mass). The local factors of safety for Ailc and Aglc for the present problem are shown in Figure 5.20. The results have illustrated that the first few slices as measured from the left are more difficult to fail, and this results are reasonable as the α values for these slices are either negative or small positive numbers. The variation of β with different slice as shown in Figure 5.21 is basically equivalent to a complicated $f(x)$ which is far from 1.0 (Spencer's assumption).

Example 6 is a slope in layered soils which is considered by Zolfaghari (2005) using genetic algorithm with the Spencer's method. The geometric layout of the slope is shown in Figure 5.22 while the geotechnical properties for soil layers 1 to 4 are given in Table 5.6. The critical factors of safety by Ailc, Aglc and the Spencer's method by Cheng et al. (2007a) using the PSO as shown in Table 5.7 are all smaller than those by Zolfaghari (2005). Cheng et al. (2007a) have commented that the result by Zolfaghari (2005) is possibly trapped by a local minimum, as the portion of the critical failure surface lying within the soft band zone by Zolfaghari is less than that by Cheng (2007a). For the present problem, the critical failure surfaces by Cheng using the Spencer's method is very close to those by Ailc, Aglc, which indicate that the present formulation will gives results close to that by the Spencer's method. The results have also indicated the effectiveness of the mixed optimization algorithm to overcome the local minimum for a relatively difficult problem. The distribution of the local factor of safety and β are shown in Figures 5.23 and 5.24. These results correspond to the left portion of the failure surface close to the failure surface with high basal angles which from the optimization analysis are also physically reasonable.

The local factor of safety along the interface between two adjoining slices is defined as $\zeta = \dfrac{K_i \cos\beta_i \tan\phi_{vi} + C_{vi}}{K_i \sin\beta_i}$, where ϕ_{vi} is the average friction angle along the ith inter-slice and C_{vi} is the average cohesion along ith inter-slice. The distribution of $1/\zeta$ along the failure surface for the critical failure surfaces by Ailc, Aglc, the Spencer's method (classical and extremum principle) for examples 5 and 6 are shown in Figures 5.25 and 5.26. It is found that the factors of safety are much greater than unity, which is greatly different from the assumption by Sarma and Tan (2006) which assumed that the factor of safety along the interfaces between slices/blocks is unity at all the interfaces or in the limit analysis by Chen (1975). In this respect, the present approach has the advantage of requiring less assumption in the basic formulation.

5.4.3 Assessment of residual strength and progressive failure

Before the initiation of the ultimate condition, part of the soil mass has yielded and stress will re-distribute until a failure mechanism is formed. This process is called the progressive failure which is well known but is seldom considered. To overcome this problem, local safety of factor with consideration of residual strength can be introduced to investigate the actual failure mechanism.

From the previous studies, it appears that there is no special advantage to the present formulation, even though an acceptable set of internal forces will always be determined from the present formulation without an assumption of $f(x)$ or the thrust line. It also appears that the redistribution of stress in Aglc is not important for normal problems. There are however some cases where the consideration of approximate progressive failure may greatly affect the results of analysis and design. The design of slope in such condition is difficult because:

1. For normal condition, the weak zone at the front of the slope will be stressed beyond the peak strength from a normal elastic finite element stress analysis. The latter part of the weak zone will still be controlled within the peak strength.
2. If the residual strength is used for the design, the factor of safety will be very low and seems unrealistic.
3. If the peak strength is used for the design, the factor of safety will be high which also seems unrealistic, as part of the weak zone should be stressed beyond the peak strength so that the residual strength is activated.
4. It is not easy to define the regions where the peak strength and residual strength are used for the analysis and design.

Consider a slope problem in Hong Kong (example 7) where the soil properties are given in Table 5.8 and the ground profile is shown in Figure 5.27. Since there is a 200mm thick weak zone which is shown by the region from A to B in Figure 5.27, 9 layers of soil nails are provided in the slope stabilization design. The minimum factor of safety and the critical failure failures are obtained by the particle swarm optimization method by Cheng (2007 a, 2007c) with a precision of 0.0001 for the objective function in the optimization search (not precision for the factor of safety determination). Based on the Spencer's method, the minimum factors of safety are 1.154 and 0.963 using the peak strength and the residual strength for soil layer 3. The critical failure surfaces based on the peak strength and the residual strength are virtually the same (follow line AB) as the failure is controlled purely by the weak zone. Using the formulation Aglc where the peak strength is used initially, but under stress-redistribution the residual strength will be used which is similar to the concept by Lam et al. (1987), a global factor of safety 1.034 will be obtained. The base normal forces for the three cases are shown in Figure 5.28. Under the Aglc formulation, the initial 7.2m of the failure surface will be controlled by the residual strength with a local factor of safety 1.0 while the later part of the failure surface will still be controlled by the peak strength with a local factor of safety greater than 1.0. This phenomenon can be viewed as an assessment of the progressive failure development, where the initial 7.2m of the weak zone which has attained the residual strength is no longer able to take up additional increase of loads. The concept by Lam et al. (1978) which is actually not possible to be implemented into the classical limit equilibrium formulation can now be adopted under the present formulation. It is also noticed that the residual strength has played a significant role in the factor of safety of this slope and cannot be neglected in the analysis and design.

5.5 Study on convergence

Failure to converge for “rigorous” methods is well known to many engineers, particularly when there are external loads and soil nails. Cheng et al. (2008b) have carried out a detailed study on the convergence problem of Morgenstern-Price’s method (1965), and they found that one of the reasons for divergence is the use of an iteration method with zero interslice shear force in the first step of the iteration. Cheng (2003) has proposed the double QR method which determines the factor of safety directly without the requirement of an initial trial, and the factors can be classified into three groups: negative numbers, imaginary numbers, and positive numbers. If no physically acceptable solution is found from the positive results from the double QR method, the problem under consideration has no solution by nature. Every failure surface should physically bear a factor of safety, and for this kind of “failure to converge” which is the basic limitation of the assumed $f(x)$, it is possible to ensure convergence by tuning $f(x)$ until a physically acceptable factor of safety is obtained. Based on the extremum principle as outlined in section 5.2, the problem of convergence will be investigated in this section.

Consider the slope with a steep failure surface as shown in Figure 5.29. The factors of safety are 1.542, 1.570, 1.526, and 1.550 based on Bishop's method (1955), Janbu's simplified method (without the correction factor), the Swedish method, and Sarma's method. The extrema are 1.602 and 1.547 if Eq.(5.3) is not enforced and are 1.564 and 1.559 if Eq.(5.3) is considered. No physically acceptable result can be found for Spencer's method (1967) using the double QR method, and "failure to converge" is the fundamental problem in assuming $f(x)$=1.0.

If there is vertical loading of 30 kPa applied at the right hand side on the top of the slope as shown in Figure 5.4, the critical circular failure surface is to be determined. The minimum factors of safety from Spencer's method (1967) using the double QR method and the iteration method are 0.995 and 0.989, respectively. Based on the harmony search, the percentages of surfaces that fail to converge are 6.2 and 24.6 for Spencer's method (1967) for this problem, based on the double QR method and the iteration method respectively. It can be noted that there is a high percentage of failure by the classical iteration analysis, which has been investigated in detail by Cheng et al. (2008b). The double QR method has greatly overcome the limitations of the iteration method by direct evaluation of the factor of safety, but 6.2% of those slip surfaces still fail to converge due to the enforcement of $f(x)$=1.0 for the present simple problem. The minimum factors of safety using the harmony search for the extrema are 1.013 and 0.85 if Eq.(5.3) is not applied, and they are 1.002 and 0.901 if Eq.(5.3) is used; and there is virtually no failure to converge based on the present approach. It can be observed that the lower bound of the factor of safety is relatively low as compared with the result by Spencer's method (1967), which means that the choice of $f(x)$ is actually important for this case and is contrary to the comment by Morgenstern (1992) that $f(x)$ is not important except for isolated cases .

Though the use of the simulated annealing method to determine the factor of safety of a single failure surface is time-consuming, the objective function factor of safety is practically a continuous function so that the more efficient harmony search method can be used to locate the critical failure surface. The present method is hence a practical solution for the engineer, and the time required to obtain the critical circular failure surface is about 10 minutes for the present problem, which can be considered as acceptable. A further advantage of the present method is that the upper and lower bounds of the factor of safety for the critical failure surface can be evaluated for reference.

For the problem as shown in Figure 5.4, if c'=5 kPa and ϕ'=20°, there are about 5700 $f(x)$ during the optimization search for which no factors of safety associated with acceptable internal forces are found. These 5700 cases have been carefully examined and grouped into three major categories, apart from some cases that are completely random. The first two cases constitute about 15% of all the failure to converge cases and are shown in Figures 5.30 and 5.31. Type 1 $f(x)$ fluctuates randomly with x, and the magnitude of the fluctuation is quite significant. For Type 2 $f(x)$, $f(x)$ is high at the two extremes of x and is low in the middle. Type 3 $f(x)$ in Figure 5.32 constitutes about 80% of all the failure-to-converge cases and is particularly important. Type 3 $f(x)$ looks like Eq.(5.5) except that $f(x)$ is near the maximum at the left for a short interval of x. Type 3 $f(x)$ decreases rapidly toward 0 at about x=0.3 and is practically zero beyond that. It should be noted that a spike have appeared after x=0.3 which is actually case dependent in general. In general, these three types of $f(x)$ also apply to other soil parameters when there is no soil nail or external load.

5.6 Conclusions and Discussions

Factor of safety and the critical slip surface are the main interests to the engineers in slope stability analysis. In this chapter, the author has developed the extremum principle and the concept of variable factor of safety based on the Pan's postulate (lower bound principle). Under such condition, the unknown $f(x)$ becomes determinate. Actually, the use of the concept of ultimate limit state is the missing equation which will complement the force and moment equilibrium to give the factor of safety without additional assumption as in all the classical limit equilibrium methods. Besides the limit equilibrium method, the author has also adopted the SRM in determining $f(x)$ and thrust line. Based on LEM and SRM, it is found that the interslice force function varies with slopes with different soil properties and geometry and should not be arbitrarily specified. Basically, for slopes controlled by self weight, interslice force function is a bell-shaped function which is similar to the results by Fan, Fredlund and Wilson (1986), except for a part near to the toe of slope.

Cheng et al. (2007) and many others have found that the results from the LEM and SRM are similar in general. In the present study, one important difference is found, at least for all the existing limit equilibrium formulations. From the results in SRM, it is noticed that the factor of safety is introduced to the whole soil mass so that the factor of safety must be introduced into the interslice force relation. Such a requirement is however not mandatory in the LEM, and the factor of safety is only enforced at the slice base while the

Mohr-Coulomb relation along the vertical interface can be used without the application of the factor of safety. It is possible that the factor of safety can also be introduced to the interface force relation (though not used in any LEM method at present). For practical application, since the interslice shear force is not sensitive to the overall factor of safety, the enforcement of the factor of safety in the interslice force relation appears to be not a critical factor, though conceptually the factors of safety from LEM and SRM cannot be compared directly because of this requirement.

In Janbu's Rigorous Method (1973), the position of the thrust line is assumed at the 1/3 of slice length from the base to render the problem statically determinate. The above investigations on simple slope basically agree well with the Janbu's Rigorous method (1973). Slight difference exists at the exit end of the sliding soil mass where the points of thrust line are located at nearly half of the slice height. When the slope angle is steep, the difference between the actual thrust line and 1/3 slice height is found to be small. When the sliding soil mass is deep-seated or the properties of slope is complex leading to below toe failure, more attention should be paid in defining the thrust line.

For the two extrema from the present analysis, it is proposed that the maximum extremum should be taken as the factor of safety of the prescribed failure surface. As discussed, the internal forces within the soil mass should redistribute until the maximum resistance capacity of the soil mass is fully mobilized. Beyond that limit, the soil mass will start to fail. The present proposal also possesses an advantage in that it is independent of the definition of $f(x)$. It is well known that there are also cases where $f(x)$ may have a noticeable influence on the factor of safety. There is no clear guideline on the acceptance of the factor of safety due to the use of different $f(x)$. The use of the maximum extremum can also avoid this dilemma, which has been neglected in the past. The approach in section 5.2 is a typical lower bound approach, as statically admissible forces associated with a prescribed $f(x)$ are considered. The selection of the maximum factor of safety is hence justified from the lower bound theorem.

While an arbitrary choice of $f(x)$ may be in conflict with Eq.(5.3) or no solution can be evaluated, the present approach, which is based on a global optimization method, provides results that are physically consistent and acceptable. The approach in section 5.2 possesses the following advantages: (1) it avoids the assumption of $f(x)$ or other similar relation, (2) it exhibits virtually no failure to converge, (3) consistent and acceptable internal forces complying with force and moment equilibrium are determined, (4) it provides the bounds to the actual factor of safety, (5) it determines $f(x)$ during the evaluation of the factor of safety, and (6) the problem of the variational principle as discussed by Jong (1980, 1981) and Castilo and Luenco (1980, 1982) is automatically eliminated by using the global optimization analysis in the present approach.

Within the context of classical slope stability analysis where the factor of safety is defined in terms of the ultimate shear strength and mobilized shear strength, there should only be a single factor of safety for a problem. On the other hand, for normal stable slope with an overall factor of safety greater than 1.0, at least part of the system is not situated at the ultimate condition. The present study has demonstrated that for such cases, the factors of safety based on a variable factor of safety and the classical approaches are similar. In this respect, the present formulation provides an alternative to the classical methods of analysis. For normal and practical problems, the present formulation provides no advantage over the classical methods of analysis. On the other hand, for those cases of stable slopes where the factors of safety is slightly above 1.0 and part of the system may be controlled by the residual strength, the present formulation provides an estimation of the factor of safety which is not possible with the classical methods of analysis.

Imposing Pan's principle, two different extremum formulations based on variable factor of safety concept are proposed in section 5.2 and 5.4, which can consider global and local equilibrium and satisfying all the equilibrium conditions without any assumption as in the classical formulations. Pan's principle is actually the combination of lower and upper bound approach which is purely a concept without any practical numerical procedures. The author has developed the global optimization methods in chapter 3 and the numerical algorithms for the Pan's principle in chapter 5. The most difficult question in slope stability analysis can now be considered as settled under the Pan's principle or the lower bound method.

Table 5.1a Factors of safety from lower bound and Spencer's analysis for Example 2 (* Spencer's result violates Eq.(5.3))

Case	Max. FOS no Eq.(5.3)	Max FOS with Eq.(5.3)	Min. FOS no Eq.(5.3)	Min. FOS with Eq.(5.3)	Spencer
c'=0 kPa, ϕ'=20°	0.759	0.749	0.738	0.743	0.745*
c'=0 kPa, ϕ'=40°	1.753	1.733	1.702	1.708	1.718
c'=5 kPa, ϕ'=20°	1.017	1.012	1.002	1.003	1.007
c'=5 kPa, ϕ'=40°	2.008	1.998	1.966	1.965	1.98
c'=10 kPa, ϕ'=20°	1.280	1.277	1.268	1.267	1.272
c'=10 kPa, ϕ'=40°	2.263	2.261	2.230	2.229	2.242

Table 5.1b λ from lower bound and Spencer's analysis for Example 2 (* Spencer's result violates Eq.(5.3))

Case	Max. FOS no Eq.(5.3)	Max FOS with Eq.(5.3)	Min. FOS no Eq.(5.3)	Min. FOS with Eq.(5.3)	Spencer
c'=0 kPa, ϕ'=20°	1.867	1.0	1.888	1.0	0.522*
c'=0 kPa, ϕ'=40°	1.82	1.151	1.886	0.901	0.522
c'=5 kPa, ϕ'=20°	1.89	0.892	1.873	1.758	0.457
c'=5 kPa, ϕ'=40°	1.857	1.208	1.896	1.903	0.491
c'=10 kPa, ϕ'=20°	1.711	1.024	1.889	1.893	0.407
c'=10 kPa, ϕ'=40°	1.855	1.432	1.846	1.907	0.464

Table 5.2 Soil parameters of Example 2

Soil	Unit weight (kN/m^3)	Saturated unit weight (kN/m^3)	c' (kPa)	ϕ' (°)
Top	18	20	5	36
Second layer	15	17	3	30

Table 5.3a Factors of safety from lower bound approach and Spencer's analysis of Example 2

Case	Max. FOS no Eq.(5.3)	Max FOS with Eq.(5.3)	Min. FOS no Eq.(5.3)	Min. FOS with Eq.(5.3)	Spencer
Bottom nail	1.856	1.841	1.750	1.763	1.790
2 nails	2.661	2.600	2.398	2.498	2.515

Table 5.3b λ from lower bound approach and Spencer's analysis of Example 2

Case	Max. FOS no Eq.(5.3)	Max FOS with Eq.(5.3)	Min. FOS no Eq.(5.3)	Min. FOS with Eq.(5.3)	Spencer
Bottom nail	1.149	0.944	0.924	1.902	0.488
2 nails	1.435	1.281	1.149	2.011	0.547

Table 5.4 Summation of λ obtained by different methods

		LEM	FDM	FEM
c'=2kPa β=45°	ϕ'=10°	0.7522	0.7889	0.7645
	ϕ'=20°	0.9324	0.8192	0.8213
	ϕ'=30°	0.9885	0.8232	0.8174
	ϕ'=40°	1.2477	0.8830	0.8069
ϕ'=10° β=45°	c'=2kPa	0.7522	0.7889	0.7645
	c'=10kPa	0.8996	0.7313	0.6792
	c'=20kPa	0.4936	0.5996	0.6510
	c'=30kPa	0.0320	0.5519	0.6467
c'=30kPa ϕ'=40°	β =30°	0.5297	0.4536	0.4478
	β =45°	1.7007	0.7424	0.7644
	β =60°	0.7979	0.8837	0.9877

Table 5.5 Minimum factors of safety for example 5

Methods of analysis	Ailc		Aglc		MP	Cheng (Spencer)	Greco (Spencer)	Yamagami (Spencer)
	n=11	*n*=15	*n*=11	*n* =15				
Factor of safety	1.349	1.376	1.320	1.354	1.345	1.325	1.327	1.338

Table 5.6 Geotechnical parameters for example 6

Layers	γ (kN/m^3)	c' (kPa)	ϕ' (°))
1	19.0	15.0	20.0
2	19.0	17.0	21.0
3	19.0	5.00	10.0
4	19.0	35.0	28.0

Table 5.7 Minimum factors of safety for example 6

Methods	Ailc		Aglc		Cheng (Spencer)	Zolfaghari (Spencer)
	n=11	*n*=21	*n*=11	*n*=15		
Factor of safety	1.053	1.150	1.170	1.187	1.11	1.24

Table 5.8 Geotechnical parameters of example 7

Layers	γ (kN/m^3)	c' (kPa) (peak)	ϕ' (°) (peak)	c' (kPa) (residual)	ϕ' (°) (residual)
1	20	10	40		
2	18	2	34		
3	18	2	24	0	21
4	18	5	38		

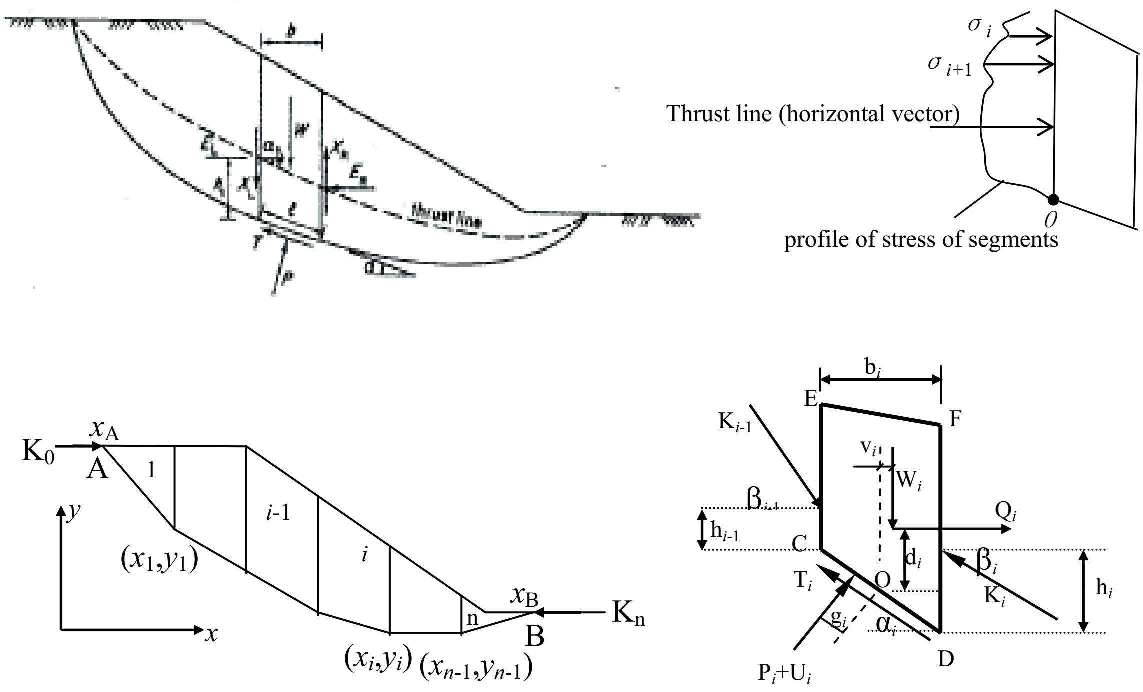

Figure 5.1 Interslice forces and determine of thrust line

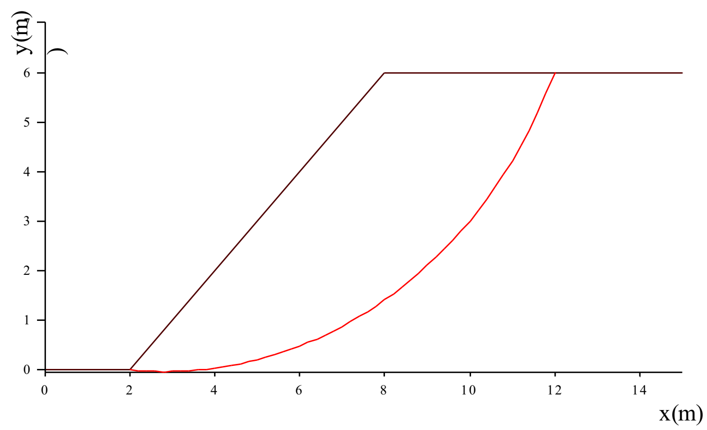

Figure 5.2 A simple slope with a circular failure surface – example 1

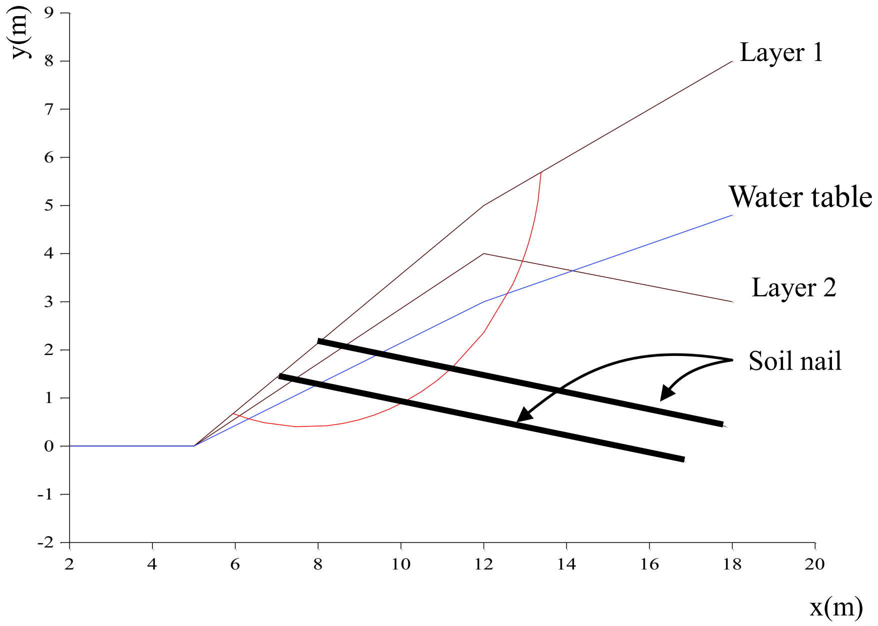

Figure 5.3 A problem with two soils, two soil nails, and a water table – example 2

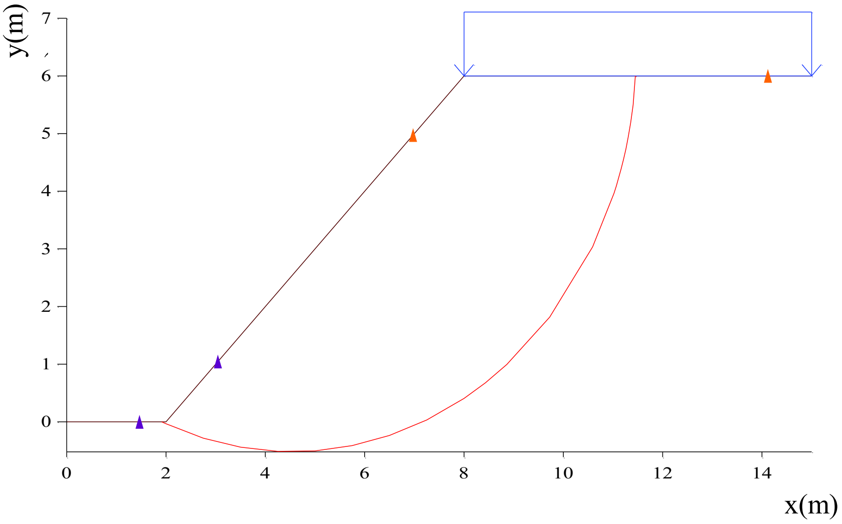

Figure 5.4 Slope with a deep-seated failure surface and a vertical pressure – example 3

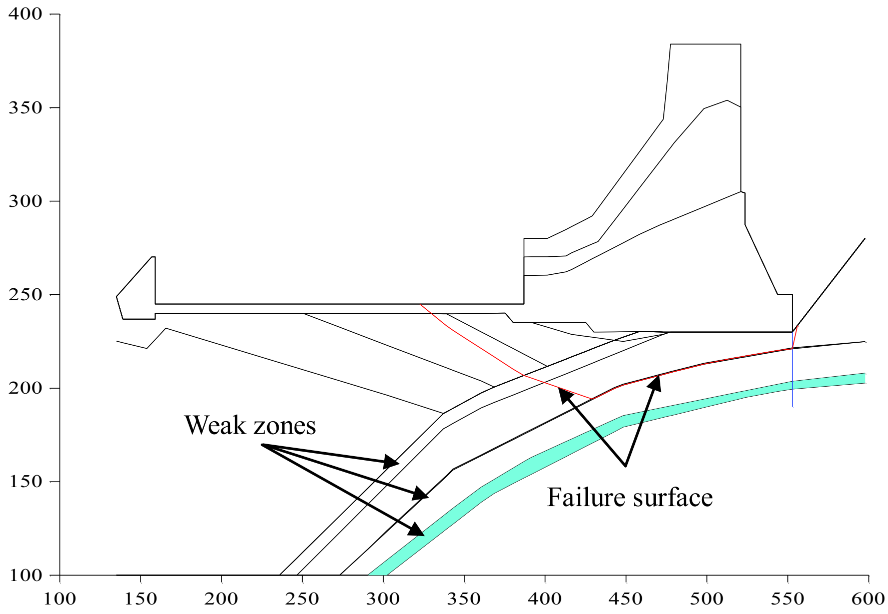

Figure 5.5 A complicated problem where there is a wide scatter in the factor of safety – example 4

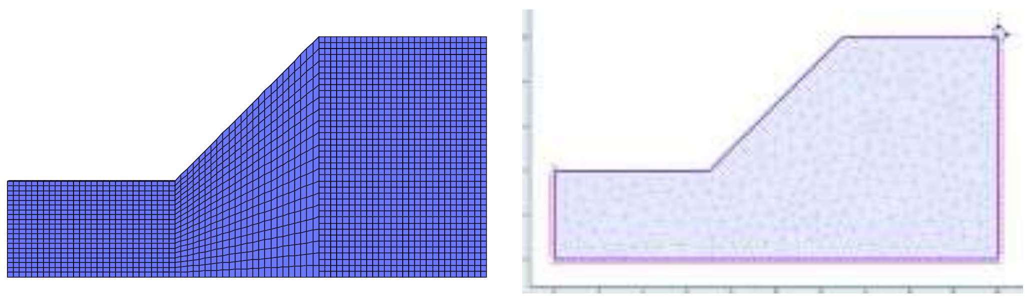

a FDM b FEM

Figure 5.6 Numerical models for 1:1 slope in FDM and FEM

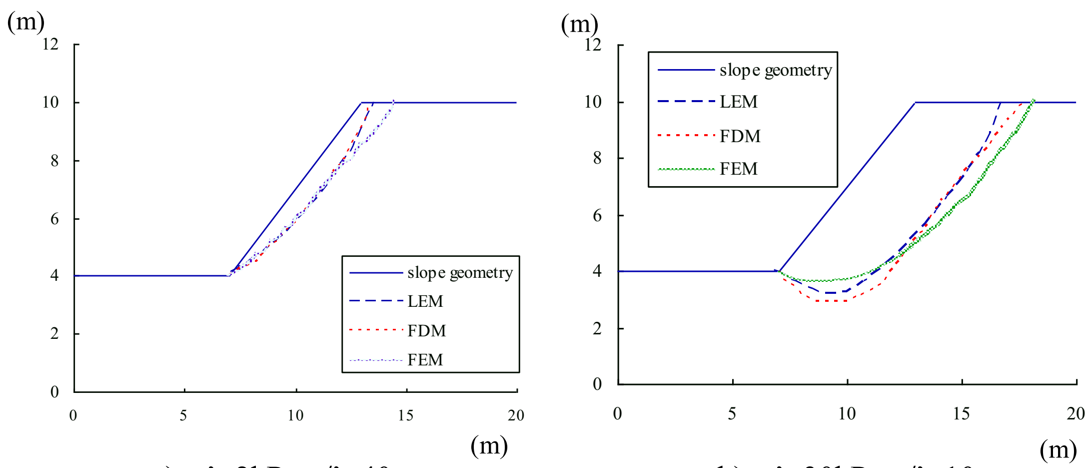

a) c'=2kPa, ϕ'=40 b) c'=30kPa, ϕ'=10

Figure 5.7 Comparisons of critical slip surfaces

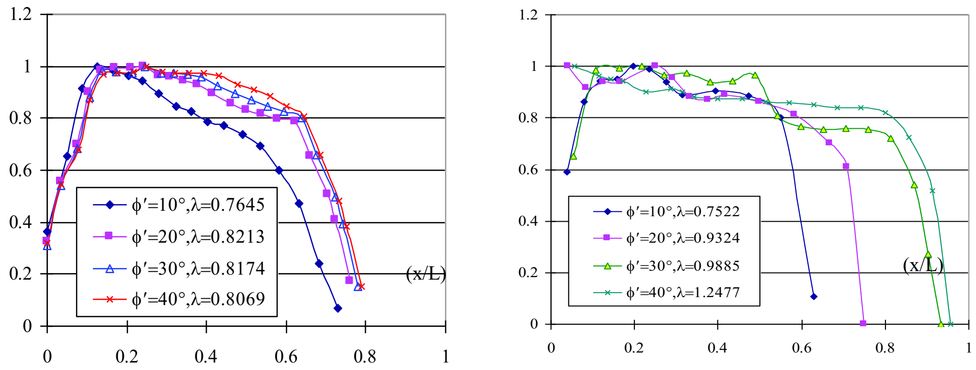

a) SRM b) LEM

Figure 5.8 $f_1(x)$ of slope with varying ϕ' when c'=2kPa

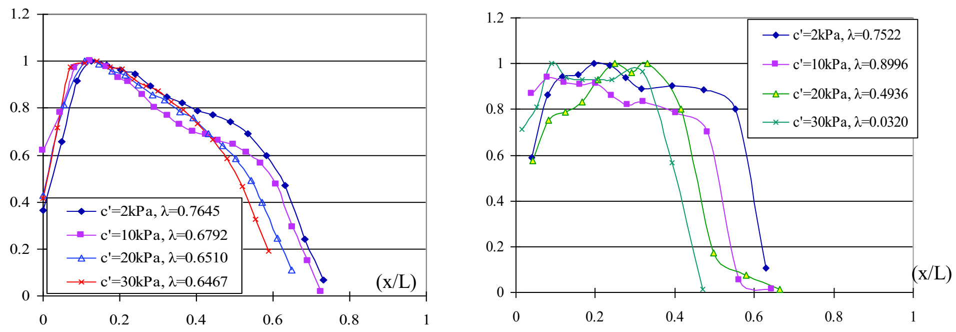

a) SRM b) LEM

Figure 5.9 $f_1(x)$ of slope with varying c' when ϕ'=10°

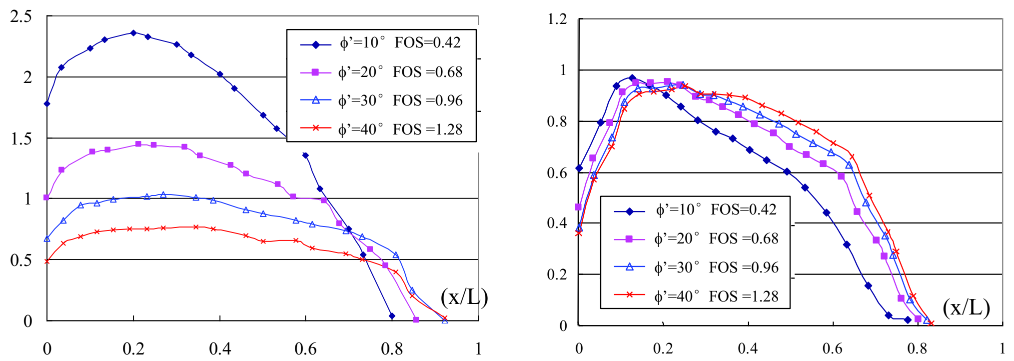

a) SRM (when FOS is not used) b) SRM (when FOS is used)

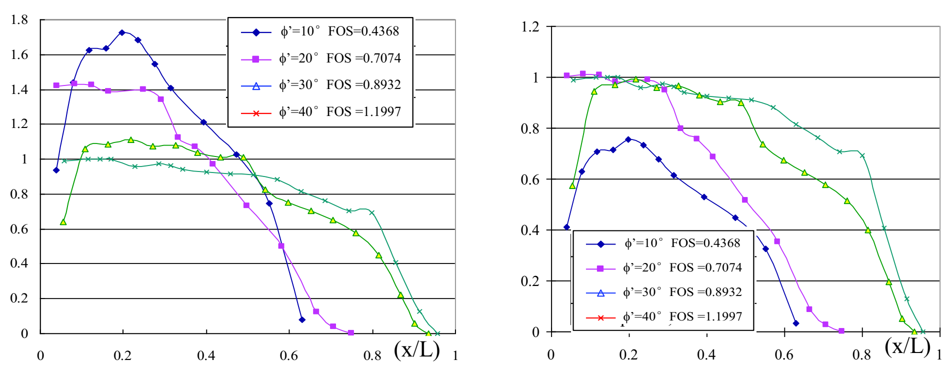

c) LEM (when FOS is not used) d) LEM (when FOS is used)

Figure 5.10 $f_2(x)$ of slope with varying ϕ' when c'=2kPa

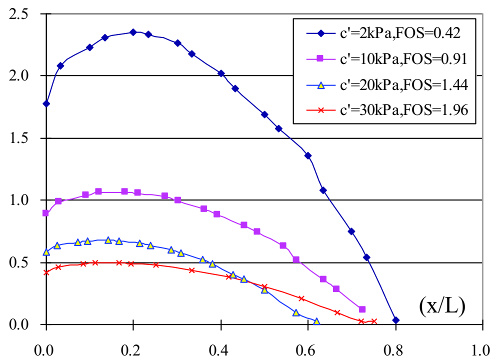

a) when FOS is not used

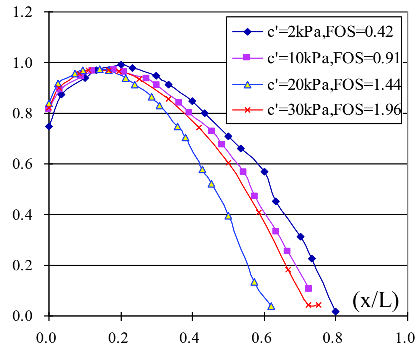

b) when FOS is used

Figure 5.11 $f_2(x)$ of slope with varying c' when ϕ'=10°

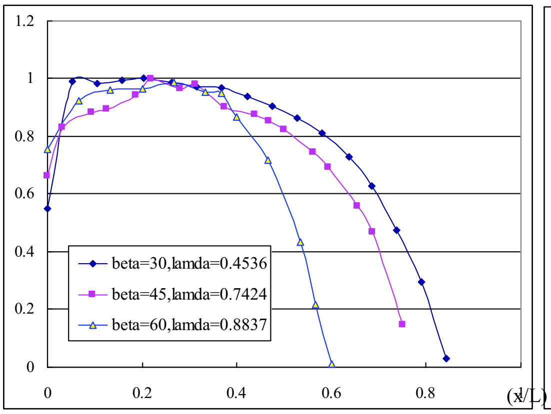

a) FDM

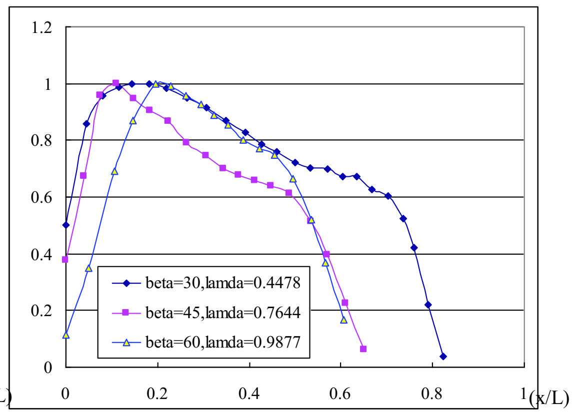

b) FEM

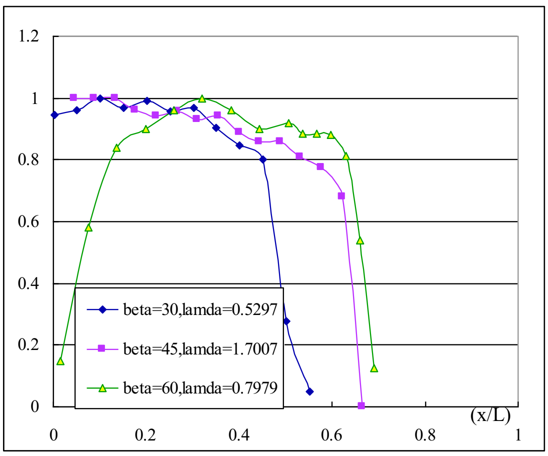

c) LEM

Figure 5.12 $f_1(x)$ when c'=30kPa and ϕ'=40°

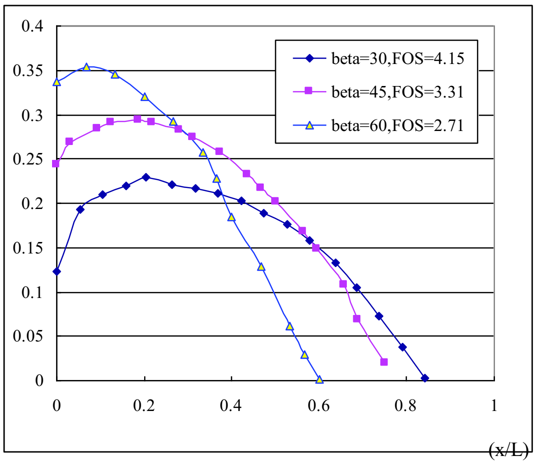

a) FDM (when FOS is not used)

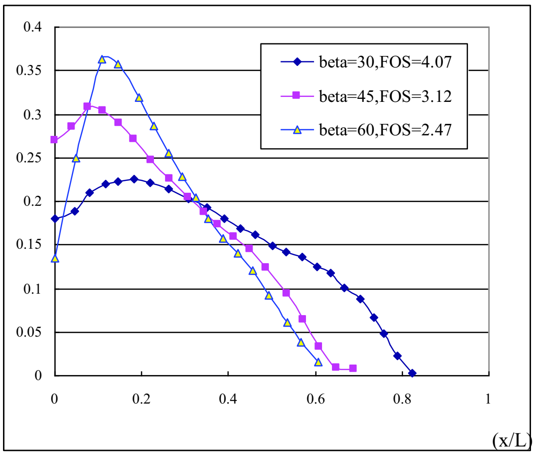

b) FEM (when FOS is not used)

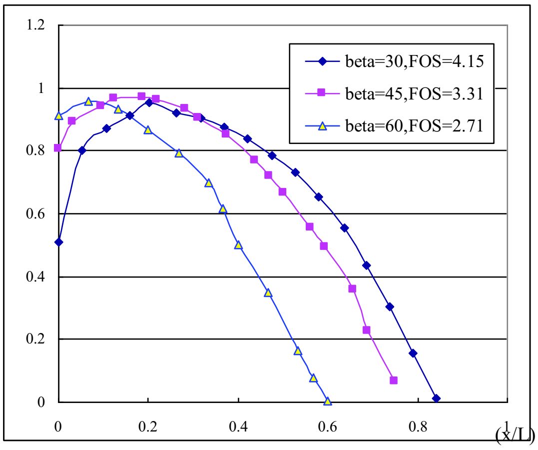

c) FDM (when FOS is used)

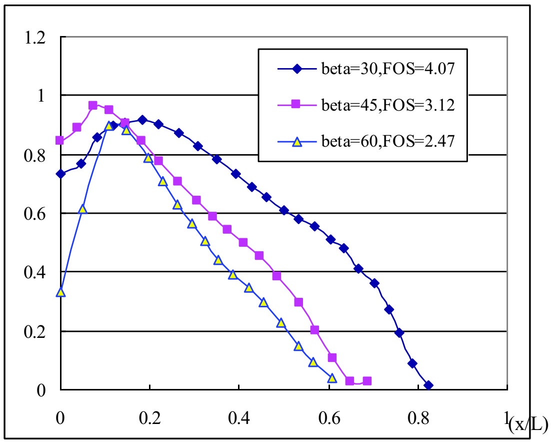

d) FEM (when FOS is used)

Figure 5.13 $f_2(x)$ with varying slope angle when c'=30kPa and ϕ'=40°

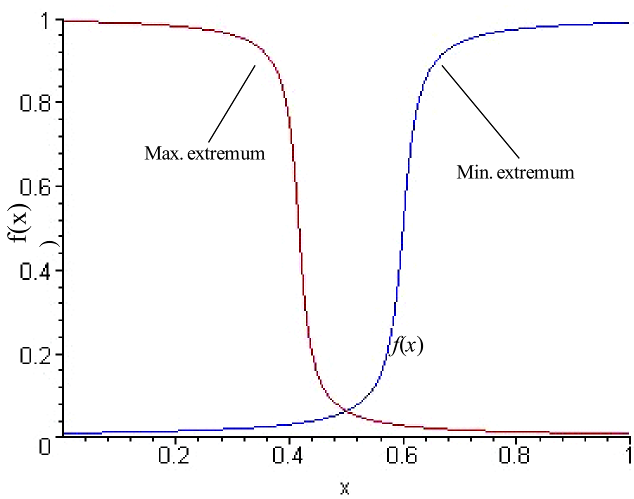

Figure 5.14 Simplified $f(x)$ plotted against dimensionless x for the determination of the maximum and minimum extrema

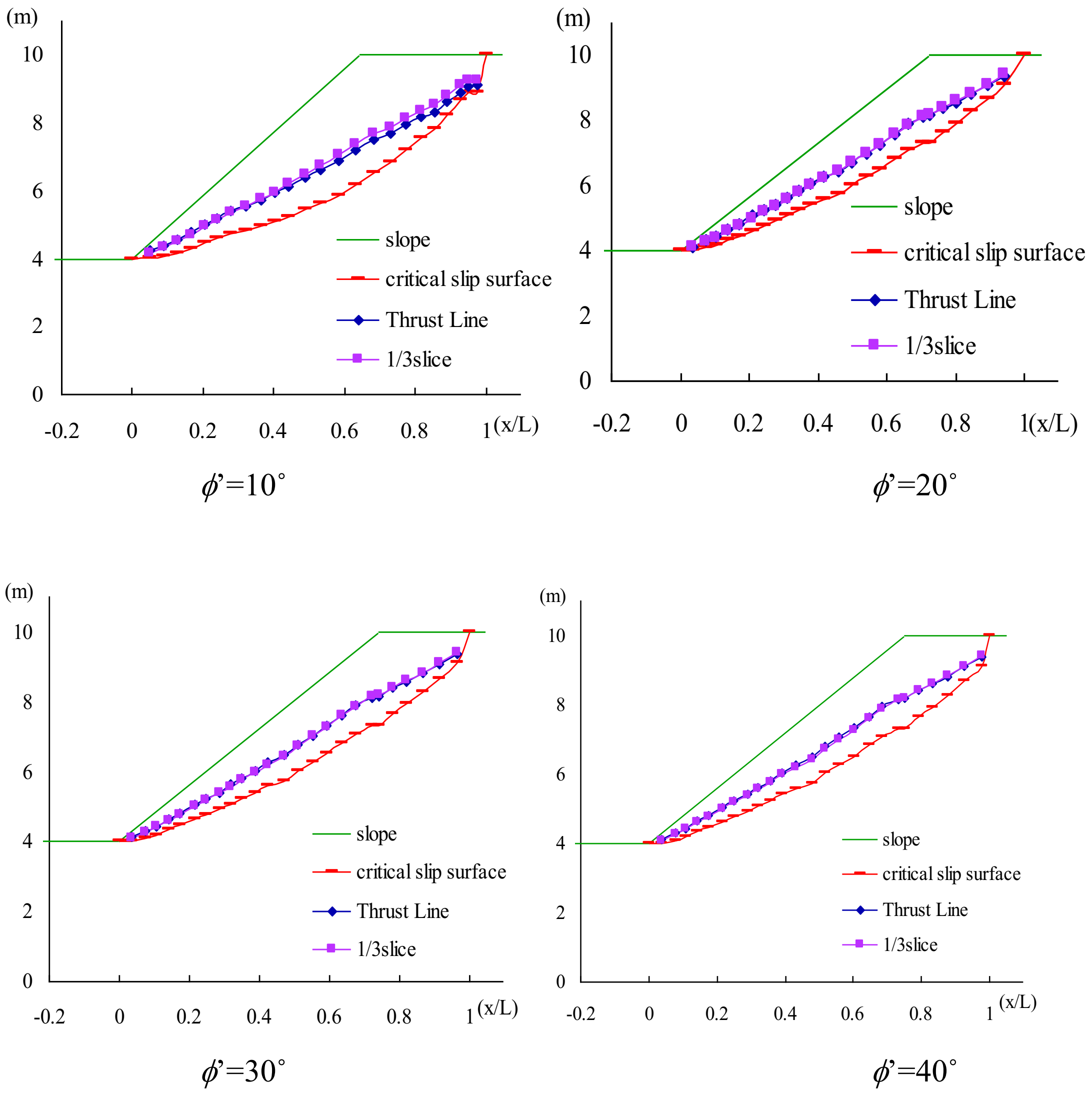

Figure 5.15 Thrust line of slope with varying ϕ' when c'=2kPa

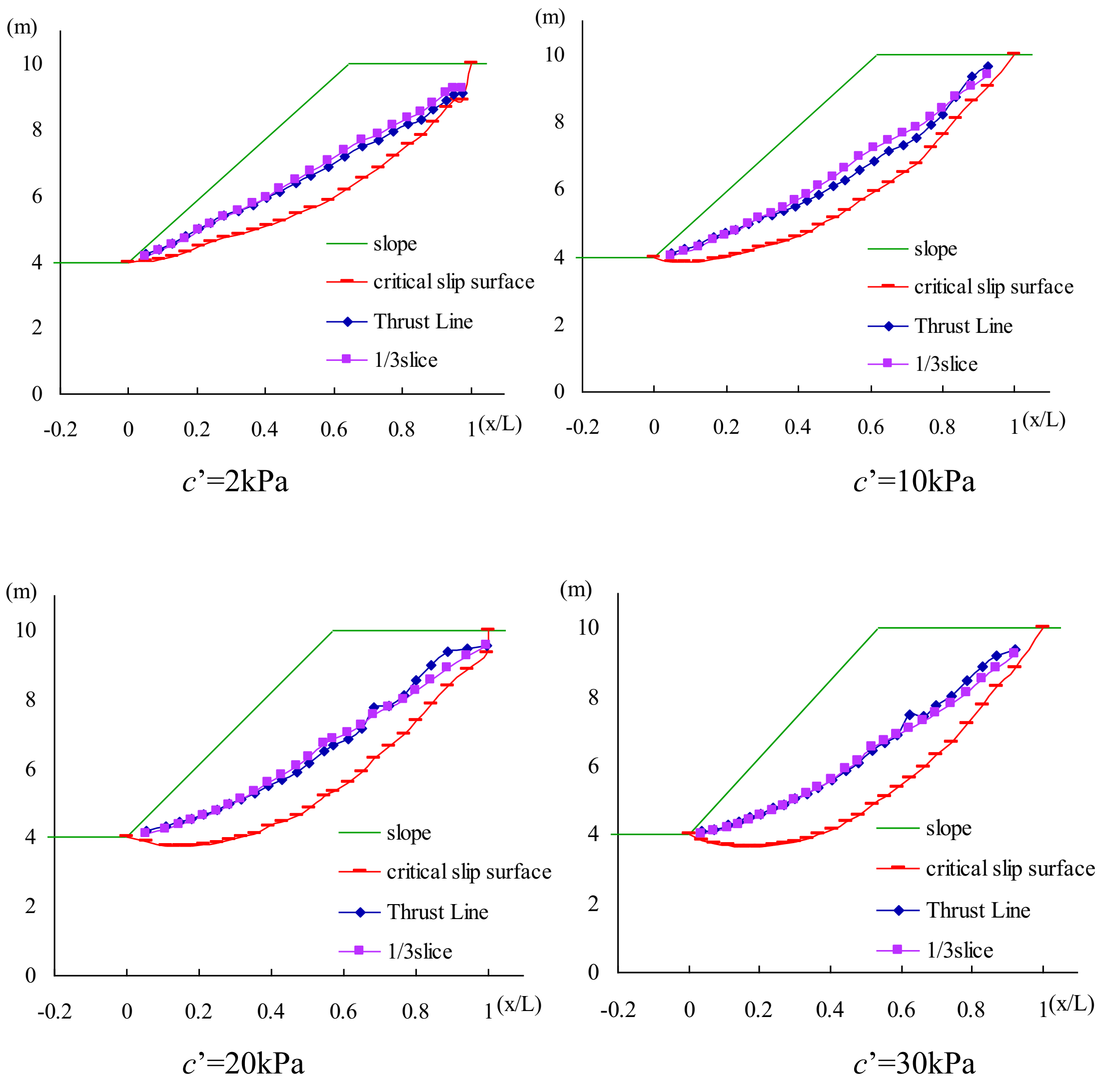

Figure 5.16 Thrust line of slope with varying *c*' when ϕ'=10°

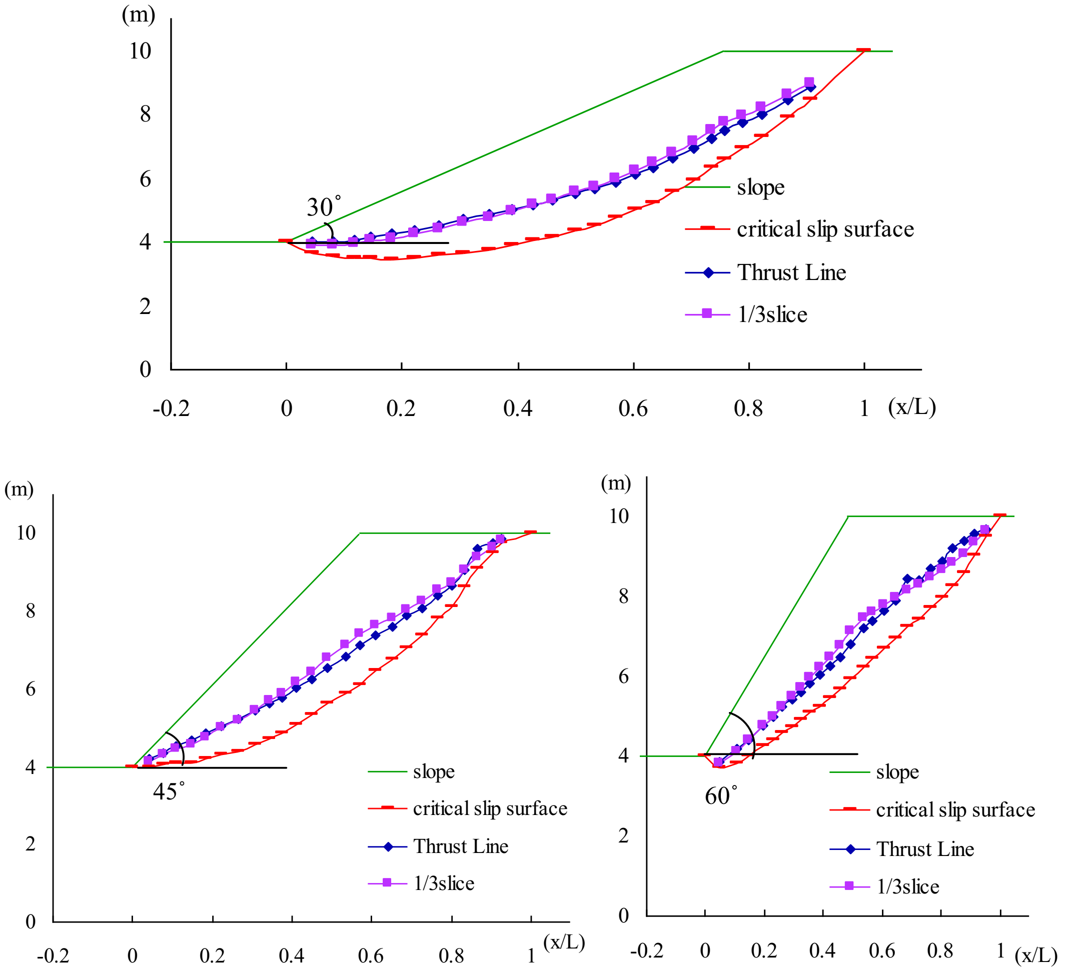

Figure 5.17 Thrust line of slope with varying slope angle when c'=30kPa and ϕ'=40°

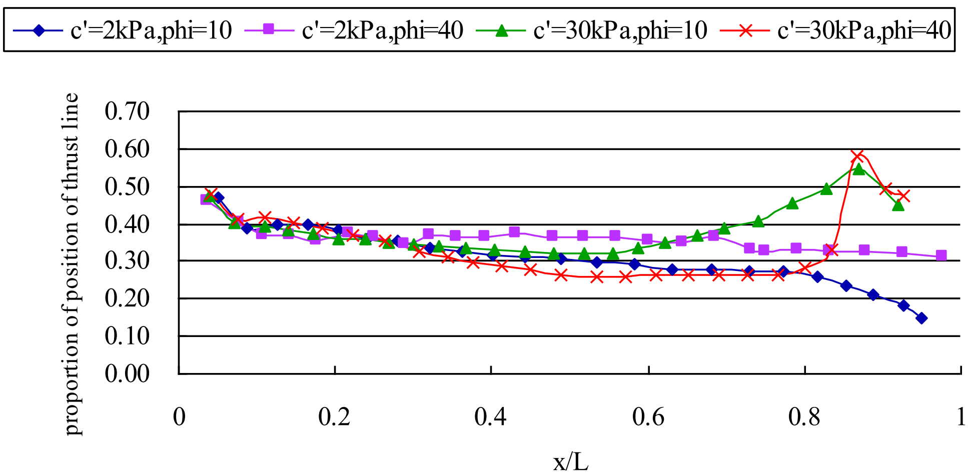

Figure 5.18 Proportion of position of thrust line to slice length

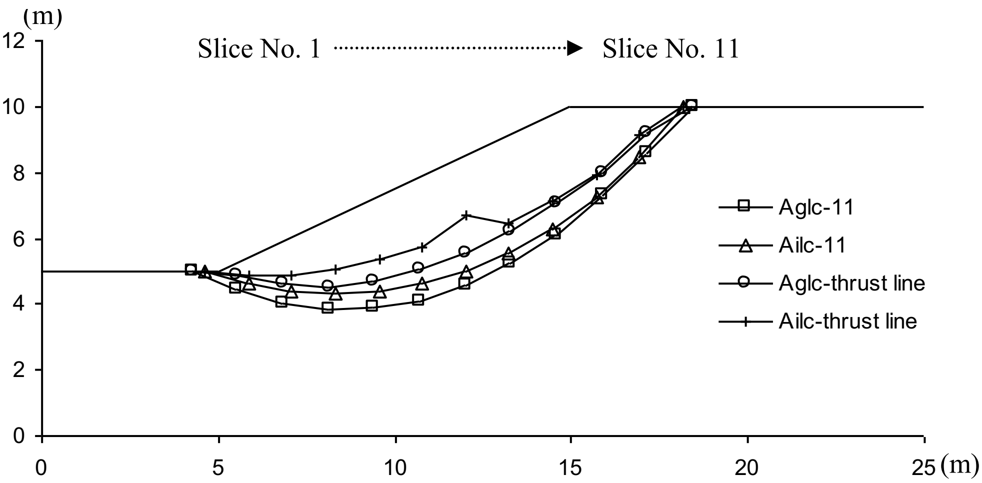

Figure 5.19 Critical slip surfaces and corresponding thrust lines by different methods for example 5

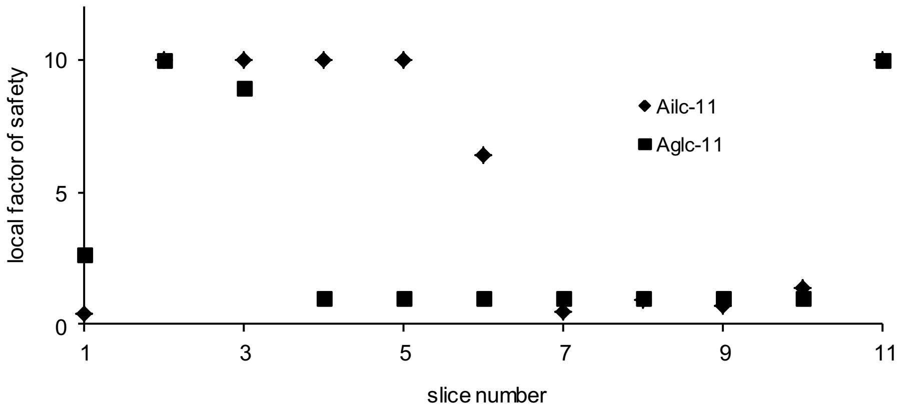

Figure 5.20 Distribution of the local factor of safety for example 5 (n=11)

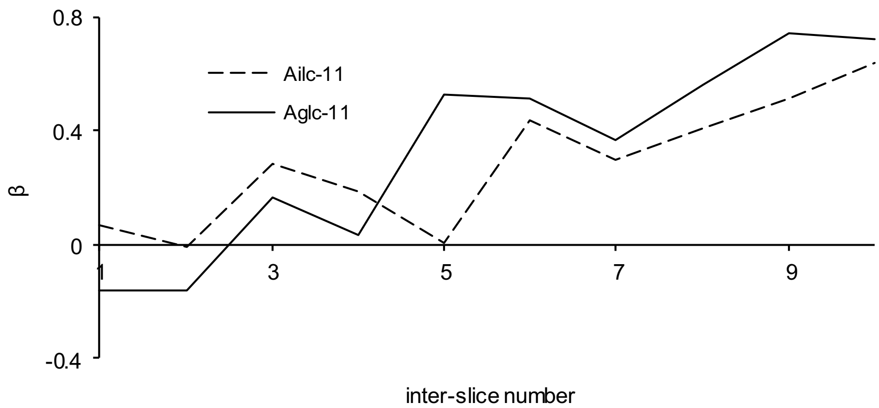

Figure 5.21 Distribution of β_i (in radian) for example 5 (n=11)

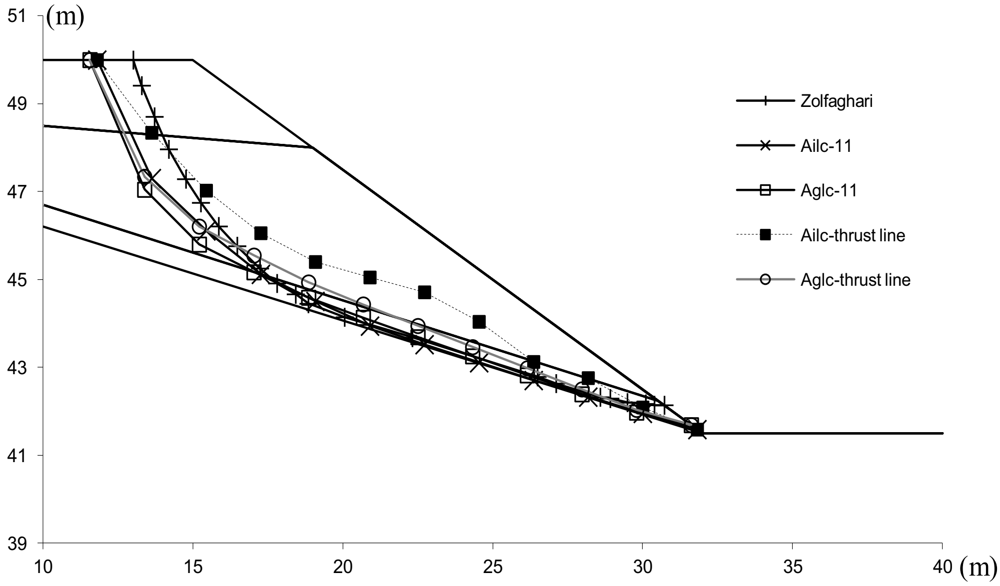

Figure 5.22 Critical slips surfaces and thrust lines by different methods for example 6

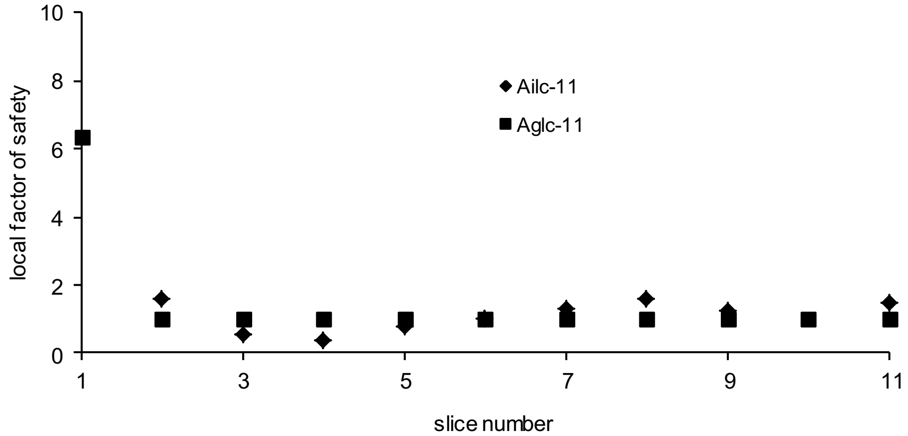

Figure 5.23 Distribution of the local factor of safety for example 6 (n=11)

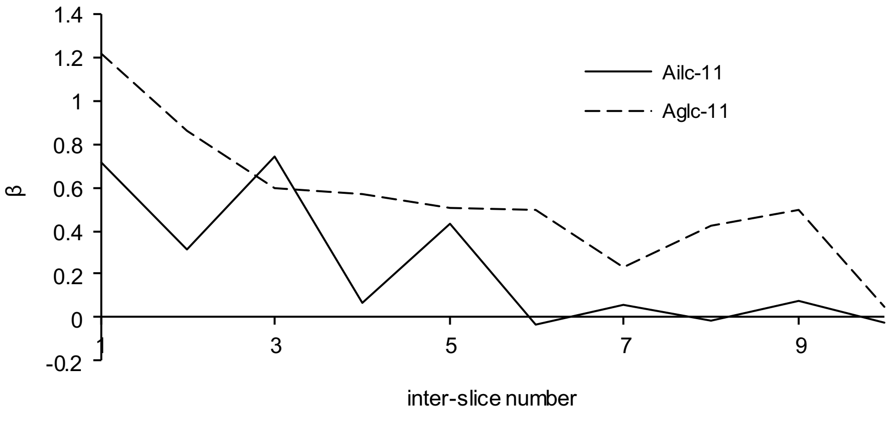

Figure 5.24 Distribution of β_i for example 6 (n=11)

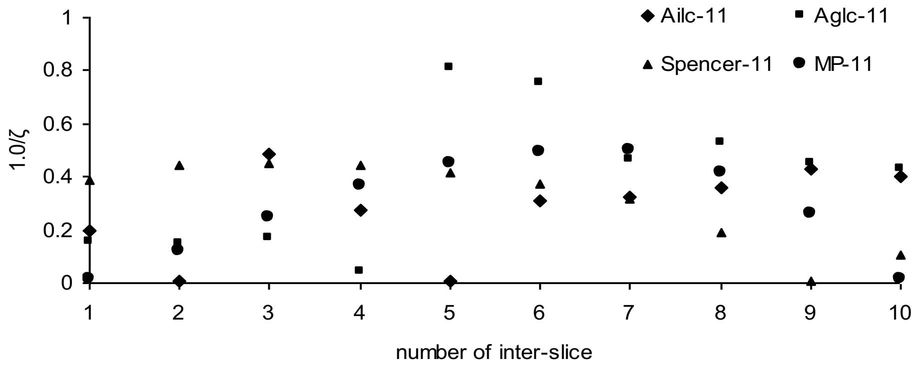

Figure 5.25 The local factor of safety ζ at interfaces for example 5

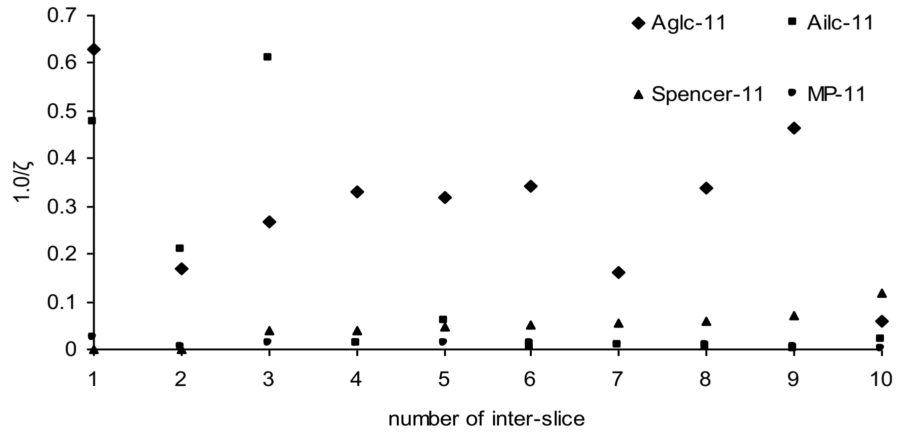

Figure 5.26 The local factor of safety ζ at interfaces for example 6

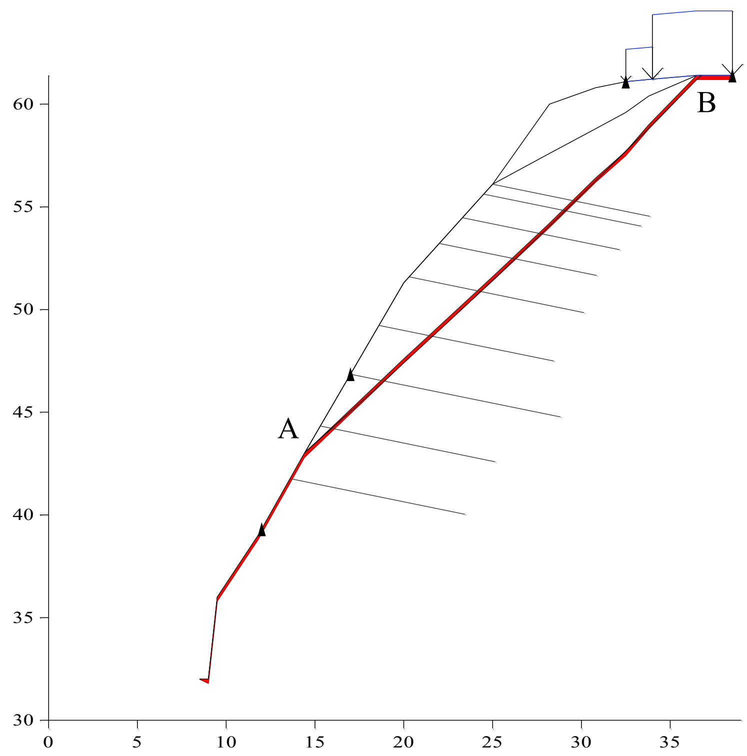

Figure 5.27 A slope with a thin weak zone in Hong Kong – example 7

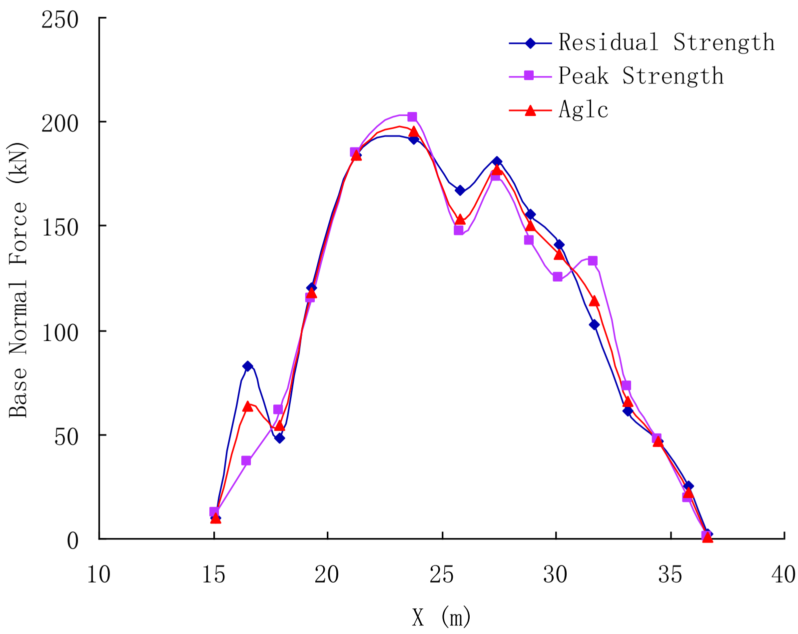

Figure 5.28 Base normal forces based on peak strength, residual strength and Aglc analyses

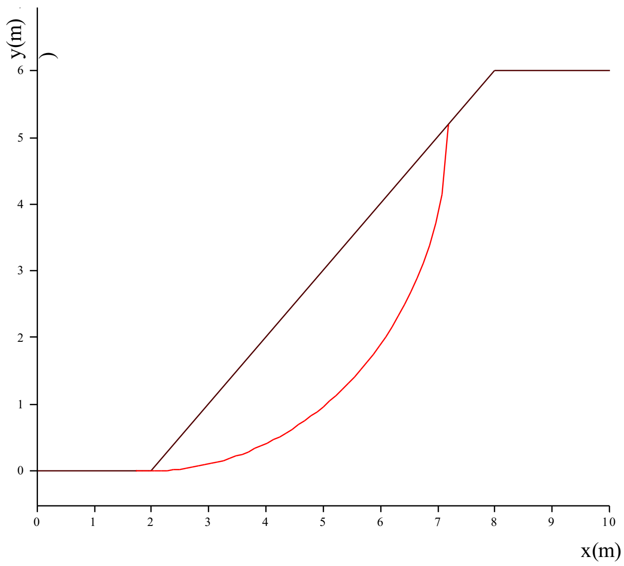

Figure 5.29 An example with a steep failure surface – example 8

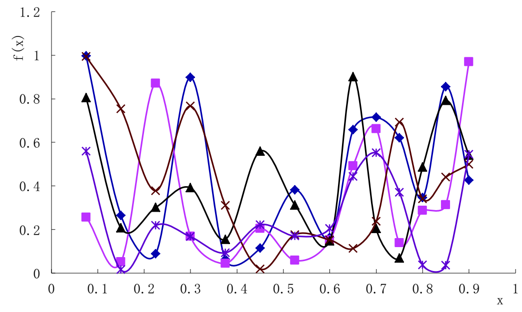

Figure 5.30 Type 1 *f*(*x*) plotted against dimensionless x for failure to converge

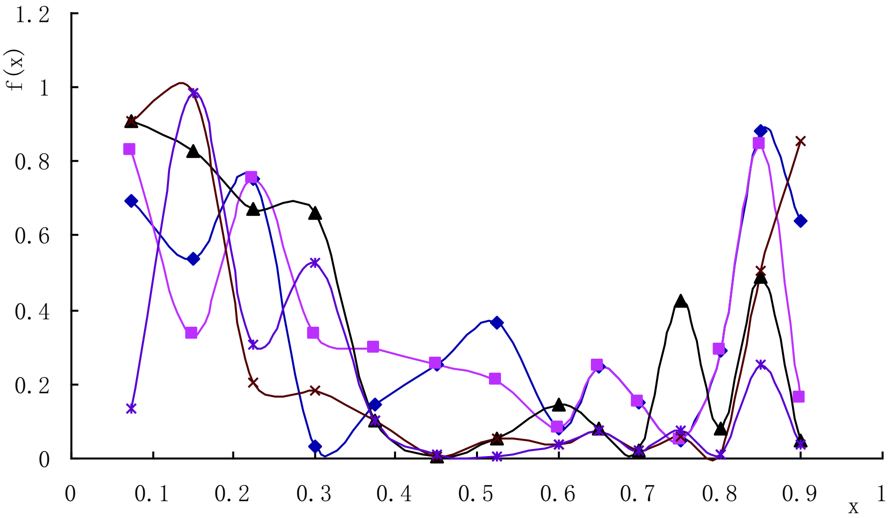

Figure 5.31 Type 2 *f*(*x*) plotted against dimensionless x for failure to converge

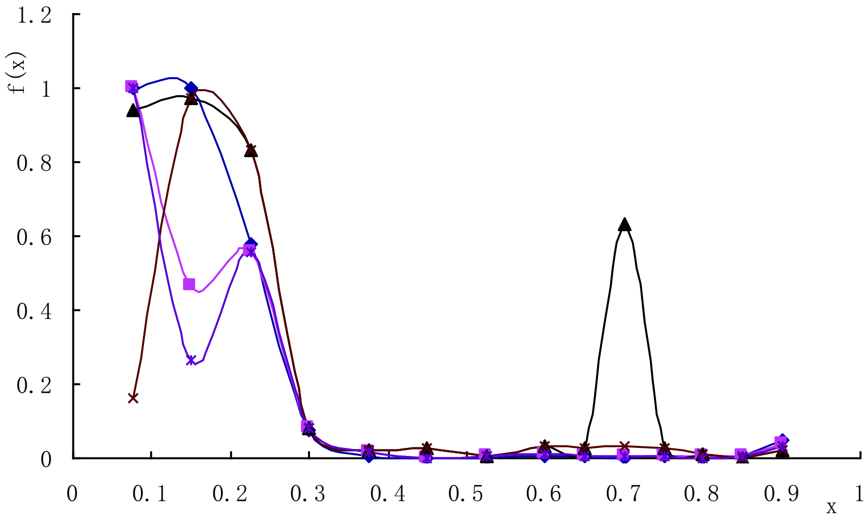

Figure 5.32 Type 3 *f*(*x*) plotted against dimensionless x for failure to converge

CHAPTER 6 Slope Stability Analysis in Three-dimension

6.1 Introduction

Although all slope failures are three-dimensional (3D) in nature, two-dimensional (2D) analysis is still adopted in most of the slope stability analysis because of various reasons. Most of 3D LEM methods including those by Hovland (1977), Chen and Chameau (1983), Zhang (1988), Ugai (1988), Lam and Fredlund (1993), Chang (2002), Chen et al. (2003a) adopt the assumption of symmetrical slip surface with a certain sliding direction. Such methods are basically the extension of 2D methods, where the interslice force relationship is extended to intercolumn force assumptions and the corresponding equilibrium equations are considered under 3D framework. Among these works, Lam and Fredlund (1993) in their development of a general LEM method have found that dominating intercolumn force functions are X/E and V/P with regard to the normal and vertical shear forces on the xy- and yz- plane (xz- and yz- plane in this study) respectively. Huang et al. (2002) in their general method for 3D slope stability analysis have also involved the intercolumn force, but their formulation suffers from several limitations which are discussed by Cheng and Yip (2007). Cheng and Yip (2007), on the other hand, developed an asymmetric model prescribing only one sliding direction for the whole failure mass. The convergence problem under transverse load in the Huang and Tsai formulation (2000) has been overcome under this new formulation, and Cheng and Yip (2007) have demonstrated that this approach is equivalent to rotation of sliding axis until the minimum factor of safety is determined. The advantage of this formulation is that there is no need to carry out the axis rotation explicitly, which will save tremendous computations with no loss of accuracy. 3D NURBS surface and the simulated annealing method proposed by Cheng et al. (2005) are incorporated to locate the 3D critical slip surface.

3D analysis by SRM is robust provided that sufficient computer time is allowed in the modelling. Many researchers have considered the 3D stability under different complex conditions of slope. Ugai and Leshchinsky (1995) have included a pseudo-static seismic force component in their 3D SRM analysis for vertical cuts. Zheng et al. (2005) have used program ANSYS to conduct an extensive SRM analysis in slope, tunnel and ultimate bearing capacity of foundations. Griffiths and Marquez (2007) have considered both vertical and inclined boundaries to investigate the constraint effect of slopes with finite length for several 3D slope examples by SRM. Deng et al. (2007) have also conducted 3D SRM to analyze the stability of a pre-existing landslide with multiple sliding directions.

For many slopes, due to route selection, geology, neighbor constructions and other necessary consideration, the slopes are curved in the geometric layout. For the previous 3D analysis methods, there are only limited works on the effect of curvature on the stability of slope. Rassam and Williams (1999) have conducted a survey on the curvature effect on fill slope stability with concave and convex faces by configuring the axi-symmetric option in FLAC2D. To investigate the three-dimensional geometry effect for both convexity and concavity conditions, this chapter will conduct 3D analyses on different geometry by FLAC3D. Intercolumn force function will also be investigated to supplement the intercolumn force function which is an outstanding work up to present.

6.2 Failure mechanism of curvilinear slope

Intuitively, curvature is the amount by which a geometric object deviates from being flat or straight. In general mathematics, curvature is in the inverse of the radius of curvature of 2D circle or 3D surface. In the point of view of civil engineering, curvature can be classified as concavity and convexity. The curvature of plane facing can be regarded as zero with infinite radius.

By changing the orientation relative to the axis of symmetry, both convex and concave slopes can be obtained by extension of 2D slope using the basic section as shown in Figure 6.1. The simple slope is with section of similar geometry as those adopted in 2D analysis in Chapter 5. The friction angle of soil is prescribed as 20°, slope angle is 45°, height of slope is 6m, soil unit weight of 19kN/m^3 and cohesive strength of 20kPa or 4kPa are assumed. For pure convex and concave slopes with no transverse load, the problem domain is axi-symmetric. Similar to 2D plane-strain analysis, the tangential force or stress vector is zero in theory and only stress and force on the radial plane are considered as significant. Therefore, the radial intercolumn force function corresponds to f(x) and tangential intercolumn force function corresponds to f(y). For simplicity and clarity in this study, a slope is defined as locally convex when the curvature is positive or locally saddle when the curvature is negative according to the theorem of Gauss curvature. The radius of rotation about the axis of symmetry (R) is accordingly positive for convex and is negative for concave, and cylindrical coordinate system O(r, θ, z) will be adopted instead of the Cartesian coordinate system O(x,y,z) for the investigation of intercolumn force function, and f(r) and f(t) represent the radial and tangential intercolumn force function. By such definition, plane slope is the extreme situation of curvilinear slope with R=∞.

In general, the slip surfaces for 2D and 3D analyses are very similar for the present situation. The curvature seems to have not a noticeable influence on the 3D slope failure mechanism when the critical slip surface and the overall displacement vector are observed as shown in Figure 6.2(a), that is the critical slip surface is similar and the displacement is pointing to the slope toe in the radial direction in both convex and concave slope. However when the displacement vector at middle portion where influence by boundary condition can be eliminated are investigated as shown in Figure 6.2(b), the displacement vectors in convex slope is mainly downstream and only slight sliding out could be found at the slope toe while for concave slope the soil mass sliding out is obvious. Combined with the results of shear stress on middle section shown in Figure 6.2(c), the failure mechanism behind might be explained as: (1) failure soil mass in the convex slope evenly slides down from the concentrated ground at crest and through the diverging geometry until reaching the toe where the shear stress is mainly mobilized; noticeable shear stress mobilized could be found near the crest because possibly the concentrated ground at crest restricts the trigger of failure; (2) the converging geometry of concave slope forms arching effect; such effect increases shear stress significantly in almost whole failure mass and results in accumulation of soil hence larger upheaval displacement at toe as compared with that in convex slope (shown in Figure 6.3); the converging geometry towards downstream restricts the develop of failure. These restrictions from curvilinear geometry may be regarded as the reason why curvilinear slope obtains higher / slightly higher safety than plane slope (see Table 6.1). Furthermore, it should be noted that the diverging geometry in convex slope, compared to converging geometry in concave slope, imposes no positive influence on the restriction of failure development especially at middle height of slope as we have already spotted in the stress analysis (see Figure

6.12(c)). This result accounts for the fact that the factor of safety of convex slope (1.86) is about 10% lower than that of concave slope (2.05).

In addition, different curvatures are also studied. Factors of safety of slope with different radii of curvature and different cohesive strength are investigated and the results are shown in Figure 6.4 and Table 6.1 with reference to the slope with plane facing as well. Different curvatures (0.2, 0.1, 0.667, 0.05) correspond to different radius of rotation about the symmetric axis (see Figure 6.1), i.e. R=5m, R=10m, R=15m, and R=20m, respectively. As shown in Figure 6.4, the effect of curvature is beneficial on factor of safety but is noticeable and important only when the curvature is significant. That means, unless the radius of curvature is small, the effect of curvature on factor of safety is not critical for most of the highway slopes if the soil is homogeneous. This result is however not necessarily true if the soil is nonhomogeneous, but then the effect of inhomogeneity will be more important than the effect of curvature.

If the geometry of slope is complex, the slope profile is hardly defined by a single radius of curvature and thus the failure is complicated. Figure 6.5 shows two types of complex slope with similar basic section and properties as previous parameters. Type 1 complex slope combines directly convex and concave portions while type 2 complex slope adopts a plane portion to connect both curvilinear portions. Bearing the findings from above study in mind, we anticipate the stability of complex slope would be enhanced by existence of curvilinear portions and be weakened by existence of plane portion. As shown in Figure 6.5, factor of safety for Type 1 complex slope is 2.0 and for Type 2 complex slope is 1.89. Compared with the results of simple slope with c=20kPa (FOS=2.05 for concave slope, FOS=1.86 for convex slope and FOS=1.82 for plane slope), factor of safety for complex slope ranges among the maximum and minimum factors of safety of constituent portions. These results agree well with the anticipation and can be further explained by studying the critical slip surface. Due to the local stabilization effect from curvilinear portion, the plastic zone initiated at portions with low stability only partly develops in portion with high stability and no continuous, thorough failure surface is essentially formed. So there is only local failure in complex slope.

From the above investigations on simple slope, for homogeneous slope with 3D curvature, the failure is symmetric about the rotation axis with an axi-symmetrical shear failure. For the same radius of curvature, the concavity geometry shows higher factor of safety than the convex geometry which is an indication of the arch action introduced by the obvious confining action of the geometry. When different radii are concerned, the concavity geometry has more positive effect to the stability when the radius of curvature is small. Both curvilinear geometries are beneficial to the slope stability, but such merit is relatively small and is only significant when the curvature is significant.

6.3 3D intercolumn force function on plane slope by stress analysis

Compared with 2D plane strain analysis, 3D analysis on slope with plane slope is expected to give similar factor of safety and stress distribution if the length of the slope is large enough. The procedure to determine the intercolumn force function is similar to the interslice force function. The intercolumn force function is studied along both x-direction and y-direction as shown in Figure 6.6 and Figure 6.7, where x=0 indicates the exit end of the slip surface. For f(x), it is basically a simple extension of the 2D interslice force function. On the other hand, there seems to be no simple rule to define f(y) distribution. The actual distribution of f(y) is however not critical, as λ_y is as small as 1.9e-4 and 4.8e-

4 for c=20kPa and c=4kPa respectively. In fact, λ_y should be equal to 0 exactly for a plane slope. For this case, f(y) is actually a meaningless item as λ_y is zero. The peak value of f(x) is situated and maintained around the exit end of soil mass near the toe and decreases rapidly at the middle of the soil mass as shown in Figure 6.8. The abnormality is located at the later proportion of the soil mass where tension crack may exist. For this 3D failure which is actually a simple extension of 2D failure with same factor of safety and internal stresses, a 2D analysis is completely sufficiently good, and f(x) is similar to that by 2D SRM as shown in Chapter 5.

6.4 Curvature effect on the internal force distribution

Figure 6.9 illustrates f(r) and f(t) of curvilinear slope. It is obvious that there is no solid trend for f(t) while f(r) is still basically similar to that for 2D situation. The f(t) is investigated along different θz-planes as shown in Figure 6.10 where for both convex and concave slope, the distribution of f(t) is very random. This might result from the symmetric slope profile - actually most of the vertical intercolumn shear force is small as seen from attained λt shown in Figure 6.10 - therefore the f(t) can be neglected in this respect.

In the investigation of f(r) as shown in Figure 6.11, both f(r) of convex and concave slope with R=±10m and c=20kPa is similar on different rz-planes which again due to the property of symmetry. However, it should be noted that f(r) seems to take different form when compared with 2D interslice force function. Further study is carried out among slopes with same properties except for different geometry, or saying different radii of rotation. The results on f(r) is given in Figure 6.12. Compared with the obvious platform of f(r) in the plane slope case, concave slope have peak f(r) at the lower exit end of soil mass and f(r) continuously decreases towards the inner section of soil mass. For the convex slope, f(r) maintains high value for a shorter or longer distance from the toe of slope and then drops rapidly at about $x/L=0.6$ (where similarly as those in Chapter 5, x represents the distance from the exit end of slip surface and L represents the horizontal extent of slip mass). The main difference of f(r) among different geometries thus can be regarded as the starting locations where the function decreases. The formula of f(x) adopted in 2D analysis is still applicable to f(r) provided that some adjustment of the three constants (a,b, and c) in Eq.(5.5) is made. It should be noted that unlike plane and convex slope, the concave slope gives slightly higher factor of safety but the location of the maximum intercolumn force function has decreased to about 0.1-0.2 in length. This phenomenon indicates that the internal strength is well mobilized within concave slope. Such merits can also be found when factor of safety is relatively high as shown in Figure 6.4. Table 6.1 summarizes attained factors of safety and maximum λr as well for slopes with different geometries. The relation of maximum λr and slope curvature is plotted in the same form as Figure 6.4. It is of interest that as shown in Figure 6.13 the maximum λr, i.e. maximum ratio of shear stress to normal stress on different θz-directional intercolumn surface increases as the curvature.

The thrust line in 2D slope stability analysis has been demonstrated to be located generally at 1/3 or slightly higher of the interslice height from the base of slices and been proved as an alternative to interslice force function. In 3D analysis, the same result can be found in plane slope which are shown in Figure 6.14. The locations of radial and tangential thrust line of plane slope agree well with the assumption of 1/3. For the thrust line of curvilinear slope, however, the assumption is not always true. The radial thrust line in convex slope is found to be close to the 1/3 line as shown in Figure 6.15. The tangential thrust line, on the other hand, deviates from the assumption evidently at different sections (Figure 6.15). As for thrust line location of concave slope shown in Figure 6.16, the radial and tangential thrust line are in the good accordance with each other while the difference between thrust line location and 1/3 line is noticeable at different sections. At the section near boundary where the displacement is confined, the resulted thrust line is slightly higher than the 1/3 line but the deviation becomes significant at the middle portion as Figure 6.16(b) indicates. That is to say, while location of thrust line is relatively stable in 2D analysis and 3D plane slope, it varies from case to case in 3D slopes influenced by curvature effect and the assumption of 1/3 line should not be regarded anymore as a stable and trustful assumption.

6.5 Stability of locally loaded slope with curvature

If local load is superimposed on a curved slope, the difference between concave and convex geometry becomes more apparent. Figure 6.17 illustrates the failure mode when the slope is bearing a 1m×1m square loading of 200kPa at the top and 1m away from the rim. It can be seen from Figure 6.17(a) that the failure becomes local failure and clustered around the loaded district as expected. For the failure at toe for the case of concave slope, there are two failure zones at the toe which are not connected. The factor of safety under such local loading decreases by about 5.9% in convex slope (from 1.86 dropping to 1.75 as listed in Table 6.2) and 2.4% in concave slope (from 2.05 dropping to 2.0 as listed in Table 6.2), which indicates the concave slope is more unstable under local loading.

6.6 Assessment of different soil nailing modes on curvilinear slope

The consideration of soil nailing modes is considered in this section and the factor of safety is summarized in Table 6.2. Generally, soil nails are installed into the slope in parallel mode in rows for ease of construction. For slope with no curvature, nails are parallel to each other at different section. For slope with curvature, however, nailing perpendicular to the slope which corresponds to the state that nails are in the radial direction is another possible installation method. In literature, the differences between these two nail installation methods have not been considered. In this section, two nailing mode will be investigated: (1) for radial mode, soil nails are installed radially with a possibility that there is some overlap of the stabilized zones, especially for the convex slope; (2) for parallel mode, soil nails are installed parallelly to each other and thus are installed with different horizontal angles with respect to the slope surface on plan. The soil nails are installed horizontally with length equal to 8m and vertical interval equal to 2m as shown in Figure 6.18. The basic convex and concave slope are modeled in the way same as that in the former section and horizontal interval of soil nails is 1.6m, so there are totally 30 soil nails in 3 rows (namely: top, middle, and bottom) for each curvilinear slope. From the view of factor of safety only as listed in Table 6.2, for convex slope the parallel nailing mode is more beneficial and for concave slope radial nailing mode takes advantage.

Using radial nails, the problem under consideration is still an axi-symmetric problem. factor of safety of both curvilinear slopes is enhanced by 0.14 compared with corresponding non-nailed slope. For the failure modes which are shown in Figure 6.19, the critical slip surface is a pronounced below toe failure for both cases. On the other hand, due to the concentration of soil nails near to the top for convex slope, the failure zone extends to a much greater horizontal extent which is not observed for the case of concave slope. These findings which have not been reported previously are interesting, and the results reflect the combined effect of curvature and soil nail stabilization distribution.

Figure 6.20 demonstrates the critical slip surface for the slope nailed in parallel mode. There are several changes in the results when the nails are installed in parallel mode as compared with radial mode for convex slope, but the changes to concave slope are not significant in general. For convex slope, below toe failure is much less significant and the thickness of the failure zone near to the toe is greatly reduced as compared with the case for radial mode nail installation.

If the nail force distribution is examined which is shown in Figure 6.21, it is noticed that the nail installation mode is more important for convex slope but is not sensitive to concave slope. Another interesting phenomenon is that there are greater variations in the nail forces for different row of nail for different nail installation mode. Since a more uniform nail load distribution is good for economic design, it appears that the use of parallel nail installation mode which is easier for field installation is also a more economic design in general.

6.7 Conclusions and Discussions

This chapter investigated the intercolumn force function and the curvature effect on the stability of simple 3D slope. The effect of localized loading under different nailing modes is also investigated. The radial intercolumn force function f(r) in simple curvilinear slopes is demonstrated to be similar to the 2D interslice force function and by some minor adjustments of the parameters, the same function can also be adopted for 3D radial intercolumn force function. It is thus proved that analysis of plane 3D slope can be simplified as 2D slope problem with good accuracy considering the tangential intercolumn force function of 3D plane slope is minor. On the other hand, for simple axi-symmetric cases, since the tangential intercolumn force is minor or even zero, it is acceptable to conclude that the radial intercolumn force function is dominating in the overall stability. However, if the geometry is complex comprising of several portions with different curvature, it would be difficult to specify one radial and one tangential direction and thus the intercolumn force function is as almost impossible to be referred in similar form with 2D interslice force function. To generalize the intercolumn force function, the concept of spatial principal surfaces can be introduced which corresponds to the surface containing the principal stress σ_1 and σ_3. σ_1 thus is related to maximum principal surface within which the intercolumn force function is dominating. The other principal surface contains intercolumn force function less significant which is f(t) in this study. The intercolumn force function within the surface perpendicular to the principal surfaces is small as investigated by Lam and Fredlund (1993). With this concept, the direction of maximum principal stress is consistent with the direction of dominating interslice/intercolumn force function. The overall potential sliding direction of instable soil mass can be hence determined as the overall resultant vector of the principal stress.

The curvature of slope has a beneficial effect on the global stability due to restriction of failure trigger by convex slope and restriction of failure development by concave slope, especially when the resistance of soil is relatively high. Concave slope usually gives higher global stability than convex slope under the same loading and nailing mode conditions which are shown in Table 6.2. In addition, the factor of safety of concave slope is less sensitive to the localized loading as compared with that of convex slope.

The thrust line locations for 2D analysis agree well with the assumption of 1/3 column height, therefore, the thrust line is a good alternative to the interslice force function. However it is found in this study that such fitness is not always correct in 3D analysis. When the maximum ratio of vertical shear force to horizontal normal force on single intercolumn surface i.e. λr is investigated, it can be found in Table 6.1 that the λr is generally sensitive to sign (positive or negative) of the curvature but not sensitive to the value of curvature. Compared with the convex slope, concave slope has smaller peak value of intercolumn force function, which shows that concave slope is more capable of resisting driving force.

In comparison with parallel nailing mode, the radial nailing mode gives lower factor of safety in convex slope but higher factor of safety in concave slope. This can give a reference guidance that parallel mode in reinforcing convex slope and radial mode in reinforcing concave slope are preferred.

Table 6.1 Summary of factor of safety and λ of simple slope with no loading

geometry	plane		convex				concave			
R	∞	∞	R=+10		R=+20		R=-10		R=-20	
c	c=20kPa	c=4kPa	c=20kPa	c=4kPa	c=20kPa	c=4kPa	c=20kPa	c=4kPa	c=20kPa	c=4kPa
FOS	1.82	0.49	1.86	0.49	1.82	0.49	2.05	0.52	1.94	0.51
λrmax	0.7	0.7	1.7	1.0	1.7	0.9	0.36	0.4	0.36	0.4

Table 6.2 Summary of factor of safety of different loading and nailing mode (R=±10m)

geometry	local loading	nailing mode		
		no nailing	radial	parallel
convex	0	1.86	2.00	**2.10**
	200kPa	1.75	1.82	**1.87**
concave	0	2.05	**2.19**	2.16
	200kPa	2.00	**2.16**	2.15

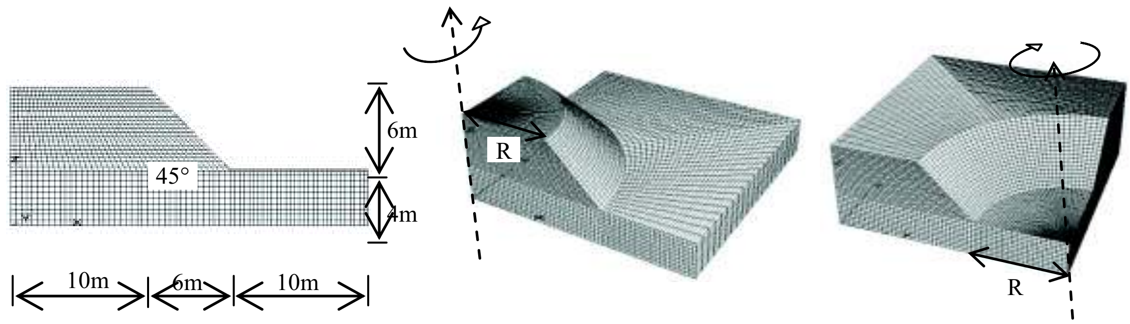

(a) Plane slope (basic section) (b) convex slope (c) concave slope

Figure 6.1 Geometry of plane, convex and concave slopes

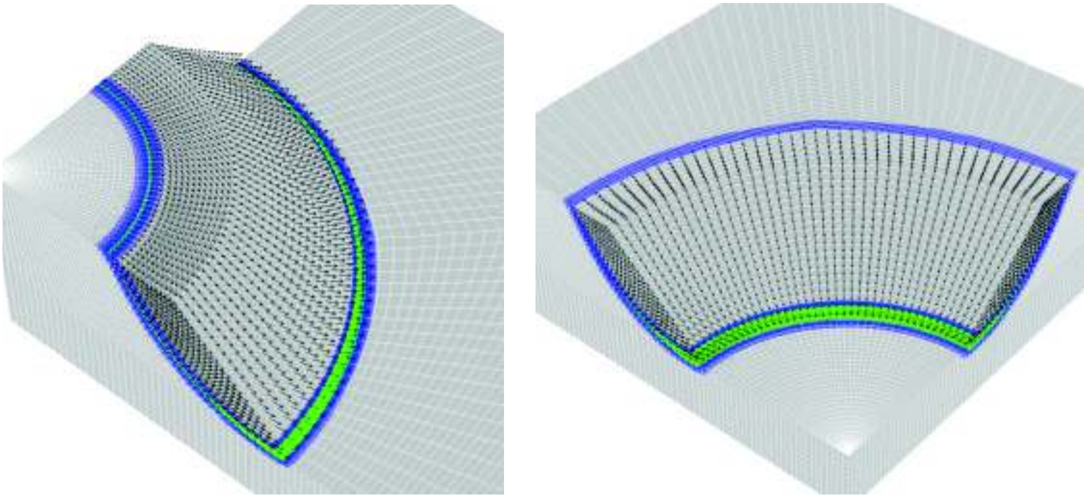

convex(FOS=1.86) concave(FOS=2.05)

(a) critical slip surface and overall displacement

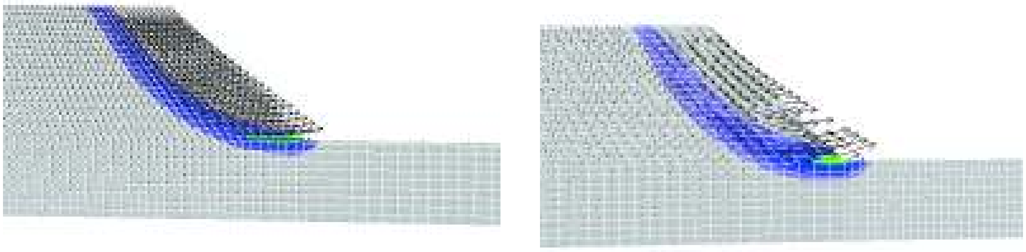

convex(FOS=1.86) concave(FOS=2.05)

(b) section view of displacement at middle portion

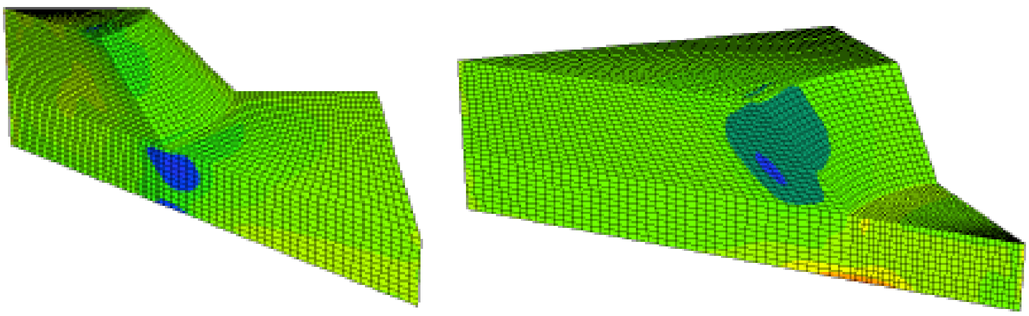

(c) shear stress distribution near the middle portion

Figure 6.2 Failure mode of simple curvilinear slope (R=10m, c=20kPa)

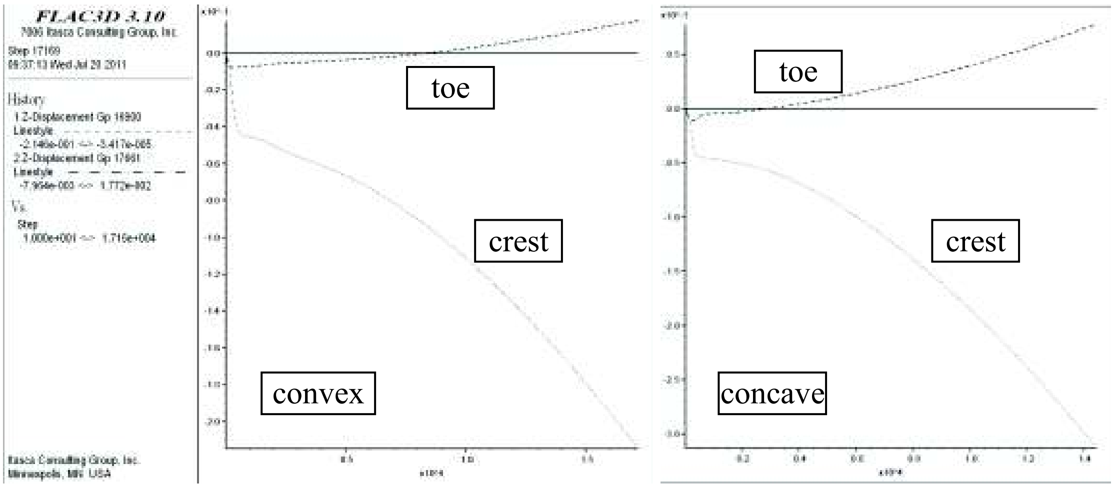

Figure 6.3 Displacement history of simple curvilinear slope (R=10m)

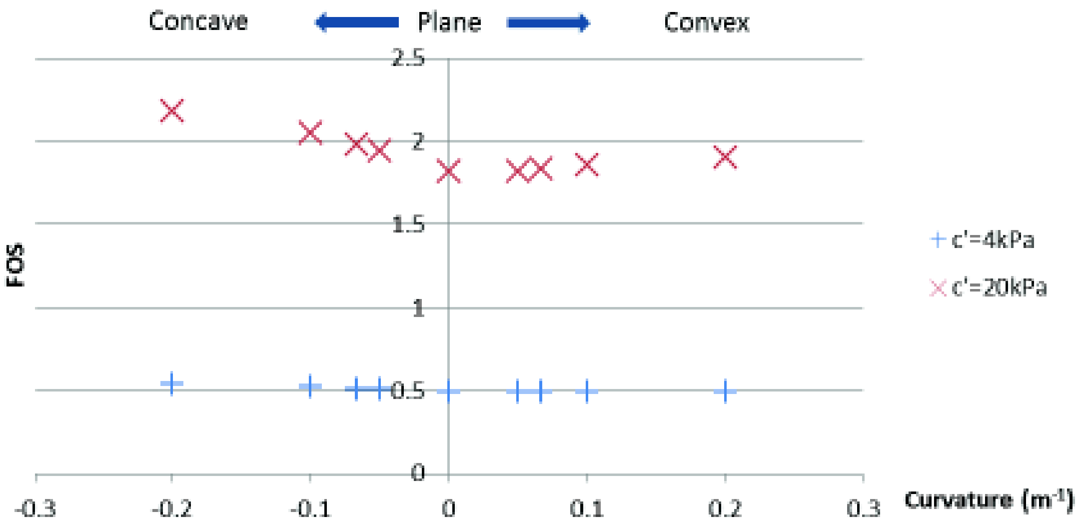

Figure 6.4 Factor of safety of slopes with different curvature

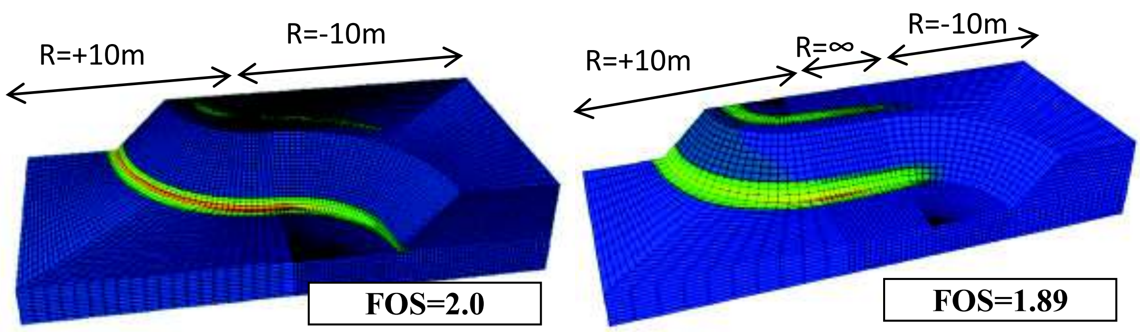

(a) Type 1 complex slope (b) Type 2 complex slope

Figure 6.5 Critical slip surface of complex slope (c=20kPa)

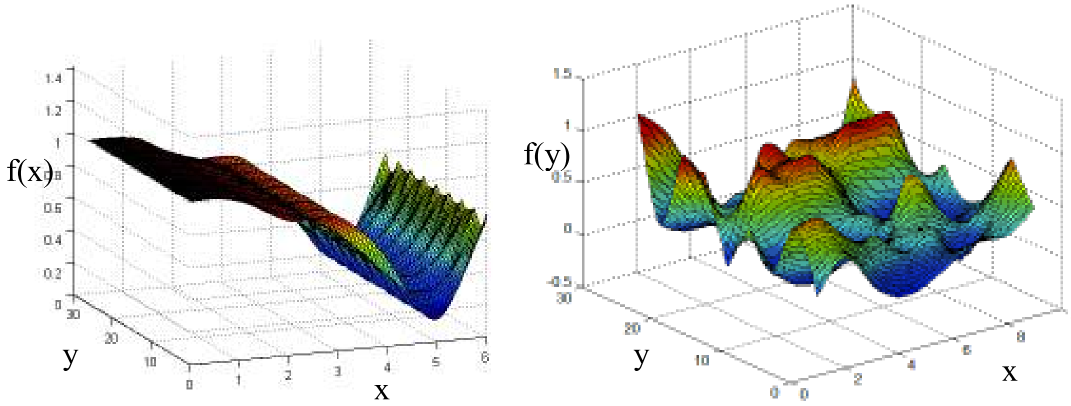

(a) f(x) (λ_{max}=λ_{min}=0.74) (b) f(y) (λ_{max}=1.9e-4)

Figure 6.6 f(x) and f(y) of plane slope (c=20kPa)

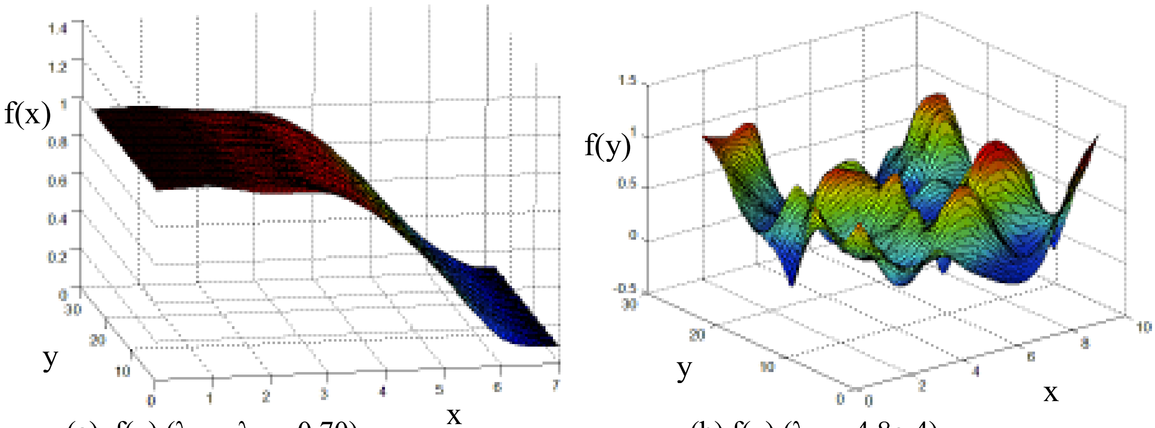

(a) f(x) (λ_{max}=λ_{min}=0.70) (b) f(y) (λ_{max}=4.8e-4)

Figure 6.7 f(x) and f(y) of plane slope (c=4kPa)

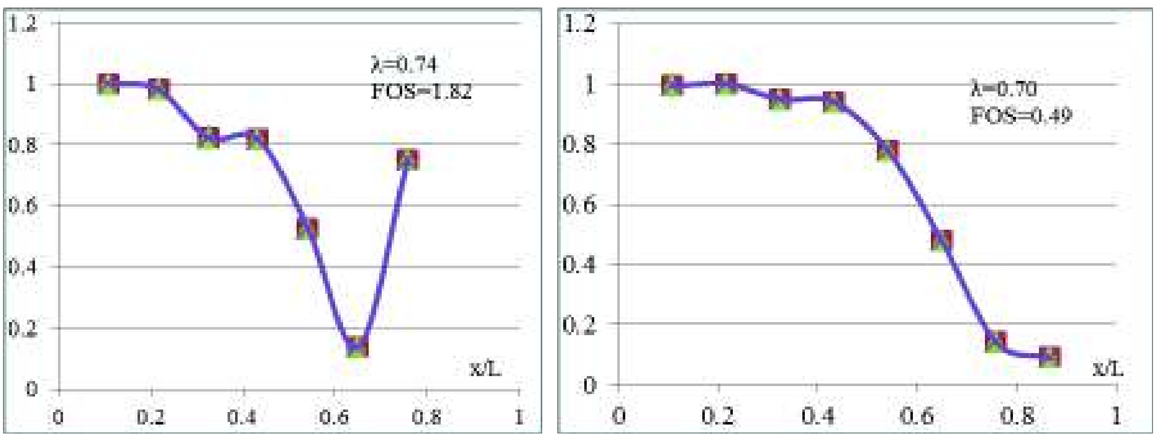

(a) c=20kPa (b) c=4kPa

Figure 6.8 f(x) of plane slope on xz-plane

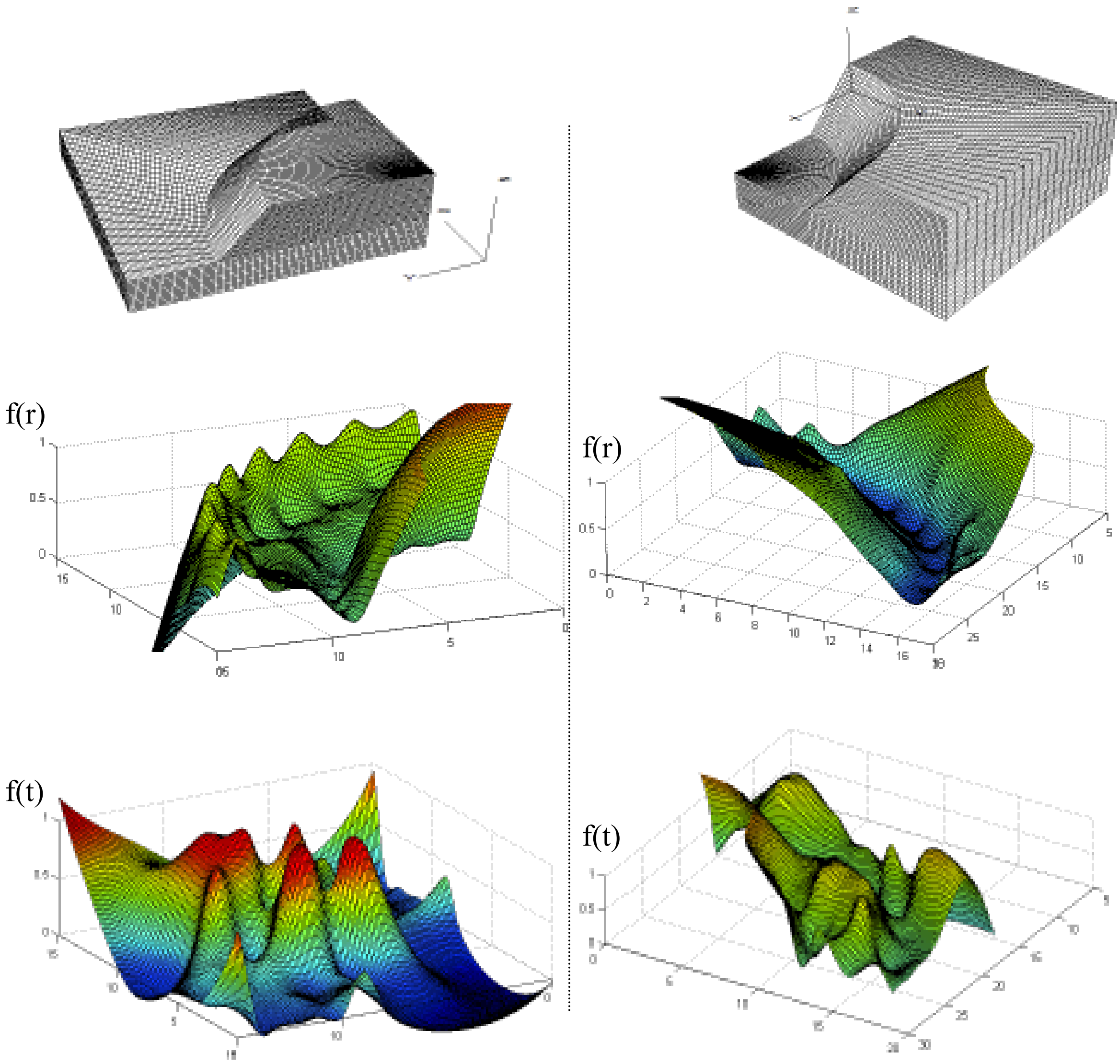

Figure 6.9 Intercolumn force function f(r) and f(t) for curvilinear slope (R=±10m, c=20kPa)

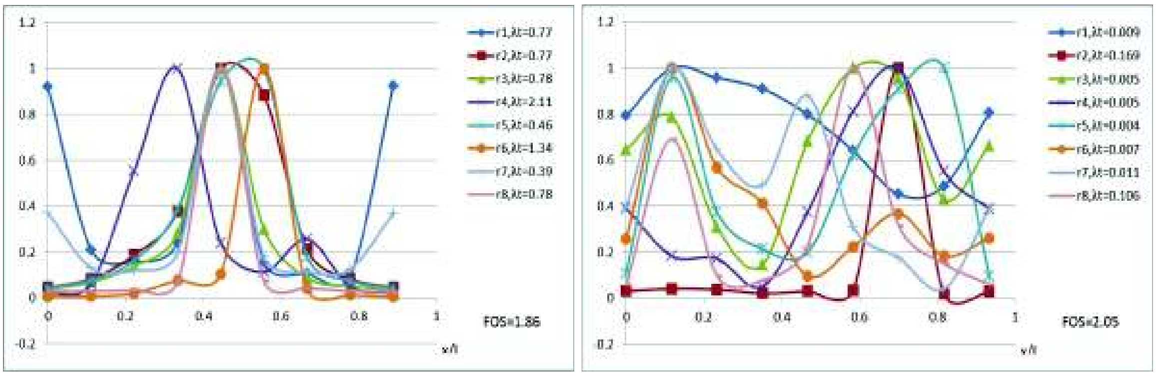

(a) convex slope (b) concave slope

Figure 6.10 f(t) of curvilinear slope (R=±10m, c=20kPa)

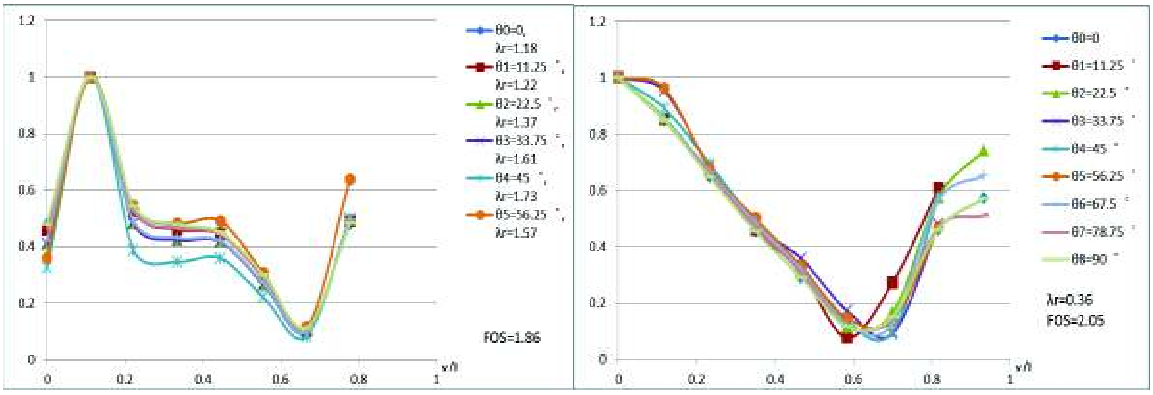

(a) convex slope (b) concave slope

Figure 6.11 f(r) of curvilinear slope (R=±10m, c=20kPa)

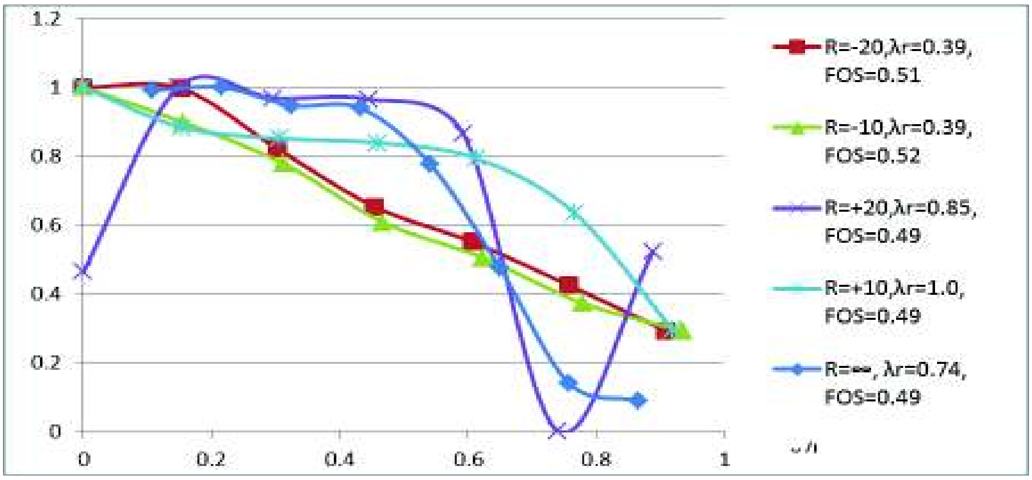

Figure 6.12 Summarized f(r) graph for slope with different R (c=4kPa)

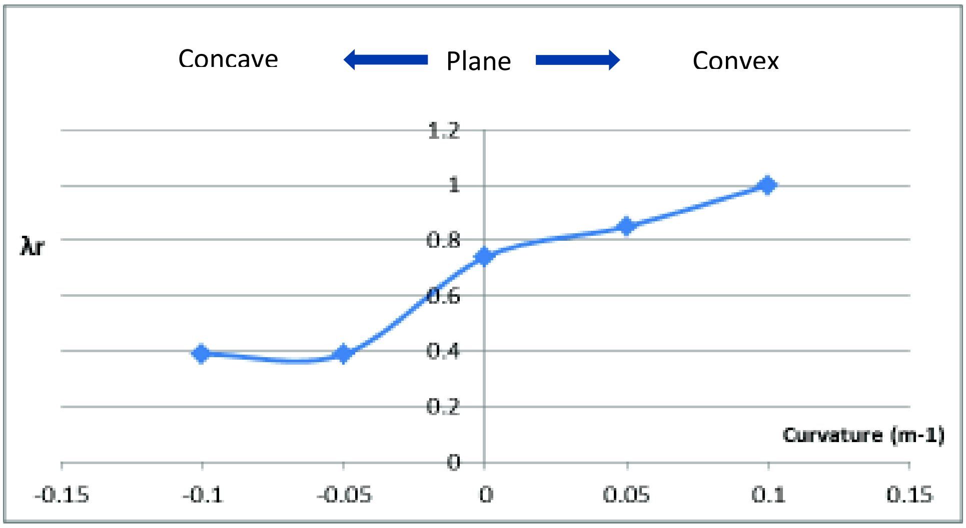

Figure 6.13 Maximum λr of slopes with different curvature

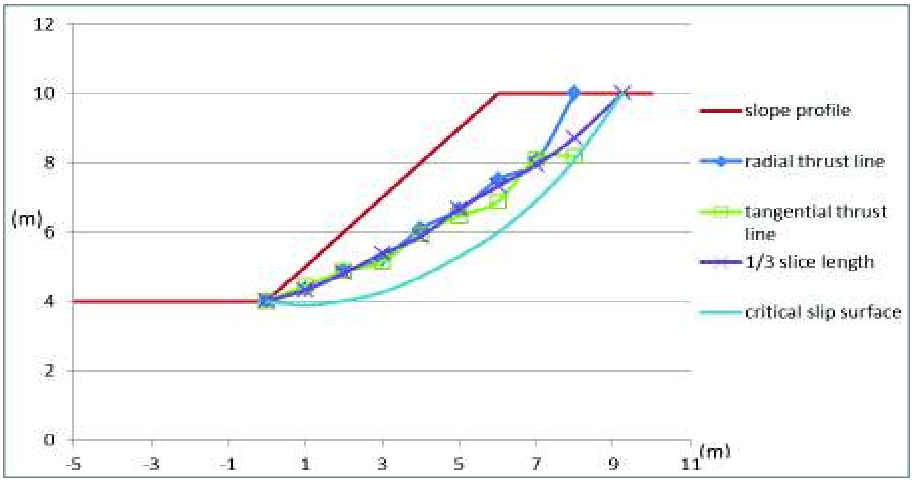

Figure 6.14 Thrust line of plane slope (R=∞, c=20kPa)

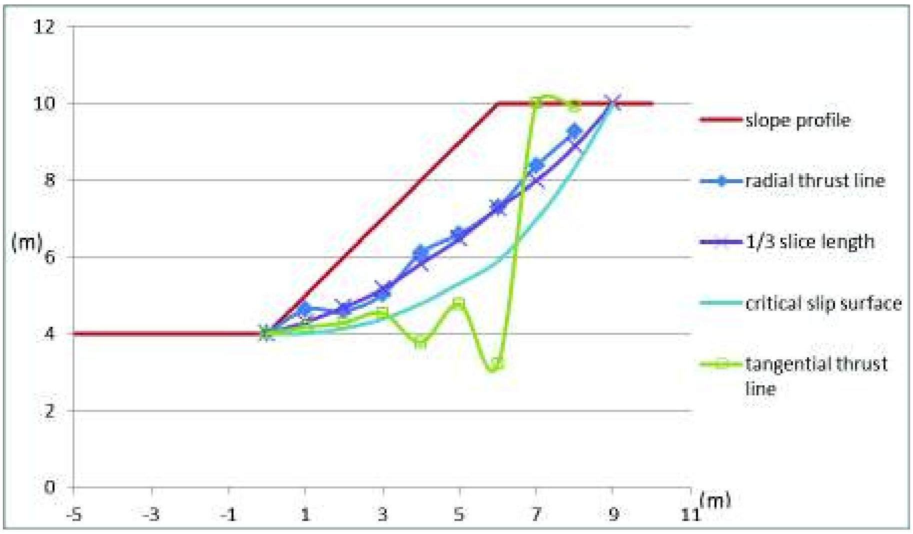

(a) at section near boundary

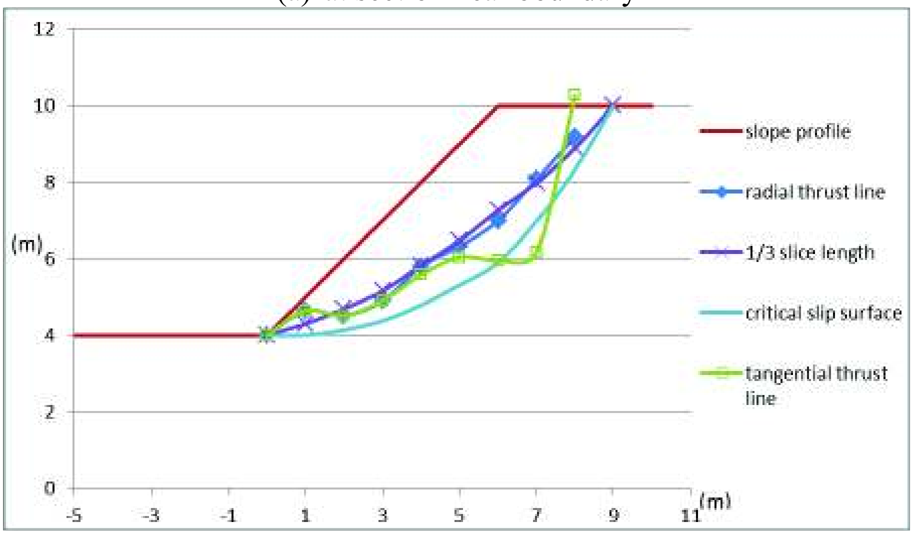

(b) at section of middle portion

Figure 6.15 Thrust line of convex slope (R=+10m, c=20kPa)

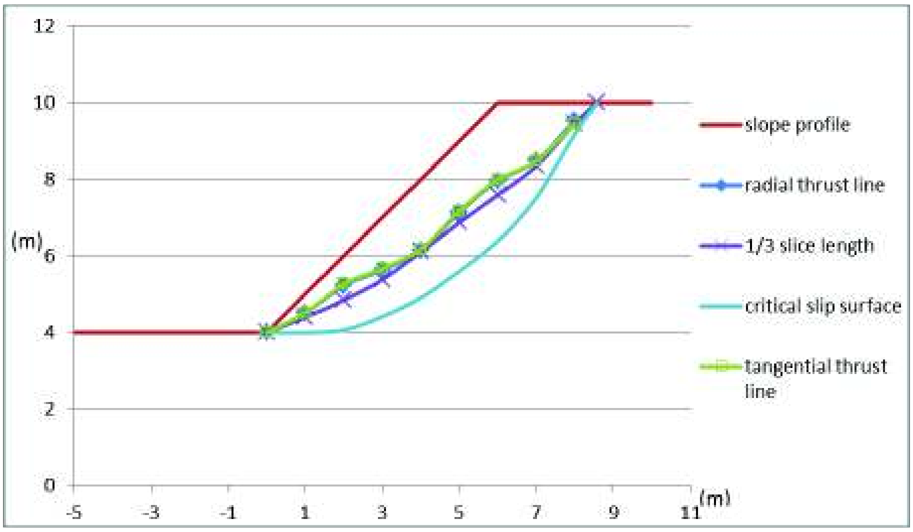

(a) at section near boundary

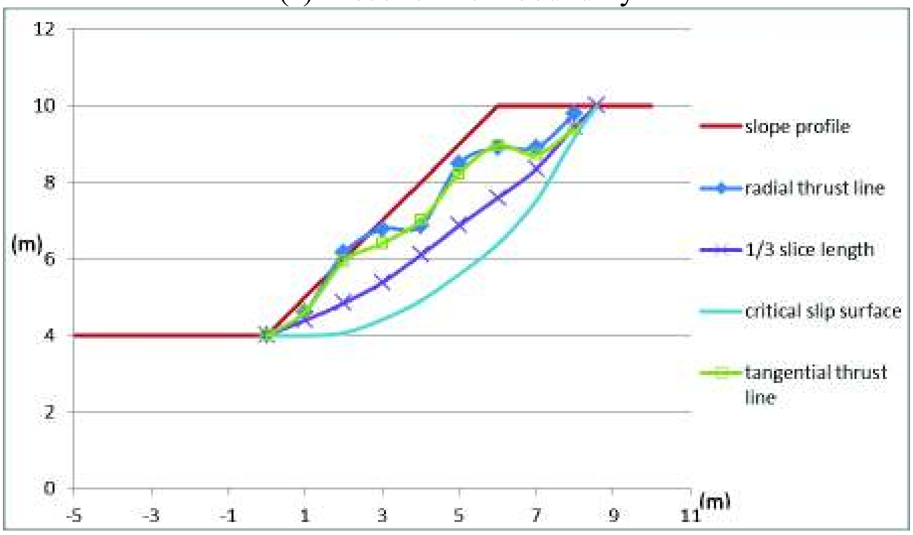

(b) at section of middle portion

Figure 6.16 Thrust line of concave slope (R=-10m, c=20kPa)

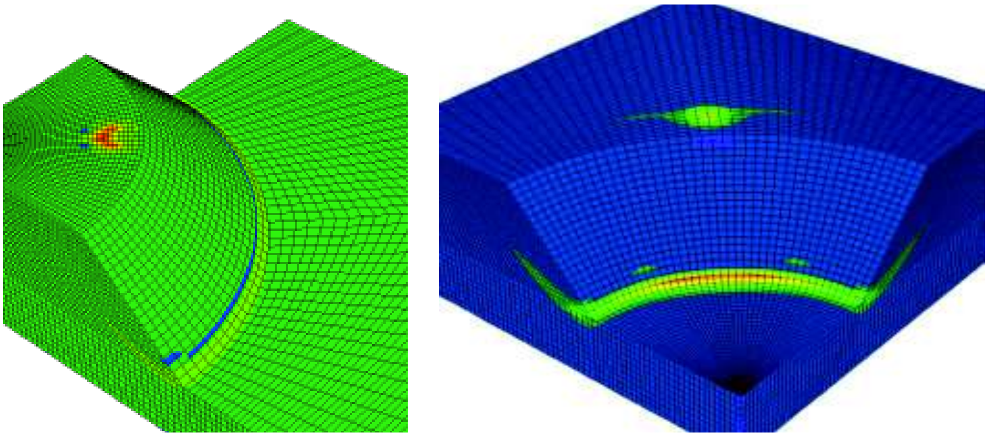

convex(FOS=1.75) concave(FOS=2.00)

(a) overall view

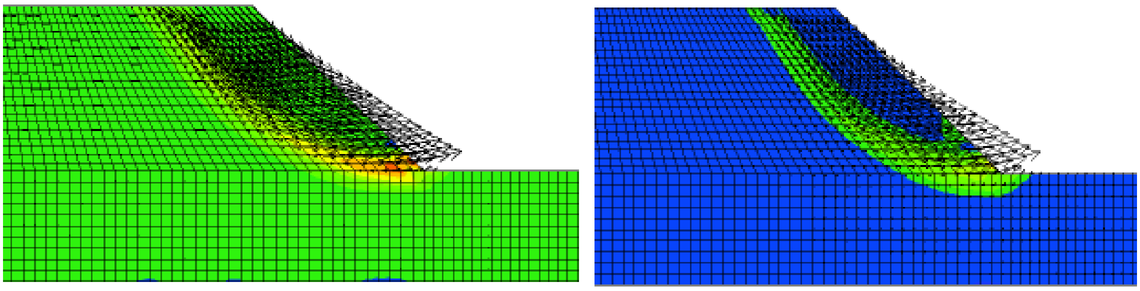

convex(FOS=1.75) concave(FOS=2.00)

(b) section view

Figure 6.17 Failure mode of locally loaded curvilinear slope (200kPa, R=±10m)

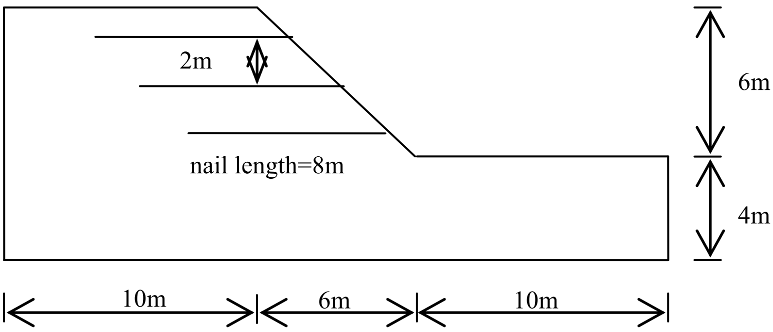

Figure 6.18 soil nailing on the slope section

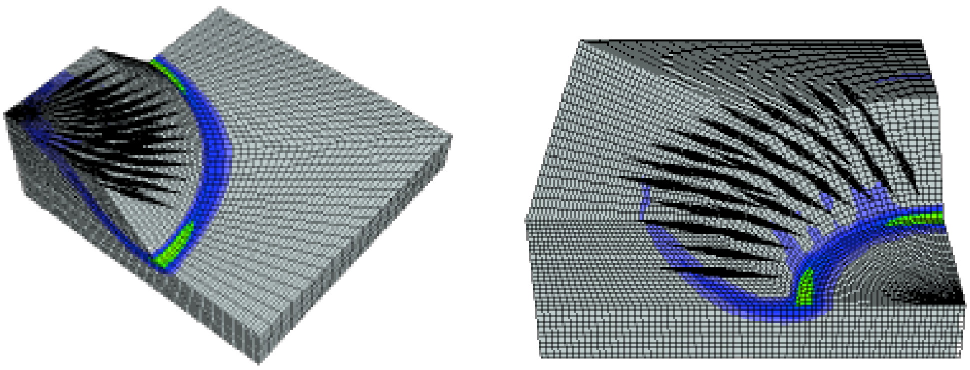

convex(FOS=2.00) concave(FOS=2.19)

Figure 6.19 Critical failure surface and soil nail stress of radially nailed curvilinear slope

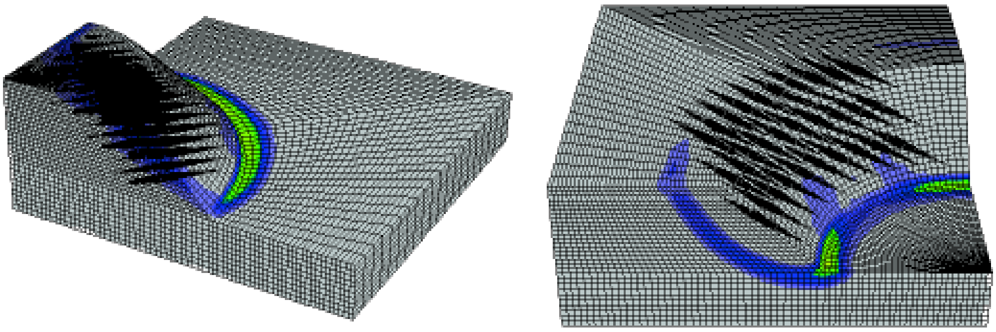

convex(FOS=2.10) concave(FOS=2.16)

Figure 6.20 Critical failure surface and soil nail stress of parallely nailed curvilinear slope

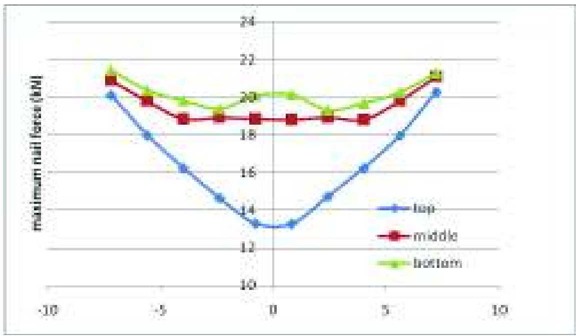

(a) radially nailed convex slope

(b) parallelly nailed convex slope

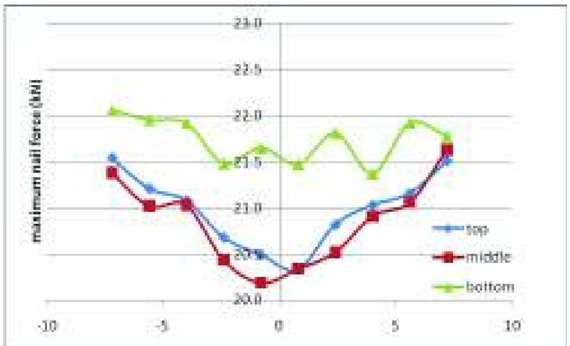

(c) radially nailed concave slope

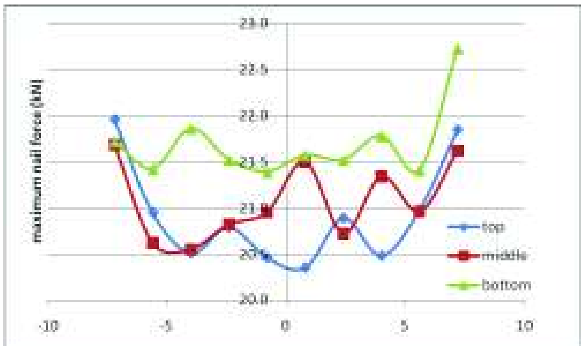

(d) parallelly nailed concave slope

Figure 6.21 Maximum nail force on the convex and concave slope with no loading

CHAPTER 7 Conclusions, Discussions and Suggestions

7.1 Conclusions

Although many slope stability methods have been developed and slope stability problems have been considered for many years, there are still various limitations to the previous studies, and some of these limitations are considered in this study. In this study, Limit Equilibrium Method (LEM), Finite Element Method (FEM), Strength Reduction Method (SRM), Distinct Element Method (DEM) and Finite Difference Method (FDM) are adopted. The location of critical slip surface, the internal force distribution function, calculation of slope global stability, identification of local failure and failure mechanism are studied by different methods in this study.

7.1.1 Findings from location of critical slip surface

In this part of work, several optimization algorithms are implemented and improved to efficiently and precisely locate the critical slip surface. For slope stability problems, the critical slip surface is the surface on which the factor of safety is minimum among all the possible failure surfaces. The minimum factor of safety is thus a typical global optimization objective function. Practically all the modern optimization methods can work well if the geometry and ground conditions are relatively simple. Difficulties are that the objective function might be trapped into local minimum and “failure to converge” is relatively common for complicated problems.

An improved harmony search method MHS is developed in this study, and this new method is found to be efficient for large problems in the present study. In fact, it performs better than the original harmony method in most cases, especially when the number of control variables is large. Another new approach is developed by coupling the PSO and HS. HS/PSO algorithm is efficient and effective for complicated geotechnical problems. When Morgenstern-Price method is used for the analysis, 'failure to converge' is relatively common and a large value is assigned to those cases that fail to converge (equivalent to a discontinuous objective function), and this will create further difficulties in the search direction. The proposed coupled optimization method has been clearly proved of the advantages under these difficult cases. This part of work also provides the mathematical tools which are required for the later part of the work in LEM.

7.1.2 Findings from analysis of failure mechanism by distinct element method

By adopting DEM (PFC), it is found in the present study that for a slope with cohesionless soil, failure firstly occurs at the crest of the slope, and the failure gradually extends to the base of the slope until the final geometry where the slope angle is equal to the friction angle of soil. Due to the downward movement of the particles at the crest which induces tensile failure, tension crack may be found at the crest of the slope. Soil is deposited at the toe of slope, and the failure is in the forms of sliding out and upheaval; while middle part of the slope actually turns into a shear failure zone due to the continuous sliding of soil. When the cohesive strength is relatively high or soil nails are installed, the overall stability can be enhanced and the displacement is limited. The effectiveness of the cohesive strength and soil nails are hence important factors in slope stability which is actually a well-known fact. In particularly, the soil nails are found to distribute the stresses within the soil mass and limit the development of local failure zones, so the overall stability is greatly improved by the presence of soil nail. It is also found that the use of nail head/facing is vital to the stress-redistribution and the prevention of local failure. Without the facing, local failure will control the stability of the slope.

The basic failure mechanism of slope influenced by water flow is similar to that of a simple slope: failure begins from the crest of slope due to gravity and extends to the middle of slope and then the toe. Water flow with a noticeable seepage force will result in a thrust pushing the soil mass above the water table outwards with an obvious decrease in the stability of the slope and extended failure zone.

It is found that DEM can simulate large scale deformation which is impossible in FEM and FDM, but a precise slip surface as given by LEM and SRM is difficult to be established due to the continuous change in the geometry and the fluctuation of the local stresses within the soil mass. A rough slip surface which is basically similar to that by LEM and SRM can however still be defined in general. Although DEM is seldom used by the engineers for assessing the stability of a slope, it appears that DEM possesses some advantages which are not possible for the classical LEM and SRM.

7.1.3 Findings from interslice/intercolumn force function

The present study has investigated the internal force function within 2D and 3D framework. The classical LEM based method of slices/columns includes many assumptions to solve the statically indeterminate problem. Either the interslice/intercolumn force function or thrust line can render the slope stability problem statically determinate. By the use of extremum principle which is actually a lower bound principle, there is no need to make the assumptions on the internal force function. Treating this function as a variable, the function can be determined when the maximum strength of the system is fully mobilized. This function which is taken as indeterminate and impossible to be determined can now be determined under a rigorous framework.

By employing SRM, interslice force function $f(x)$ is found to vary with slopes with soil different properties and geometry and should not be arbitrarily specified. Basically, for slopes which are mainly controlled by self weight, $f(x)$ is a bell-shaped function which is similar to the results by Fan, Fredlund and Wilson (1986), except for a part near to the toe of slope. The location of thrust line basically agrees well with the Janbu's Rigorous method at 1/3 of slice height from the base. It can be considered that those variables which are taken as indeterminate in the past are now fully determinate, and these variables are sometimes important for some special case, even though Morgenstern (1992) has observed that these variables are not important for normal problems.

For 3D internal force function, this study has introduced the concept of principal surface to determine the sliding direction and the corresponding dominating internal force function. For simple slopes with either plane surface or curvilinear profile intercolumn force function agrees well with the 2D interslice force function because of the symmetry. By some adjustments of the parameters in the 2D interslice force function, the same function can be adopted for 3D radial intercolumn force function. But for complex problems, 3D internal force function is complicated and 2D interslice force function will not apply.

7.1.4 Findings from development of variable factor of safety

The extremum principle and the concept of variable factor of safety based on Pan's postulate are developed in this study. Even though the minimum extremum of factor of safety within whole domain is also determined, the maximum extremum should be taken as the factor of safety of the prescribed failure surface. The internal forces within the soil mass should redistribute until the maximum resistance capacity of the soil mass is fully mobilized. Beyond that limit, the soil mass will start to fail. The present proposal is independent of the definition of $f(x)$ and exhibits virtually no failure to converge. There are also cases where $f(x)$ may obviously influence on the factor of safety but no clear guideline on the acceptance of the factor of safety due to the use of different $f(x)$ is available. The use of the maximum extremum can also avoid this dilemma, which has been neglected in the past. The approach in section 4.2 is a typical lower bound approach, as statically admissible forces associated with a prescribed $f(x)$ are considered. The selection of the maximum factor of safety is hence justified from the lower bound theorem.

The factor of safety is defined in terms of the ultimate shear strength and mobilized shear strength in classical slope stability analysis, so only one single factor of safety globally for a problem. The present study has demonstrated that for normal stable slope with an overall factor of safety greater than 1.0, the factors of safety based on a variable factor of safety and the classical approaches are similar. In this respect, the present formulation provides an alternative to the classical methods of analysis but no advantage is guaranteed. On the other hand, for those cases of stable slopes where the factors of safety is slightly above 1.0 and part of the system may be controlled by the residual strength, the present formulation provides an estimation of the factor of safety which is not possible with the classical methods of analysis.

Pan's principle is actually the combination of the lower and upper bound approach which is purely a concept without any practical numerical procedures. Imposing Pan's principle, two different extremum formulations based on variable factor of safety concept are proposed which can consider global and local equilibrium and satisfying all the equilibrium conditions without any assumption as in the classical formulations. This new formulation has the advantage that progressive failure can be considered for LEM which is not possible for all the previous LEM formulation. On the other hand, the present proposal is based on an equivalent variational principle with a solid theoretical background which is also not possible for all the previous LEM formulation.

7.1.5 Findings from analysis of 3D effect on slope stability

In the past, analysis for the stability of slope with curved geometry which is common in practical engineering is usually analyzed as a 2D problem, and the effect of curvature is usually neglected for simplicity. In this study, it has been demonstrated that the curvature is an evidently beneficial effect on global stability of concave slopes where arch action can develop, especially when the resistance of soil is relatively high. The concave slope generally gives higher global stability than convex slope under the same loading and nailing mode conditions as discussed. In addition, the factor of safety of concave slope is less sensitive to the localized loading. In comparison with parallel nailing mode, the radial nailing mode gives lower factor of safety in convex slope but higher factor of safety in concave slope.

7.2 Discussions

7.2.1 Discussions on LEM and SRM

SRM has the advantage that it can automatically locate the critical slip surface, and the failure modes can be detected by the shear strain distribution. Another advantage of SRM is that it can easily simulate more complex conditions with inclusions. On the other hand SRM can be sensitive to the convergence criterion and possible tedious computational time.

LEM is more suitable and generally accepted for typical design with fast analysis. LEM is flexible in finding different local minima factor of safety and the corresponding slip surface which may be more difficult for SRM. However, LEM includes many assumptions to render the problem statically determinate. These assumptions have been taken to be indeterminate in the past, but have been solved within a rigorous framework under the present study. LEM is also not as powerful as SRM to simulate the interaction between reinforcement and soil, and to analyze some very complex situations.

Both the LEM and SRM have their own advantages and disadvantages. Cheng et al. (2007) and many others have found that the results from the LEM and SRM are in general similar. In the present study, one important difference is found, at least for all the existing limit equilibrium formulations. From the results in SRM, it is noticed that the factor of safety is introduced to the whole soil mass so that the factor of safety must be introduced into the interslice force relation. Such a requirement is however not mandatory in the LEM, and the factor of safety is only enforced at the slice base while the Mohr-Coulomb relation along the vertical interface can be used without the application of the factor of safety. It is possible that the factor of safety can also be introduced to the interface force relation (though not used in any LEM method at present). For practical application, since the interslice shear force is not sensitive to the overall factor of safety, the enforcement of the factor of safety in the interslice force relation appears to be not a critical factor, though conceptually the factors of safety from LEM and SRM cannot be compared directly because of this requirement.

7.2.2 Discussions on FEM/FDM and DEM

The major difference between FEM/FDM and DEM is the mechanical relation including the movement and interaction of discretized elements. The assumption of continuity in FEM/FDM requires that at all points in a problem domain, the material cannot be torn open or broken into pieces. All material points originally in the neighborhood of a certain point in the problem domain remain in the same neighborhood throughout the whole physical process. In DEM like PFC, the particles are assigned normal and shear stiffness and friction coefficients in the contact relation. Therefore large-scale deformation or post-failure can be simulated by DEM while methods based on continuum can only simulate the situation before the failure launches. There is no way to assess the post-failure phenomenon using the classical approach.

DEM can also define a slip surface, but not in a way as precise as LEM and DEM, since the geometry of slope changes continuously. Furthermore, it is also difficult to define the concept of factor of safety as in the traditional concept. The main limitation of DEM is that there is great difficulty in relating the microscopic and macroscopic variables/parameters, hence DEM is mainly tailored towards qualitative instead of quantitative analysis.

7.2.3 Discussions on 2D and 3D slope stability analysis

In normal practical design, 3D slope is commonly analyzed in simplified 2D model. This study has elaborated the investigation on the 3D slope internal force function and analyzed localized loading effect and soil nailing systems in the scope of slopes influenced by 3D curvature effect. The obtained 3D internal force function is found to be similar to 2D internal force function only when the geometry is symmetric and the radial internal force function is concerned. If a slope with irregular geometry no matter how simple the basic cross-section is, the internal force function cannot be predicted using 2D internal force function equation. Assumption of thrust line located at 1/3 slice height is a good alternative as demonstrated in 2D analysis, but it is proved to either apparently deviated from assumed location or even distribute randomly in even different sections of 3D simple curvilinear slope.

2D internal force function and thrust line can be used to predict 3D situation only for very limited 3D problems. Otherwise the problem will be simplified too much. Besides, considering that curvature effect is of significance to slope overall stability, 2D and 3D problems are clearly different though critical slip surface and factor of safety may be similar by 2D and 3D analysis in some cases.

7.3 Recommendations and Suggestions

This study has investigated various problems by LEM, SRM and DEM. LEM takes advantage on the efficiency but engineers should pay careful attention on the interslice force assumption. SRM essentially does not require such assumption but can give clear stress analysis, but the analysis is time-consuming and there are also many limitations to

SRM under special cases. DEM can give better understanding than other methods about the post-failure mechanism, but no index like the factor of safety is available. By the understanding of these methods and mechanism revealed by these methods, the slope stability problem can be solved effectively by combining all the merits of different methods.

Based on the investigated interslice force function and the understanding of progressive failure from DEM, concept of variable factor of safety in 2D can be established. And making the use of the heuristic algorithms developed in this study, the complicated procedure to achieve variable factor of safety can be solved more stably. From these respects of this study, 2D slope stability problems are well understood.

3D curvature effect which is usually ignored and simplified in the past is demonstrated as significant for even simple slopes. Besides, due to the existence, the prediction of 3D internal force becomes difficult. This study mainly focused on pure convex and concave slope or slopes with simple combination of different curvilinear portions. Further development on the internal force distribution by 3D analysis and determination of sliding direction of complicated slope can be expected based on the findings.

Reference

Abramson, L. W., Lee, T. S., Sharma, S., and Boyce, G. M. (2002). Slope Stability and Stabilization Methods, 2nd edition, John Wiley, USA

Anderheggen, E. and Knopfel, H. (1972). Finite element limit analysis using linear programming. International Journal of Solids and Structures, 8, 1413-1431

Arai, K. and Tagyo, K. (1985). Determination of noncircular slip surfaces giving the minimum factor of safety in slope stability analysis. Soils and foundations, 21: 43–51.

Azzouz, A. S. and Baligh, M. M. (1983). Loaded areas on cohesive slopes. Journal of Geotechnical Engineering, ASCE, 109(5), 724-729

Baker, R., and Leshchinsky, D. (1987). Stability analysis of conical heaps. Soils and Foundations, 27(4), 99-110

Baker R. and Garber M. (1978), Theoretical Analysis of the Stability of Slopes, Geotechnique, 28:395-341.

Baker R (1980), Determination of the critical slip surface in slope stability computations, International Journal of Numerical and Analytical Methods in Geomechanics, 4:333-359.

Baker R. (2003), Sufficient conditions for existence of physically significant solutions in limiting equilibrium slope stability analysis, International Journal of Solids and Structures, vol.40(13-14), 3717-3735.

Baligh, M. M. and Azzouz, A. S. (1975). End effects on stability of cohesive slopes. Journal of the Geotechnical Engineering Division, ASCE, 101(GT11), 1105-1118

Bishop, A. W. (1955). The use of the slip circle in stability analysis of slopes. Geotehnique, 5(1), 7-17

Bottero, A., Negre, R., Pastor, J., and Turgeman, S. (1980). Finite element method and limit analysis theory for soil mechanics problems. Computer Methods in Applied Mechanics and Engineering, 22, 131-149

Cavounidis, S. (1987). On the ratio of factors of safety in slope stability analyses. Geotechnique, 37 (2), 207- 210

Chang, M. (2002). A 3D slope stability analysis method assuming parallel lines of intersection and differential straining of block contacts. Canadian Geotechnical Journal, 39, 799-811

Chen, W. F. (1975). Limit Analysis and Soil Plasticity. Elsevier Scientific Publishing Co., New York.

Chen, W. F. and Giger, M. W. (1971). Limit analysis of stability of slopes. Journal of the Soil Mechanics and Foundations Division, 97(1), 19-26.

Chen, J. (2004). Slope stability analysis using rigid elements. PhD Thesis, The Hong Kong Polytechnic University

Chen, R. H. and Chameau, J. L. (1983). Three-dimensional limit equilibrium analysis of slopes. Geotechnique, 32(1), 31-40

Chen Z. and Morgenstern N. R U. (1983), Extensions to the generalized method of slices for stability analysis. Can. Geotech. J. vol.20: 104-119

Cheng, Y. M. (2003). Locations of critical failure surface and some further studies on slope stability analysis. Computers and Geotechnics, 30, 255-267

Cheng, Y. M. and Zhu, L. J. (2004). Unified formulation for two dimensional slope stability analysis and limitations in factor of safety determination. Soils and Foundations, 44(6), 121-127

Cheng, Y. M., Liu, H. T., Wei, W. B., and Au, S. K. (2005). Location of critical threedimensional non-spherical failure surface by Nurbs Functions and Ellipsoid with applications to highway slopes. Computers and Geotechnics, 32, 387-399

Cheng Y. M. (2007). Global optimization analysis of slope stability by simulated annealing method with dynamic bounds and 'Dirac function'. Eng Optimiz 2007;39(1):17–32.

Cheng Y. M. and Yip C. J. (2007), Three-dimensional Asymmetrical Slope Stability Analysis -Extension of Bishop's, Janbu's and Morgenstern-Price's Techniques, Journal of Geotechnical and Geoenvironmental engineering, ASCE, 133(12):1544-1555

Cheng Y. M., Li L. and Chi S. C. (2007a), Studies on six heuristic global optimization methods in the location of critical slip surface for soil slopes, Computers and Geotechnics, vol.34, 462-484.

Cheng Y. M., Li L., Chi S. C., Wei W. B. (2007b), Particle swarm optimization algorithm for location of a critical non-circular failure surface in two-dimensional slope stability analysis, Computers ad Geotechnics, 34(2):92-103.

Cheng Y. M., Lansivaara T, Wei W. B. (2007c), Two-dimensional Slope Stability Analysis by Limit Equilibrium and Strength Reduction Methods, Computers and Geotechnics, vol.34, 137-150, 2007.

Cheng Y. M., Li L., Chi S. C. (2008a). Performance studies on six heuristic global optimization methods in the location of critical slip surface. Computers and Geotechnics, 34(6), 462-484

Cheng Y. M., Li L., Lansivaara T., Chi S. C., Sun Y. J. (2008b). An improved harmony search minimization algorithm using different slip surface generation methods for slope stability analysis

Cheng Y.M., Li L., Chi S.C. and Wei W.B. (2008c), Determination of the critical slip surface using artificial fish swarms algorithm, Journal of Geotechnical and Geoenvironmental Engineering, ASCE, ASCE, 134(2):244-251.

Cheng Y.M., Lansivaara T. and Wei W.B. (2008d), Reply to the comments on 'Two-dimensional slope stability analysis by limit equilibrium and strength reduction methods' by Bojorque, Roeck and Maertens, Computers and Geotechnics, vol.35, 309-311.

Cheng Y.M., Li L., Lansivaara T and Chi S.C. (2008e), Minimization of factor of safety using different slip surface generation methods and an improved harmony search minimization algorithm, Engineering Optimization, vol.40, 95-115.

Cheng Y.M., Lansivaara T and Siu J. (2008f), Impact of Convergence on Slope Stability Analysis and Design, Computers and Geotechnics, 35(1):105-113.

Cheng Y.M., Zhao Z.H., and Sun Y.J. (2010a). Evaluation of interslice force function and discussion on convergence in slope staility analysis by the lower bound method. Journal of geotechnical and geoenvironmental engineering , ASCE, 136(8):1103-1113

Cheng Y.M., Li L, Sun Y.J., Au S.K.(2010b). A coupled particle swarm and harmony search optimization algorithm for difficult geotechnical problems. Structural and Multidisciplinary Optimization. Volume 45, Number 4, 489-501

Ching R.K.H. and Fredlund D.G. (1983). Some difficulties associated with the limit equilibrium method of slices. Can. Geotech. J. vol.20:661-672

Chugh A.K. (1986). Variable Factor of Safety in Slope Stability Analysis. Variable factor of safety in slope stability analysis. Geotechnique, 36:57-64.

Colorni A., Dorigo, M., and Maniezzo V. (1992). Distributed optimization by ant colonies, in *Proceedings of the First European Conference on Artificial Life*, F. J. Varela and P. Bourgine, Eds., MIT Press, Cambridge, MA, pp. 134–142, 1992.

Daud W. and Williams, David J.(1999). 3-Dimensional effects on slope stability of high waste rock dumps. International Journal of Mining, Reclamation and Environment, 13: 1, 19-24

Deng, J. H., Tham, L. G., Lee, C. F., and Yang, Z. Y. (2007). Three-dimensional stability evaluation of a preexisting landslide with multiple sliding directions by the strength-reduction technique. Canadian Geotechnical Journal, 44, 343-354

Donald, I. and Chen, Z. Y. (1997). Slope stability analysis by the upper bound approach: fundamentals and methods. Canadian Geotechnical Journal, 34, 853-862

Dawson, E. M., Roth, W. H., and Drescher, A. (1999). Slope stability analysis by strength reduction. Geotechnique, 49(6), 835-840

Dawson, E., Motamed, F., Nesarajah, S., and Roth, W. (2000). Geotechnical stability analysis by strength reduction. Slope stability 2000: proceedings of sessions of Geo-Denver 2000, August 5-8, 2000, Denver, Colorado, 99-113

Dorigo M., Maniezzo V., and Colorni A. (1996). The ant system optimization by a colony of cooperating agents, IEEE Transactions on Systems, Man, and Cybernetics—Part B, Vol. 26, No. 1, pp. 29–41, 1996.

Drucker, D. C. and Prager, W. (1952). Soil mechanics and plastic analysis or limit design. Quarterly of Applied Mathematics, 10, 157-165

Duncan, J. M. (1996). State of the art: limit equilibrium and finite-element analysis of slopes. Journal of Geotechnical Engineering, 122(7), 577-596

Duncan, J. M. and Wright, S. G. (2005). Soil Strength and Slope Stability. John Wiley & Sons, Inc.

Fan K., Fredlund D.G. and Wilson G.W. (1986), An interslice force function for limit equilibrium slope stability analysis. Can Geotech. J. vol.23: 287-296

Farzaneh, O. and Askari, F. (2003). Three-dimensional analysis of nonhomogeneous slopes. Journal of Geotechnical and Geoenvironmental Engineering, 129(2), 137-145

Fredlund D.G. and Krahn J. (1977), Comparison of slope stability methods of analysis. Can. Geotech. J. vol.14: 429-439

Geem Z.W., Kim J.H.，Loganathan G.V. (2001). Harmony search. Simulation, 76(2):60-68.

Giger, M. W. and Krizek, R. J. (1975). Stability analysis of vertical cut with variable conner angle. Soils and Foundations, 15(2), 63-71

Giger, M. W. and Krizek, R. J. (1976). Stability of vertical corner cut with concentrated surcharge load. Journal of the Geotechnical Engineering Division, 102(1), 31-40

Greco,V.R. (1996). Efficient Monte Carlo technique for locating critical slip surface. Journal of geotechnical engineering–ASCE, 122, 517–525.

Griffiths D. V. and Lane P. A. (1999). Slope stability analysis by finite elements. Geotechnique, 49(3), 387-403

Griffiths D.V. and Lane P.A. (2001), Discussion on 'Slope stability analysis by finite elements'. Geotechnique, vol. 51(7): 653-654.

Griffiths, D. V. and Marquez, R. M. (2007). Three-dimensional slope stability analysis by elasto-plastic finite elements. Geotechnique, 57(6), 537-546

Holland J. H.(1975). *Adaptation in Natural and Artificial Systems*, University of Michigan Press, Ann Arbor, MI, 1975.

Hovland, H. J. (1977). Three-dimensional slope stability analysis method. Journal of the Geotechnical Engineering Division, ASCE, 103(GT9), 971-986

Huang, C. C. and Tsai, C. C. (2000). New method for 3D and asymmetrical slope stability analysis. Journal of Geotechnical and Geoenvironmental Engineering, ASCE, 126(10), 917-927

Huang, C. C., Tsai, C. C. and Chen, Y. H. (2002). General method for three-dimensional slope stability analysis. Journal of Geotechnical and Geoenvironmental Engineering, ASCE, 128(10), 836-848

Hungr, O. (1987). An extension of Bishop's simplified method of slope stability analysis to three dimensions. Geotechnique, 37(1), 113-117

Hungr, O. (1994), A general limit equilibrium model for three-dimensional slope stability analysis: Discussion. Can. Geotech. J., 31: 793–795.

Hungr, O., Salgado, F. M., and Byrne, P. M. (1989), Evaluation of a three-dimensional method of slope stability analysis. Can. Geotech. J., 26, 679–686.

Itasca Consulting Group, Inc. (2006). FLAC 3D Version 3.1 User's Guide. Minneapolis, Minnesota, USA

Izbicki, R. J. (1981). Limit plasticity approach to slope stability problems. Journal of the Geotechnical Engineering Division, 107(2), 228-233

Janbu N. (1973), Slope stability computations in Embankment-Dam Engineering, John Wiley, p.47-86

Jiang, J. C. and Yamagami, T. (1999). Determination of the sliding direction in threedimensional slope stability analysis. Proc. 44th Symposium on Geotechnical Engineering, 193-200

Jing L.R. and Stephansson O. (2007). Fundamentals of Discrete Element Methods for Rock Engineering Theory and Applications. Elsevier Science Publishing Company

Jong, G. D. J. D. (1980). Application of the calculus of variations to the vertical cut off in cohesive frictionless soil. Geotechnique, 30(1), 1-16

Karal, K. (1977a). Application of energy method. Journal of the Geotechnical Engineering Division, 103(5), 381-397

Karal, K. (1977b). Energy method for soil stability analyses. Journal of the Geotechnical Engineering Division, 103(5), 431-445

Lam, L., and Fredlund, D. G. (1993), A general limit equilibrium model for three-dimensional slope stability analysis. Can. Geotech. J., 30: 905–919.

Lam, L., and Fredlund, D. G. (1994), A general limit equilibrium model for three-dimensional slope stability analysis: Reply. Can. Geotech. J., 31: 795–796.

Lee, K.S. and Geem, Z.W. (2005). A new meta-heuristic algorithm for continuous engineering optimization: harmony search theory and practice. Computer methods in applied mechanics and engineering, 194, 3902–3933.

Leshchinsky, D. and Baker, R. (1986). Three-dimensional slope stability: end effects. Soils and Foundations, 26(4), 98-110

Leshchinsky, D., Baker, R., and Silver, M. L. (1985). Three-dimensional analysis of slope stability. International Journal for Numerical and Analytical Methods in Geomechanics, 9(2), 199-223

Leshchinsky D. and Huang C.C. (1992). Generalized slope stability analysis: interpretation, modification and comparison. Jour. of Geotechnical Eng, vol.118(10):1559-1576

Liang R.Y., Zhao J. and Vitton S. (1997), Determination of interslice force in slope stability analysis. Soils and foundations, vol.37(1):65-72

Loukidis, D., Bandini, P., and Salgado, R. (2003). Stability of seismically loaded slopes using limit analysis. Geotechnique, 53(5), 463-479

Lyamin, A. V. (1999). Three-dimensional lower bound limit analysis using nonlinear programming. Ph.D Thesis, University of Newcastle, Australia

Lyamin, A. V. and Sloan, S. W. (2002a). Lower bound limit analysis using nonlinear programming. International Journal for Numerical Methods in Engineering, 55(5), 573-611

Lyamin, A. V. and Sloan, S. W. (2002b). Upper bound limit analysis using linear finite elements and non-linear programming. International Journal for Numerical and Analytical Methods in Geomechanics, 26, 181-216

Malkawi, A.I.H, Hassan,W.F., and Sarma, S.K (2001). Global search method for locating general slip surface using Monte Carlo techniques. Journal of geotechnical and geoenvironmental engineering, 127, 688–698.

Matsui T. and San K. C. (1992), Finite element slope stability analysis by shear strength reduction technique. Soils and foundations, vol.32(1):59-70

Michalowski, R. L. (1989). Three-dimensional analysis of locally loaded slopes. Geotechnique, 39(1), 27-38

Morgenstern, N. R. and V. E. Price, (1965). The analysis of the stability of general slip surfaces. Geotechnique, vol.15: 70-93.

Morgenstern N.R. and Price V.E. (1967). A numerical method for solving the equations of stability of general slip surfaces. Computer Journal. vol. 9(4): 388-393.

Morgenstern N.R. (1992), `The Evaluation of Slope Stability – A 25 Year Perspective', Stability and Performance of Slopes and Embankments –II, Geotechnical Special Publication No. 31, ASCE, 1992.

Pan Jiazheng (1980), Analysis of stability and landslide for structures, hydraulic press, Beijing, 25-28. (in Chinese).

Rao S.S. (2009). Engineering optimization : theory and practice. John Wiley & Sons, Inc.

Rechenberg (1965). Cybernetic Solution Path of an Experimental Problem, Library Translation 1122, Royal Aircraft Establishment, Farnborough, Hampshire, UK, 1965

Revilla J. and Castillo E. (1977), The Calculus of Variations applied to Stability of Slopes, Geotechnique, 27:1-11.

Sarma S.K. and Tan D. (2006), Determination of critical slip surface in slope analysis, Geotechnique, 56(8):539-590.

Sloan, S. W. (1988). A steepest edge active set algorithm for solving sparse linear programming problems. International Journal for Numerical Methods in Engineering, 26, 2671-2685

Sloan, S. W. (1989). Upper bound limit analysis using finite elements and linear programming. International Journal for Numerical and Analytical Methods in Geomechanics, 13, 263-282

Sloan, S. W. and Kleeman, P. W. (1995). Upper bound limit analysis using discontinuous velocity fields. Computer Methods in Applied Mechanics and Engineering, 127, 293-314

Spencer, E., (1967), A method of analysis of the stability of embankments assuming parallel inter-slice forces. Geotechnique, 17, 11-26.

Sridevi, B. and Deep, K. (1991). Application of global optimization technique to slope stability analysis. In Proceedings of the 6th international symposium on landslides, 1991, pp. 573–578.

Terzaghi, K. and Peck, R. B. (1967). Soil Mechanics in Engineering Practice. John Wiley and Sons, Inc., New York

Ugai, K. (1985). Three-dimensional stability analysis of vertical cohesive slopes. Soils and Foundations, 25(3), 41-48

Ugai, K. (1988). Three-dimensional slope stability analysis by slice methods. Proceedings of the Sixth International Conference on Numerical Methods in Geomechanics, Innsbruck, 11-15 April, edited by G. Swoboda, 1369-1374

Ugai, K. and Leshchinsky, D. (1995). Three-dimensional limit equilibrium and finite element analysis: a comparison of results. Soils and Foundations, 35(4), 1-7

Wei W.B., Cheng Y.M. and Li L. (2009), Three-dimensional slope failure by strength reduction and limit equilibrium methods, Computers and Geotechnics, 36:70-80.

Yamagami T and Ueta Y. (1988), Search for noncircular slip surfaces by the Morgenstern-Price method, Proceeding 6th International Conference on Numerical Methods in Geomechanics, 1219-1223.

Yang X.S. (2008). Introduction to Mathematical Optimization. Cambridge International Science Publishing, Cambridge, UK.

Zhang P.W. and Chen Z.Y. (2004), Finite element method for solving safety factor of slope stability (in Chinese). Rock and Soil mechanics, vol.25(11): 1757-1760

Zhang, X. (1988). Three-dimensional stability analysis of concave slopes in plan view. Journal of Geotechnical Engineering, 114(6), 658-671

Zhang, X. (1999). Slope stability analysis based on the rigid finite element method. Geotechnique, 49(5), 585-593

Zheng, Y. R., Zhao, S. Y., Kong, W. X., and Deng, C. J. (2005). Geotechnical engineering limit analysis using finite element method. Rock and Soil Mechanics, 26(1), 163-168 (in Chinese)

Zhu D.Y., Lee C.F., Qian Q.H. and G.R. Chen (2005). A concise algorithm for computing the factor of safety using the Morgenstern-Price method. Can. Geotech. J. vol.42: 272-278

Zhu D.Y. (2001), A method for locating critical slip surfaces in slope stability analysis. Can. Geotech. J. vol.38: 328-337

Zhu D.Y., Lee C.F., Qian Q.H. (2001), A new procedure for computing the factor of safety using the Morgenstern-Price method. Can. Geotech. J. vol.38:882-888

Zolfaghari A.R., Heath A.C. and McCombie P.F (2005). Simple genetic algorithm search for critical non-circular failure surface in slope stability analysis. Computers and Geotechnics, 2005, 32:139-152.